PERFORMANCE MODELLING AND ASSESSMENT OF PLASTIC TUBULAR FALLING FILM TOWER FOR THE DEVELOPMENT OF LOW FLOW LIQUID DESICCANT SYSTEM

Ph.D. Thesis

By

KHAN REHAN WASIM

DISCIPLINE OF MECHNICAL ENGINEERING

INDIAN INSTITUTE OF TECHNOLOGY INDORE

JUNE 2023

PERFORMANCE MODELLING AND ASSESSMENT OF PLASTIC TUBULAR FALLING FILM TOWER FOR THE DEVELOPMENT OF LOW FLOW LIQUID DESICCANT SYSTEM

A THESIS

Submitted in partial fulfillment of the

requirements for the award of the degree

of

DOCTOR OF PHILOSOPHY

by

KHAN REHAN WASIM

DISCIPLINE OF MECHNICAL ENGINEERING

INDIAN INSTITUTE OF TECHNOLOGY INDORE

JUNE 2023

INDIAN INSTITUTE OF TECHNOLOGY INDORE

CANDIDATE'S DECLARATION

I hereby certify that the work which is being presented in the thesis entitled **PERFORMANCE MODELLING AND ASSESSMENT OF PLASTIC TUBULAR FALLING FILM TOWER FOR THE DEVELOPMENT OF LOW FLOW LIQUID DESICCANT SYSTEM** in the partial fulfilment of the requirements for the award of the degree of **DOCTOR OF PHILOSOPHY** and submitted in the **DISCIPLINE OF MECHANICAL ENGINERRNG, Indian Institute of Technology Indore**, is an authentic record of my own work carried out during the time period from January 2017 to June 2023 under the supervision of **Prof. Ritunesh Kumar, IIT Indore.**

The matter presented in this thesis has not been submitted by me for the award of any other degree of this or any other institute.

16-06-2023

Signature of the student with date

(KHAN REHAN WASIM)

This is to certify that the above statement made by the candidate is correct to the best of my/our knowledge.

Ritunesh Kumar

16-06-2023

Signature of Thesis Supervisor with date

(PROF. RITUNESH KUMAR)

KHAN REHAN WASIM has successfully given his Ph.D. Oral Examination held on **1st May 2023**

Ritunesh Kumar

16-06-2023

Signature of Thesis Supervisor with date

(PROF. RITUNESH KUMAR)

Acknowledgement

The development of the thesis has been a long journey, and that would not have been possible without the blessings and support of many people.

I want to thank Almighty for his continuous blessings and for granting me the valuable opportunity to carry out the thesis work.

First and foremost, I would like to express my sincere gratitude to my supervisor **Prof. Ritunesh Kumar** for his patience, continuous support, and encouragement during the entire research work. This work could not have been accomplished without his valuable guidance and monitoring of the whole research work.

I am highly thankful to my committee members **Prof. D. Deshmukh,** Discipline of Mechanical Engineering, and **Prof. Sanjay. S**, Discipline of Chemistry, for their valuable suggestions.

Furthermore, I would like to thank my lab manager Mr. Mahesh Jhade, Mr. Kailash Patel, and my Seniors, Dr. Kadam, Dr. Vikas, Dr. Digvijay, and Dr. Gurjeet. They helped me a lot in my research work. Also, thankful to different intern students, Gaurav, Shubham, and Yogesh, for their support in carrying out the experiments and numerical modeling.

I am indebted to my friend Dr. Parvez, Dr. Eshan, and Dr. Faizal for their encouragement and moral support during the critical phase of my thesis.

Finally, I express thanks to my mother, brother, and sister for their support and encouragement to finish this work. Special thanks to my wife **Sameena** and my son **Rizwan**. Without their sacrifice and patience, it would have been impossible for me to complete this research.

Khan Rehan Wasim

Dedicated in memory of

my loving father

Late Dr. KHAN WASIM

List of papers in International Journal from PhD Thesis

1. Kumar R., **Khan R**., Ma Z. (2021), Suitability of plate versus cylinder surface for the development of low flow falling film liquid desiccant dehumidifier, Renew Energy, 179, 723–736 (DOI: 10.1016/j.renene.2021.07.076) **[IF 8.001].**
2. **Khan R**., Kumar R., Ma Z. (2021), Experimental assessment of mass transfer characteristics of polypropylene surfaces for low flow falling film liquid desiccant air- conditioning applications, Chem Eng Process - Process Intensif, 169, 108605 (DOI: 10.1016/j.cep.2021.108605) **[IF 4.237].**
3. **Khan R**., Kumar R., Ma Z. (2022), Experimental investigations on the performance characteristic of plastic surfaces for developing low flow falling film liquid desiccant regenerator, Sol Energy, 236, 356–368 (DOI: 10.1016/j.solener.2022.03.012) **[IF 5.742].**
4. **Khan R**., Neyer D., Kurzina I., Kumar R. Coupled heat and mass transfer characteristics of vertical plastic falling film regenerator at partial wetting conditions. International journal of heat and mass transfer **(under review)**

List of papers in International Journal outside PhD Thesis

1. **Khan R**., Patil D.A., Kumar R. (2022), Development of high-performance vertical falling film plastic dehumidifier exploiting surface modification technique, J Sol Energy Eng, 144, 1–40. (DOI: 10.1115/1.4053905)

List of Book chapters outside PhD Thesis

1. **Khan R**., Kumar R., Rohatgi N. (2019), Sustainable Air-Conditioning, Ref Modul Mater Sci Mater Eng, 1–18 (DOI: 10.1016/b978-0-12-803581-8.11465-1).
2. **Khan R**., Deshmukh S., Kumar R. (2020), Energy Needs for Sustainable Buildings and Transportation. Sustainability; Fundamentals and Applications (DOI: 10.1002/9781119434016.ch27)

ABSTRACT

Low flow falling film liquid desiccant systems are promising due to their overall efficiency and energy-economic value. Two main limitations: corrosive nature of liquid desiccant and incomplete wetting of the working surface hinders the development of low flow liquid desiccant systems. Corrosion of the working surface reduces the system reliability and affects the overall performance (due to breakage of falling liquid film), while incomplete wetting severely weakens the heat and mass transfer performance of the system. The current research investigations aim to address both the above issues. The plastic surfaces can effectively eliminate the corrosion problem. They are cheap, lightweight, and have long longevity. However, unlike metallic surfaces, plastic surfaces suffer from poor wettability due to their inherent hydrophobic nature. Plastic surfaces can be successfully employed as desiccant air contacting surfaces in the liquid desiccant system to address corrosion issues and revamp the development of small-size hybrid liquid desiccant systems for residential thermal comfort needs. But it requires uplifting the wettability of the plastic surface equivalent to the commonly used metallic surfaces. The wettability of the liquid desiccant on the working surface, apart from the basic nature of liquid desiccant solution and surface (plastic/metallic), also depends on the geometry and orientation of the working surface.

Firstly, a preliminary wetness experimental investigation is carried out on the vertical plastic circular cylinder surface, and the wetness behaviour of the circular cylinder surface is compared with that of the vertical plastic plate surface. It is found that the circular cylinder surface showed superior wetness performance in comparison to the plate surface. An experimental setup is fabricated and developed to carry out the experimental investigation on the performance of circular cylinder surfaces in adiabatic mode. Comprehensive dehumidification and regeneration experiments are conducted on circular cylinder surfaces under the influence of air and solution operating parameters. The mechanical surface modification method is utilized to enhance circular

cylinder performance at low flow conditions. The performance of the circular cylinder surface is compared with plate surface to find a better surface for developing a low flow falling liquid desiccant system. It is found that the Plain PP circular cylinder offered 55.9% and 50.5% improvement in dehumidification rate and regeneration rate as compared to the Plain PP plate surface. The Modified PP circular cylinder intensified the dehumidification rate and regeneration rate of the Plain PP circular cylinder by 31.1% and 44.9%. The findings of dehumidification and regeneration study could be useful for designing small capacity low flow falling film tower-based solar hybrid liquid desiccant systems for residential and commercial applications. Based on the experimental readings, new generalized dehumidification and regeneration effectiveness correlations are proposed to predict the effectiveness of adiabatic and non-adiabatic falling film towers by incorporating shear force, enthalpy/temperature difference, and mass transfer potential between liquid desiccant and air along with wetness behavior parameters. The mean effective error of the dehumidification correlation against eight datasets is 11.7%, and for regeneration correlation, it is 16.5% against nine datasets.

In addition to performance analysis, heat and mass transfer characteristics are essential for developing liquid desiccant systems. Existing heat and mass transfer correlations are available mostly for packed bed systems or metallic surface falling film towers; these correlations are not suitable for simulation/modelling of low flow plastic falling film towers. In the current work, parametric analysis of experiment variation of mass transfer coefficient of Plain and Modified PP circular cylinder is studied. The mass transfer coefficient of the circular cylinders and plate surface are compared, and it was found that under the tested conditions, the mass transfer coefficient of the Plain PP circular cylinder is 1.65 times superior to the Plain PP plate. The optimal mass transfer coefficient of ~20 g/m^{2}s for the Plain PP circular cylinder is obtained at ~1.5 ratio of the mass flow rate of liquid to air. In contrast, the mass transfer coefficient of the Modified PP circular cylinder continuously increases for the studied range of the mass flow rate of the liquid to air ratio. Further, efforts are made to develop a generalized mass transfer coefficient correlation by incorporating the wetting characteristics difference, flow dynamics, enthalpy potential, and sensible cooling information. The developed correlation presented good accord with experimental observations of plastic/metallic surfaces of adiabatic and non-adiabatic dehumidifiers. The mean effective error of the current correlation against nine experimental datasets is 16.6%. The regenerator plays a critical role in the overall efficiency and energy-economics of LDS. However, compared to the dehumidification study, the experimental heat and mass transfer analysis on falling film regeneration is almost nil. The heat and mass transfer coefficient of the Plain PP and Modified PP circular cylinder surface for the regeneration process are evaluated using the finite difference method considering actual wetting characteristic as well as heat transfer from the dry surface. It was found that the performance difference between the Plain and Modified circular cylinder surface mainly depends on the operating flow rate conditions: partial or complete wetting. To ascertain the behaviour of above observation, the transfer coefficients variation against two strong parameters: air mass flow rate and solution temperature are analysed and studied at partial wetted conditions, whereas the effect of process air temperature and humidity are analysed at complete wetting conditions. Based on the observation, a new heat and mass transfer coefficient are developed to facilitate the numerical simulation needs of partial and complete wetted operating conditions of the falling film tower. It is found that the partial wetting correlations predicted the experimental outlet values with greater accuracy compared to complete wetting correlations. Developed correlations through full wetting assumption approach (Sh_{CW} and Nu_{CW}) highly underpredicted the experimental observation (MAPE 27.2% and 15.2%) unlike the correlations developed based on actual wetting of the solid surface (Sh_{PW} and Nu_{PW}) approach, which predicted experimental observation with much superior accuracy (MAPE 7.5% and 11.2%). The developed partial wetting heat and mass transfer correlations will be helpful for

designing and developing falling film towers operated in wide range of liquid flow rate conditions. Several researchers have used ANN techniques to reproduce the experimental observations accurately. However, previous ANN performance models were mainly developed based on training performance with limited datasets. In the current work, a new generalized ANN model is developed to predict the performance of the dehumidifier, considering both training and simulation performance. The developed ANN model showed good accuracy and predicted the performance of sixteen experimental dehumidification studies with an average error of 4.2%. The optimized ANN models are useful for accurately predicting the performance of falling film dehumidifiers operating at different at different operating range.

TABLE OF CONTENTS

LIST OF FIGURES

Title **Page No.**

LIST OF TABLES

Title **Page No.**

NOMENCLATURE

Ø	diameter (mm)
a	Packing density (m^2/m^3)
A	area (m^2)
A_w	wetted area (m^2)
B	breadth (mm)
d	depth of cut (mm)
C_p	Specific heat (kJ/kg)
C_{pm}	Specific heat of moist air (kJ/kg)
D	diffusion coefficient (m^2/s)
F_g	gravity force (N)
F_τ	shear force (N)
h	enthalpy (kJ/kg)
h_m	mass transfer coefficient (g/m^2 s)
$h_m{}'$	molar mass transfer coefficient (mol/m^2 s)
h_t	heat transfer coefficient (W/m^2 K)
h'_t	corrected heat transfer coefficient (W/m^2 K)
h_{fg}	enthalpy of vaporization (kJ/kg)
H	height (mm)
k	thermal conductivity (W/mK)
Le	Lewis number
$\dot{m}$	mass flow rate (kg/s)
N	number of data points
Nu	Nusselt number
p	pitch of groove (mm)
P_a	partial vapor pressure in air (Pa)
Pr	Prandtl number
P_s	partial vapor pressure in solution (Pa)
Re	Reynolds number
Sc	Schmidt number
Sh	Sherwood number
t	air channel gap (mm)
T	temperature (^{0}C)
W	width (mm)

X	concentration of the solution (%)

Greek symbols

δ	film thickness (mm)
ω	humidity ratio (g/kg)
ε_Y	effectiveness (%)
μ	dynamic viscosity (Pa s)
ρ	density (kg/m^3)
γ	surface energy (m J/mm^2)

Sub and superscripts

*	interface equilibrium
a	air
abs	absorption/dehumidification
c	solid surface
eqls	equilibrium with solution
exp	experimental
in	inlet
out	outlet
pred	predicted
reg	regeneration
s	solution
v	water vapor
w	water

Abbreviations

ABS	acrylonitrile butadiene styrene
CCS	circular cylinder surface
DBT	dry bulb temperature (ºC)
HCOOK	potassium formate
HCFC/CFC	hydro/chlorofluorocarbons
HX	heat exchanger
LDS	liquid desiccant system
LiBr	lithium bromide
LiCl	lithium chloride
LMTD	log mean temperature difference (ºC)
LMWD	log mean humidity difference (g/kg)
MSE	mean square error

MAPE	mean absolute percentage error
NTU	Number of transfer units
PP	polypropylene
PS	plate surface
PTFE	polytetrafluoroethylene
SiO_2	silicon dioxide
S.S.	stainless steel
TiO_2	titanium dioxide
TEG	triethylene glycol
VAS	vapor absorption system
VCS	vapor compression system
WBT	wet bulb temperature (ºC)

CHAPTER 1

Introduction

1.1 Research background

Air-conditioning (AC) represents an indispensable part of building energy consumption. Around 50% of the energy utilized in buildings is mainly consumed by air-conditioners to provide thermal comfort for building occupants. In addition to basic food, clothing, and shelter, thermal comfort has become a vital necessity in modern times, as it affects not only human working productivity but also health and well-being [1–3]. AC systems are meant to maintain comfortable levels of temperature, humidity, purity, and air quality. The energy consumption for AC in residential and commercial buildings has increased during the last decades and is still rising at an unprecedented rate. The increased energy consumption is primarily caused by rapid population growth, economic progress, and thermal comfort demand. Conventionally, AC is still achieved by the vapor compression technology, a technology suggested at the beginning of the 20th century by a person later recognised as the "Father of Modern Air-Conditioning": Willis Haviland Carrier. He invented the first electrical AC system to control humidity. Billions of vapor compression systems (VCSs) have been installed worldwide since then due to its outstanding compactness, low cost, maintenance-free operation, and scalability. Fig. 1.1 shows the simple vapor compression-based AC system. This technology work in a closed cycle, where the peculiar working fluid (HFCs/ HFOs refrigerant) continuously flows in a closed loop of components facilitating compression and expansion of the refrigerant. Cooling and dehumidification of the process air (at warm and humid conditions) are accomplished simultaneously by allowing it to contact with an evaporator coil that is kept below the dew point temperature of the process air. In many incidences reheating of the cool and dehumidified process air is required to get the desired supply air conditions. The compressor is a main energy (electrical energy) consuming component in the entire cycle. The required cooling capacity of the AC system depends on the desired total load (sensible and latent) through it.

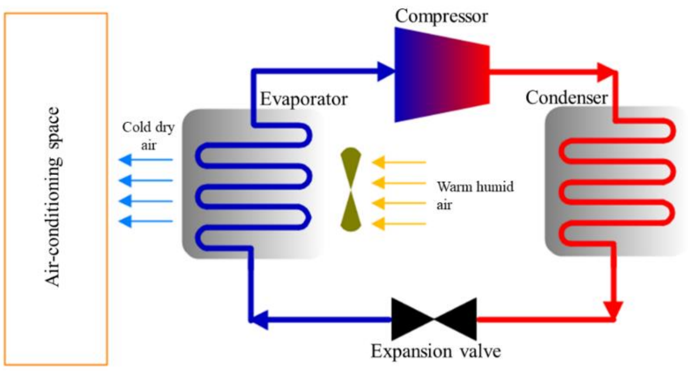

Fig. 1.1 Simple vapor compression AC system

In the 1970s, the world was introduced to rapidly spreading environmental malignancy by the CFC/HCFC refrigerant based ACs. Apart from the severe environmental concerns of global warming and ozone layer depletion, several other problems: such as sole dependency on electrical energy, coupled cooling and dehumidification process, inefficient dehumidification, and human health issues associated with VCSs have been identified. The global environmental concerns and a deteriorating level of left primary energy created an opportunity for exploring more efficient, eco-friendly AC technology driven by low grade energy. Evaporative cooling and sorption-based AC technology emerged as alternatives to VCS. The evaporative cooling technique is a simple and passive method of providing cooling, in which cooling is obtained through the evaporation of water. Evaporative cooling systems are mainly useful for hot and dry conditions, where the desired cooling can be obtained without crossing the acceptable humidity levels.

Sorption-based AC systems can be categorized as vapor absorption systems (VASs) and desiccant systems. Fig. 1.2 depicts simple VAS. Some of the VAS working components are the same as used in VCS. In VAS, the mechanical compression process (through compressor) is replaced by heat-based compression process (by an absorber, pump, and regenerator together). The refrigerant vapor leaving the evaporator is absorbed by the absorbent solution, which has a high affinity for the refrigerant. After that, the refrigerant-rich solution is pumped to high pressure and heated in the regenerator to separate the absorbed refrigerant. The pure refrigerant is subsequently condensed and returned to the evaporator. The hot and strong absorbent solution generated in the regenerator is throttled back to the absorber. Similar to VCS, the simultaneous cooling and dehumidification of process air is realized by the condensation process across the low-temperature evaporator coil. The regenerator is the main energy-consuming component in VAS. Renewable sources of energy or waste heat can be used to power the regenerator. The VAS is a potentially useful alternative to the VCS; however, due to its low COP and bulky size, the VAS could not compete with the VCS commercially. The desiccant AC system can help overcome the technical limitations of both VCS and VAS. Following are the advantages of liquid desiccant over VCS/VAS.

1) The desiccant directly removes the moisture from the air through physical contact. Hence, it can can effectively control the air humidity compared to VCS/VAS (e.g highly humid conditions).
2) The energy required for the regeneration process in desiccant systems can be supplied by renewable sources or waste heat at even low exergy levels.
3) The desiccant system uses environment-benign hygroscopic salt solutions for dehumidification instead of highly environment-malignant CFC/HCFC refrigerants.
4) Desiccant systems can be integrated with other cooling systems (e.g., evaporative cooling, VCS, or closed absorption cooling) to independently handle cooling and dehumidification load.

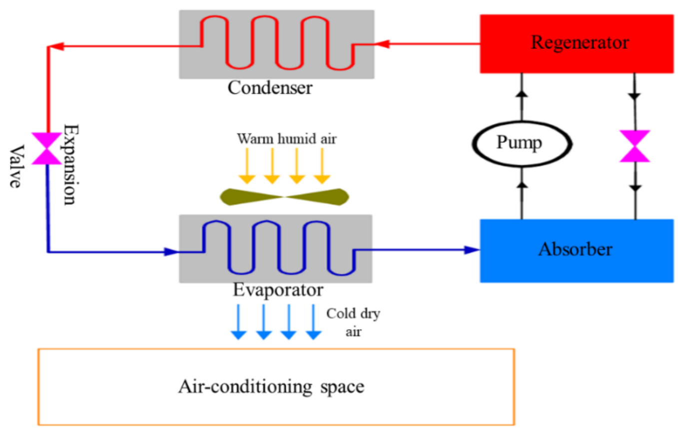

Fig. 1.2 Vapor absorption AC system

1.2 Desiccant system

Desiccant is a term used for any substance that has a strong affinity toward the water vapor present in the air. Dehumidification in the desiccant system is achieved by allowing the humid air to contact with desiccant. The absorbed moisture is then expelled out by heating the desiccant to realize continuous dehumidification. Based on their physical state, desiccants are classed as solid desiccants or liquid desiccants. The physical mechanism of removing moisture is different for both desiccants. In the case of a solid desiccant, moisture removal is accomplished by physical holding the water vapour within the porous structure of the desiccant (adsorption). In contrast, the liquid desiccant absorbs moisture at the interface of the liquid solution (absorption). The absorbed moisture gets completely integrated with the liquid desiccant solution.

1.2.1 Solid desiccant system

Solid desiccants are solid adsorbent materials consisting of microporous holes with a high potential to attract moisture from air. The solid desiccant dehumidification was proposed by Hausen in 1935. Solid desiccant materials are impregnated, embedded, or coated over a cylindrical shape honeycomb structure known as a desiccant wheel (rotor), which rotates at a low speed continuously. The compact honeycomb structure coated with adsorbent material provides a large surface area for air dehumidification. Fig. 1.3 shows a typical solid desiccant wheel. The desiccant wheel is divided into two sections: 75 % of the desiccant wheel for the adsorption process and remaining 25% for regeneration process. There are two opposing airstreams: process air stream and reactivation air stream. On the adsorption side, the humid process air interacts with desiccant material and transfers its moisture to the micropores of the desiccant material. The reactivation air stream is initially heated and passed through the regeneration side, where it picks up the excess moisture from the desiccant wheel and discharges it to the outside air. The adsorption and reactivation processes happen continuously during the circular motion of the wheel to provide continuous dehumidification. The dry and hot air leaving the desiccant wheel can be cooled using evaporative cooling or VCS/VAS to obtain the desired supply conditions. The most commonly used solid desiccant materials are silica gels, zeolites, synthetic zeolites, activated alumina, carbons, and synthetic polymers.

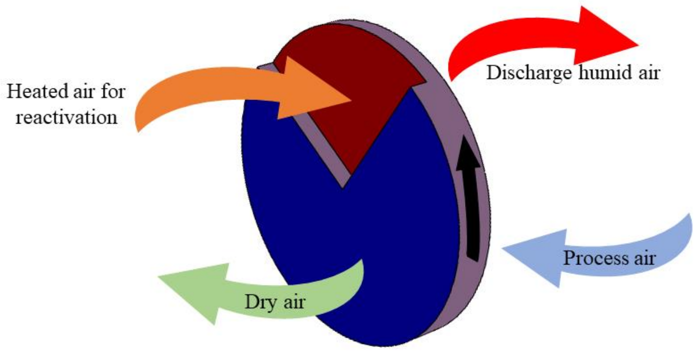

Fig. 1.3 Solid desiccant wheel

1.2.2 Liquid desiccant system

Another type of desiccant-based AC system is the liquid desiccant AC system. Fig. 1.4 shows a simple liquid desiccant-based AC. Concentrated and cold desiccant solution at low vapor pressure (state 1) enters from the top of the dehumidifier and interacts with humid air flowing in parallel/counter/cross direction. The difference in vapor pressure between moist air and desiccant solution dehumidifies the air. The solution becomes diluted due absorption of moisture from the air.

For continuous dehumidification, the diluted solution must be concentrated again. The diluted solution (state 2) is first passed through a solution-to-solution heat exchanger to raise its temperature, and then a heating coil heats it to the required regeneration temperature. In the regenerator, the hot and diluted solution (state 3) at relatively higher vapor pressure expels excess moisture to atmospheric air. The hot concentrated (state 4) is cooled initially using the solution-to-solution heat exchanger and then by cooling coil before being sent back to the dehumidifier to complete the cycle. LDS has the following advantages over a solid desiccant system:

1. LDS requires a lower regeneration temperature to concentrate the desiccant solution (around 50ºC - 80ºC) unlike the solid desiccant systems (150ºC - 260ºC). Hence, they offer better chances of using the waste heat/renewable energy.
2. The liquid desiccant solutions have strong thermo-chemical energy storage capability in the form of concentrated solutions. The excess concentrated desiccant solution can be utilized for dehumidification when sufficient energy for regeneration is not available (analogous to electrical batteries).
3. Apart from removing dust particles, the liquid desiccant can absorb many inorganic and organic impurities along with different bacteria present in the air. Hence, they have become exclusive option for AC applications requiring highly sterilize air such as hospital, operation theatre etc.
4. LDS are more flexible; unlike solid desiccant systems, the dehumidification and regeneration process in LDS can be disintegrated from each other. Thus, localized and disintegrated dehumidification and regeneration processes are possible in LDS.
5. Simultaneous cooling/heating can be easily done to obtain isothermal dehumidification and regeneration. Along with the above-discussed advantages, LDS has some limitations, such as corrosion, liquid desiccant carryover, salt crystallization, and higher initial cost. On the commercial front, the solid desiccant system has proven successful, but

LDS continues to face technical challenges due to various limitations cited above.

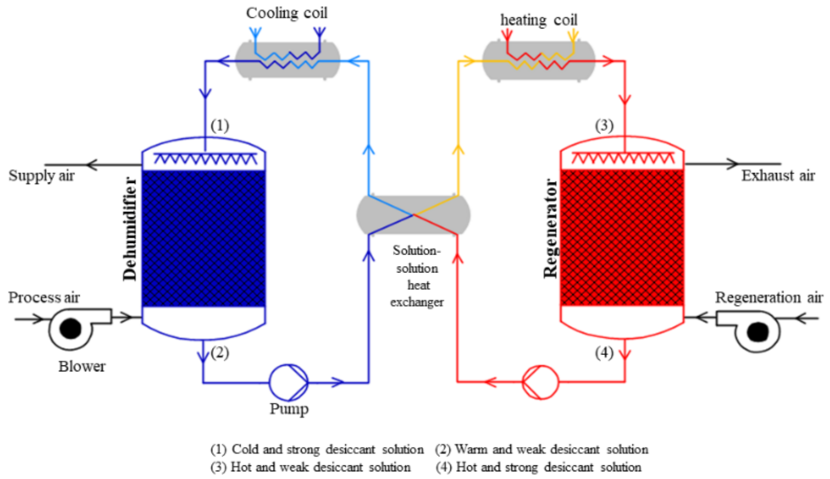

Fig. 1.4 Simple liquid desiccant system

1.3 Organization of thesis

The main objective of the current work is to find the best non-corrosive solid surface for the development of low-flow LDS to improve their energy performance and economic value. The research includes both experimental and numerical investigations on plastic vertical LDS falling film towers. The complete thesis is organized into seven chapters. A brief introduction about the research area and its importance are presented in the **Chapter 1** of the thesis.

Chapter 2 presents a detailed literature survey of previous work on LDS. It includes different aspects of experimental and numerical work on the packed bed and falling film towers. Finally, the conclusions of the literature survey and the objectives of the present work are summarized.

Chapter 3 describes the findings of the preliminary study on the wetting characteristic of circular cylinder surface (CCS) and the experimental test facility developed for the dehumidification and regeneration study. Experimental investigations of the dehumidification and the regeneration processes on the CCS, performance comparison of CCS with plate surface (PS), and development of generalized dehumidification and regeneration effectiveness correlations for the falling film tower have been presented in **Chapter 4**.

The numerical modelling of coupled heat and mass transfer characteristics of vertical circular cylinder dehumidifiers and regenerators and the development of new Nu and Sh number correlations for low flow falling film dehumidifiers and regenerators have been presented in the **Chapter 5**.

In **Chapter 6**, data-driven predictive models are developed for falling film dehumidifiers using artificial neural networks (ANN).

Finally, conclusions and recommendations for future work are discussed in **chapter 7**.

Useful supplementary information associated with the present research work is included in the **appendices**.

CHAPTER 2

LITERATURE REVIEW

2.1 Historical overview of liquid desiccant

The use of liquid desiccant started during the early 20th century for drying in the chemical processing and textile industries. The idea of using the inorganic salt solution in AC was initially proposed in 1935 by Bichowsky and Kelley [4]. After 20 years, Lof [5] proposed the concept of solar liquid desiccant AC. Earlier research on liquid desiccant could not generate the required interest for developing liquid desiccant AC technology, as more attention was given to contemporary vapor compression AC systems due to astonishing compactness, high COP, favourable thermophysical properties, i.e., odourless, non-toxic, non-flammable, high level of scalability and maintenance free operation. Also, the low cost of electricity was another important reason behind the wide acceptance of the VCS in thermal comfort cooling. The energy crisis of the 1970s, combined with environmental concerns associated with VCS (ozone depletion and global warming), has forced the attention back on the VASs. Research groups started exploring closed VAS and LDS as an alternatives to conventional VCS [6–15]. Closed VAS as an alternative to high-capacity VCS and LDS systems as an alternative to small-capacity applications such as residential air-conditioners. In the last two decades, much attention has been given to efficient design, performance improvement, use of new desiccants, and overcoming the limitations of LDS mentioned in section 1.2.2.

2.2 Liquid desiccant characteristics

The type of liquid desiccant used is one of the most important parameters in LDSs. The liquid desiccant characteristic significantly influences the design and overall performance of LDS. The hygroscopic strength of liquid desiccant can be evaluated by measuring its vapor pressure. The vapor pressure is the most critical property of liquid desiccant as it directly determines the dehumidification ability. Apart from vapor pressure, other properties such as surface tension, density, viscosity, thermal conductivity, and corrosiveness play an important role in deciding the potential usability of liquid desiccant for AC. Ideally, desiccant should have the following characteristics to ensure good performance and overall economics of the LDS.

1. Low vapor pressure corresponding to atmospheric temperature conditions for better dehumidification ability.
2. Low cost.
3. High crystallization temperature.
4. Low surface tension and viscosity to ensure proper wetting of solid surface facilitating desiccant air contact.
5. Low regeneration temperature to minimize energy consumption.
6. Non-corrosive, non-toxic, odourless, zero vapor pressure in purest form and inflammable.
7. High thermal conductivity for good performance of LDS

2.3 Liquid desiccant material

Liquid desiccants are of two types: conventional and ionic liquids. Conventional liquid desiccants are sub-categorized as organic and inorganic desiccant solutions. The most common organic desiccants are glycol solutions such as monoethylene glycol (MEG), diethylene glycol, and triethylene glycol (TEG). Earlier, research on LDS started with glycol solution as a liquid desiccant. Lof [5] utilized TEG solution as a working fluid for their solar LDS. Factor and Grossman [8] drew attention to the problem with the use of MEG glycol. They found that although the MEG is hygroscopic, due to high evaporation, it gets easily carried away by the process air stream (liquid desiccant carryover). They suggested that MEG is not useful for AC, but TEG can be used because it has a lower vapor pressure than MEG. Several studies utilized TEG as a desiccant to carry out experimental and theoretical work on LDS [16–19]. However, the high viscosity and non-zero vapor pressure of pure TEG solution made it extremely difficult to separate the mist carried over along with the process and the scavenging air across the absorber and regenerator. Mist carryover along with process air induces serious health hazards such as strong skin irritation and respiratory problems. Hence, researchers stopped exploring the use of glycol solution in air-conditioning. It resulted in a gain in interest for inorganic desiccant solutions. The aqueous solution of halide salts of LiCl, LiBr, $CaCl_2$, and the mixtures of these salts are used as an inorganic desiccant solution. These desiccants have low viscosity and low vapor pressure; most importantly, their anhydrous salts have zero vapor pressure. Hence, they carry almost all desired characteristics required in thermal comfort applications except for the high price issue. Among them, LiCl is the most extensively studied, followed by LiBr and $CaCl_2$. The preferred range of these desiccants is: LiCl 30-40%, $CaCl_2$ 35-45%, and LiBr 50-60%. One of the biggest setbacks of using an inorganic desiccant solution is that they are highly corrosive to most of the commonly used metallic surfaces in LDS. Expensive coating and corrosion inhibitors are required to increase the durability of the system. Recently, ionic liquids have been explored to overcome the corrosion problem and limited availability of rare earth Lithium metal-based salt. Lithium is quite popular in various other engineering applications, especially energy storage applications such as lithium-ion batteries. Ionic liquids are aqueous solutions typically composed of organic cation/anion and inorganic cation/anion. The different possible combinations of organic cation/anion and inorganic cation/anion can be tuned to obtain the desired vapor pressure for a specific application. The important properties of the ionic liquid are low volatility, good thermal conductivity, low corrosion, and high chemical stability [20]. Few examples of ionic liquids are 1-butyl-3-methylimidazolium tetrafluoroborate ([Bmim]BF4, 1-Ethyl-3-methylimidazolium acetate ([Dmim]OAc) etc. Ionic liquids are promising, but they are costly, and the research is still in the developing stages. Apart from the above, potassium formate (HCOOK) is explored as a liquid desiccant due to its low corrosiveness and volatility.

2.4 Liquid desiccants comparative performance analysis

The key qualities necessary for air dehumidification by liquid desiccant have already been covered in section 2.2. In addition, the ultimate choice of liquid desiccant depends on several other factors, such as type of application (industrial or domestic), working surface material, and the load across the system. The summary of the comparative performance analysis of different liquid desiccants are discussed below.

2.4.1 Comparative performance studies of different liquid desiccants

Ertas et al. [21,22] proposed the concept of mixing desiccant solutions to normalize the limitations of participating desiccant solutions. The drawbacks of $CaCl_2$ are low stability, high crystallization temperature, and high vapor pressure, and the drawbacks of LiCl are high cost and high viscosity. They mixed LiCl and $CaCl_2$ in different proportions: 30% LiCl + 70% $CaCl_2$, 50% LiCl + 50% $CaCl_2$, and 30% LiCl+ 50% $CaCl_2$ and concluded that 50% LiCl + 50%$CaCl_2$ mixture is the best option due to its optimum vapor pressure, viscosity, stability, and cost. Chung et al. [17] experimentally compared the performance of 40% LiCl and 95% TEG desiccants. They found that the dehumidification effectiveness of LiCl ranged from 65-70% and 90-95% for TEG. Additionally, they demonstrated the effective removal of air contaminants using TEG. Lazzarin et al. [23], in a numerical study, compared the mass transfer capabilities of 40-65% LiBr and 30-50% $CaCl_2$ solutions. They found that the mass transfer performance of LiBr solution was superior to $CaCl_2$ solution at the 30^{o}C temperature and 40% concentration. Liu et al. [24] theoretically compared the mass transfer performance of two liquid desiccants: LiCl and LiBr. They concluded that at the same desiccant volumetric flow rate for the dehumidification process, the performance of 27.8-36.7% LiCl is better than 42.2-54.1% LiBr, and for the regeneration process performance of 38.4-54.0% LiBr is better than 23.7-40.7%LiCl. Longo and Gasparella [25] experimentally compared the performance of 40% LiCl and 52% LiBr with an organic desiccant solution of 74% HCOOK for three years. They concluded that the LiBr desiccant solution showed the best performance and suggested that the HCOOK solution as a promising desiccant for LDS due to its low cost and low causticity. Bouzenada et al. [26] experimentally compared the performance of 33% LiCl and 40% $CaCl_2$ desiccants in absorber and regenerator modes. They claimed better dehumidification capability of LiCl solution, but the regeneration process was more effective for $CaCl_2$ solution. Koronaki et al. [27] compared the heat and mass transfer performance the LiCl, LiBr and $CaCl_2$ desiccant solutions in a packed column dehumidifier. They concluded that at 40% concentration, the performance of LiCl is better than LiBr and $CaCl_2$. Wen et al. [28] experimentally tested the performance of 35% LiCl and 68% HCOOK desiccants on a plate falling film regenerator. They found that the performance of both the desiccants was almost equivalent under similar experimental working conditions. Bhowmik et al. [29] explored the performance of a mixed desiccant solution made from 37.2% LiBr and 17.8% HCOOK. The newly prepared desiccant solution enhanced the dehumidification/regeneration rate compared to LiBr/HCOOK desiccant due to improvement in the wetted area. They found through economic analysis that the optimal mixed desiccant was almost 9% cheaper than conventional LiBr desiccant. Jiang et al. [30]compared the performance of mixed liquid desiccant (LiCl and $CaCl_2$) with LiCl and $CaCl_2$. The dehumidification rate of the mixed desiccant solution was higher than the $CaCl_2$ desiccant. Based on the economic analysis they claimed that the optimal mixed desiccant 1:3 ($CaCl_2$: LiCl) cost is lower than pure LiCl.

2.4.2 Ionic liquids

Luo et al. [31] tested the dehumidification performance of 1-Ethyl-3-methylimidazolium Tetrafluoroborate ([Emim]BF4) and compared it with conventional LiBr desiccant solution. They found that the dehumidification rate of [Emim]BF4 was 13% lower than LiBr. However, they claimed that at higher concentration levels, the performance of ionic liquid can approach the performance level of LiBr. In subsequent research, Luo et al. [32] investigated the dehumidification ability of 1-butyl-3-methylimidazolium tetrafluoroborate ([Emim]BF4) as well as 1,3-dimethylimidazolium acetate ([Dmim]OAc). They showed that ([Emim]BF4) with 85.5% and ([Dmim]OAc) with 81.7% concentrations can approach the dehumidification rates of 40.9% LiCl and 45.0% LiBr under the same simulated conditions. Qu et al. [33] tested thirteen different ionic liquids and found that the [Emim][OAc] was the most suitable liquid for desiccant dehumidification and regeneration. They also developed empirical correlations to calculate thermophysical properties of [Emim][OAc]. Watanabe et al. [34] compared the dehumidification performance of sixteen types of ionic liquids. They reported that the tributyl(methyl)phosphonium dimethyl phosphate ([P4441] [DMPO4]) gave the best dehumidification performance among the tested ionic liquids. Furthermore, the best ionic liquid and 30% LiCl were compared for corrosion tests against four different metals (steel, S.S. 304, copper, and aluminium) to prove the usefulness of the best ionic liquid against the corrosion process. Similarly, Maekawa et al. [35] explored and compared the dehumidification capacity of seven different ammonium type-ionic liquids and reported that 2-hydroxy-N,N,N-trimethylethan-1-aminium dimethyl phosphate ([Ch][DMPO4]) gave best dehumidification performance due to its low vapor pressure.

Table 2.1 present the comparative property analysis of liquid desiccants. The properties are calculated at typical dehumidification/regeneration temperature of different liquid desiccant. The properties of LiCl and $CaCl_2$ are taken from Conde [36], LiBr from Kaita [37] and Patterson and Blanco [38], ionic liquid from Luo et al. [32], and HCOOK from Wen et al. [39], and Nasr-El-Din et al. [40]. The following important points can be concluded from

Table 2.1 Comparative analysis of liquid desiccants

Properties of desiccants	Inorganic desiccant solutions			Ionic liquid	Other desiccant
	LiCl (40%) 25ºC/ 70ºC	LiBr (60%) 25ºC/ 70ºC	$CaCl_2$ (45%) 25ºC/ 70ºC	[Dmim]OAc (91.77%) 20.3ºC/ 68ºC	KCOOH (68%) 25ºC/ 70ºC
Vapor pressure (kPa)	0.590/ 7.377	0.216/ 3.637	0.946/ 11.60	0.586/ 7.013	0.968/ 9.870
Surface tension (m N/m)	95.73/ 90.45	91.60/ 81.16	96.42/ 91.76	NA	61.77/ 56.77
Viscosity (mPa s)	8.38/ 3.17	9.11/ 4.33	14.17/ 5.25	NA	6.88/ 2.84
Density (kg/m^3)	1252/ 1228	1717/ 1687	1446/ 1418	NA	1488/ 1456
Cost (INR/kg)	1850	2500	300	36,000	250

1. Among inorganic desiccant solutions, LiBr and LiCl have the lowest vapor pressure i.e., higher dehumidification ability, followed by $CaCl_2$. The vapor pressure of [Dmim]OAc and LiCl are comparable at the dehumidification and the regeneration conditions. Similarly, the vapor pressure of HCOOK and $CaCl_2$ are comparable.

2. The higher vapour pressure of the $CaCl_2$ and HCOOK solutions at regeneration conditions indicates that these solutions require a relatively low temperature to regenerate the solution (suitable for regeneration mode only). However, ideally, the desiccant solution should have low vapor pressure for the dehumidification temperature range of (20-30ºC) and high vapor pressure for the regeneration temperature range (60-70ºC).

3. Surface tension and viscosity affect the wetting of solid surfaces. Higher values of these properties lead to poor dehumidification and regeneration performance. While higher value of density indicated more pumping power. The surface tension of the KCOOH is lower than conventional liquids, whereas the density of LiBr solution is the highest.
4. The $CaCl_2$ and HCOOK are the cheapest desiccants followed by LiCl and LiBr. The ionic liquid cost is expensive.

2.5 Liquid desiccant-based AC system

The liquid-based AC system can be standalone or hybrid LDS depending on the type of method utilized for cooling the dry air. LDS in conjunction with evaporative cooling is referred as standalone LDS. The dry air leaving the dehumidifier of LDS is cooled with the help of evaporating cooling. Different types of evaporative cooling such as direct [41], indirect [42], or regenerative cooler [43], have been utilized in combination with LDS to obtain dry and cool supply air. The combination of VCS and LDS is commonly referred to as hybrid LDS. The dehumidified air is passed over the evaporator coil of the VCS for sensible cooling. In a hybrid system, there are two common configurations of LDS and VCS to take care of the cooling requirements. First, dehumidification in LDS followed by cooling of the air using VCS, and second simultaneous dehumidification and cooling through the integration of dehumidifier-evaporator as a single unit. Pena et al. [44] designed a hybrid LDS to control humidity and temperature of air for high latent load conditions. The desired supply condition of air was attained first by dehumidification in LDS and then by cooling in VCS. The proposed design could provide a 30% savings in electrical consumption as compared to conventional VCS. Yadav [45] presented modelling of hybrid LDS, which consisted of dehumidifier-evaporator and regenerator-condenser as a single unit. They found that energy savings of 80% could be achieved as compared to a conventional VCS in a hot and humid climate. In a hybrid system, the heat rejected by the VCS is utilized for desiccant regeneration. Chen et al. [46] proposed a hybrid LDS that works at low temperatures and solution concentrations.

The heat rejected across the condenser is utilized to regenerate the liquid desiccant. The hybrid system's overall COP was 1.16 times higher than a conventional VCS system. Several advantages of hybrid LDS are mentioned below:

1. The hybrid LDS system offers a huge amount of electricity saving potential currently employed in thermal comfort cooling applications; they offer higher COP than the standalone VCS.
2. Clean sources of energy such as solar and geothermal can be used effectively in hybrid LDS.
3. The heat rejected by the condenser can be utilised efficiently to regenerate the desiccant solution. Thus, eliminating the requirement of an auxiliary thermal heater.
4. The desired thermal comfort can be achieved using small compact VCS in a hybrid system, resulting in reduced energy consumption by VCS.

2.6 Liquid desiccant towers

The dehumidifier (also known as absorber) and regenerator (as known as desorber/stripping column) are the two most important components of the LDS. These components work as simultaneous heat and mass exchangers. The heat and mass transfer process in LDS is governed by the type of tower utilized for liquid desiccant air-interaction. Packed bed and falling film towers are primarily used as dehumidifiers/regenerators in the LDS.

2.6.1 Packed bed tower

Packed bed columns consist of a vertical column filled with packing material (Fig. 2.1). The packing provides a large interfacial surface area for the mass transfer inside the packed column. Hence, they are the most compact tower, unlike other contemporary designs such as falling film and spray towers. As the liquid flow inside the packed column is highly irregular and liquid film contracts between the packing, packed columns generally operate at a high mass flow rate of liquid to air ($\dot{m}_s/\dot{m}_a$ ratio 2.5 - 12) to properly wet the packing surface. Apart from a high parasitic power requirement for the liquid pump, high parasitic power requirement for the air blower (due to high air side pressure drop) and the difficulty in providing internal cooling/heating are other limitations associated with packed columns.

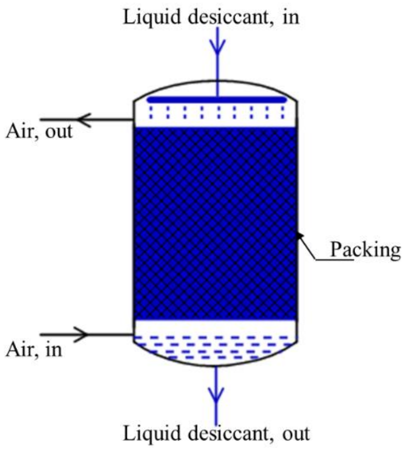

Fig. 2.1 Packed bed tower

The packing material is the medium for liquid desiccant and air to interact. The packing can be classified as random packing, which is assembled inside the tower in the random manner, and structure packing, which is formed by structuring the packing in a regular way. Random packings (Raschig rings, Berl and Intalox saddles, Pall rings) are arranged in a random pattern inside the tower. They are traditionally being used as they provide good contact for air-liquid descant interaction. However, the hydraulic resistance to air and solution is relatively high due to the irregular arrangement of packing. The structure packings (wood grids, corrugated structure packing, gauze structure) are easier to install and provide less airflow resistance, but they are more expensive than random packings. Several studies have reported on packed bed towers with random or structure packings. However, in the last two decades, attention has shifted towards structure packing as they offer better performance for the same loading condition without additional liquid and air side pressure drop. The experimental and theoretical studies on packed bed towers are summarized in section 2.9

2.7 Falling film towers

Falling film tower or wetted wall columns (Fig. 2.2) consist of a vertical plate or horizontal tube over which the liquid solution flows in the form of a thin film by gravity. They operate at a relatively lower pressure drop keeping the $\dot{m}_s/\dot{m}_a$ ratio close to almost unity. The unique feature of the falling film tower is that it can provide simultaneous cooling/heating during dehumidification/regeneration, which increases the effectiveness of the absorption/regeneration process as heat liberated during the absorption or required during regeneration is supplied externally, facilitating in achieving process close to isothermal dehumidification/regeneration. Falling film towers had been one of the most preferred designs for closed VAS [47–56].. Horizontal tubes (refrigerant vapor and absorbent solution contacting outside the tubular surface) [49,50,54,56] and vertical plates or tubes (refrigerant vapor and absorbent solution contacting inside the tubular surface) designs [47,48,51–53,55] were used frequently. The pattern of the liquid film falling on a vertical surface is more stable and stretched in comparison to flow over a horizontal tube arrangement, whereas the uniform distribution of liquid in the vertical tubes is more complicated compared to the horizontal tube arrangement. Peng and Howell [50] and Gutkowski and Ryduchowski [51] reported the first numerical and experimental studies on liquid desiccant falling film towers. The researchers explored three types of designs: flow inside the vertical tubes, flow over the vertical plates and horizontal tube. The studies on falling film liquid desiccant towers are summarized in section 2.10.

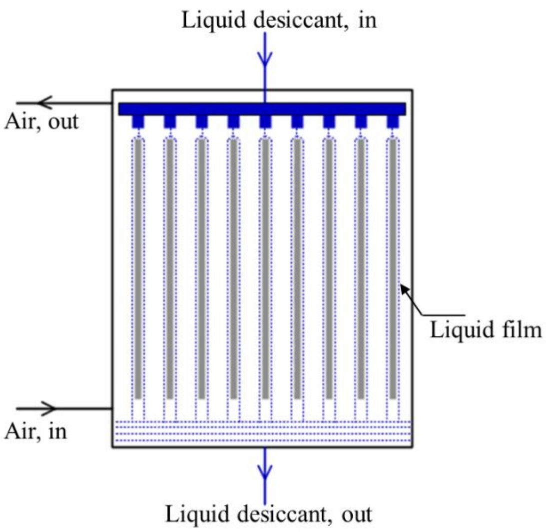

Fig. 2.2 Falling film tower

2.8 Types of liquid desiccant dehumidifiers/regenerators

One of the serious problems associated with the adiabatic dehumidifier is that the solution temperature increases along the bottom part of the dehumidifier due to absorption of latent heat of vaporization (exothermic process) and sensible heat transfer from air. The increasing solution temperature reduces the moisture transfer potential between air and solution, which deteriorates the performance of dehumidifier. Exactly, similar problem exists in the regeneration process. Hence, to retard the increase/decrease of solution temperature in dehumidifier/regenerator internal cooling /heating systems are developed. Generally, water is used as the cooling/heating media in internally cooled/heated system. Several studies highlighted the advantages of using internally cooled/heated dehumidifier/regenerator.

Chung and Wu [57] compared the performance of internally cooled finned-tube dehumidifier with a adiabatic dehumidifier. It was shown that the effectiveness of internally cooled dehumidifier was 1.2 times that of the adiabatic dehumidifier.

Yin and Zhang [58] numerically compared the adiabatic and non-adiabatic falling film regenerator performance. They concluded that the internally heated regenerators offered better regeneration thermal efficiency than adiabatic regenerators. They also concluded that the increasing desiccant flow rate showed weak impact on regeneration rate of internally heated regenerators, whereas for the adiabatic regenerator the impact was significant.

Bansal et al. [59] experimentally compared the performance of adiabatic packed dehumidifier with an internally cooled packing (embedded with a cooling coil) dehumidifier. It was found that the internal cooling intensified the effectiveness of the dehumidifier by 35%.

2.9 Experimental and theoretical studies on packed bed towers

Bichowsky and Kelly [4] found that drying chemical agents such as sulphuric acid, and phosphoric acid are not suitable for AC due to their highly corrosive nature. They successfully demonstrated the use of aqueous LiCl solution for AC in a packed bed tower filled with Raschig rings. During dehumidification experiments, they observed that air humidity reduced from 9.55 g/kg to 7.15 g/kg.

Patnaik et al. [60] examined the performance of a random packed column containing PP spheres in dehumidification and regeneration mode using LiBr desiccant solution. They found that the dehumidification and regeneration rates were substantially influenced by the air inlet temperature, humidity ratio, desiccant flow rate, and desiccant concentration. They also compared the performance of two liquid distributors: a gravity tray distributor and a spray nozzle and claimed that the spray nozzle considerably enhanced the performance of LDS.

Chung et al. [61] experimentally compared the dehumidification ability of two different random packings (PP Flexi rings and Berl saddles) and structure packing (cross corrugated cellulose packing and PVC structure packings). They claimed that all packings were equally efficient under similar working conditions. However, the heat transfer coefficient of the random packing was higher than structure packing.

Fumo and Goswami [62] experimentally investigated the dehumidification and regeneration performance of a random packing

(PP Rauschert Hiflow) using LiCl as a liquid desiccant. The effect of variation of air and desiccant flow rate, air temperature and humidity, and desiccant temperature and concentration were analysed on dehumidification rate and regeneration rate. They claimed that the desiccant concentration had the greatest impact on the dehumidification rate and desiccant temperature on the regeneration rate.

Gandhidasan et al. [63] experimentally studied the gauze type structure packed bed absorber using $CaCl_2$ as desiccant of a 5 TR capacity hybrid LDS. They presented a variation of air humidity ratio and temperature, desiccant temperature, and concentration with time and the effect of these variables on change in air humidity ratio. They concluded that low desiccant temperature significantly improves the dehumidifier performance.

Elasrrag et al. [64] experimentally studied the regeneration ability of a cross-corrugated cellulose structuring packing using TEG desiccant. The packing was arranged in a zig-zag manner to minimize the liquid carryover. The effect of various operating operators was comprehensively analysed on regeneration rate and regeneration effectiveness. They found that higher solution flow rates ($\dot{m}_s$ / $\dot{m}_a \sim 1.1\ to\ 1.6$) did not have significant impact on performance indicators. Furthermore, they suggested that regeneration of the liquid desiccant in a humid climate should be carried out at higher temperatures.

Abu-Arabi et al. [65] carried out a parametric analysis of structured (wood) packed regenerator bed using TEG as a desiccant. They found that higher desiccant temperature and lower desiccant concentration improved the regeneration process. They observed that although the air mass flow rate enhanced the regeneration rate, it decreased the effectiveness of the regeneration process.

Liu et al. [66] estimated the performance of a crossflow desiccant dehumidifier by using Celdeck structured packing with a LiCl desiccant solution. They presented the experimental variation of dehumidification rate and dehumidification effectiveness against operating parameters of air and solution. They concluded that the dehumidification rate increases with an increase in air and desiccant mass flow rate, air inlet humidity ratio and desiccant concentration and decreases with an increase in inlet solution temperature. Similarly, the dehumidification effectiveness increased with an increase in desiccant mass flow rate and temperature and decreased with an increase in air mass flow rate.

Yin et al. [67] experimentally investigated the performance of an evaporative cooling system coupled with a liquid desiccant system using packed bed absorber and regenerator. The impact of air and solution flow rate on the dehumidification and regeneration process were analysed comprehensively. They found that for the dehumidification process, there is an optimal efficiency at the suitable value of inlet air humidity ratio.

Longo and Gasparella [68] conducted experiments with random (Pall rings) and structured packing (MellaPack 250Y) for desiccant regeneration using LiBr solution. The random packing showed a 20%~25% higher regeneration performance than the structured packing; however, the air-side pressure drop in the structured column was 65% ~75% lower than random packings.

Babakhani and Soleymani [69] developed analytical model to study the dehumidification performance of a packed column. To simplify the complex heat and mass transfer processes, they assumed constant value of equilibrium humidity of air (due to high operating flow rate of solution). On validation with previous experimental studies [62], they found that the analytical model predicted that outlet conditions of air and solution within 7% error.

Bassouni [70] investigated the performance of a structured packing crossflow dehumidifier and regenerator using $CaCl_2$ as a liquid desiccant. They concluded that the dehumidification rate and effectiveness of the dehumidifier and regenerator increase with structured packing thickness.

Gao et al. [71] experimentally analysed the influence of air and solution parameters as well as packing size on the performance of packed tower with structured packing (Celdeck). The enthalpy effectiveness and dehumidification were selected to illustrate the heat and mass transfer performance of the dehumidifier. The mass flow rate of air and solution were claimed to have stronger leverage on dehumidification and enthalpy effectiveness. They claimed that the dehumidification performance can be improved without affecting the pressure drop by increasing the thickness, height, or width of the packing simultaneously.

Park et al. [72] used experimental data to develop a simplified model for a packed dehumidifier working with LiCl desiccant solution. They used the response surface methodology (RSM) technique to develop an effectiveness correlation in terms of air and solution operating parameters. The model predicted the experimental values within ±10% error band.

Wang et al. [73] investigated the performance of a counter flow structure packing having a very high surface density (Celdeck 650 m^2/m^3). The performance of the compact packing was compared with the experimental results of Yin et al. [67] (PP gauze type 315 m^2/m^3) and Gao et al. [71] (Celdeck 396 m^2/m^3). They recommended the use of high surface density Celdeck Packing over PP gauze packing in small-scale applications such as residential AC.

Mohamed et al. [74] demonstrated the performance of a dehumidifier using channel gauze packing and LiCl solution as a desiccant. They observed that increase in air flow rate had no significant impact on the change in air humidity ratio and dehumidification effectiveness for $(\dot{m}_s/\dot{m}_a) \geq 2$. They also showed that the pressure drop in the gauze packing was comparatively lower than random packing studies [62,75].

Dong et al. [76] experimentally compared the performance of three different structured packings with different surface densities but for the same volume: corrugated structured, S-shaped PVC, and globular-shaped PP. They found that the dehumidification and enthalpy effectiveness of the corrugated structured packing were 69% and 60% higher than S-shaped PVC packing, and 97% and 87% higher than globular-shaped PP packing due to its high surface density compared to other packings.

Dong et al. [77] investigated the performance of a packed bed LDS to determine the optimum regeneration temperature of LiCl liquid desiccant. They recommended 65ºC as the optimum solution regeneration temperature after balancing the regenerator performance and solution heating energy requirement. They also demonstrated that increasing the $\dot{m}_s/\dot{m}_a$ ratio from 0.5 to 4 did not affect the optimum solution temperature.

Gu and Zhang [78] implemented the concept of rotating packed bed in LDS to improve the heat and mass transfer performance of a counter flow regenerator. Centrifugal force acting on the surface of rotating packing improved wetted area and mixing of desiccant film and air stream. They compared the mass transfer coefficient of the developed regenerator with experimental observations of [79][24] and claimed six times improvement in comparison to the conventional design.

2.10 Experimental and theoretic studies on falling film tower

Jain et al. [80] experimentally and theoretically investigated a falling film copper tubular dehumidifier and a parallel galvanized iron plate regenerator using LiBr solution. They emphasized the importance of the incomplete wetting area to corroborate the differences between the theoretical model and experimental observation.

Ren et al. [81] developed an analytical model to investigate the combined heat and mass transfer performance of counter, and parallel flow internally cooled/heated dehumidification systems. The model was developed by considering the incomplete wetting conditions, non-unity Le number, and linear variation of equilibrium humidity with temperature and concentration. They concluded that the counterflow configuration between air and solution gave the best performance

Yin et al. [82] experimentally studied the dehumidification/regeneration performance of a counter flow S.S. multi- plate-fin heat exchanger using LiCl solution in adiabatic and non-adiabatic mode. They concluded that the dehumidification and regeneration performance could be improved by increasing the air flow rate. The non-adiabatic dehumidifier and regenerator performance were higher than the adiabatic dehumidifier and regenerator.

Liu et al. [83] conducted an extensive numerical analysis to study the effect of different air-solution flow configurations on the performance of the internally cooled dehumidifier. They concluded that desiccant concentration was the most influencing parameter for internally cooled dehumidifiers and the desiccant temperature was the most significant parameter for adiabatic dehumidifiers.

Zhang et al. [84] experimentally investigated the performance of an S.S tube-fin dehumidifier using LiBr solution. They tested the influence of the inlet parameters of the solution and cooling water on the dehumidification rate, dehumidification efficiency, and mass transfer coefficient. In addition, they extended the study for the simulation of an internally heated regenerator for the same geometry, and it was found that regeneration at low temperatures could be achieved through internal heating.

Qi et al. [85] experimentally investigated the impact of surface temperature on the wetted characteristic of S.S plate falling film regenerator and developed a theoretical model to calculate the wetted area. They concluded that enhancement of wetted area due to an increase in plate surface temperature corresponded to low solution flow rate conditions. The proposed model predicted the actual wetted area with an average error of 10.8%.

Luo et al. [86] experimentally analysed the dehumidification ability of internally cooled S.S plate dehumidifiers in different climatic conditions of Hong Kong. They recommended low inlet solution temperature and solution concentration range of 36% - 39% for best dehumidification effectiveness. Further, they observed water condensation on the non-wetted part of the plate surface at very low temperature of the cooling water.

Dong et al. [87] developed a theoretical heat and mass transfer model to examine the influence of contact angle on the performance of S.S plate dehumidifiers. The incomplete wetting and variable falling film thickness information were included in the model. They found that by reducing the contact angles (from 85º to 5º), the wetting area was enhanced, which improved the mass transfer performance of the system.

Dong et al. [88] examined the performance of a TiO_2 coated plate dehumidifier. They found that the dehumidification efficiency of the coated surface was 63% higher than the conventional surface due to a reduction in the contact angle of liquid desiccant solution (from 84.6º to 8.8º).

Wen et al. [89] experimentally compared the performance of plain aluminium and anodized aluminium plate dehumidifiers using LiCl solution as the desiccant. They concluded that the dehumidification effectiveness of an anodized aluminium plate was found 36.7% superior to plain aluminium due to improvement in the wetted area.

Qi et al. [90] developed a theoretical mass transfer coefficient correlation by considering different aspects of liquid desiccant-air interaction, such as flow characteristics, Marangoni effect, and partial wetting conditions. The liquid film Reynolds number and wetting factor were found to have the most significant impact on mass transfer coefficient than airflow rate and solution temperature. The developed correlation showed good agreement with the experimental data, within an error range of 20 - 30%.

Cheng et al. [91] designed an S.S fin-tube type heat exchanger to conduct dehumidification experiments with LiCl as the liquid desiccant. The process air and desiccant interacted inside the tube, and the outside surfaces of fins and tubes were evaporatively cooled. The performance of the evaporatively cooled dehumidifier was found 1.25 times higher than the adiabatic operated dehumidifier.

Wen and Lu [92] did experiments and modelling to study the performance of an internally cooled S.S plate dehumidifier. The effect of falling film shrinkage and water condensation on the non-wetted part of the pate surface were considered in the model. They reported that the error between the calculated results and experimental values was 4.5%.

Wen et al. [93] used CFD tool to extensively study a metallic plate dehumidifier's heat and mass transfer process by applying different surface modification methods such as super hydrophilic coatings, wavy surface, and coated plate with wavy-fin structure. They found that the surface modification method intensified the performance of the plate dehumidifier from 7.8% to 47.1%, and the coated plate with a waved fin provided the maximum enhancement.

Lu et al. [94] numerically studied the nature of liquid film on metallic smooth and micro-baffled plate dehumidifiers and compared their performance characteristics. Five different geometries (with varying baffles height/spacing) of micro-baffled dehumidifiers were considered in their study. It was reported that the maximum improvement in dehumidification performance offered by micro-baffles plate was 25.1%.

It is evident that most of the studies on the falling film towers have been reported on metallic surfaces. However, despite possessing favourable thermophysical characteristics for comfort AC, most inorganic desiccant solutions cause severe corrosion to the metallic surfaces. The corrosion problem has been identified as the primary limiting concern for developing LDS. Researchers proposed remedial action such as surface treatment, solution modification, or alternate desiccants to mitigate the corrosion problem.

2.11 Remedial actions against surface corrosion

2.11.1 Surface treatment

Lowenstein [95] used commercially available plastic-coated aluminium plates desiccant conditioner to prevent the corrosion LiCl desiccant. They discovered that the plastic coating did not adequately protect the plates, and that the desiccant caused severe corrosion to several components of LDS.

Luo et al. [96] experimentally investigated the internally cooled fin-tube dehumidifier performance. To enhance the corrosion resistance of the S.S working surface, some covert antiseptic was adhered to the fins surface by electroplating surface treatment technique. The newly fabricated surface demonstrated good anti-corrosion performance compared to normal S.S 304 and copper surface. They observed that the developed surface sustained corrosion even after 48 hours in concentrated LiCl solution.

Turgut and Coban [97] used epoxy coating on a S.S plate-fin dehumidifier to alleviate the corrosive effect of LiCl desiccant solution. They observed that initially, the coated plate was able to withstand the corrosion effect of LiCl. However, with the progress of time, the dehumidification performance deteriorated due to the corrosion of the solid surface.

Wen et al. [98] experimentally verified that an anodized aluminium plate showed good resistance to corrosion as compared an ordinary aluminium plate. They concluded that in addition to low corrosiveness, the anodized plate offered 23.7% and 24.0% improvement in regeneration rate and regeneration effectiveness rate due to higher wetting.

Jaradet [99] applied a powder coating with a layer thickness of 0.24 mm on the external surface of the vertical copper tube regenerator. The powder coating comprised polyester, polyurethane, polyester-epoxy, and acrylics. They recommended continuous monitoring of the coated surface at higher temperatures.

2.11.2 Solution modification/ alternate desiccants

Wen et al. [100,101] proposed mixing hydroxyethyl urea to minimize the corrosion of S.S surfaces of the dehumidifier and the regenerator using LiCl desiccant solution. The mixed solution's corrosion rate was lower than the normal LiCl. Additionally, the hybrid solution enhanced the average dehumidification and regeneration effectiveness by 15.3 % and 14.1%, respectively, due to an increase in the wetted area of the solid surface. Nevertheless, inhalation of urea causes respiratory problems and several other health hazards. Researchers even explored using other alternate desiccants to combat the corrosion problem. Low corrosive desiccant solutions such as ionic liquids and potassium formate were investigated as replacements for commonly used conventional desiccants. The studies on ionic liquids are already covered in section 2.3.

2.12 Studies on plastic surface

At the end of the 20th century, researchers started putting efforts in search of new avenues for replacing corrosion prone metallic solid surfaces in falling film dehumidifier/regenerators. Plastic as an alternative of metallic surface was the first obvious choice. As they do not react with inorganic desiccant solution thus extremely useful in eliminating corrosion problem of solid surfaces, plastics are inexpensive, light in weight and are easy to fabricate. The progress in research related to the used of plastic surface is summarized below

Saman and Alizadeh [102] carried experimental study on a cross flow plate HX made from thin polyethylene plastic (0.2 mm thick). One side of plate was dedicated to dehumidification and other side for evaporative cooling. The HX module was tested for three different conditions: evaporative cooling, desiccant dehumidification, and combined dehumidification and evaporative cooling. The primary air mass flow rate (process air for dehumidification) and HX angle showed significant impact on dehumidification effectiveness. At HX angle of 45º and mass flow rate of 0.3 kg/s the HX module yielded maximum dehumidification effectiveness of 75%. The mathematical model developed earlier by Saman and Alizadeh [103] showed good agreement with experimental results.

Mesquita [104] developed a two-dimensional mathematical model for counter flow internally cooled plate dehumidifier made from PP plastic by applying three different approaches: simplified model based on heat and mass transfer correlations, constant falling film thickness model, and variable falling film thickness models. They found that simplified model and constant film thickness model over precited experimental values especially at low flow rate condition, while variable thickness model closely validated the experimental results.

Chen et al. [105] fabricated and compared the thermal performance a three plastic PP fin-tube heat exchanger having different thermal conductivity. Two modified PP HX having high values of thermal conductivity ($k_{PP-\alpha}$ = 2.3 and $k_{PP-\beta}$ = 16.5 W/mK) and one ordinary PP HX (k = 0.1 - 0.22 W/mK). The effect of material thermal conductivity on HX performance was analysed in detail. They concluded that the thermally conductive plastic dehumidifier can offer an equivalent performance to the metallic dehumidifier, if threshold influence of thermal conductivity on overall thermal conductance is considered.

Gommed et al. [106] experimentally compared the performance of internally cooled horizontal tube titanium tubes and HDPE plastic dehumidifiers of different dimensions and surface area. The titanium dehumidifier was designed with 258 tubes with a specific area of 75 m^2/m^3 while HDPE includes 800 tubes and has a specific area of 116 m^2/m^3. They concluded that low wetting of the plastic was primarily responsible for poor heat and mass transfer performance of plastic dehumidifiers.

Mun et al. [107] experimentally investigated the regeneration of LiCl desiccant solution on multi-plates regenerator made from ABS. The surface of the plates was vertically grooved, and a hydrophilic coating was applied. They found that the regeneration rate is significantly influenced by the inlet solution concentration and air relative humidity; similarly, air velocity was found most influencing parameter for regeneration effectiveness.

Park et al. [108] tested a cross-flow dehumidifier fabricated from corrugated polyethylene plastic. The dehumidifier was designed for dehumidification on one side (process air) and evaporative cooling (working air) on another side. They observed the maximum dehumidifier performance corresponding to working air to process air ratio of 0.5. Further, a detailed numerical simulation analysis was carried on the evaporatively cooled plate dehumidifier which agreed with experimental results within ±20% error bound.

Dong et al. [109] experimentally compared the performance of titanium, S.S and PTFE plate dehumidifier. The best performance was obtained for the titanium plate dehumidifier, they further claimed that an energy saving of 9.6% could be achieved for LDS with titanium plate compared to plastic one. The poor performance of the plastic surface was primarily due its low wettability.

2.13 Performance intensification

The partial/incomplete wetting of the solid surfaces have been discussed in previous studies [85,87,92]. The wettability of the liquid desiccant solution on the working surface determines the area available for liquid-air interaction, and thus significantly effects the heat and mass transfer performance during the dehumidification/regeneration process. At partial/incomplete wetting conditions falling film contracts gradually in the direction of flow, resulting in the formation of dry patches on the working surface. Consequently, the wetted area decreases, resulting in decrease in heat and mass transfer performance. The surface modification and solution modification techniques have been explored by researchers to improve the wettability and thus the overall performance of the system. The surface modification indicates altering the texture of the surface by physical or chemical method. The solution modification highlights the performance improvement by adding additives (surfactants/nanoparticles/ethanol) in the solution. The research studies on these modification techniques are summarized below.

2.13.1 Surface modification

Mortazavi et al.[110] designed a vertical plate absorber installed with fin structure, as shown in Fig. 2.3. To improve the wetness characteristic of LiBr solution, the fin surfaces were sandblasted with fine aluminium oxide particles in order to make them hydrophilic. Preliminary wetness experiments were conducted using dye to decide the fins spacing and size. They claimed that new absorber offered around two times higher performance in comparison to conventional absorber.

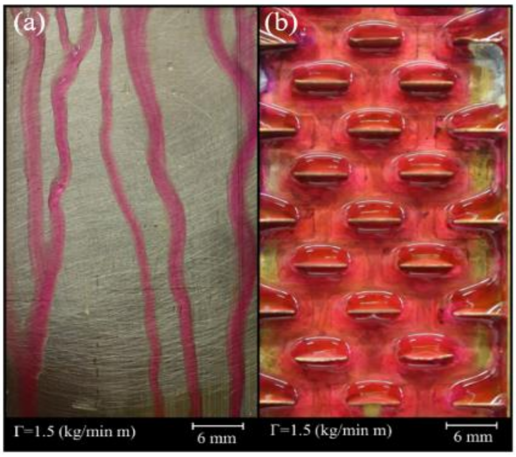

Fig. 2.3 a) Flat surface b) Pattern surface [110]

Lee et al. [111] fabricated and did experimental and numerical analysis on a single plate type dehumidifier made from vertical grooved and hydrophilic coated ABS plastic. Firstly, vertical parallel grooves were generated on the surface and then a double layer hydrophilic coating was applied to elevate the wettability of the plate. They claimed that the air velocity has the most significant impact on the dehumidification rate.

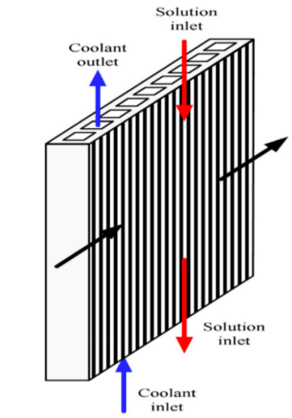

Fig. 2.4 Hydrophilic grooved surface [111]

Michel et al. [55] experimentally and numerically investigated the absorption performance of vertical grooved S.S plate using LiBr solution. The optimized size of the grooves was selected based on experimental trials by applying the concept of capillary length $\left(L_C = \sqrt{\sigma/\rho g}\right)$. Various pertinent parameters of desiccant solution were investigated in adiabatic and non-adiabatic mode, and they reported that modified surface offered maximum absorption rate of 0.007 kg/sm^2.

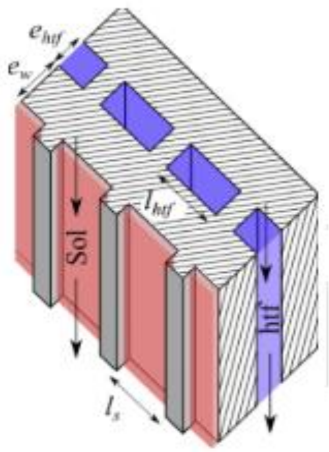

Fig. 2.5 Vertical grooved absorber [55]

Prieto et al. [112] modified the surface of internally cooled PP horizontal tube dehumidifier by a plasma treatment. A comparative experimental assessment was carried out between plasma treated PP dehumidifier and Plain PP dehumidifier. It was reported that 54% and 20% improvement could be obtained in overall heat transfer coefficient (between water and solution) and dehumidification rate through plasma treatment process.

Fig. 2.6 Plasma treated PP dehumidifier[112]

Zhi et al. [113] investigated the dehumidification performance of Plain PTFE plate and Modified PTFE. The Modified surface was prepared initially by etching process to generate a micro-rod structure and subsequently by applying a super-hydrophilic SiO_2 coating over it. The dehumidification performance of Modified PTFE plate was found 30 - 80% higher than the Plain PTFE Plate.

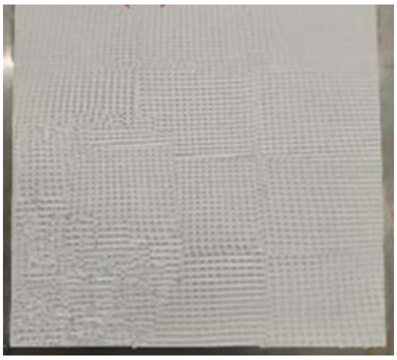

Fig. 2.7 Superhydrophilic PTFE Plate [113]

Jaradet et al. [114] conducted experiments to analyse the performance of an adiabatic polycarbonate parallel plate dehumidifier. They suggested the idea of attaching textile sheets on the plate surface to ensure complete wetting of the surface at low flow rate conditions.

Yi et al. [115] conducted research to investigate the wetting characterise and heat and mass transfer performance of a vertical chevron corrugation plate absorber. They found that the chevron corrugation intensified the overall heat transfer coefficient of waterside by 33.8% and solution side by 249%.

Fig. 2.8 Chevron corrugated plate [115]**.**

Ahmadi et al. [116] extensively studied the capillary and wickability effects of liquid desiccant on a textured polycarbonate plate dehumidifier. Mechanical surface modification was applied to create an optimized texture on the Plain surface: drop-shaped and partitioned offset strip-fin. The textured surface was then sandblasted with aluminium oxide abrasives to improve wettability and desiccant flow. They found that the performance of optimized textured surface was 1.28 time superior to Plain surface.

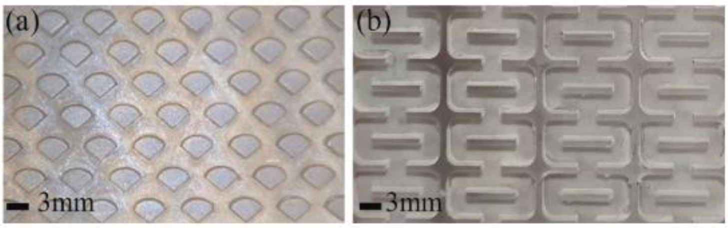

Fig. 2.9 Textured surfaces a) Drop-shaped b) Offset strip-fin [116]

2.13.2 Solution modification

Zheng and Worek [117] experimentally investigated the regeneration heat and mass transfer characterise of LiCl desiccant by mixing surfactants sodium lauryl sulphate (SLS) and polymer polyacrylamide. They concluded that the addition of small amount of SLS was able to improve the heat and mass transfer rates due to decrease in the surface tension, while no improvement was observed for the polymer polyacrylamide surfactant.

Ali and Vafai [118] numerically studied the dehumidification performance of parallel plate by adding Cu-ultrafine particles to $CaCl_2$ desiccant. They concluded that the addition of small number of Cu-particles had negligible influence on the dehumidification performance.

Abu-Hamdeh and Almitani [119] experimentally examined the feasibility of using ZnO, Fe_3O_4, and Al_2O_3 as nanofluid for performance improvement of LDS. They reported an enhancement in the heat transfer coefficient of 5.50–9.01%, 6.20–12.30%, and 7.20–14.40% for ZnO, Fe_3O_4, and Al_2O_3 nanofluids, respectively.

Cihan et al. [120] experimentally investigated the dehumidification and regeneration processes of polycarbonate plastic packed column using LiCl desiccant with surfactant Polyether modified siloxane (BYK349). They observed that the although the wetted area increased with addition of surfactant, the mass transfer performance deteriorated due to the foaming problem.

Wen et al. [121] mixed odourless, non-volatile PVP-K30 surfactant with LiCl desiccant solution to intensify the dehumidification ability of an internally cooled S.S plate dehumidifier. They achieved 22.7% and 19.9% enhancement in the dehumidification rate and dehumidification effectiveness primarily due to increase in wetted area.

Wen et al. [122] studied the influence modified solution on the performance of S.S plate dehumidifier. The modified solution was prepared by adding multi-walled carbon nanotubes (MWNTs) into LiCl solution. They found that modified solution could enhance the dehumidification rate by 25.9% due to reduction in contact angle.

Lun et al. [123] investigated a distinct approach to dehumidify the air by mixing cooling liquid (ethanol) with LiCl desiccant. Comparative analysis indicated that for the same operating conditions, the relative increment of 40% in dehumidification performance could be gained by the proposed system. However, inhalation of ethanol is toxic to human health.

2.14 Heat and mass transfer simulation/numerical modelling

Apart from experimental analysis on liquid desiccant dehumidifier and regenerators, lot of efforts have also been made on developing numerical/simulation models for the dehumidifier/regenerator to study the study the behaviour of dehumidifier/regenerator and the combined system in wide range of operating conditions. According to the available open literature four types of modelling approaches are reported: finite difference modelling, effectiveness-NTU (ε-NTU) modelling, empirical correlation based on experimental/numerical data and ANN modelling.

2.14.1 Finite difference model

Factor and Grossman [8] proposed a theoretical model to predict the performance of a counter flow packed bed absorber. The absorber was divided into 'n' number of small control volumes as shown in Fig. 2.10. To simply the complex heat and mass transfer process several assumptions were made. They are as follows

1. The heat and mass transfer process are adiabatic
2. The air and desiccant flow are assumed as slug flows
3. The change in the air temperature and humidity occurs in the direction of flow
4. The packing is completely wetted (100% wetting)
5. The resistance to heat transfer in liquid side is negligible
6. The interface temperature is equal to bulk liquid temperature

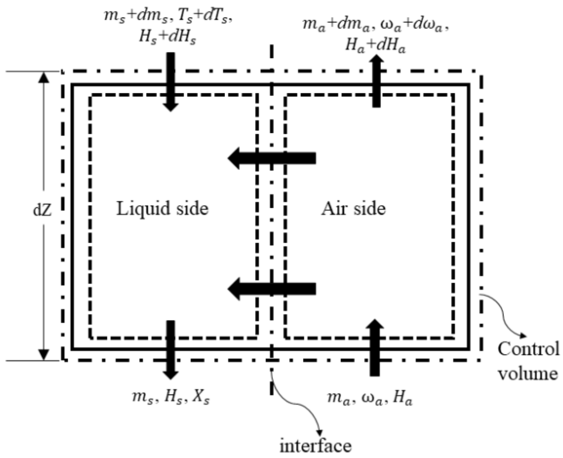

Fig. 2.10 Heat and mass transfer modelling

Based on the assumptions following governing equation were derived

Mass balance of control volume

$$d\dot{m}_s = \dot{m}_a d\omega_a \qquad (2.1)$$

According to the mass and heat transfer rates across the interface between air and solution, the air humidity ratio change was

$$\frac{d\omega}{dz} = \frac{h'_m M_v A}{\dot{m}_a} ln\left(\frac{1-\frac{p_s}{p_t}}{1-\frac{p_a}{p_t}}\right), \qquad (2.2)$$

Similarly, the change in air temperature according to sensible heat from air to solution side and energy balance from air side was

$$\frac{dT_a}{dz} = \frac{h'_{t,a}A(T_a - T_s)}{\dot{m}_a C_{p,a}} \qquad (2.3)$$

$$h'_{t,a}A = \frac{-\dot{m}_a C_{p,v}\frac{d\omega}{dz}}{1-exp\left[\frac{\dot{m}_a C_{p,v}\frac{d\omega}{dz}}{h_{t,a}A}\right]} \qquad (2.4)$$

Where $h_{t,a}$ and $h'_{t,a}A$ are the heat transfer coefficient of air side due to sensible heat transfer and corrected heat transfer coefficient for coupled heat and mass transfer process. The above heat and mass transfer governing equation cannot be solved analytically. The most basic approach is numerical differentiation/integration along the length of the tower.

Khan and Ball [124] developed a simplified form of the above equation called NTU-Le model to solve the coupled heat and mass transfer equations. They assumed that the overall heat and mass transfer process air side controlled. Hence, the mass transfer and heat transfer rate across the air film form bulk air to interface was equal to the change in air humidity ratio and temperature as shown below

$$\frac{d\omega_a}{dz} = \frac{NTU}{L}\left(\omega_a - \omega_{eqls}\right) \quad (2.5)$$

$$\frac{dT_a}{dz} = \frac{NTU.Le}{L}\left(T_a - T_s\right) \quad (2.6)$$

In the above equation NTU and Le are defined as

$$NTU = \frac{h_m A}{\dot{m}_a} \quad (2.7)$$

$$Le = \frac{h_t}{h_m C_{p,m}} \quad (2.8)$$

2.14.2 Effectiveness NTU ($\varepsilon - \boldsymbol{NTU}$) model

Stevens [125] introduced the concept of effectiveness-NTU model for liquid desiccant dehumidifiers/regenerators following the effectiveness model of cooling towers. In addition to finite difference assumption, two more assumptions were considered. The first was the linear variation of saturation enthalpy with temperature, and the second was the omission of the water loss term from the solution energy balance. In addition, the effective heat and mass transfer process was assumed. The developed equations are analogous to heat exchanger equations. They are as follows

effectiveness of the dehumidifier

$$\varepsilon_Y = \frac{1 - e^{-NTU(1-m^*)}}{1 - m^* e^{-NTU(1-m^*)}} \quad (2.9)$$

NTU is calculated from Eq. (2.7)

Outlet air enthalpy

$$h_{a,out} = h_{a,in} + \varepsilon_Y\left(h_{T_s,sat} - h_{a,in}\right) \quad (2.10)$$

effective saturation enthalpy

$$h_{T_s,sat,eff} = h_{a,in} + \frac{(h_{a,out}-h_{a,in})}{1-e^{-NTU}} \quad (2.11)$$

Outlet air humidity ratio

$$\omega_{a,out} = \omega_{T_s,sat,eff} + (\omega_{a,in} - \omega_{T_s,sat,eff})e^{-NTU} \quad (2.12)$$

2.14.3 Empirical correlations

Finite difference method has been widely used to study the heat and mass transfer characteristic of dehumidifiers and regenerator due to its high prediction accuracy. The finite difference and ε-NTU modelling require numerical differential/integration techniques and iterative approach to investigate the heat and mass transfer performance of dehumidifier/regenerator. Hence, for quick prediction of outlet conditions of air and solution both these methods are not suitable. Many researchers developed empirical correlation based one experimental/numerical data to estimate the outlet conditions of air and solution. The summary of the empirical correlation studies is discussed as follows.

2.14.3.1 Heat and mass transfer coefficient correlations

2.14.3.1.1 Packed bed dehumidifier and regenerator

Chung et al. [61] compared the performance of random and structure packing dehumidifier using TEG as desiccant. They calculated the heat and mass transfer coefficient following Eqs. (2.13) and (2.14). Eq. (2.13) was solved numerically by applying Simpson's 1/3 numerical integration technique and Eq. (2) by applying logarithm mean temperature difference. Heat and mass transfer correlations for random and structure packing were proposed according to the experimental results (Eqs. 2.15-2.18).

$$h'_m = \left(\frac{\dot{m}_a}{aZ}\right)\int_{y_{A,in}}^{y_{A,out}} \frac{(1-y_A)*M}{(1-y_A)(y_A-y_A^*)}\, dy_A \quad (2.13)$$

$$h_t = \frac{G\prime(C_{p,a}+Y_A C_{p,w})}{aZ} ln\frac{T_{a,in}-T_i}{T_{a,in}-T_i} \quad (2.14)$$

$$Nu_{a(random\ packings)} = 8.76 \times 10^{-6}(1 - X_s)^{1.23} \left(\frac{m_s}{m_a}\right)^{0.47} Re_a^{1.12}\, Pr_a{}^{0.333} \tag{2.15}$$

$$Nu_{a(structure\ packings)} = 1.76 \times 10^{-6}(1 - X_s)^{0.07} \left(\frac{m_s}{m_a}\right)^{0.49} Re_a^{1.52}\, Pr_a{}^{0.333} \tag{2.16}$$

$$Sh_{a\ (random\ packings)} = 6.33 \times 10^{-5}(1 - X_s)^{-0.09} \left(\frac{m_s}{m_a}\right)^{0.27} Re_a^{1.38}\, Sc_a{}^{0.333} \tag{2.17}$$

$$Sh_{a(structure\ packings)} = 9.03 \times 10^{-6}(1 - X_s)^{-0.05} \left(\frac{m_s}{m_a}\right)^{0.26} Re_a^{1.34}\, Sc_a{}^{0.333} \tag{2.18}$$

Elsarrag et al. [64] experimentally studied the mass transfer performance of a packed bed dehumidifier using TEG desiccant . Utilising their own experimental data; they estimated mass transfer coefficient following the method used by Chung [61] and proposed Sherwood number correlations for two distinct liquid loading range: $0.88 < \frac{m_s}{m_a} < 2$ (Eq. 2.19) and $2 < \frac{m_s}{m_a} < 11$ (Eq. 2.20). The correlation predicted the experimental data within ±15 error band.

$$Sh_a = 6.18 \times 10^{-6} \left(1 - \frac{P_s}{P_w}\right)^{-0.77} \left(\frac{m_s}{m_a}\right)^{0.55} Re_a^{1.3}\, S\, c_a{}^{0.333} \qquad 0.88 < \frac{m_s}{m_a} < 2 \tag{2.19}$$

$$Sh_a = 0.52 \left(1 - \frac{P_s}{P_w}\right)^{-0.48} \left(\frac{m_s}{m_a}\right)^{0.55} Re_a^{0.2}\, S\, c_a{}^{0.333} \qquad 2 < \frac{m_s}{m_a} < 11 \tag{2.20}$$

Liu et al. [126] developed theoretical NTU-Le model to study the heat and mass transfer characteristic of cross flow packed tower using LiBr desiccant solution.. A mass transfer correlation similar to the form of Chung et al [61] was proposed for dehumidifier and regenerator with complete surface wetting assumptions. They found that developed correlation predicted the moisture effectiveness and enthalpy effectiveness with an average error of 8.5% and 7.9%, respectively for dehumidification process and 6.9% and 5.8% respectively, for regeneration process.

$$Sh_{a,dehumidifier} = 1.11 \text{ X } 10^{-3}(1 - X_s)^{1.913} \left(\frac{m_s}{m_a}\right)^{0.396} Re_a^{1.363}\, S\, c_a{}^{0.333}$$

(2.21)

$$Sh_{a,regenerator} = 5.59 \text{ X } 10^{-6}(1 - X_s)^{-5.353} \left(\frac{m_s}{m_a}\right)^{0.617} Re_a^{1.546}\, S\, c_a{}^{0.333}$$

(2.22)

Zhang et al. [79] evaluated the mass transfer coefficient of a structure packing dehumidifier and regenerator from experimental data following Eq. (2.23) and proposed an empirical model for the same. Apart from air side Re_a and Sc_a, the developed Sh number correlations also assumed to be influenced by Re_s and Sc_s, thus they included the effect of heat and mass transfer resistance of the solution side also. They reported that the difference between the experimental and predicted values were within ±20% error band.

$$h_m = \frac{\dot{m}_a}{A} \frac{(\omega_{a,in} - \omega_{a,out})}{(\omega_{a,avg} - \omega_{eqls,in})} \text{, where} \tag{2.23}$$

$$\omega_{a,avg} = \frac{\omega_{a,in} + \omega_{a,out}}{2}$$

$$Sh_{a,dehumidifier} = 0.0038\, Re_a^{0.52}\, S\, c_a{}^{0.33}\, Re_s^{0.28}\, S\, c_s{}^{0.33} \tag{2.24}$$

$$Sh_{a,regenerator} = 0.0038\, Re_a^{0.39}\, S\, c_a{}^{0.33}\, Re_s^{0.39}\, S\, c_s{}^{0.33} \tag{2.25}$$

The effectiveness-NTU model was used by Langroudi et al. [127] to investigate the heat and mass transfer performance of a packed dehumidifier. The random glass beads and LiBr solution were the packing and desiccant material. Based on experimental results, they build Nu and Sh correlation. They found that the average error between the predicted and experimental values of Nu and Sh number were 5.27%, and 2.14%, respectively.

$$Nu_a = 0.173(1 - X_s)^{-0.091} \left(\frac{m_s}{m_a}\right)^{0.081} Re_a^{0.617}\, Pr_a{}^{0.333} \tag{2.26}$$

$$Sh_a = 0.158(1 - X_s)^{1.102} \left(\frac{m_s}{m_a}\right)^{0.115} Re_a^{0.689}\, S\, c_a{}^{0.333} \tag{2.27}$$

Chen et al. [128] developed a modified NTU-Le model to evaluate the heat and mass transfer coefficient of packed bed dehumidifier working at low temperature (20ºC) and low concentration (33%). They proposed a heat and mass transfer correlation to predict the experimental values.

$$Nu_a = 4.7756 \times 10^{-5} \left(\frac{T_s}{T_a}\right)^{0.3846} \left(1 - \frac{\omega_{eqls}}{\omega_a}\right)^{0.8198} \left(\frac{m_s}{m_a}\right)^{-1.001} Re_a^{1.7936}\, {Pr_a}^{0.3333} \tag{2.28}$$

$$Sh_a = 7.3492 \times 10^{-7} \left(\frac{T_s}{T_a}\right)^{0.2376} \left(1 - \frac{\omega_{eqls}}{\omega_a}\right)^{-0.8956} \left(\frac{m_s}{m_a}\right)^{0.5235} Re_a^{2.1576}\, S\,{c_a}^{0.3333} \tag{2.29}$$

Varela et al. [129] proposed a heat and mass transfer correlation for packed bed dehumidifier and regenerator. The heat and mass transfer coefficient were derived from the experimental data by applying FDM. Using the proposed correlation, they predicted the outlet conditions of air (temperature and humidity) and found that the correlation predicted the experimental values with good accuracy in comparison to previous correlation of Zhang et al. [79].

$$Nu_{a,dehumidifier} = 0.0295 Re_a^{0.7117} Re_s^{01339} \tag{2.30}$$

$$Sh_{a,dehumidifier} = 0.0307 Re_a^{0.5519} Re_s^{0.2833} \tag{2.31}$$

$$Nu_{a,regenerator} = 0.0335 Re_a^{0.7731} Re_s^{00809} \tag{2.32}$$

$$Sh_{a,regenerator} = 0.0109 Re_a^{0.4642} Re_s^{0.4818} \tag{2.33}$$

Su et al. [130] developed a FDM mathematical model to predict the heat and mass transfer characteristic of a frost-free hybrid LDS in winter conditions (outside humidity below 5 g/kg). They concluded that the mass transfer coefficient is influenced by mass flow rate of air and solution and desiccant concentration, whereas the heat transfer coefficient is influenced by mass flow rate of solution.

$$Nu_a = 1.2971 {m_s}^{-0.5122} m_a^{2.3414} \tag{2.34}$$

$$Sh_a = 2.2596 {X_s}^{-0.5818} m_s^{-0.31952} m_a^{1.1019} \tag{2.35}$$

Recently, Lim et al. [131] proposed an empirical correlation for packed regenerator utilised of humidification purpose in dry outside conditions.

The NTU-Le model was applied on the experimental data to derive the heat and mass transfer coefficient by assuming unity Le number.

$$Sh_a = 5.12 \text{ x } 10^{-4}(1 - X_s)^{1.51} \left(\frac{m_s}{m_a}\right)^{0.91} Re_a^{1.363}\, S\, c_a{}^{0.333} \tag{2.36}$$

2.14.3.1.2 Falling film dehumidifier and regenerator

Yin et al. [132] developed empirical model to predict the air side Sh number of an internally cooled/heated plate dehumidifier and regenerator using experimental observations. The mass transfer coefficient of vertical S.S plate surface was calculated from Eq. (2.37). LiCl solution was used as desiccant. They reported that the deviation between experimental and predicted values was less than 5%.

$$h_m = \frac{\dot{m}_a}{A} \frac{(\omega_{a,in} - \omega_{a,out})}{(\omega_{a,in} - \omega_{eqls,in})} \tag{2.37}$$

$$Sh_{a,dehumidifier} = 0.345 T_s^{-2.991}\, Re_a{}^{1.56}\, Sc_a{}^{0.33} \tag{2.38}$$

$$Sh_{a,regenerator} = 2.582 \text{ x } 10^5 T_s^{-3.36}\, Re_a{}^{1.55}\, Sc_a{}^{0.33} \tag{2.39}$$

Gao et al. [133] experimentally analysed the mass transfer performance of single S.S plate dehumidifier by providing internal cooling at three different segments (A,B and C) of the working surface. They developed a mass transfer prediction model for both adiabatic and internally cooled system. The mass transfer coefficient was determined using Eq. (2.37) at compete surface wetting assumptions.

$$Sh_{a,adiabtic} = 2.5 \text{ x } 10^{-4}(1 - X_s)^{-1.31} \left(\frac{m_s}{m_a}\right)^{0.231} Re_a^{2.27}\, S\, c_a{}^{0.333} \tag{2.40}$$

$$Sh_{a,segment\ A} = 2.76 \text{ x } 10^{-4}(1 - X_s)^{-1.22} \left(\frac{m_s}{m_a}\right)^{0.253} Re_a^{2.55}\, S\, c_a{}^{0.333} \tag{2.41}$$

$$Sh_{a,segment\ B} = 3.04 \text{ x } 10^{-4}(1 - X_s)^{-1.33} \left(\frac{m_s}{m_a}\right)^{0.243} Re_a^{2.32}\, S\, c_a{}^{0.333} \tag{2.42}$$

$$Sh_{a,segment\ C} = 3.22 \text{ x } 10^{-4}(1 - X_s)^{-1.12} \left(\frac{m_s}{m_a}\right)^{0.273} Re_a^{2.35}\, S\, c_a{}^{0.333} \tag{2.43}$$

Lee et al. [134] did modelling and experiments to analyse the coupled heat and mass transfer process of a ABS plastic plate dehumidifier. They proposed solution side Nu and Sh correlations and found that the modelling overpredicted the experimental results due to unity Lewis number (Le) and complete surface wetting assumptions.

$$Nu_s = 5.7\text{x}10^{-6}\, Re_a^{0.71}\, {Re_c}^{0.68}\, Re_s^{0.179}\, {Pr_s}^{0.051} \quad (2.44)$$

$$Sh_s = 4\text{x}10^{-6}\, Re_a^{0.71}\, {Re_c}^{0.403}\, Re_s^{0.514}\, {Sc_s}^{0.051} \quad (2.45)$$

Kim et al. [135] experimentally studied the regeneration process of LiCl on internally heated vertical ABS plastic plates having vertical grooves. They proposed a Nu and Sh empirical correlation for the regeneration process using numerical data and reported that the Nu correlation precited the heat transfer coefficient above 60 W/m^{2}K within ±20% error range. However, it over predicted the heat transfer coefficient in the range less than 5 W/ m^{2}K.

$$Nu_a = 0.04607\ {Re_a}^{0.6606}\, {Re_s}^{0.3217} {Pr_a}^{0.4} \quad (2.46)$$

$$Sh_a = 0.7351\ {Re_a}^{0.6716}\, {Re_s}^{0.5966} {Sc_a}^{0.4} \quad (2.47)$$

Wen et al. [28,136] compared the dehumidification and regeneration performance of LiCl desiccant with KCOOH desiccant on single S.S plate surface and reported the mass transfer coefficient correlation for dehumidification and regeneration mode. In the experiments, the operating mass flow rate of the solution was well above 100% wetting of the plate surface and mass transfer coefficient was calculated according to Eq. (2.37).

$$Sh_{a,dehumidifier} = 3385\, Re_a^{0.103}\, \omega_{a,in}^{0.853} \left(\omega_{a,in} - \omega_{eq,in}\right)^{0.239} \quad (2.48)$$

$$Sh_{a,regenerator} = 0.00355\, Re_a^{0.767}\, \omega_{a,in}^{-0.733} \left(\omega_{eq,in} - \omega_{a,in}\right)^{-0.14} \quad (2.49)$$

Peng et al. [137] compared the performance of LiCl and $CaCl_2$ on vertical S.S. tube dehumidifier. They determined the transfer coefficients following the logarithmic mean temperature and humidity difference approach (Eqs. 2.50-2.51) and proposed a transfer coefficients correlation for both the desiccants assuming complete surface wetting conditions (Eqs. 2.52-2.55)

$$h_m = \frac{\dot{m}_a}{A} \frac{(\omega_{a,in} - \omega_{a,out})}{\Delta\omega_{LMWD}} \quad (2.50)$$

$$h_t = \frac{\dot{m}_a}{A} \frac{(T_{a,in} - T_{a,out})}{\Delta T_{LMTD}} \quad (2.51)$$

$$Nu_{a(LiCl)} = 7.05\ x\ 10^{-2}(1 - X_s)^{0.648} \left(\frac{T_a}{T_s}\right)^{-3.288} \left(\frac{m_s}{m_a}\right)^{-0.155} Re_a^{0.725}\ Pr_a^{\ 0.33}\ Re_{a,ev}^{0.0221} \tag{2.52}$$

$$Nu_{a(CaCl_2)} = 0.176(1 - X_s)^{0.762} \left(\frac{T_a}{T_s}\right)^{-3.611} \left(\frac{m_s}{m_a}\right)^{-0.198} Re_a^{0.626}\ Pr_a^{\ 0.33} Re_{a,ev}^{0.0196} \tag{2.53}$$

$$Sh_{a(LiCl)} = 1.16 \times 10^{-3}(1 - X_s)^{0.557} \left(\frac{T_a}{T_s}\right)^{-1.199} \left(\frac{m_s}{m_a}\right)^{0.355} Re_a^{1.196}\ S\,c_a^{\ 0.33} Re_{a,ev}^{0.0232} \tag{2.54}$$

$$Sh_{a(Cacl_2)} = 3.61 \times 10^{-4}(1 - X_s)^{0.532} \left(\frac{T_a}{T_s}\right)^{-1.035} \left(\frac{m_s}{m_a}\right)^{0.523} Re_a^{1.348}\ S\,c_a^{\ 0.33} Re_{a,ev}^{0.0213} \tag{2.55}$$

2.14.3.2 Effectiveness correlations

2.14.3.2.1 Packed bed dehumidifier and regenerator

Ullah et al. [12] presented an empirical correlation to predict the dehumidification effectiveness of a random packed bed (Raschig rings) tower using $CaCl_2$ desiccant.

$$\varepsilon_{Y,abs} = \left(1 - \frac{C_1\, exp\left(-C_2\left(\frac{T_{a,in}}{T_{s,in}}\right)\right)}{X_{s,in}^{C_3}}\right) \Bigg/ \left(1 - \frac{C_4\, exp(C_5 T_{s,in})}{\omega_{a,in} X_{s,in}^{C_6}}\right) \tag{2.56}$$

In Eqn. (2.56) C_1, C_2, and C_3 are regression coefficients dependent on the type of packing, height of the packing and flow rates of air and liquid desiccant, whereas C_4, C_5, and C_6 are regression coefficients independent of the tower geometry and operating conditions, but dependent on the type of liquid desiccant used.

Chung [138] modified the above correlations by introducing a new term called vapor pressure difference. The correlation was developed by comparing the mass transfer performance of two different desiccant solutions, LiCl and TEG. He reported that the average error between the experimental and predicted values were 7%.

$$\varepsilon_{Y,abs} = \left(1 - \frac{0.205\left(\frac{m_{a,in}}{m_{s,in}}\right)^{0.174} exp\left(0.985\frac{T_{a,in}}{T_{s,in}}\right)}{(aZ)^{0.184}\,\theta^{1.680}}\right) \Bigg/ \left(1 - \frac{0.152\,exp\left(-0.686\frac{T_{a,in}}{T_{s,in}}\right)}{\theta^{3.388}}\right) \quad (2.57)$$

A simple prediction model for dehumidifier and regenerator was reported by Khan [139] in terms of NTU and Lewis number (Le). The model was developed based on sensitivity analysis of some pertinent operating parameters of air and solution.

$$\varepsilon_{Y,abs} = c_0 - c_1(Le) - c_2(NTU.Le) - c_3(NTU.Le)^2 \quad (2.58)$$

Chung and Luo [140] developed a correlation to calculate the vapor pressure of liquid desiccant. Using vapour pressure data they modified the Chung [138] correlation to predict the effectiveness of different liquid desiccant and packing materials. They reported that 80% of the data points lies within ±10% error band, and the average errors between the experimental and predicted value was around 10%.

$$\varepsilon_{Y,abs} = \left(1 - \frac{0.0204\left(\frac{m_{a,in}}{m_{s,in}}\right)^{0.6} exp\left(1.507\frac{T_{a,in}}{T_{s,in}}\right)}{(aZ)^{-0.185}\,\theta^{0.638}}\right) \Bigg/ \left(1 - \frac{0.192\,exp\left(0.615\frac{T_{a,in}}{T_{s,in}}\right)}{\theta^{-21.498}}\right) \quad (2.59)$$

Martin and Goswami [141] proposed an improved non-dimensional effectiveness correlation valid for packed bed dehumidifier as well as regenerator by introducing wetting characteristic information of desiccant solution and packing material in their prediction model. They found that the accuracy of the prediction model was within 15% for dehumidifier/regenerator.

$$\varepsilon_{Y,abs/reg} = 1 - 48.345\left(\frac{m_{s,in}}{m_{a,in}}\right)^{\left(0.396\frac{\gamma_S}{\gamma_C}-1.573\right)}\left(\frac{h_{a,in}}{h_{s,in}}\right)^{-0.751}(aZ)^{\left(0.033\frac{\gamma_S}{\gamma_C}-0.906\right)} \quad (2.60)$$

Wahab et al. [142] developed effectiveness regression model by conducting experiments on packed bed dehumidifier with packing density ranging from 77 to 200 m^2/m^3.

$$\varepsilon_{Y,abs} = 0.601 + 0.257m_{s,in} - 0.00072\,a - 0.0107T_{a,in} \quad (2.61)$$

Liu et al. [143] developed empirical model to investigate the effects of inlet parameters of air and solution on cross flow dehumidifier. The developed model showed good accuracy, and on validation with experimental values of Chung et al. [61], Chung and Wu [144], and Fumo and Goswami [62] the average error was only 1.3%, 4.7% and 5.1%, respectively.

$$\varepsilon_{Y,abs} = c_0\, m_{a,in}{}^{-0.2804}\, m_{s,in}{}^{0.3657} \tag{2.62}$$

Liu et al. [66] developed a correlation for cross-flow packed bed dehumidifier following Ullah et al. [12] and Chung [138] correlation form. The accuracy of their model was 5%, and almost 99.4% of data was predicted within 20% error range. In another study Liu et al. [145] proposed an empirical correlation to predict the effectiveness of a packed bed regenerator.

$$\left(1-\frac{0.642\left(\frac{m_{a,in}}{m_{s,in}}\right)^{0.1} exp\left(-0.2\frac{T_{a,in}}{T_{s,in}}\right)}{X_s{}^{0.537}}\right)\Bigg/\left(1-\frac{0.496\, exp\left(-0.945\frac{T_{a,in}}{T_{s,in}}\right)}{X_s{}^{1.558}}\right) \tag{2.63}$$

Moon et al. [146] found that the previous dehumidifier effectiveness model of Chung [138] and Liu et al. [66] failed to predict their experimental data. Hence, they proposed a new correlation model to predict the experimental values of a cross flow dehumidifier. However, they did not consider the packing size in correlation equation.

$$\varepsilon_{Y,abs} = \left(1-\frac{0.363\left(\frac{m_{a,in}}{m_{s,in}}\right)^{-0.038} exp\left(1.012\frac{T_{a,in}}{T_{s,in}}\right)}{\theta^{0.342}}\right)\Bigg/\left(1-\frac{0.267\, exp\left(1.401\frac{T_{a,in}}{T_{s,in}}\right)}{\theta^{0.363}}\right) \tag{2.64}$$

Gao et al. [71] established a prediction model for effectiveness of packed bed dehumidifier in terms of flow rates of air and solution.

$$\varepsilon_{Y,abs} = 0.67 m_{a,in}^{-0.352}\, m_{s,in}^{0.403} \tag{2.65}$$

Wang et al. [40] proposed a new empirical correlation for the effectiveness of packed bed dehumidifiers in terms of air and solution operating parameters. The correlation equation included the effect of air humidity ratio which was neglected in the previous models. The comparison result showed a deviation of ±10% with experimental values and ±15% with Fumo and Goswami [62].

$$\varepsilon_{Y,abs} = 3.5823\, m_{s,in}^{0.256} T_{s,in}^{-0.634} \omega_{a,in}^{0.350} m_{a,in}^{-0.322} T_{a,in}^{-0.327} \tag{2.66}$$

2.14.3.2.2 Falling film dehumidifier and regenerator

Qi et al. [147] used numerical data to formulate an effectiveness correlation for falling film dehumidifier/regenerator. In addition to common operating parameters, heat and mass driving potential was taken into consideration. The developed model indicated an accuracy of 14.5% for dehumidifiers and 6.83% for regenerators in comparison to previous mathematical models.

$$\varepsilon_{Y,abs} = \frac{0.0829\,(|h_{a,in}-h_{l,in}|)^{0.195}\left(\frac{m_{s,in}}{m_{a,in}}\right)^{0.350} m_f{}^{0.0619}\, a_w^{0.07}\, wf^{\,0.0977}(-0.0032.L+0.0248.H)^{0.0854}}{(|t_{f,in}-t_{s,in}|)^{0.009}(\omega_{a,in}-\omega_{l,in})^{0.0441} th^{0.375}} \tag{2.67}$$

$$\varepsilon_{reg} = \frac{46.219\,(1000(\omega_{l,in}-\omega_{a,in}))^{0.728}\left(\frac{m_{s,in}}{m_{a,in}}\right)^{0.844} a_w^{0.0691}\, m_f{}^{\,0.001}\, th^{0.324}\,(1.552L+0.118H)^{0.0242}\, wf^{0.0248}}{(|h_{a,in}-h_{l,in}|)^{1.332}(|t_{f,in}-t_{s,in}|)^{0.0168}} \tag{2.68}$$

Qi et al. [148] derived a regression model for falling film dehumidifier/regenerator by considering significant parameters of air, solution and water.

$$\varepsilon_{Y,abs} = k\left(1 - 0.06\,\frac{th^{0.12}\left(\frac{m_{a,in}}{m_{s,in}}\right)^{0.25} T_{s,in}^{0.66}}{(-0.19L+1.44H)^{0.06} X_{s,in}{}^{0.5}}\right) \Big/ \left(1 - 0.27 X_{s,in}{}^{-0.46}\right) \tag{2.69}$$

$$\varepsilon_{Y,reg} = k\left(1 - 25.9\,\frac{\left(\frac{m_{a,in}}{m_{s,in}}\right)^{0.43}}{T_{s,in}^{0.93}.\theta^{0.14}(L.H)^{0.35}.\omega_{a,in}^{0.22}}\right) \Big/ \left(1 - \frac{1.39}{\theta^{0.72}.(L.H)^{0.45}}\right) \tag{2.70}$$

Wen et al. [100,149] experimentally compared the performance of LiCl and mixed liquid desiccant (LiCl+Urea) in regeneration and dehumidification mode and proposed a effectiveness correlation based on air humidity ratio, air Reynolds number and mass transfer potential between air and liquid desiccant. They reported an average error of 4.01% and 4.51% for regenerator and dehumidifier, respectively.

$$\varepsilon_{Y,reg} = 0.0184\, Re_a^{-0.217}\, \omega_{a,in}^{-0.886} (\omega_{eqls,in} - \omega_{a,in})^{-0.06} \tag{2.71}$$

$$\varepsilon_{Y,abs} = 159.97\, Re_a^{-0.161}\, \omega_{a,in}^{1.151} (\omega_{a,in} - \omega_{eqls,in})^{0.254} \tag{2.72}$$

Cheng et al. [91] built an effectiveness correlation for a vertical tube dehumidifier assisted with evaporative cooling. However, they did not validate their model with other studies.

$$\varepsilon_{Y,abs} = 2.85 \frac{m_{s,in}^{0.165} T_{s,in}^{0.835} m_{a,ev}^{0.146} m_{w,in}^{0.354}}{m_{a,in}^{0.328} T_{a,in}^{0.043} \omega_{a,in}^{1.081} X_{s,in}^{2.09} T_{w,in}^{0.958}} \tag{2.73}$$

Kumar et al. [150] proposed a generalized correlation model for plastic/metallic plate regenerator of adiabatic and non-adiabatic studies. The model predicted the experimental values of eight data sets with an accuracy of 18.1%. However, it performed poorly against studies other than LiCl.

$$\varepsilon_{Y,reg} = 1.294 \frac{m_{s,in}^{0.102} T_{a,in}^{0.87} X_{s,in}^{1.347} A_W^{0.628}}{m_{a,in}^{0.515} T_{s,in}^{1.237} \omega_{a,in}^{0.036} \left(1+\frac{T_{w,in}}{T_{s,in}}\right)^{0.021}} \tag{2.74}$$

Khan et al. [151] extended the correlation model of Kumar et al. [150] to developed generalized effectiveness model for falling film dehumidifier. The model was developed by incorporating the wetting characteristics of solid surface, the sensible cooling information in addition to operating parameters of air and solution. They reported that the model showed good validation accuracy against vertical metallic/plastic plate dehumidifier of adiabatic/non-adiabatic studies and against different desiccants LiCl, $CaCl_2$, LiBr and KCOOH with an overall average error of 12.7%.

$$\varepsilon_{Y,abs} = 39.95 \frac{m_{s,in}^{0.025} \omega_{a,in}^{0.468} A_W^{0.968} \left(1+\frac{T_{s,in}}{T_{w,in}/T_{w,out}}\right)^{0.180}}{m_{a,in}^{0.496} T_{s,in}^{0.095} T_{a,in}^{0.230} \omega_{eqls}^{0.451}} \tag{2.75}$$

2.14.4 ANN Modelling

As discussed in section 2.14.3, numerical models to solve the complex heat and mass transfer process in dehumidifiers and regenerators involve many assumptions and are time consuming because of its iterative procedure. Further, to prove the reliability of the numerical model it has to be validated with experimental results. Regression models developed based on experimental/numerical data have limited generalizability are valid only for the fitted range of datasets. Recently, artificial neural network (ANN) has emerged as the popular tool among the researchers to predict the experimental observations accurately.

Gandhidasan and Mohandas [152] demonstrated the potential application of ANN to accurately predict the vapor pressure of commonly used inorganic desiccant solution such as LiCl, $CaCl_2$ and LiBr. They found that the ANN model results showed good agreement for LiCl and LiBr experimental data but perform poorly against $CalCl_2$ due to a smaller number of data points.

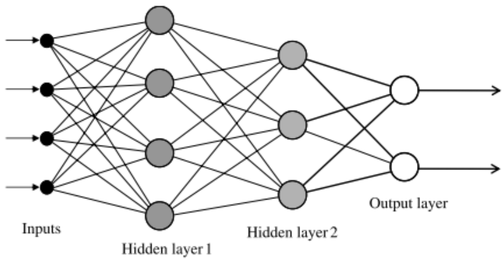

Fig. 2.11 A three layer feed forward ANN [152]

Gandhidasan and Mohandas [153] used three different multilayer ANN model to predict dehumidification rate, outlet temperature and concentration of desiccant. They found that the ANN model predicted the dehumidification rate and outlet solution concentration with good accuracy. However, for solution temperature the values predicted by ANN models were 0.8-1.8ºC less than experimental values.

Mohammed et al. [154] proposed a single and multilayer ANN model to predict the dehumidification rate and dehumidification effectiveness of a packed bed dehumidifier. They concluded that 6-3-3-1 and 6-6-6-1 were the optimum ANN model for predicting dehumidification rate and dehumidification effectiveness and the maximum error between the

ANN and experimental value for dehumidification rate and dehumidification effectiveness were 8.1% and 9.0%, respectively.

Mohammed et al.[155,156] extended the ANN technique to predict the performance of a dehumidifier and regenerator performance of a solar hybrid liquid desiccant system. In case of dehumidifier, they found that 5-5-5-1 and 5-11-11-1 ANN model were optimal models for MRR and ME and similarly 5-5-5-1 and 5-11-1 provided the best performance for regenerator.

Zendehboudi et al. [157] compared the performance of different intelligent computing models such as Least Square Support Vector Machine (LSSVM), Adaptive Neuro Fuzzy Inference System (ANFIS) and ANN. They concluded that among different intelligent models ANN gave the best performance for predicting the experiment data.

Longo et al. [158] applied ANN technique to predict the dynamic viscosity of KCOOH solution. They showed that the ANN model predicted the experimental data with an average error of 0.92%. Similarly, Aly et al. [159] used ANN technique to predict the outlet conditions of a solar hybrid LDS.

2.15 Low flow falling film LDS

The development of low flow falling towers has been the subject of interest due to the higher energy efficiency of the overall system. AIL research was the first to develop and design the low flow LDS [160]. Lowenstein et al. [161] tested the performance of a novel multiplate plastic low flow internally cooled liquid desiccant dehumidifier experimentally. The dehumidifier was made of 198 PP plates, each with a cross section of 2.5 mm by 305 mm and 110 cooling passages running along the length of the plate. To ensure complete wetting by the liquid desiccant, the plates were covered with 0.5 mm wick. The liquid desiccant operating mass flow rate was significantly lower than that of conventional packed bed towers (by a factor of 10 to 20). The proposed system provided dehumidification performance comparable to traditional packed bed towers. In addition, they focused on the development of low flow liquid desiccant systems for successful use of LDS in residential cooling. A design similar to above discussed dehumidifier was used by Abdel-Salam et al. [162] to analyse the field performance of low flow LDS. The thermal and electrical COP of LDS were in the ranges of 0.35 to 0.52 and 2.7 to 3.6 respectively. They suggested that while evaluating the energy consumption of LDS, the transient conditions can be ignored, and the quasi-steady performance of LDS can be predicted by averaging the transient field tests with acceptable uncertainty. Recently, Jaradet [163] built a low flow falling film vertical tube regenerator with a solution to air mass flow ratio ranging from 0.03 to 0.2. He reported a maximum thermochemical energy storage capacity of 117 kWh/m^3 for their system.

2.15.1 Advantages of low flow falling film LDS

1. Low parasitic power requirement for liquid pump and air blower.
2. At low flow rate, the change in concentration of desiccant solution is relatively higher. The energy required to regenerate the solution at low concentration is comparatively lower. Hence, the regeneration process will be more efficient at low flow rate.
3. Low thermal energy is required to precool/preheat the desiccant solution before the dehumidifier/regenerator.

2.16 Literature summary

Based on the extensive literature review analysis following important points are highlighted.

1. LiCl is the most widely used desiccant due to its high dehumidification ability, followed by LiBr and $CaCl_2$. Ionic liquids are less corrosive and possess comparable dehumidification ability to LiCl/LiBr, but they are still extremely costly and at the research stage. HCOOK seems to be a promising desiccant solution, but poor dehumidifying capability does not let it qualify as the suitable list of desiccant solutions. Hence, alternative liquid desiccant solution search is still at a nascent stage. At present, inorganic liquid desiccant salt solutions and their mixture look to process potential to be used in commercial systems.

2. The packed bed tower is most widely used and extensively studied due to its outstanding compactness and higher efficiency. However, packed bed towers are energy-intensive due to their increased airside pressure drop and large desiccant flow requirements. Thus, they seem to be suitable for large-scale hybrid liquid desiccant systems. For the small-scale and residential systems, the falling film tower-based hybrid liquid desiccant system seems to be a more suitable option. The falling film tower operates at a lower pressure drop than the packed bed tower. Nevertheless, comparatively less number of experimental studies on falling film towers had been carried out.

3. Most of the existing work on the falling film dehumidifiers and regenerators have been reported on metallic surface. However, most inorganic salt-based liquid desiccants such LiCl, LiBr and $CaCl_2$ cause severe corrosion problems to most metals. The surface treatment and solution modification corrosion minimization techniques certainly prolong the life of the metallic surfaces; however, they are not a permanent solution. The surface/solution treatment processes are generally cost expensive and require frequent replacement.

4. Plastic surfaces are promising to eliminate the corrosion problem permanently. However, they suffer from poor performance due to their hydrophobic nature. The performance improvement techniques such as plasma treatment, hydrophilic coatings, and textile sheets were explored to elevate the performance of the plastic surface. The plasma treatment and hydrophilic coatings are expensive and have limited durability, while textile sheets require frequent replacement. Mechanical surface modification appears to be the possible solution to the above problem. However, comparatively very few efforts have been made on LDS.

5. In conventional packed bed towers, FDM had been mostly used to determine the accurate values of heat and mass transfer coefficients. For falling film towers, heat and mass transfer coefficients are mainly evaluated based on the logarithmic mean temperature (humidity) difference approach and based on terminal heat and mass transfer potential difference. Also, most of the existing Nu and Sh correlations based on the above techniques are developed at complete surface wetting and unity Le number assumptions. These correlations are not usable for predicting experimental observation on plastic falling film LDS.

6. Low flow falling film towers are promising for the development of small-scale compact size AC for residential/commercial applications. They offer a tremendous opportunity of saving energy consumption as precooling/internally cooling of the desiccant solution during dehumidification as well as preheating/internally heating of the solution during regeneration (the main energy-consuming process of LDS) becomes energy economical.

7. Theoretical models have limited prediction ability and mostly rely on verification from experimental data. Empirical models developed based on experimental/numerical data lack generalizability and are limited only to the range of fitted data. ANN computing technique models have emerged as the popular choice among researchers to reproduce the experimental observation accurately.

2.17 Research gaps

1. Most of the research on the falling film LDS is carried out on vertical plates, a few on horizontal arrayed tubes. However, there has been limited research on the use of vertical tubes with external liquid desiccant flow.

2. Existing mass transfer correlations were developed for the packed bed towers or metallic surfaces; these mass transfer correlations may not suffice the need for simulation/numerical modelling of the plastic surface.

3. The regenerator plays a critical role in the overall efficiency and energy-economic viability of the LDS. However, compared to dehumidifiers, the heat and mass transfer studies on the falling film regeneration process are almost nil.

4. In heat and mass transfer modelling of liquid desiccant system generally full wetting of the working surface and unity Lewis number is assumed. The studies on non-unity Lewis number and considering the actual wetting characteristics of the surface is rare.

5. ANN modelling has been used by several researchers to develop predictive models for dehumidifiers and regenerators. However, the existing work focused mainly on training performance of ANN modelling to limited number of experimental datasets.

2.18 Research objective of the thesis

Based on the above literature summary following main research objectives have been identified for the current research work.

1. The first objective is to identify a suitable plastic (to eliminate corrosion problem) surface as an alternative to PS for the development of low flow falling film towers. For that purpose, the wetting characteristic of a vertical CCS is studied, and it is compared with the PS.

2. The vertical CCS geometry exhibited superior wetting characteristics compared to PS. Hence to prove the usefulness of CCS over PS for the development of compact low-flow falling film LDS, detailed experimentation investigations on the dehumidification and regeneration performance of CCS have been planned. Also, a comparison between CCS and PS surfaces needs to be drawn, covering a wide range of operating parameters of air and liquid desiccant to conclude, “Which one is more suitable for the development of low flow falling film liquid desiccant systems”. Additionally, exploring the possibility of developing generalized empirical effectiveness correlations for the dehumidifier and regenerator of falling film liquid desiccant system.

3. Evaluation of heat and mass transfer coefficients apart from performance analysis is crucial for enriching the design and development of falling film LDAC. Therefore, the third objective is to develop a new generalized Sh number correlation for the metallic/plastic falling film dehumidifiers.

4. The fourth objective is to study the coupled heat and mass transfer characteristics of plastic regenerators. The finite-difference numerical technique is applied to determine the heat and mass transfer coefficients, and a correlation for Nu and Sh numbers is proposed at partial as well as complete wetting conditions.

5. The last objective is to develop a generalized data-driven predictive model using the ANN technique for falling film dehumidifier.

2.19 Research contributions

1. A new experimental dehumidification and regenerating study on vertical plastic circular cylinder with external flow of the liquid desiccant and air is investigated in this work. The outcome of the study provides the scope of finalizing the superior non-corrosive solid surface out of vertical plate and vertical circular cylindrical surfaces for the development low flow hybrid liquid desiccant systems. The circular cylinder surface offered 55.9% and 50.5% enhancement in dehumidification rate and regeneration rate over the plate surface. This study also proposed new generalized effectiveness models for liquid desiccant dehumidifiers and regenerators, which predicted dehumidification and regeneration performance with greater accuracy than previous correlations. Journal papers based on these results have been published in Renewable Energy and Solar Energy.

2. A new generalized correlation is proposed to predict the mass transfer coefficient of plastic and metallic surfaces of adiabatic and non-adiabatic dehumidifier operating with different solution such as LiCl, $CalCl_2$ and KCOOH. The developed correlation predicted 70% of the data points of nine experimental dehumidification studies (three adiabatic and six non-adiabatic) within an error band of ±20%. The developed correlation will be useful for researchers interested in numerical/simulation modelling of falling film towers. Journal paper based on the results has been published in Chemical Engineering and Processing - Process Intensification.

3. The performance of a liquid desiccant system is significantly impacted by the wetting characteristics of the surface. This study deviates from the conventional full wetting approach and investigates the coupled heat and mass transfer characteristics of the surface, considering the actual wetting conditions of surface as well as heat transfer from the dry surface. The heat and mass transfer correlation developed using full wetting assumption underpredicted the experimental observations (with a MAPE 27.2% and 15.2%). In contrast, the correlation developed based on the actual wetting of the solid surface predicted the experimental observations with far greater accuracy (with a MAPE of 7.5% and 11.2%). The developed heat and mass transfer correlations are highly promising for designing and developing falling film regenerators that operate in a wide range of liquid flow rate conditions.

CHAPTER 3

WETNESS STUDY OF CIRCULAR CYLINDERS AND EXPERIMENTAL TEST FACILITY

3.1 Introduction

Adverse corrosion problem of the commonly used metallic materials by the liquid desiccant solutions is well evident, and it has been identified as one of the primary limiting concerns for the development and commercialization of LDS for end-user applications [96,109,164]. Presently, plastic falling film towers are gaining more attention than metallic columns in LDS due to their excellent anti-corrosive characteristics. The use of plastic surfaces faces very poor wetness setbacks as most of the plastics are hydrophobic. Existing research on the plastic surface is mainly reported on vertical plates, and a few studies are available on the horizontal tube. Apart from surface wettability, its geometry also plays a vital role in the formation of the continuous thin film over it. In this chapter, the wetness characteristic of vertical circular cylinders has been experimentally investigated and compared with the wetness characteristics of vertical plastic surface [165] to find the superior surface for the developing low flow falling film towers. Apart from the wetness study, the main experimental test facility, experimentation procedure, different measuring instruments, and devices used in dehumidification and regeneration experimentation of circular cylinders are also discussed in this Chapter.

3.2 Identification of suitable surface for developing low flow falling film tower

Four commercially available solid PP circular cylinders with sizes of D = 22, 32, 40, and 64 mm are chosen for the preliminary wetness experimentation on a circular cylindrical surface. Four vertical lines at an angular distance of 90° are marked throughout the CCS surface length to estimate average surface wetness accurately. Then, the still photographs are taken from all four sides at different flow rates for each CCS to calculate the total wetted area of the solid surface. The wetting factor indicates the fraction of the total wetted area of liquid on solid CCS. The details of the wetness study, experimental set-up, and procedure are given in Patil et al. [165]. Fig. 3.1 shows the wetting behavior of all four solid circular cylinder and plain plate experimental observations published by Patil et al. [165]. The wetting factor increases with an increase in flow rate for the entire studied CCS. The wetting factor is a measure of the ability of a liquid to spread over a solid surface It is defined as the ratio of wetted area to the total solid surface area. Although the best wetting behavior is found for the solid circular cylinder of *D* = 22 mm, *D* = 32 mm CCS is chosen for further study considering the serious maldistribution problem. The equal flow distribution responsibility increases almost 50% more than *D* = 22 mm [166].

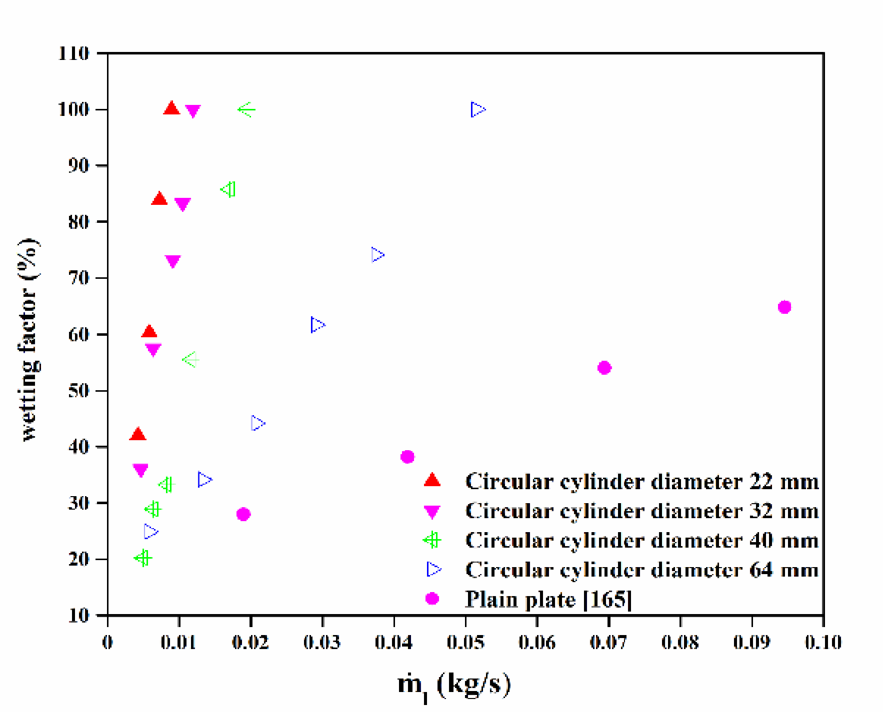

Fig. 3.1 Comparison of the wetting behavior of different CCS with PS [165]

3.3 Mechanical surface modification

Apart from targeting the influence of solid surface shape, it is also decided to study the influence of surface modification on the performance intensification provided by the enhancement technique. The performance intensification technique suggested by Patil et al. [165] is shortlisted for that purpose, in which the authors suggested that horizontal grooves (inclined opposite to the direction of flow) enhanced the performance of falling film towers by improving the wetting as well as ensuring liquid holdup in the dry patches of the plate. Following the procedure suggested by Patil et al. [165], the radially inclined grooves (p = 2mm and d = 1.5mm) were generated on the vertical PP rods using CNC turning machine. Fig. 3.2 shows the front view of Plain PP and Modified PP solid circular cylinder surfaces.

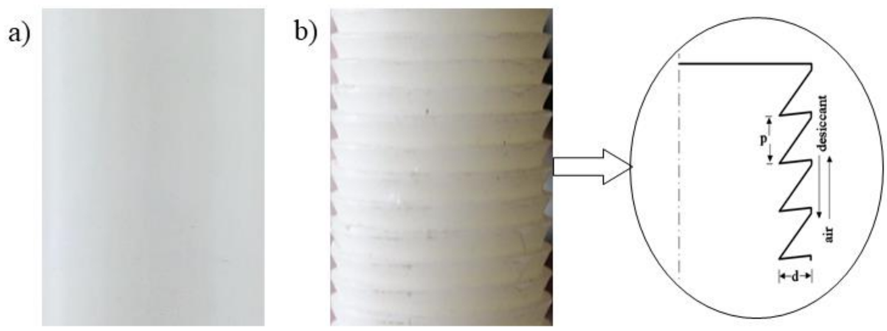

Fig. 3.2 Front view of a) Plain PP CCS and b) Modified PP CCS

3.4 Experimental test facility and experimentation procedure

An experimental test facility is constructed in Applied Thermal Engineering and I.C. Engine Laboratory of IIT Indore, India to investigate the performance of the vertical solid PP circular cylinders. Fig. 3.3 and Fig. 3.4 show the schematic diagram and photograph of the experimental setup. The complete setup is a combination of three main facilities: vertical falling film tower (I), desiccant pre-conditioning section (II), and air pre-conditioning section (III).

3.4.1 Description of the experimental setup

The vertical tower is an assembly of three main parts: liquid distributor header (1), vertical column (2) and bottom sump (3). The vertical tower is constructed from a 10 mm thick transparent acyclic sheet for clear visualization purposes. The vertical column with a size of 450 x 80 x 700 mm (W x B x H) is connected with the solution distributor header on the top side and through the bottom duct on the bottom side using S.S. 316 bolts and nuts. An acrylic duct (4) with the size of 250 x 75 x 270 mm (W x B x H) is fused on the top front portion of the vertical column to provide an exit passage for the processed air. The CCS diameter is finalized through an initial wetness study on commercially available PP CCS (Ref. Section 3.2). The vertical solid PP CCSs (5) with a size of 32 x 700 mm (Ø x H) are placed inside the vertical column in an inline manner at its mid-section. Eight number of the CCS is decided to keep its total surface area equal to the vertical PS study of Patil [167].

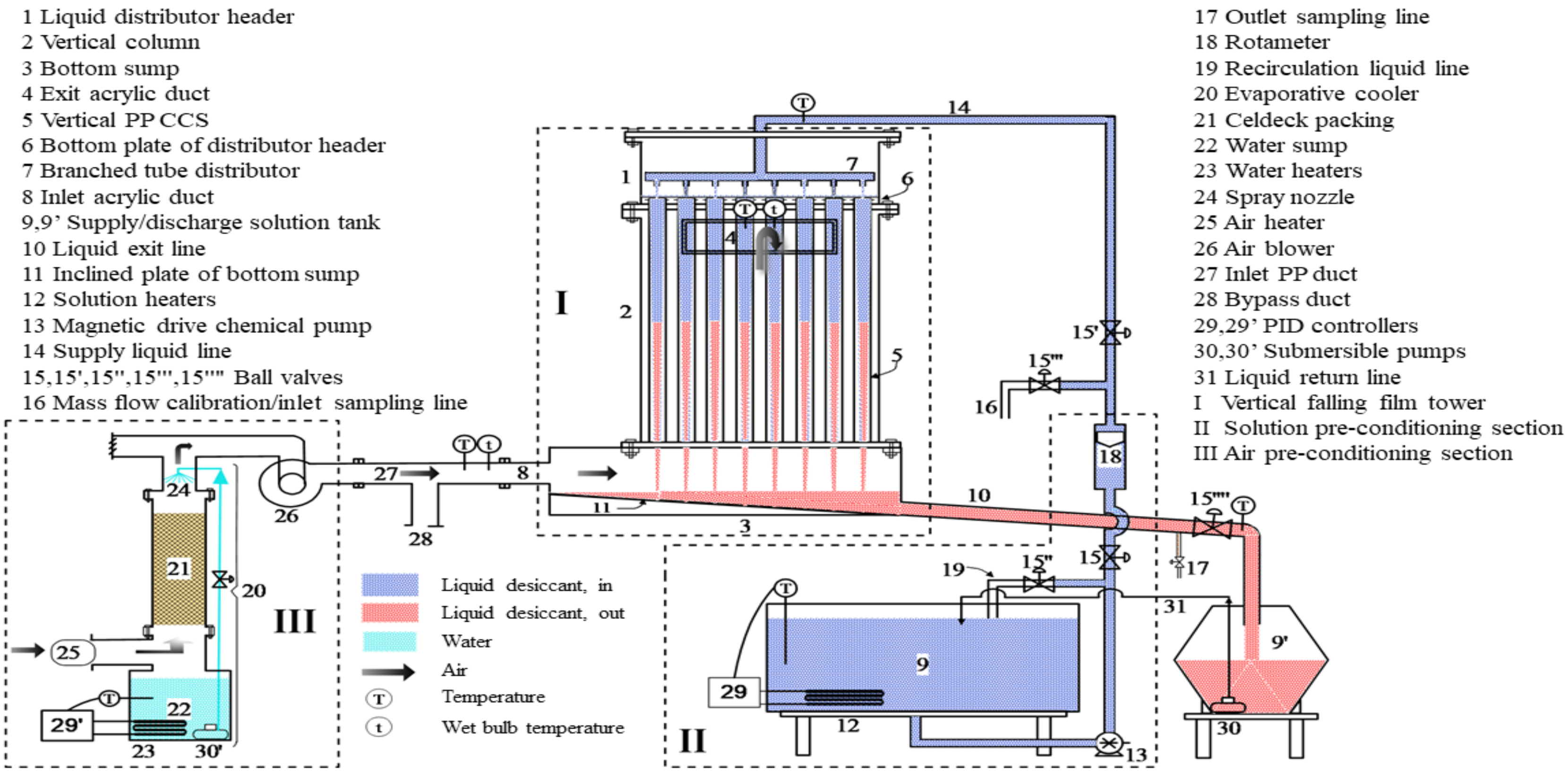

Fig. 3.3 Schematic diagram of experimental setup

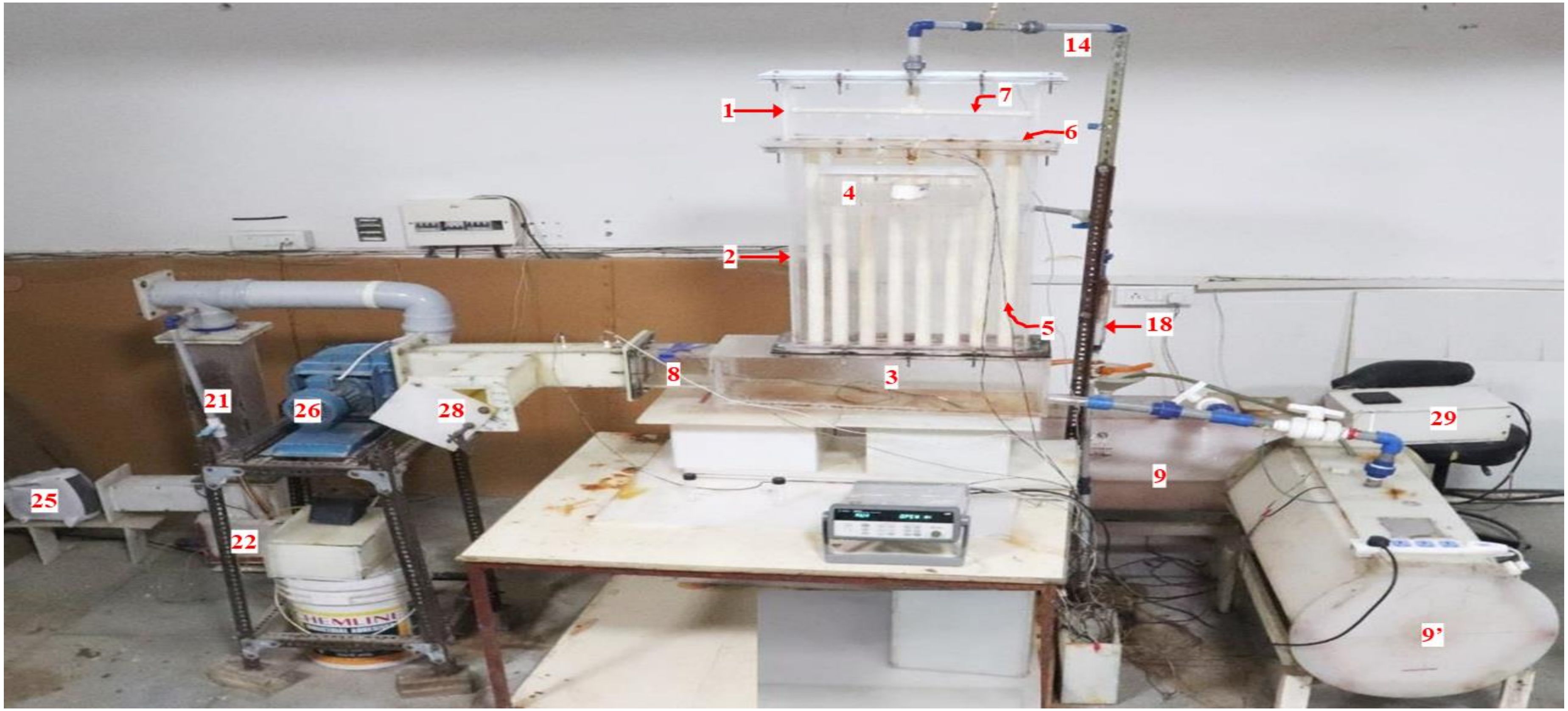

Fig. 3.4 Photoview of experimental setup

The major challenge is “how to generate and maintain a continuous flow of liquid on the outside of CCS?”. For that purpose, separate arrangements are made to generate and maintain the falling film outside the CCS. Eight precise circular holes of a diameter 34 mm along with four rectangular slots with a size of 4 x 6 mm per hole are cut on the bottom plate of the distributor header (6) through a CNC machine (CNC EMCO 350) to provide uniform flow through each solid surface (Fig. 3.5). The circular holes generate a slit opening of 1 mm around the periphery of each CCS. The straight alignment is essential to maintaining continuous falling film, as any eccentricity in the alignment would lead to poor performance because of the slippage of liquid film out of the cylindrical surface. Fig. 3.6 shows the 3D of the falling film tower along the vertical arrangement of circular cylinders. At a 3.5 mm distance from the top surface of each PP CCS, two through-holes of 3 mm diameter are drilled accurately on a vertical milling machine assisted with an indexing chuck. Then, S.S. 316 headless bolts are inserted from all sides in each hole of PP CCS, and they are fixed firmly at the rectangular slots of the bottom plate of the distributor header. Space of 1 mm is kept between the top surface of the bottom plates and circular cylinder to reduce liquid splashing at higher flow rates. At the bottom surface of each PP rod, a slot of size (6 mm) wide is cut parallel to one of the top-drilled holes to place it straight on a S.S. 316 solid rod and kept fixed at the bottom of the vertical tower. The above arrangement also helps to avoid any vertical misalignment generated due to thermal distortion. The top distributor header of size (W x B x H) (450 x 100 x 200 mm) encloses a branched solution distributor (7), which is fabricated following the recommendations of Kumar et al. [166]. The bottom sump of size on one side is connected with the air pre-conditioning section via acrylic inlet duct (8), and on the other side, it is connected to the discharge solution tank (9’) via the liquid exit line (10). Moreover, the bottom sump has an inclined plate (11) to enable an easy flow of the diluted/concentrated desiccant solution to the discharge tank.

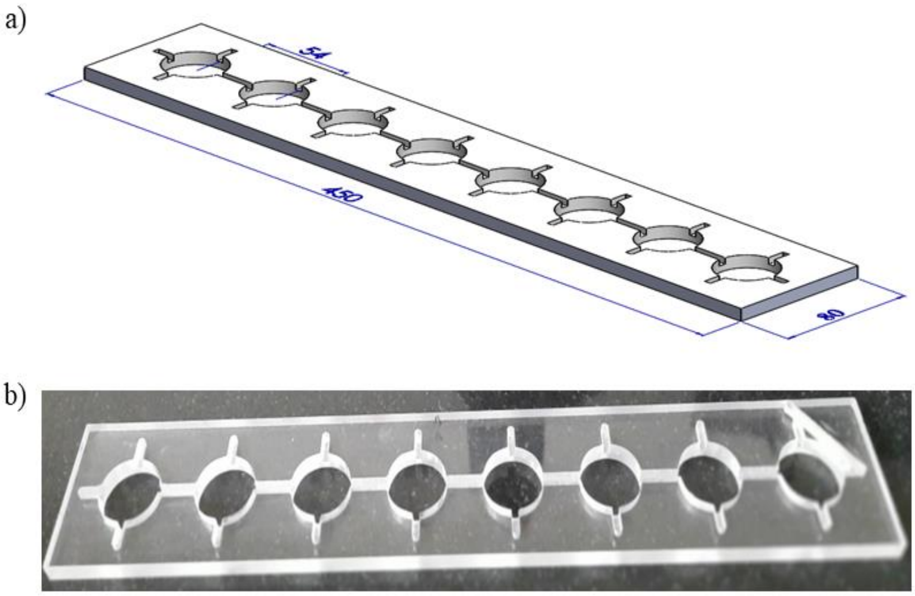

Fig. 3.5 a) 3D view of bottom plate b) photoview of bottom plate

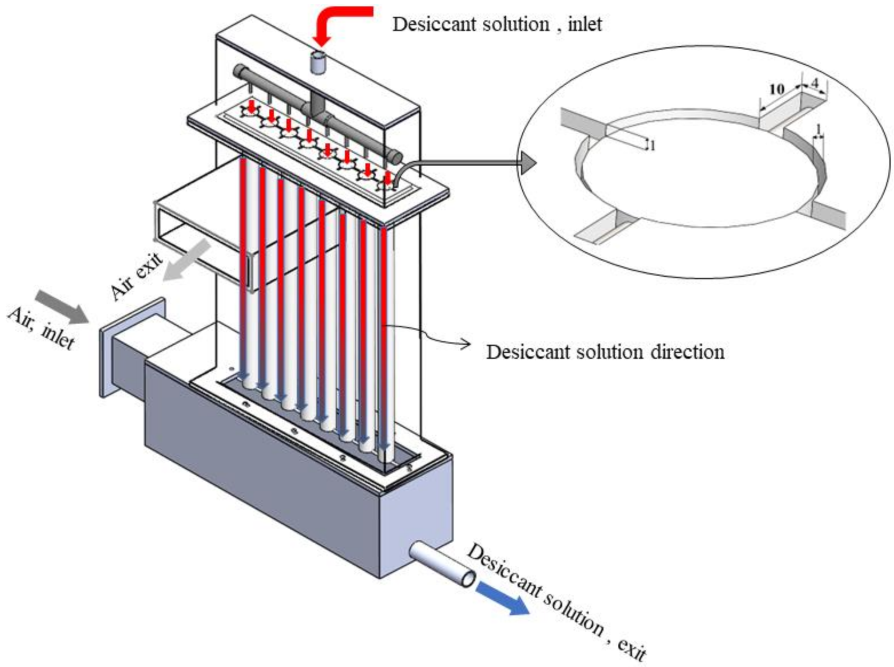

Fig. 3.6 3D view of vertical falling film tower

The desiccant pre-conditioning section consists of a solution pump, a solution heater, a supply tank, main/recirculation liquid line, and a flow rotameter. The desiccant solution prepared from laboratory-grade anhydrous lithium chloride (LiCl) (~99% pure) is kept in the PP supply tank (9). On one side of the supply tank, highly anti-corrosive (Titanium, 3kW) solution heaters (12) are attached, which are regulated by a PID controller (29). A magnetic drive chemical pump (13) (Promivac MP50) is connected to the liquid line for pumping the solution inside the vertical tower through the supply line (14). The flow through the supply line is controlled by regulating ball valves 15 and 15’’ (keeping 15’ open and 15’’’ closed). Liquid desiccant solution through the discharged solution tank is pumped back to the supply solution tank by a submersible liquid pump (30) through the liquid return line (31).

The air pre-conditioning section consists of a variable capacity air preheater (1-2 kW), an evaporative cooler, and an air blower. The evaporative cooler (20) of size (W x B x H) (150 x 150 x 600 mm) is filled with Celdeck packing (21) of surface density 660 m^2/m^3. At the bottom, it has a 20 L capacity water sump (22) equipped with a 1.5 kW PID controlled heater (23), while at the top nozzle (24) is attached for spraying water inside the tower. The air blower (26) is connected with the inlet PP duct (27) to supply the pre-conditioned air inside the tower. The air flow rate supplied inside the falling film tower is regulated by varying the opening of the bypass duct (28). Fig. 3.7 presents a photo view of the different devices used in the experimental set up.

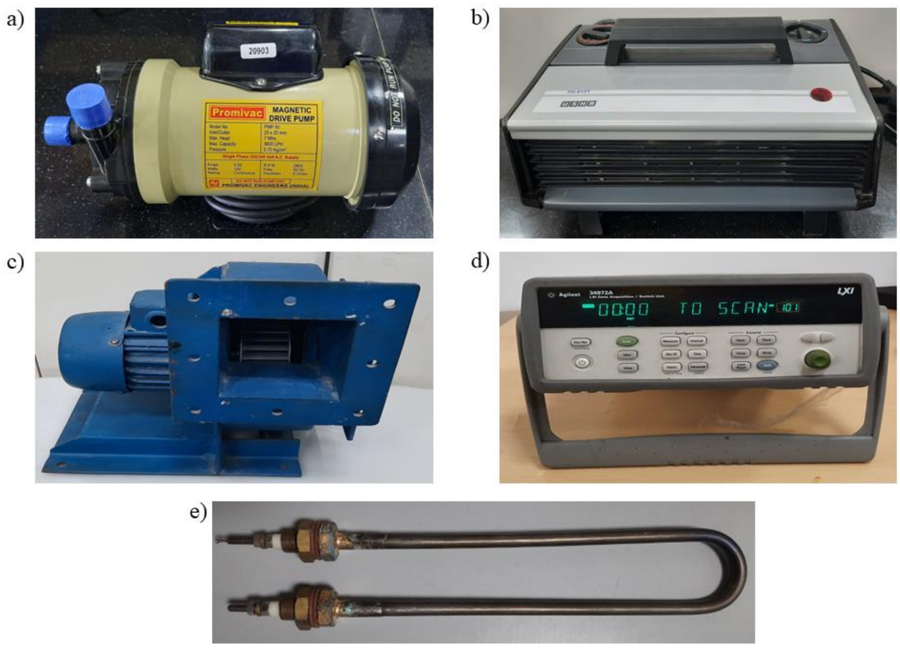

Fig. 3.7 Different devices used in experimental set up: a) Chemical pump b) Air heater c) Air blower d) Datalogger c) Titanium heater

3.4.2 Measurements and instrumentation

Different instruments were used to measure the desiccant solution and air parameters accurately. Fig. 3.8 shows the photo view of different measuring instruments used for experimentation. The details of the different measuring instruments are illustrated in Table 3.1. The mass flow rate of air is computed by measuring the average air velocity at the exit of the acrylic duct using an accurate anemometer (Testo-400). The mass flow rate of the solution is measured with the help of a plastic float rotameter, ball valves (15 and 15'''), weighing balance, stopwatch, and a plastic container. The desired level of solution flow rate is set via the rotameter by regulating the ball valves (15 and 15''). By keeping the ball valves 15''' open and 15' closed, the solution is allowed to flow through the liquid calibration/sampling line (16). The liquid discharged through the sampling line is collected in a plastic container for a time duration of at least 2 minutes. The weight of the solution in the plastic container divided by the sampling time gives the calibrated mass flow rate of the solution. The air temperature (DBT and WBT) and liquid desiccant temperature have been measured using calibrated 4-wire Pt-100 RTDs. DBT and WBT of the air are measured by the dry and wet cotton wick covered RTDs. The cotton wick is kept wet throughout the experiments by keeping the lower portion of the wick dipped inside a cup filled with distilled water. Two RDTs, one for DBT and another for WBT are installed at the inlet and outlet duct to measure the temperature and humidity ratio of air. The humidity ratio of air is derived from the measured DBT and WBT values using empirical correlations. One RTD is kept at the tower inlet (just before the liquid distributor) and one RTD is placed at the bottom sump to measure the liquid desiccant temperature. One long RTD (equivalent to the height supply tank) is also kept inside the supply tank to monitor/regulate the solution temperature before liquid desiccant-air interaction. All the RTDs are connected to the data logger (Agilent 34972A) for continuous monitoring of air and liquid desiccant temperatures. During each experiment, the DBT and WBT RTDs (air humidity) behaviours are cross-checked against the highly precise Testo-400 instrument. A thermal camera (Fluke RSE 600) was used to capture the falling film pattern on Plain PP and Modified PP CCS. The concentration of desiccant solutions is calculated first by measuring the solution density using a densitymeter at a particular temperature and by applying the Conde [36] empirical correlation. The detailed procedure for density measurement is discussed in the subsequent section.

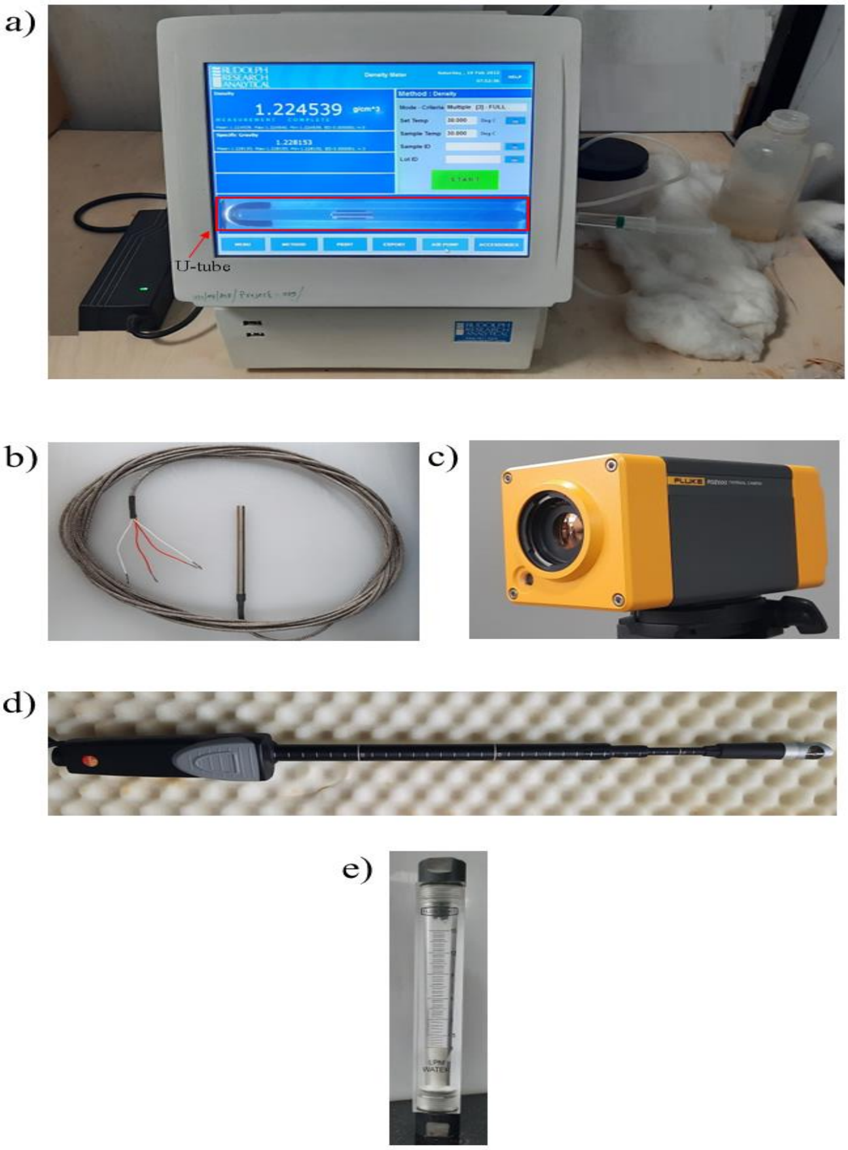

Fig. 3.8 Measuring instruments used in experimentation: a) Densitymeter b) RTD c) Thermal camera d) Anemometer e) Rotameter

Table 3.1 Details of the different measuring instruments

Parameter	Instrument	Type	Accuracy	Range
Air and solution temperature	Temperature sensor	Pt-100 RTD	±0.1 ^{0}C	0 – 100 ^{0}C
Solution density	Density meter	Rudolph-DDM2911 PLUS	±0.00001 g/cm^3	0 – 3 g/cm^3
Air flow rate	Anemometer	Testo 480	±0.03m/s+ 4% of mv	0 – 20 m/s
Solution flow rate	Flow meter	Variable area	± 0.5-1% of F.S	0 – 15 LPM
Wetted area	Thermal camera	Fluke RSE 600	±2%	−20 °C – 1000 °C

3.4.3 Density measurement of desiccant solution

Generally, the change in the concentration of the desiccant solution is very small, sometimes even lesser than 0.1% by weight during the dehumidification/regeneration process. Consider the case of dehumidification, for inlet solution concentration at 39.0%; the outlet concentration will be ≤ 38.9%. By applying Conde [36] correlation at 30ºC (assuming the measurement process is carried out after the solution acquires equilibrium with outside air condition), the inlet and outlet density is estimated as 1.24273 g/cm^3 and 1.24200 g/cm^3. The change in density is merely 0.00073 g/cm^3. Hence, a densitymeter with very high accuracy is required. The Rudolph-DDM2911 PLUS densitymeter (accuracy 0.00001 g/cm^3) is selected in the current study. Samples of fresh and used liquid desiccant are collected in 30 ml glass bottles. The inlet sample is taken via liquid sampling line/calibration line by regulating the ball valve 15''' and outlet sample is taken from the outlet sampling point 17. The following procedure is adopted for density measurement of liquid desiccant samples.

1. Before starting the measurement of the liquid desiccant density, the densitymeter U tube is thoroughly rinsed by two different solutions. Initially through soap solution to get rid of any salt crystal remaining on the U tube surface from the previous experiment. Later on, it was cleaned two times by the rinsing of hot RO water to remove any effect of soap solution remaining at the surface of glass U tube of the densitymeter (Fig. 3.8a).

2. Next, the small air pump available in the densitymeter is put ON 2 to 3 times (90 second cycle) to dry out the U-tube. While pumping, the outlet pipe of the pump connected to the inlet of U-tube is pressed and released 5 to 6 times. This is done to push out any tiny impurity that may have remained on the U-tube.

3. The temperature of the U-tube is set 30ºC, and U-tube is filled with RO water gradually till the water is visible at the outlet pipe of U-tube. Before injecting the water, the syringe is tapped manually to remove the air bubbles from the syringe. The U-tube is then zoomed in and scanned completely to check the presence of any air bubbles in the water. The density of water is measured and validated with standard values. This activity confirms that there are no powder traces of desiccant salt left in the U-tube.

4. The U-tube is once again dried with help of air pump. The air density is measured and compared with standard values of air density at 30ºC. If the measured value is confirmed, the density meter is considered ready for measurement of liquid desiccant density. Else, the procedure from point 3 is repeated.

5. The desiccant sample bottles are shaken vigorously, and it’s allowed to settle for 5-10 minutes to normalize the concentration. Samples of desiccant solution is taken in syringe. The desiccant sample is then injected in the U-tube and further the U-tube is scanned and checked for any air bubbles. The syringe is kept fixed at the inlet of the U-tube. The solution density is measured and recorded. After one sample readings, the syringe plunger is pushed, and another measurement is carried out. This procedure repeated at least 2 to 3 times and the average density is considered for concentration calculation.

6. After completion of one sample bottle measurement, the procedure 1-4 is repeated for another sample density measurement.

3.5 Experimentation

3.5.1 Preparation for experiments

The following activities are carried out before the start of experiments.

1. Sampling glass bottles are cleaned with hot RO water and dried with a hot air gun before being used to collect desiccant solution samples. The activity is strictly followed for each experimental run to avoid any side influence of salt and water particles remaining inside the sampling bottles from the previous day's experiments.
2. The inlet and outlet DBT and WBT sensors are detached from their installed position. The small bottles used for providing the saturated environment on the outside surface of the WBT sensors (by the continuous evaporation of water around the wick surface covering the RTD sensors) are cleaned and filled with fresh RO water. The DBT and WBT sensors are cleaned with a dry cotton cloth. The covering wicks are separately washed in hot water to remove the possibility of any dust/desiccant accumulation on them. The above activity ensures accurate DBT and WBT measurements.
3. As the outlet sampling line is made from a very thin diameter flexible tube, it is initially cleaned with metallic wire and hot water (injecting hot water through a syringe) to remove the accumulated salt crystal, if any, from the previous experiments.
4. The outlet air duct is wiped using white tissue paper before each experiment. It keeps the outlet duct clean and removes very fine tiny drops of desiccant solution (small in numbers) that are found at the edges of the outlet duct near the entrance (observed only at high air flow rate ~0.086 kg/s and high solution temperature >72ºC readings).
5. To subside the influence of any salt crystal remaining on the CCS surfaces and other inner parts of the setup on experimental observation; the experimental setup is initially run with hot air circulation only (for 20-30 minutes), until the humidity of air coming out from the outlet duct

becomes equal to the humidity of the air set at inlet duct. Above is the air pre-conditioning stage.

3.5.2 Experiments in dehumidification mode

The dehumidification experiments were performed during the monsoon season of Indore city from July - October 2019. In monsoon, the outdoor ambient air temperature reaches above 27 ºC with a humidity ratio of around 18 g/kg, naturally high outside humid conditions of air facilitated in performing the dehumidification experiments. The following section describes the method and procedure followed for conducting the dehumidification experiments.

1. Air inlet conditions at different desired levels can be set by the simultaneous control of the air preheater and evaporative cooler. Air preheater (1 or 2 kW) is used to control the temperature of the air at the desired level, and the humidity ratio of air is controlled by the combined regulations of water flow rate and recirculation water temperature across the evaporative cooler. The recirculated water temperature is controlled with the help of a liquid water heater (1.5 kW) coupled with a PID controller. A conventional room air convector is used as an air preheater so that its position can be regulated precisely to get desired value of air temperature. Initially, the desired condition of air is set by the regulation of the above components.
2. During the air pre-conditioning state, simultaneously, on the solution side, the desiccant pre-conditioning is carried out. Initially, the concentration and temperature of solution salt kept in the supply tank are normalized by circulating the solution through the recirculation for 10-15 minutes.
3. A sample of the desiccant solution is collected from the inlet sampling line to measure the concentration level of the desiccant solution available in the supply tank.
4. The calculated amount of anhydrous pure LiCl salt/pure water is added to the supply tank based on the measured and desired levels.
5. The solution is again mixed continuously by circulating it through a recirculation line. Simultaneously during the solution mixing, the

solution inlet temperature level is set either by light heating the solution inside the supply tank or by adding a pre-cooled desiccant solution of the same concentration level. The requisite concentration of the pre-cooled desiccant solution is kept ready for instantaneous cooling by overnight cooling of salt solution inside the deep freezer (Blue Star CHF 400A).

6. Once the desired conditions of the solution are achieved, then the desired mass flow rate during experimentation is calibrated for the set level of a rotameter. Afterward, the main solution line is switched on by gradually opening the ball valve (15) and keeping the ball valve (15''') closed to get the desired level of the rotameter. The solution starts falling as a thin film on the outside surface of the PP circular cylinder surface and interacts with humid air flowing in the counter direction.

7. During air-liquid desiccant interaction (dehumidification process), it is observed that the outlet WBT of air decreases rapidly initially, followed by a gradual reduction; eventually, it becomes constant. The dehumidifier is allowed to run until any further change in air outlet condition (DBT or WBT) becomes constant. Generally, it takes 8-12 minutes to attain steady state conditions at the air outlet. The solution and air (DBT and WBT) temperatures at the inlet and exit are recorded through the data logger (Agilent 34972A).

8. The liquid desiccant solution samples are collected from the inlet and outlet sampling lines after the system attains a steady state. These samples are used to measure the accurate inlet and outlet concentration levels by their density measurement (Fig. 3.9).

9. After completion of each experiment, the used desiccant solution in the discharge tank is returned to the supply tank via the liquid return line for starting the next experimental run.

Fig. 3.9 Sampling bottles for density measurement

3.5.3 Experiments in regeneration mode

The regeneration tests were conducted during the summer season (hot and dry weather) of Indore city from April - June 2019. The outside air temperature exceeded 35°C and humidity was below 10 g/kg. Following procedure and methods were adopted to conduct the regeneration experiments.

1. The solution inside the supply tank is heated up to the required value with the help of chemical heaters. The heaters are controlled by a PID controller. Heaters are attached on one side of the tank and PID RTD is placed at the opposite end. During initial heating, the solution is continuously mixed through the re-circulation line and inlet sampling line to obtain uniform temperature throughout the supply tank.
2. The rest of the experimentation procedures remain the same as discussed in the dehumidification mode (section 3.5.2).

Fig. 3.10 shows the typical air handling process for the dehumidification and regeneration processes on the psychrometric chart.

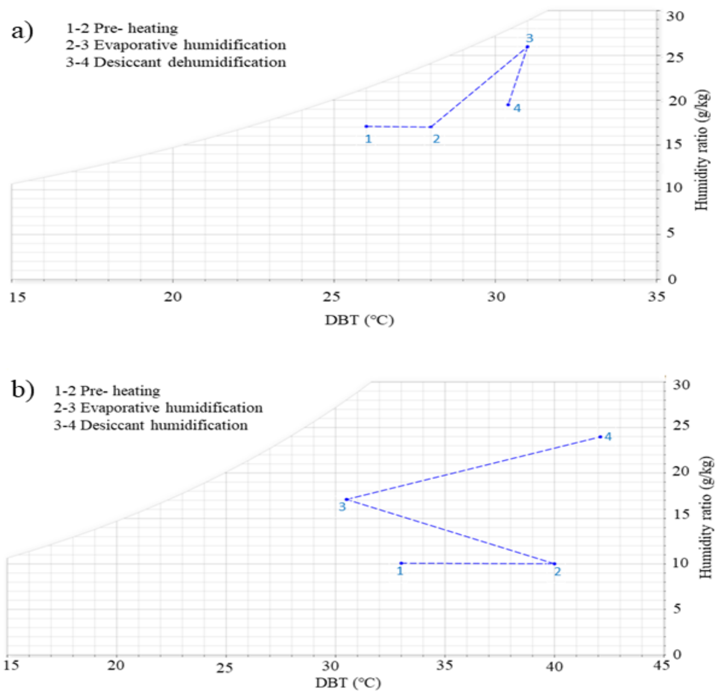

Fig. 3.10 Psychrometric chart of air handling process a) Dehumidification b) Regeneration

CHAPTER 4

PERFORMANCE ANALYSIS OF DEHUMIDIFIER AND REGENERATOR

4.1 Introduction

Experimental results presented in Chapter 3 established that the circular cylinder geometry enjoys superior wetting characteristics compared to PS. Hence, to assess the benefits of CCS surface over PS for the development of the low falling LDS, extensive experimentations are performed on the CCS in the dehumidification as well as regeneration modes, and the results are compared with the PS experimental results reported by Patil [167]. This chapter presents the experimental observations and the discussions based on the above observations. The range of independent parameters of desiccant solution and air are given in Table 4.1. The experimental observations on the Plain and Modified PP CCS are given in appendix A (Table A1 and A2).

4.2 Performance indicators for dehumidification and regeneration study

Two performance indicators: dehumidification/regeneration rate and dehumidification/regeneration effectiveness are used to evaluate the performance of vertical circular cylinder dehumidifier/regenerator falling film tower.

The dehumidification/regeneration rate indicates the actual moisture exchange rate between air and solution. It is estimated as follows:

$$\dot{m}_{abs} = \dot{m}_{da}\left(\omega_{a,in} - \omega_{a,out}\right) \tag{4.1}$$

$$\dot{m}_{reg} = \dot{m}_{da}\left(\omega_{a,out} - \omega_{a,in}\right) \tag{4.2}$$

Where, $\dot{m}_{da}$ stands for the mass flow rate of dry air and $\omega_{a,in}$, and $\omega_{a,out}$ are the humidity ratio of air at the inlet and outlet tower respectively.

The dehumidification/regeneration effectiveness represents the effectiveness of the dehumidification/regeneration process, i.e., actual change in the humidity ratio of air to the maximum possible theoretical change in the humidity ratio of air across the tower for the given inlet conditions of desiccant and air.

$$\epsilon_{Y,abs} = \frac{(\omega_{a,in} - \omega_{a,out})}{(\omega_{a,in} - \omega_{eqls,in})} \quad (4.3)$$

$$\epsilon_{Y,reg} = \frac{(\omega_{a,out} - \omega_{a,in})}{(\omega_{eqls,in} - \omega_{a,in})} \quad (4.4)$$

Where, ω_{eqls} is the humidity ratio of air in equilibrium with the desiccant solution. The overall uncertainty associated with dehumidifier performance indicators is 0.02 g/s and 1.4% respectively. Similarly, the overall uncertainly of the regeneration performance indicators is 0.03 g/s and 0.9%, respectively.

Table 4.1 Range of independent parameters

Parameters	Unit	Range for dehumidification	Range for regeneration
$\dot{m}_s$	kg/s	0.024 – 0.146	0.055 – 0.209
$\dot{m}_a$	kg/s	0.032 – 0.070	0.033 – 0.086
T_s	^{0}C	20.8 – 32.5	60.4 – 74.6
T_a	^{0}C	26.4 – 35.9	30.1 – 44.2
X_s	%	33.0 – 39.0	34.2 – 42.3
ω_a	g/kg	15.3 – 25.7	14.0 – 24.7

4.3 Dehumidification performance analysis

The dehumidification performance is one of the key controlling parameters in LDS. The dehumidification performance of Plain and Modified PP CCS is comprehensively studied and compared with Plain and Modified PP PS readings reported in Patil [167] for a wide range of operating parameters of air and desiccant solution; including three from the solution side ($\dot{m}_s, T_s, X_s$) and three from the airside ($\dot{m}_a, T_a, \omega_a$).

4.3.1 Influence of mass flow rate of liquid desiccant

The effect of the mass flow rate of the liquid desiccant solution on the dehumidification performance indices of PP PS and CCS is shown in Fig. 4.1. Both the performance indices increase with an increase in the mass flow rate of the solution. The observed influence of the mass flow rate can be justified following three distinct yet positive effects. The wetness factor increases with the increase in mass flow rate of solution (Fig. 3.1), and thus more area of the solid surface becomes available for the mass transfer between liquid desiccant and air. Also, the larger mass flow rate of the liquid desiccant helps in maintaining higher mass transfer potential, which otherwise diminishes in the downward direction due to relatively large increase in ω_{eqls} on account of decrease in solution concentration as well as increase in desiccant solution temperature (through heat generated during absorption process). With increase in the desiccant flow rates the formation of falling film waves increases, which in turn increase the interfacial contact area between liquid desiccant and air. Under the cumulative effect of above three influences, the performance trend varies. Performance curve rapidly increases in the beginning as the solid surfaces remain poorly wetted at a low flow rate, as flow increase and the wetting over the surface starts saturating, the performance in high flow region is governed by the second idea only (thus performance curve starts flattening out). At the same reference condition ($\dot{m}_s = 0.077$ kg/s), the difference in the dehumidification rate and dehumidification effectiveness between Plain PP CCS and Plain PP plate [167] is found significant (0.213g/s versus 0.139 g/s, and 19.5% versus 12.7%). The dehumidification rate and dehumidification effectiveness of Plain PP CCS is found 38.5% and 35.1% higher than the Plain PP PS for the studied range of mass flow rate. The performance curve of Plain PP CCS saturates at a significantly lower flow rate in comparison to the Plain PP PS. Spilling liquid out of the CCS at the high flow rate might be responsible for the observed behaviour. In order to understand the reason behind the high wetness of the CCS, the liquid flow behaviour over the CCS is studied using Fluke RSE 300 thermal camera.

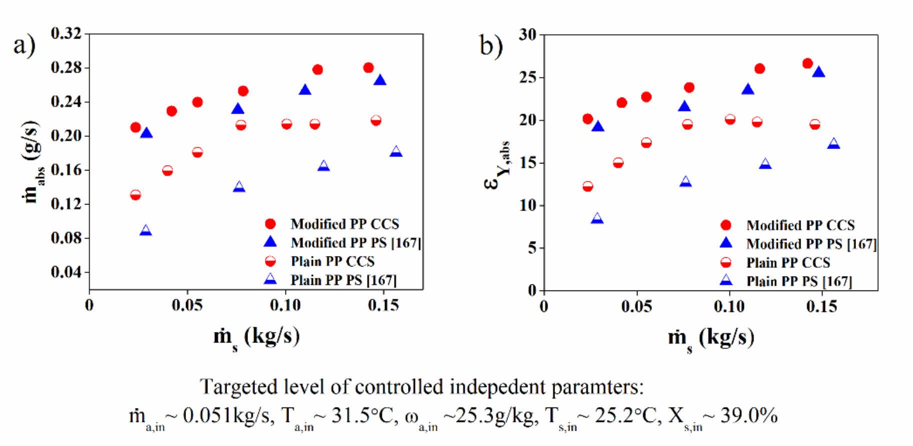

Fig. 4.1 Influence of the mass flow rate of solution on a) dehumidification rate and b) dehumidification effectiveness.

Fig. 4.2 (a, a’) and (b, b’) show the thermal images of the flow over Plain PP CCS at the flow rates of 0.040 and 0.077 kg/s, respectively. The CCS wetness attains 100% saturation at a much lower flow rate in comparison to the Plain PP PS (Fig. 3.1). Unlike, the PS in which liquid film rapidly contracts in the flow direction from top to bottom [165], the film contraction in the downward direction is very small for the CCS. Liquid spreads effectively on the radial surface and the nature of the surface helps in frequent interactions of the isolated liquid rivulets – both of the above help stretch the liquid film in the downward direction. More interfacial wetted area available on the CCS surface leads to higher heat and mass transfer between liquid desiccant and air. Besides, intermixing of isolated rivulets may retard the growth of temperature and concentration boundary layer thickness inside the falling film. The heat and mass transfer resistance decreases, which increases the heat and mass transfer between air and liquid desiccant. Therefore, Plain PP CCS demonstrates superior dehumidification characteristics in comparison to Plain PP plates. Fig. 4.2 (c, c’) and (d, d’) show the nature of the liquid film falling on Modified PP CCS. Modified surface (consecutive grooves opposite to the direction of flow) provides additional facilitation of holding the liquid in a stretched position apart of the basic benefits of

CCS (good radial spreading and frequent intermixing of liquid rivulets).

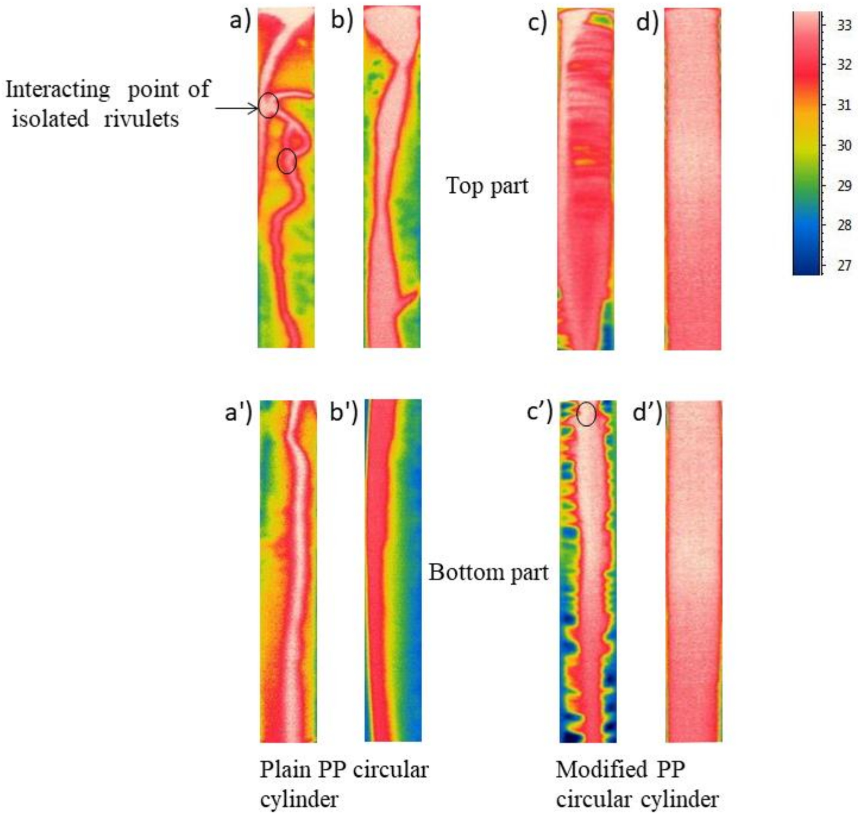

Fig. 4.2 Thermal images of the wetting pattern of Plain (a, a' – b, b') and Modified PP (c, c' – d, d') circular cylinder surfaces at mass flow rates (~0.040 – 0.077) kg/s.

The stretched position of the liquid film does not let the film break into thin liquid rivulets (even at a low flow rate), the absence of free liquid edges is responsible for very high wetness of the CCS at a low flow rate even. A very minute liquid contraction is observed towards the bottom edge of the modified surface at a low flow rate (Fig. 4.2 (c')), and the contraction in that section is even compensated by the interaction of minute liquid rivulets. The surface modification intensified the average dehumidification rate and dehumidification effectiveness of CCS by 36.1% and 38.3%, respectively, and for PS [167] by 74.5% and 76.8%, respectively. Hence, the importance of the surface modification technique is more crucial for a surface associated with poor wetting, i.e., Plain PP PS. The performance indices of the Modified PP CCS was still around 8.4% and 7.8% higher than the best Modified PP PS reported by

Patil [167]. The Modified PP CCS starts enjoying the benefits of high wetness from a very low flow rate and becomes completely wet very soon. Hence, the distinct influence of the increase in dehumidification rate and dehumidification effectiveness is not observed for the Modified PP CCS beyond ($\dot{m}_s > 0.120$ kg/s). The preeminence of the CCS over the PS for falling film towers is evident by the above observation.

4.3.2 Influence of mass flow rate of air

Fig. 4.3 shows the effect of the mass flow rate of air on the dehumidification characteristic of different PP surfaces. As the mass flow rate of air increased from 0.032 to 0.070 kg/s, the dehumidification rate of Plain and Modified PP CCS increased from 0.158 to 0.212 g/s and from 0.198 to 0.293 g/s, respectively. The increase in mass transfer coefficient of air is responsible for the observed behaviours of dehumidification rate. On the contrary, the dehumidification effectiveness for Plain and Modified PP CCS decreased from 23.1 to 14.9% and from 30.5 to 20.4%, respectively. This can be explained as follows: at higher air velocities the duration of the contact time between liquid desiccant and air is shortened as air rapidly comes out of the dehumidification column. Consequently, the outlet air humidity ratio $(\omega_{a,out})$ at the exit of the dehumidifier decreased. Therefore, the dehumidification effectiveness of the column (ϵ_Y) decreases with an increase in the mass flow rate of air. For the studied range of the flow rate, the dehumidification rate and dehumidification effectiveness through Plain PP CCS is found 39.5 – 56% and 41.7 – 53.9% higher than the Plain PP PS. The dehumidification rate and dehumidification effectiveness of the Modified PP CCS is found 19 – 37.5% and 21.5 – 37.2% higher than Plain PP CCS and 9.5 – 20.3% and 10.8 – 20.7% higher than Modified PP PS, respectively. On comparing the dehumidification rate trend of the Plain and Modified PP CCS, it is found that the trend of Plain PP CCS starts saturating at a high flow rate of air. Limited wetting of the basic surfaces seems to be the expected reason behind the observed behaviour, and additional air passes through untreated on the Plain PP CCS. The above trend was not strongly visible between the Plain and Modified PP PS. More uniform and unbiased airflow distribution across the individual falling film in the case of PS may be the expected reason behind it. The above shortcoming of the Plain PP CCS can be compensated by the provision of suitably designed air baffles between the CCS.

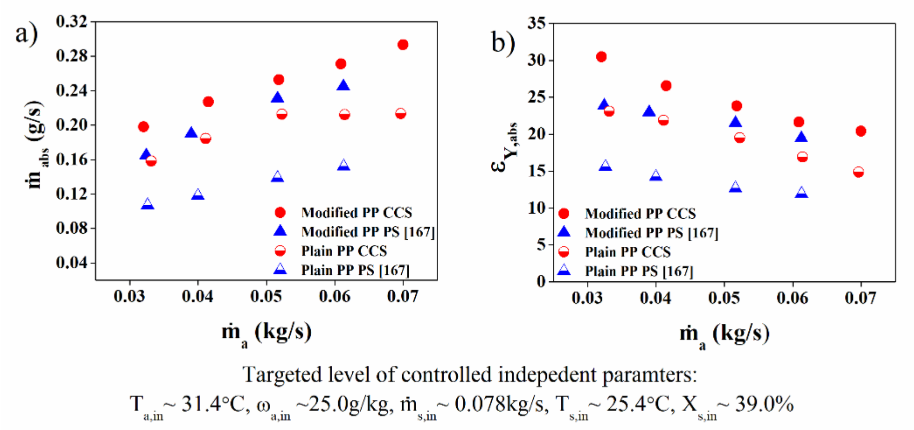

Fig. 4.3 Influence of the mass flow rate of air on a) dehumidification rate and b) dehumidification effectiveness

4.3.3 Influence of liquid desiccant inlet temperature

The influence of the liquid desiccant inlet temperature on dehumidification performance indices of different kinds of PP surfaces is shown in Fig. 4.4. Both the performance indices show a negative trend with an increase in the inlet temperature of the solution. The observed behavior is due to a decrease in mass transfer potential between liquid desiccant and air, as the equilibrium vapor pressure of the solution increases (directly proportional) with an increase in the liquid desiccant inlet temperature. The dehumidification rate and dehumidification effectiveness of the Plain PP CCS is found 41.5 – 63.7% and 48.7 – 71.9% superior to the Plain PP PS. Similarly, dehumidification rate and dehumidification effectiveness of the Modified PP CCS is found 18.9 – 33.0% and 22.3 – 32.5% superior to the Plain PP CCS for the studied range of the solution temperature. Superior wetting characteristics of the associated surfaces are the main reason responsible for the observed behaviour. The solution temperature rise penalty does not have an adverse influence on the dehumidification rate and of the CCS, unlike the PS, and more effective mixing of the desiccant solution on the CCS (due to strong radial spreading and mixing of liquid rivulets) seems to be the expected reason behind it. Following the same reason, the dehumidification rate of the Plain PP CCS becomes superior to Modified PP PS in the high solution temperature zone ($T_s > 29℃$).

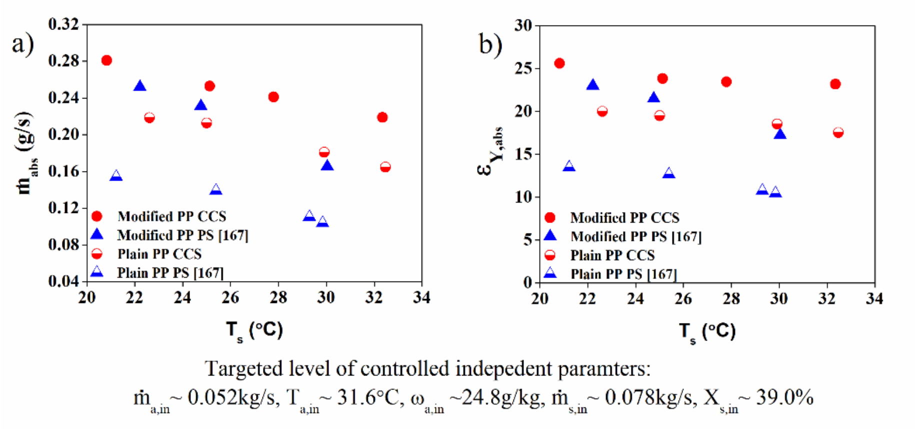

Fig. 4.4 Influence of liquid desiccant inlet temperature on a) dehumidification rate and b) dehumidification effectiveness.

4.3.4 Influence of air inlet temperature

The performance curve for the air inlet temperature of the PS and CCS is shown in Fig. 4.5. The performance behaviour does not reveal a clear distinct trend (almost flat curves) for any of the surfaces. A slight negative trend is observed for the Plain PP PS. Air temperature does not intrude directly in the dehumidification process as the humidity level of the inlet air does not depend on its dry bulb temperature. However, sensibly heating the solution by the air may inflict undesirable negative influence as evident in the case of the Plain PP PS. However, thermophysical properties of air are much weaker than the liquid desiccant solution and thus the above-mentioned reason does not have any visible impact on the performance curve of CCS. Table 4.2 shows the solution outlet temperature at different air temperature. It is clear that increasing air temperature does not have significant impact on the solution outlet temperature.

Table 4.2 Experimental observations at different air temperatures

Sr. No.	$\dot{m}_{a,in}$ (kg/s)	$\dot{m}_{s,in}$ (kg/s)	$\mathbf{T_{a,in}}$ **(^{0}C)**	$T_{a,out}$ (^{0}C)	$T_{s,in}$ (^{0}C)	$\mathbf{T_{s,out}}$ **(^{0}C)**	ϵ_Y (%)
Plain CCS							
1	0.052	0.078	**26.4**	27	25.2	**27.0**	17.5
2	0.053	0.076	**30.9**	30.1	25.0	**27.0**	19.7
3	0.052	0.077	**33.4**	31.8	25.2	**27.5**	16.1
4	0.052	0.078	**35.6**	33.3	25.3	**28.1**	18.8
Modified CCS							
1	0.053	0.078	**27.8**	28.1	25.3	**27.0**	24.7
2	0.052	0.077	**30.7**	30.0	25.3	**27.1**	24.2
3	0.051	0.078	**32.9**	31.5	25.3	**27.3**	24.9
4	0.052	0.077	**35.9**	33.5	25.4	**27.6**	23.8

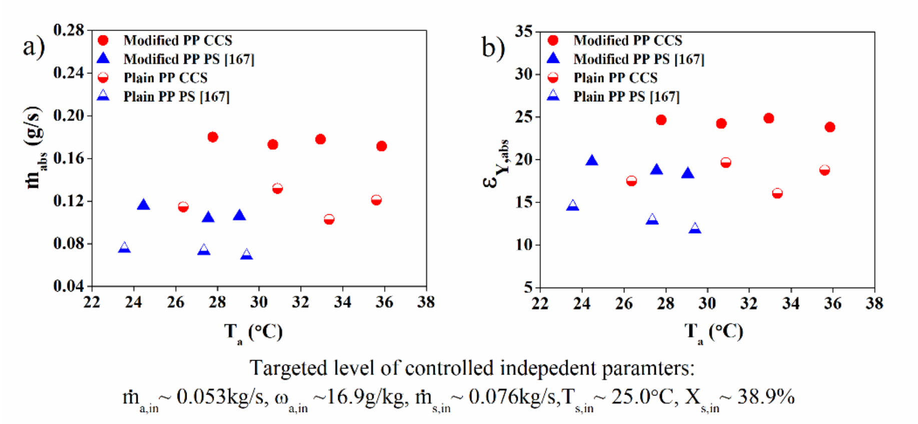

Fig. 4.5 Influence of air inlet temperature on a) dehumidification rate and b) dehumidification effectiveness.

4.3.5 Influence of liquid desiccant inlet concentration

The influence of the desiccant solution concentration on the dehumidification characteristics is presented in Fig. 4.6. The concentration range of 33.0 – 39.0% is targeted in the present study. The equilibrium vapor pressure of the desiccant solution decreases with an increase in the concentration of the desiccant solution, consequently the dehumidification rate increases. The dehumidification rate and dehumidification effectiveness of the Plain PP CCS is found 73.8 – 200.2% and 77.3 – 200.9% higher than the Plain PP PS. Similarly, Modified PP CCS dehumidification rate and effectiveness is found 23.7 – 29.8% and 23.2 – 30.7% higher than the Plain PP CCS for the tested range of the solution concentration. Superior wetting characteristics of the CCS and the formation of a thin and stable film on the modified surface are primarily responsible for the observed behaviour. In contrast to the increasing dehumidification rate trend, the dehumidification effectiveness trend is not much sensitive to the variation in the solution concentration. The dehumidification effectiveness values remained constant around 18.7% and 23.6% for the Plain and Modified PP CCS as the dehumidification rate and maximum possible dehumidification potential both increase with an increase in the solution concentration. The performance of the Plain PP CCS is found better than the Modified PP PS for the entire range of the concentration. As the inlet desiccant solution is kept around ~ 30°C, at high inlet solution temperature, low solution viscosity helps in boosting the performance level of Plain PP CCS to surpass the performance level of the Modified PP PS (Ref. Section 4.3.3). Following the same reason, the performance of Plain PP CCS and Modified PP PS starts approaching again at the higher concentration levels.

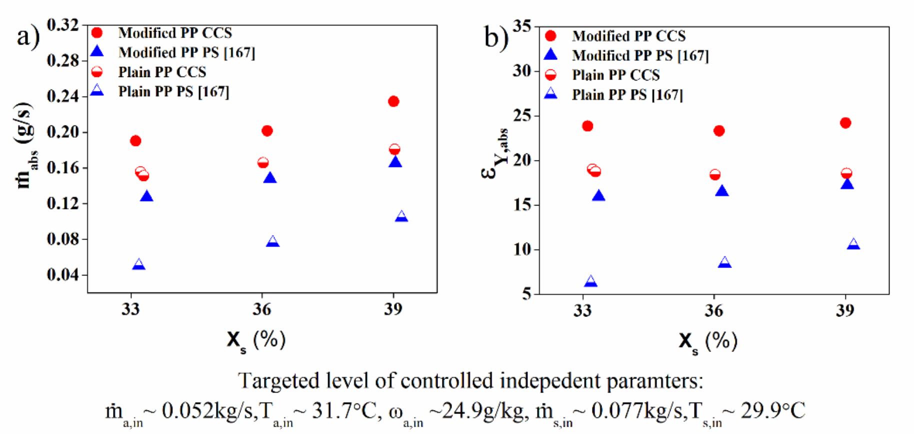

Fig. 4.6 Influence of liquid desiccant inlet concentration on a) dehumidification rate and b) dehumidification effectiveness.

4.3.6 Influence of air inlet humidity ratio

The influence of inlet air humidity on the dehumidification ability is shown in Fig. 4.7. The desiccant at given inlet conditions can better dehumidify the air associated with higher humidity levels. Hence, the dehumidification rate sharply increases with an increase in the humidity of the inlet air. However, the dehumidification effectiveness trend remains flat as the dehumidification rate and maximum potential of mass transfer improve due to an increase in the inlet humidity ratio of the air. With the change in air humidity ratio from 15.3 to 25.9 g/kg, the dehumidification rate of Plain PP CCS enhances from 0.113 to 0.213 g/s, whereas it increases only 0.056 to 0.139 g/s for Plain PP PS [167]. Similarly, the Modified PP CCS intensified the dehumidification rate from 0.136 to 0.253 g/s. The dehumidification rate enhancement offered by the Modified surfaces improves further at the high humidity level in comparison to their basis surface as the highly wetted surface (more interfacial area between desiccant solution and air) facilitates in utilizing the increased mass transfer potential.

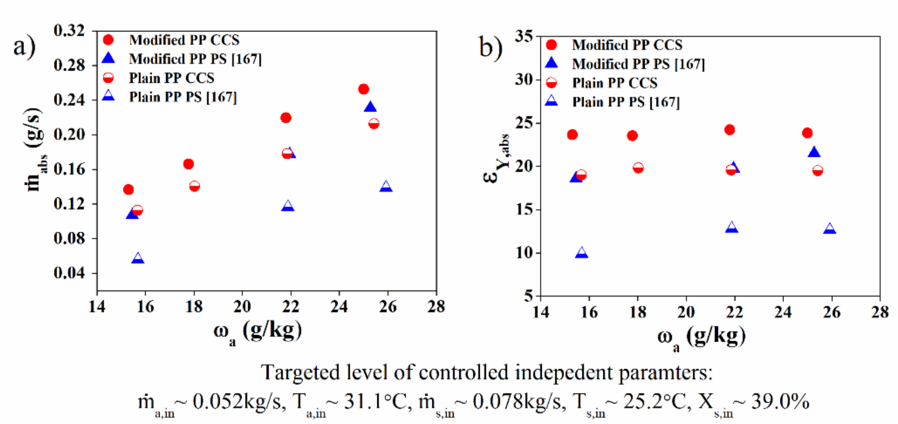

Fig. 4.7 Influence of air inlet humidity ratio on a) dehumidification rate and b) dehumidification effectiveness.

4.4 Regeneration performance analysis

Apart from dehumidification performance, the performance analysis of the regenerator is paramount as most of the energy required in LDS is consumed for concentrating the desiccant solution. The performance of CCS regenerator is extensively investigated and compared with PS regenerator [167] against pertinent parameters of air and solution.

4.4.1 Influence of the mass flow rate of liquid desiccant

Fig. 4.8 shows the influence of the mass flow rate of the liquid desiccant on the regeneration performance indices of the CCS as well as PS. The performance indices increased with an increase in the mass flow rate of the solution on account of three reasons. Firstly, the wetted area of the liquid desiccant on the solid surfaces increased rapidly with the increase in the solution flow rate, which directly improved the regeneration performance. Secondly, the decrease in ω_{eqls} along the bottom of the regeneration tower is reduced as the solution experienced more thermal inertia at higher desiccant flow rates, thus, maintaining higher mass transfer potential $(\omega_{eqls} - \omega_a)$. Lastly, at higher desiccant flow rates the formation of falling film waves increases, which in turn increase the interfacial contact area between liquid desiccant and air. Consequently, the regeneration performance improved. With the increase in mass flow rate of the desiccant solution from 0.055 kg/s to 0.209 kg/s, the regeneration rate and regeneration effectiveness of the Plain PP CCS increased from 0.267 g/s to 0.493 g/s and from 13.1% to 24.2%, whereas for the Plain PP PS [167], the regeneration rate and regeneration effectiveness increased from 0.219 g/s to 0.354 g/s and from 11.4% to 16.3% only. The average regeneration rate and regeneration effectiveness of Plain PP CCS were found to be 36.4% and 40.9% higher than those of the Plain PP PS. The enhanced performance of the CCS can be attributed to its superior wetting characteristics. The performance difference between the Plain PP CCS and Plain PP PS rises rapidly up to 0.153 kg/s; the performance difference between the two surfaces slowed down with a further increase in solution mass flow rate. It is evident from Fig. 3.1 that the CCS reaches saturation (100% wetting) very early in comparison to PS. Further increase in mass flow rate only added up in the liquid film thickness, unlike the addition of the new active surfaces (experiencing simultaneous heat and mass transfer) happening in the case of partial wetted conditions. Hence, the increasing tendency of the performance curves slowed down for the Plain PP CCS earlier.

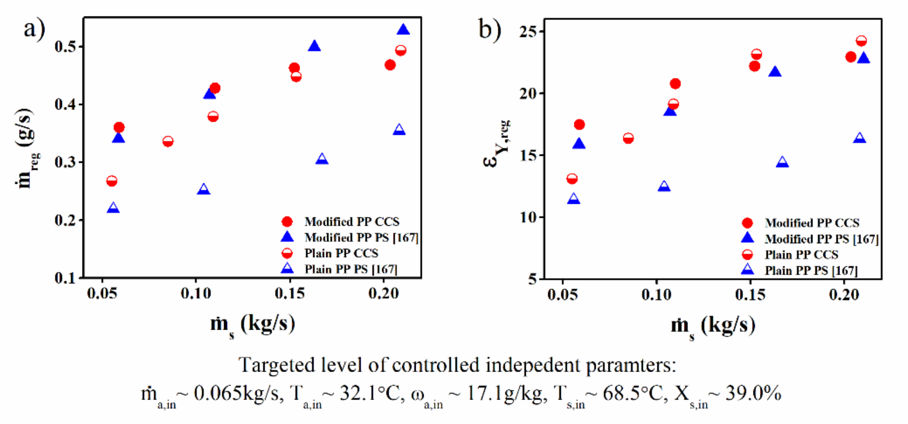

Fig. 4.8 Influence of mass flow rate of liquid desiccant on a) regeneration rate and b) regeneration effectiveness.

The Modified PP CCS - inclined concentric groves (opposite to falling film direction) obstruct the formation of the liquid rim at the free end, thus reducing the rapid contraction of the liquid film. The liquid held inside the groove formed a stationary layer of liquid, which facilitates the formation of stable liquid film on the Modified PP CCS. Further, the groves increase the intensity of the formation of falling film waves on the Modified PP surface. The improved wetting offered by the Modified PP surface helped in uplifting the performance of the circular cylinder. The surface modification improved the performance indices by 11.7% and 8.6% for CCS, and 58.1 % and 44.6% for the PS [167]. The usefulness of surface modification is found more dominant for surfaces having poor wetting characteristics. Since the CCS enjoys superior wetting characteristics to the PS, the modified circular cylinder surface exhibited lesser improvement in the performance indices of the regeneration process. As flow rates increased, the performance difference between Modified and Plain PP CCS decreased, and both converged at $\dot{m}_s = 0.153\ kg/s$. At this condition operating mass flow rate is well above the saturation limit (100% wetting) of the Plain and Modified PP CCSs (Fig. 3.1). Hence, both the studied surface attained the same performance level. At $\dot{m}_s > 0.153\ kg/s$, the Modified PP CCS showed slightly lesser performance than the Plain PP CCS. It seems to be due to the liquid splashing from the solid surface after 100% wetness condition. As the Modified PP CCS attained 100% saturation condition at a lower flow rate than the Pain PP CCS, it suffered from more liquid splashing at high flow rate conditions in comparison to the Plain PP CCS. The regeneration rate of the Modified PP CCS and Modified PP PS was found almost similar, but at higher flow rates ($\dot{m}_s > 0.110\ kg/s$) the Modified PP PS performed slightly better. The regeneration effectiveness of the Modified PP CCS was still around 5.8% higher than the Modified PP PS. This inconsistency in regeneration rate and effectiveness is due to the cumulative effect of other independent parameters, which could not be maintained strictly at the same level in the case of PS [167]. As the onset of saturation occurred much earlier for the circular cylinders, the regeneration effectiveness between the two Modified PP surfaces started to decline at higher flow rates ($\dot{m}_s > 0.153\ kg/s$). The usefulness of the CCS for the development of a low flow falling film tower was quite evident from the above discussions. The selection of a suitable diameter of the circular cylinder is also very important which needs to be decided carefully by considering the wetness curve and the mass flow range of the designed system.

4.4.2 Influence of mass flow rate of air

The influence of the change in the mass flow rate of air on the regeneration performance characteristics of different surfaces is depicted in Fig. 4.9. As the mass flow rate of air is increased from 0.033 kg/s to 0.085 kg/s, the regeneration rate of the Plain PP CCS increased from 0.290 g/s to 0.433 g/s. On the contrary, the regeneration effectiveness decreased from 30.2% to 17.5%. Similarly, the regeneration rate increased from 0.357 g/s to 0.527 g/s and regeneration effectiveness decreased from 35.4% to 19.7% for the same range of air mass flow rate for the Modified PP CCS. The increase in the mass transfer coefficient and reduction in the contact time between liquid desiccant and air are primarily responsible for the observed regeneration rate and regeneration effectiveness trends. The average regeneration rate and regeneration effectiveness of Plain PP CCS were found to be 39.4% and 42.8% higher than the Plain PP PS and the average regeneration rate and regeneration effectiveness of the Modified PP CCS were found 18.2% and 12.6% higher than the Plain PP CCS for the studied conditions. On comparing the regeneration rate curve of Plain and Modified CCS, it can be found that the Plain CCS curve saturated at higher air flow rates for $\dot{m}_a > 0.0764\ kg/s$, whereas the performance curve of the Modified CCS varied linearly. The stable and uniform thickness of the liquid film on the Modified PP CCS at high air flow rate seems to be the expected reason behind the observed behaviour.

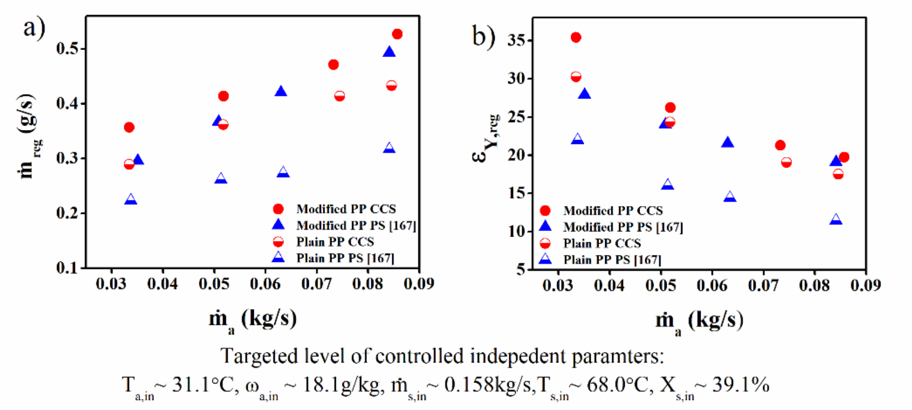

Fig. 4.9 Influence of mass flow rate of air on a) regeneration rate and b) regeneration effectiveness

The average regeneration rate and regeneration effectiveness of the Modified PP CCS were found to be 12.2% and 10.8% higher than the Modified PP PS. The regeneration rate of the Modified PP CCS and Modified PP Plate achieved the same level at higher air mass flow rates. The above observation seems to be influenced by the non-uniform distribution of air across the CCS at higher flow rates. Therefore, the regeneration rate of the Modified PP CCS did not increase as rapidly as it increased for the Modified PP PS. However, a similar difference in the regeneration rate is not observed in the case of their Plain surfaces. Poor wetting of the Plain PP PS seems to be responsible for the observed behaviour. The performance of the CCS can be improved further at a high flow rate with the provision of suitably designed air baffles for the uniform distribution of air across the CCS.

4.4.3 Influence of liquid desiccant inlet temperature

The influence of the increase in liquid desiccant temperature on regeneration performance is shown in Fig. 4.10. The regeneration rate increased, whereas the regeneration effectiveness decreased with an increase in inlet solution temperature. The increasing trend of regeneration rate is due to an increase in the mass transfer driving potential on account of an increase in ω_{eqls} with solution temperature. The decreasing trend of regeneration effectiveness can be explained using Eq. (4.4), although, with the increase solution temperature, the change in the humidity ratio of air across the regeneration tower increased; the increase in the denominator due to an increase in ω_{eqls} was comparatively higher than the numerator. For the studied range, the regeneration rate and regeneration effectiveness of the Plain PP CCS were found to be 53.6 – 80.4% and 54.2 – 62.7% superior to the Plain PS. On average, the relative enhancement in the performance indicators offered by the Plain PP CCS over the Plain PP PS was 68.6% and 58.1%, respectively. The average regeneration rate and regeneration effectiveness of the Modified and Plain PP CCS were 0.497 g/s and 23.0% respectively. The Modified PP CCS surface offered 3.5% and 9.4% improvements over Modified PP PS. The performance of the Modified PP CCS and the Modified PP PS reached almost at the same level for solution temperatures $T_s > 68$℃. The better spreading of the desiccant solution on the solid surface at high temperature seems to be the expected reason due to a decrease in the viscosity of the solution. Therefore, at high regeneration temperatures, the performance of the Modified PP PS started approaching the performance of the CCS. Unlike the CCSs, the performance difference of the PSs diverges at high solution temperatures due to the poor wetness characteristics of the PS.

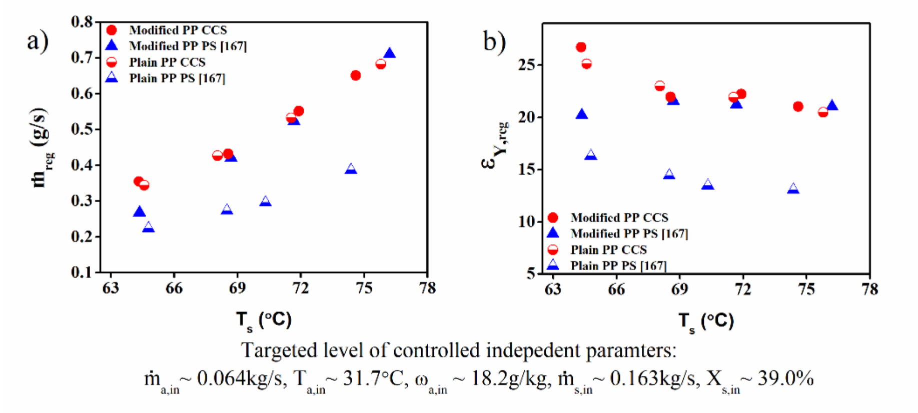

Fig. 4.10 Influence of liquid desiccant inlet temperature on a) regeneration rate and b) regeneration effectiveness

4.4.4 Influence of inlet air temperature

Fig. 4.11 shows the regeneration performance when the inlet air temperature varied from 30.4°C to 44.2°C. In the current study, the operating desiccant flow rate was almost 2.4 times the airflow rate and additionally, the specific heat of the desiccant is almost 3 times compared to that air. Hence, the inlet air temperature did not have a significant impact on both the performance indices of studied surfaces. The regeneration rate and regeneration effectiveness of the Plain PP CCS were found 54.6 – 64.6% and 51.0 – 72.7% higher than the Plain PP PS for the tested range of inlet air temperature. As the operating solution mass flow and its temperature were high, the performance level of the Plain and Modified PP CCS and Modified PP PS was found to be almost equivalent.

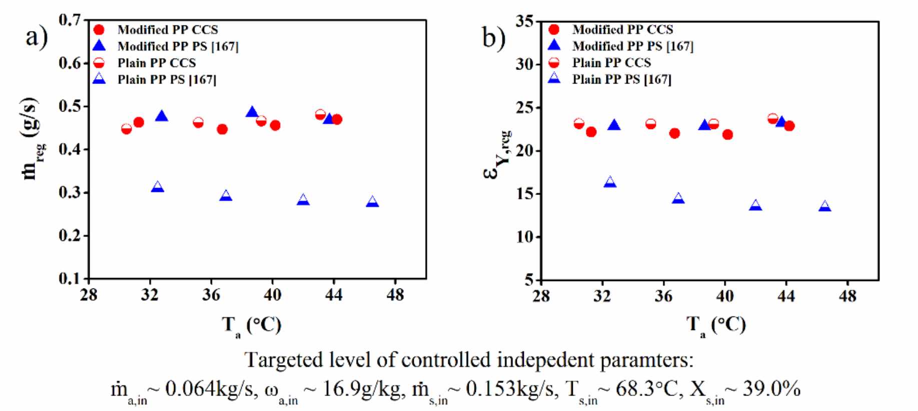

Fig. 4.11 Influence of inlet air temperature on a) regeneration rate and b) regeneration effectiveness

4.4.5 Influence of liquid desiccant inlet concentration.

The influence of the liquid desiccant inlet concentration on regeneration performance is presented in Fig. 4.12. For the studied desiccant solution concentration range from 34.2 to 42.3%, the regeneration rate of the Plain and Modified PP CCS decreased from 0.684 g/s to 0.310 g/s and from 0.670 g/s to 0.321 g/s, respectively. On the contrary, the regeneration effectiveness of the Plain and Modified CCS increased from 20.3% to 23.7% and from 19.7 to 24.4%, respectively. The observed performance trend can be attributed to a decrease in the mass transfer driving potential across the regeneration tower due to a decrease in the ω_{eqls}. As the concentration of the solution increased, the ω_{eqls} decreased due to the decrease in the surface vapor pressure of the desiccant solution. The regeneration rate and effectiveness of the Plain PP CCS were found 18.6 - 47.5% and 25.5 - 61.1% higher than the Plain PP PS. The regeneration effectiveness curve of the Plain PP CCS showed slight saturation at higher concentration levels. The increase in viscosity and surface tension of desiccant solution at higher concentration levels might be the expected reason. Unlike the Plain PP PS, the rest of the other surfaces could sustain the negative impact of the above parameters due to their high wetness. Marginally lower regeneration rate performance of Modified PP CCS with respect to Modified PP PS was due to the slightly higher operating solution temperature of the Modified PP PS ($T_s = 69.7$℃).

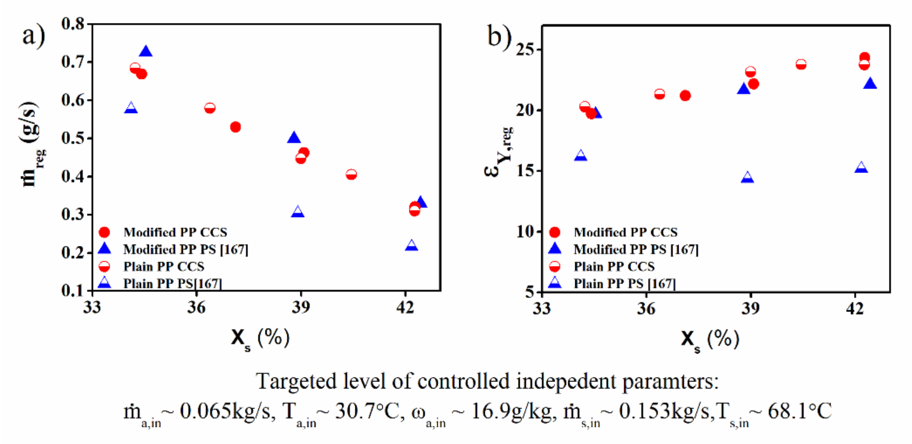

Fig. 4.12 Influence of liquid desiccant inlet concentration on a) regeneration rate b) regeneration effectiveness

4.4.6 Influence of inlet air humidity ratio.

Fig. 4.13 demonstrates the behaviour of different PP surfaces with the increase in inlet air humidity ratio. The regeneration rate and regeneration effectiveness showed a decreasing trend with an increased inlet humidity ratio of air. The potential for mass transfer between liquid desiccant and air decreased as the inlet air humidity ratio increased. Consequently, both performance indices showed a decreasing trend. It was found that the regeneration rate and regeneration effectiveness of the Plain PP CCS outperformed the Plain PP PS from 62.1% to 91.7% and from 64.9% to 83.9% for the studied range of conditions. The Modified PP CCS offered 5.2% and 6.3% improvement in regeneration rate and regeneration effectiveness against Modified PP PS. At high inlet air humidity ratio conditions, the performance of the CCSs was found higher than Modified PP PS. Hence, CCS-based regenerators can effectively tolerate the high offload outlet humidity conditions as compared to the Modified PP PS, which is indeed governed by the superior wetting characteristics of the CCS compared to the PS. No significant difference was observed in the behaviour of Plain and Modified PP CCS.

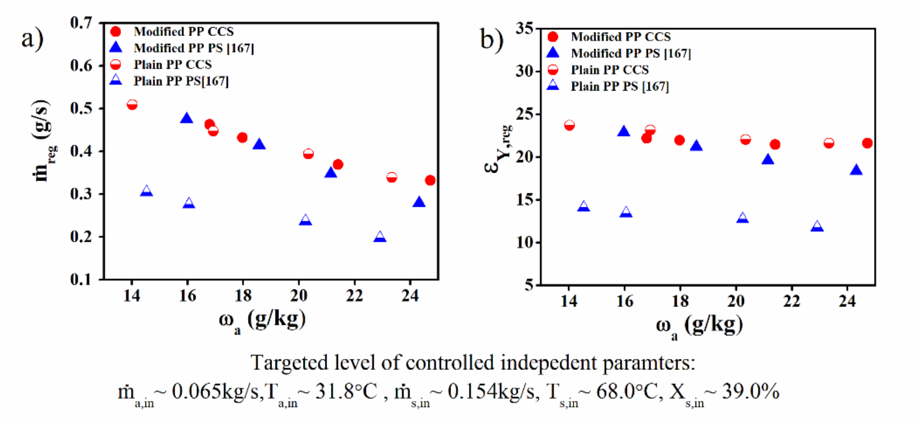

Fig. 4.13 Influence of inlet air humidity ratio on a) regeneration rate b) regeneration effectiveness.

4.5 Regeneration study of CCS at low flow rate conditions

During the regeneration experiments on the CCS surface reference operating flow rate of the desiccant solution was kept at $\dot{m}_s \sim 0.160\ kg/s$ to compare CCS with PS surface performance reported by Patil [167]. It was found that the surface modification offered an average improvement of around 4.0% and 3.4% in regeneration rate and effectiveness for the CCS surface at this operating condition. However, the same surface modification enhanced regeneration rate and effectiveness of poorly wetted PS [167] by 52.3% and 47.5% respectively. Therefore, separate regeneration experiments are conducted at low mass flow rate of the desiccant solution ($\dot{m}_s \sim 0.060\ kg/s$) to prove the usefulness of surface modification at partial/incomplete wetting conditions for CCS.

4.5.1 Influence of mass flow rate of air

Fig. 4.14 shows the influence of mass flow rate of air on the performance of Plain PP CCS and Modified CCS at a low mass flow rate of desiccant solution($\dot{m}_s \sim 0.60\ kg/s$). When the mass flow rate of air increased from 0.030 kg/s to 0.065 kg/s, the regeneration rate of the Plain PP CCS and Modified PP CCS increased from 0.189 g/s to 0.267 g/s and from 0.284 g/s to 0.360 g/s. The modified CCS surface offered an average improvement of 44% for the studied range of air flow rate. The improvement in the air side mass transfer coefficient is responsible for an increase in the regeneration rate. On the contrary, the regeneration effectiveness of the Plain PP CCS and Modified PP CCS decreased from 21.2% to 13.1% and from 29.6 % to 17.5% for the studied air mass flow rate range. The modified CCS surface offered an average improvement of 34.4% in regeneration effectiveness compared to the plain CCS surface for the studied range of air mass flow rate. The shorter residence time of air-liquid interaction with an increase in air mass flow rate is the reason for the observed effectiveness trend. Superior wetting offered by the Modified PP CCS at a low desiccant flow rate is the responsible reason behind improved regeneration rate and regeneration effectiveness.

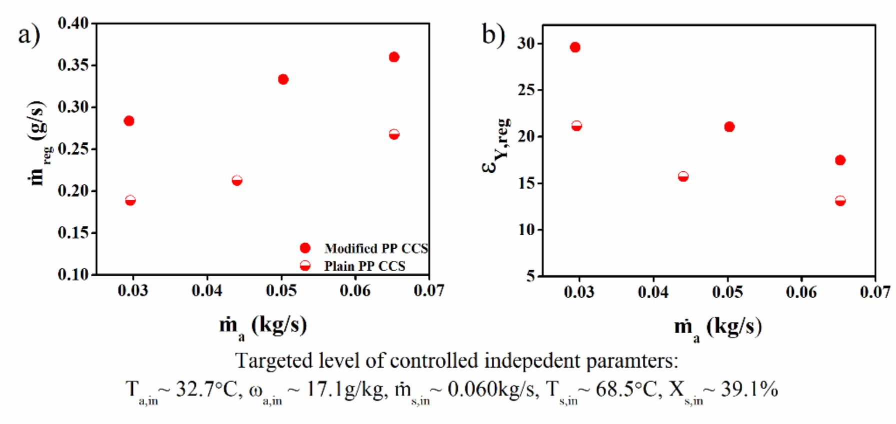

Fig. 4.14 Influence of mass flow rate of air on a) regeneration rate and b) regeneration effectiveness

4.5.2 Influence of liquid desiccant inlet temperature

Fig. 4.15 describes the behaviour of PP surfaces under the impact of varying the inlet desiccant solution temperature. With an increase in the solution temperatures, the ω_{eqls} increases due to an increase in the vapor pressure of desiccant solution. Therefore, the regeneration rate of both surfaces increases with an increase in the desiccant solution temperature. The Modified surface offered around 42.6% average improvement in the regeneration rate compared to the Plain CCS surface. For the regenerator effectiveness performance parameter, mismatching trends are observed for the Plain and Modified CCS surfaces. The performance index slightly increases for the Plain PP CCS surface, whereas for the

Modified PP CCS surface, an almost flat trend is observed. The poor wetness characteristics of the Plain PP CCS surface and positive influence of solution flow rate on the spreading of liquid over the surface (due to a decrease in viscosity of the solution) seem to be the expected reasons behind the observed behaviour.

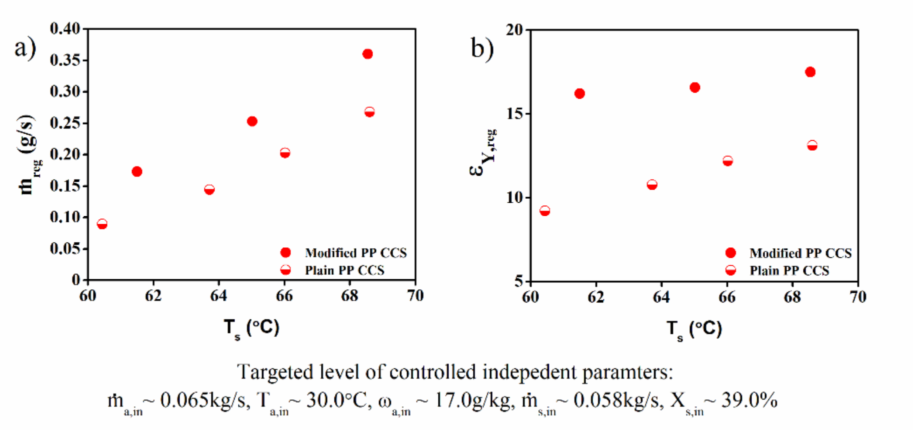

Fig. 4.15 Influence of liquid desiccant inlet temperature on a) regeneration rate and b) regeneration effectiveness

4.6 Effectiveness correlations for dehumidifiers and regenerators

From survey of previously studies is found that the majority of the effectiveness models were developed for packed bed towers [71,73,138,140–143,146], whereas falling film tower correlations are limited [100,147]. Empirical correlations of the packed bed immensely over predicted in case used for falling film towers experimental observation. As packed bed towers operate at very large $\dot{m}_s/\dot{m}_a$, large $\dot{m}_s$ clasps the influence of remaining important independent variables. Stability of the liquid film is another concern, unlike the packed bed, falling film tower performance is mainly governed by the stability of falling liquid films. Empirical correlations of falling film are expected to be more predominantly governed by the thermophysical properties of the desiccant solution. Hence, more correlations for the falling film tower are required for the future development and use of the towers in liquid desiccant area. Existing falling film correlations were developed following experimental observation on metallic/plastic PS only. These correlations failed to distinguish the performance difference arising due to change in the geometry of the basic solid surfaces. Consequently, a new correlation is required to succeed that demands.

4.6.1 Development of dehumidification effectiveness correlation

From experimental analysis, it is obvious that different operating parameters of air and desiccant solution have varying degrees of influence on dehumidification effectiveness. Hence, all the influencing parameters form air side ($\dot{m}_{a,in}, T_{a,in,} \omega_{a,in}$) and solution side ($\dot{m}_{s,in,} T_{s,in}, \omega_{eqls}$) are considered for the model development. As the desiccant systems work on the simultaneous heat and mass transfer processes. Two non-dimensional parameters: heat transfer potential between the desiccant solution and air $\left(\frac{h_{s,in}-h_{a,in}}{h_{s,in}}\right)$ and mass transfer potential between them $\left(\frac{\omega_{a,in}-\omega_{eqls,in}}{\omega_{eqls,in}}\right)$ are included as controlling parameters in the present correlation. As simple temperature difference potential $\left(\frac{T_{s,in}-T_{a,in}}{T_{s,in}}\right)$ does not map the nature of simultaneous heat and mass transfer operation, and it generates intruding undesired mathematical inconsistency with actual experimental observation. Hence, enthalpy potential is used in the current model. To incorporate the wetting characteristic difference of the plastic and metallic surfaces; surface free energy of the solid surface γ_c is used. The liquid hold up inside the grooves of the Modified PP surfaces tries to decelerate the falling film flowing over it by applying opposing shear force (drag). Hence, the ratio of shear force to gravity force is included to capture the difference of fluid flow behaviour over the Plain and the Modified PP surfaces. The shear force is determined by Eq. (4.5) following Wang and Tian [168], and its estimation method for Modified PP surfaces is shown in Fig. 4.16. The film thickness on PS and CCS is obtained from Nusselt (Eq. (4.6)) and Brauer (Eq. (4.7)) film thickness correlation [169], respectively. The gravity force is calculated using Eq. (4.8). The mass flow rate of air and solution are included as independent parameters considering the large difference in the thermodynamic properties of air and desiccant solution. In addition, $\left(1+\frac{T_{s,in}}{T_{w,in}}\right)$ is utilized to differentiate the effectiveness between adiabatic and non-adiabatic systems. The additional term becomes unity $\left(T_{w,in} = 0\right)$ for adiabatic studies.

$$F_\tau = \mu_s \frac{0.99V}{\delta} A \tag{4.5}$$

$$\delta_{plate} = 0.909 \left(\frac{\mu_s^2}{\rho_s^2 g}\right)^{1/3} Re_s^{1/3} \tag{4.6}$$

$$\delta_{circular\ cylinder} = 0.532 \left(\frac{\mu_s^2}{\rho_s^2 g}\right)^{1/3} Re_s^{1/3} \tag{4.7}$$

$$F_g = \rho_s\, g \delta A \tag{4.8}$$

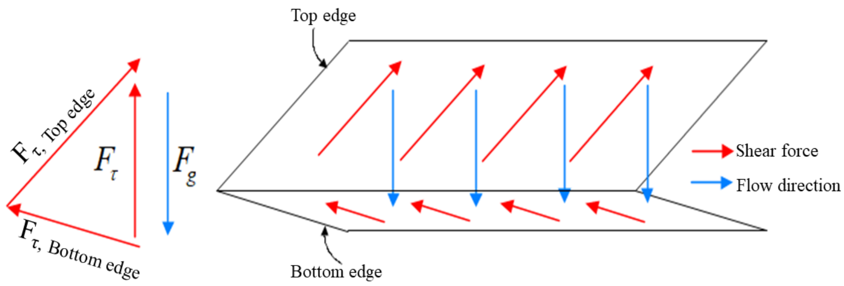

Fig. 4.16 Representation of shear force acting on the Modified PP surfaces

For regression analysis two experimental datasets i.e. one plastic adiabatic (current study) and one metallic non-adiabatic [89] are utilized so that the developed correlation can predict the behaviour of both adiabatic and non-adiabatic experimental observations of plastic/ metallic surfaces. Eq. (4.9) presents the newly developed dehumidification effectiveness correlation for the falling film towers.

$$\varepsilon_{Y,abs} = 0.024 \left(\frac{F_\tau}{F_g}\right)^{0.306} \gamma_c^{0.337} \left(\frac{A_{ext}}{A}\right)^{0.400} \left(\dot{m}_{a,in}\right)^{-0.330} \left(\dot{m}_{s,in}\right)^{0.185}$$

$$\left(\frac{h_{s,in}-h_{a,in}}{h_{s,in}}\right)^{-0.043} \left(\frac{\omega_{a,in}-\omega_{eqls,in}}{\omega_{eqls,in}}\right)^{0.058} \left(1+\frac{T_{s,in}}{T_{w,in}}\right)^{-0.076} \tag{4.9}$$

4.6.1.1 Performance of dehumidification effectiveness correlation

The current model performance is compared with past existing correlations of packed bed tower [73] and falling film tower [100,147] against eight falling film dehumidification studies. Table 5.2 presents the summary of the comparison between the current correlation and the existing past correlations on MAPE (Eq. (4.10)) basis. Only in experimental datasets of Wen et al. [100] and Wen and Lu [56] the performance of the current correlation slightly lags behind the Wen et al. [100] correlation. Also, the current model scores ~1.5% superior to Patil [167] correlation, and it capably captures the behaviour of plate and cylindrical surface, unlike the Patil [167] correlation. For the evaluated experimental datasets, the MAPE of the current model is 11.7%.

$$MAPE\ (\%) = \frac{\sum_1^N \left| \frac{\varepsilon_{Y,exp} - \varepsilon_{Y,pred}}{\varepsilon_{Y,exp}} \right|}{N} \text{ x } 100 \qquad (4.10)$$

Table 4.3 Comparison of the current dehumidification effectiveness correlation with existing correlations.

Experimental studies	Type of tower	No. of data points	Correlation by authors				
			Packed bed correlation	Falling Film correlation			
			Wang et al. [73]	Qi et al. [147]	Wen et al. [100]	Patil [167]	Current model
Patil [167]	Adiabatic	33	319.6	74.6	41.8	15.5	17.6
Current study		47	184.0	79.4	23.4	34.9	4.7
Wen et al. [89]	Non-adiabatic	85	363.6	68.4	19.6	16.6	7.3
Wen et al. [100]		100	363.7	68.8	7.6	21.0	11.8
Wen et al. [49]		129	393.8	65.8	17.5	7.4	15.0
Wen et al. [50]		154	371.3	67.8	11.1	6.5	10.9
Wen and Lu [51]		59	422.1	60.5	19.1	12.1	19.3
Wen et al. [52]		53	377.5	74.1	7.3	8.8	6.5
Overall MAPE			362.7	68.6	15.7	13.4	11.7

Fig. 4.17 shows the comparison between predicted and experimental dehumidification effectiveness for the current correlation against eight datasets. Around 83.3% of data points lie within the error band of ±20% for the current model, while it is 72.3% and 74.4% for Wen et al. [100] and Patil [167] model respectively. The dehumidification effectiveness model is tested for the following range of the operating parameters: $\dot{m}_{a,in} = 0.021 - 0.070$ kg/s, $\dot{m}_{\mathrm{s,in}} = 0.023 - 0.178$ kg/s, $T_{a,in} = 23.5 - 36.7$°C, $T_{s,in} = 20.8 - 35.3$°C, $\omega_{a,in} = 15.2 - 26.0$ g/kg, $X_{s,in} = 25 - 40$ % (LiCl) and 70.3 % (KCOOH).

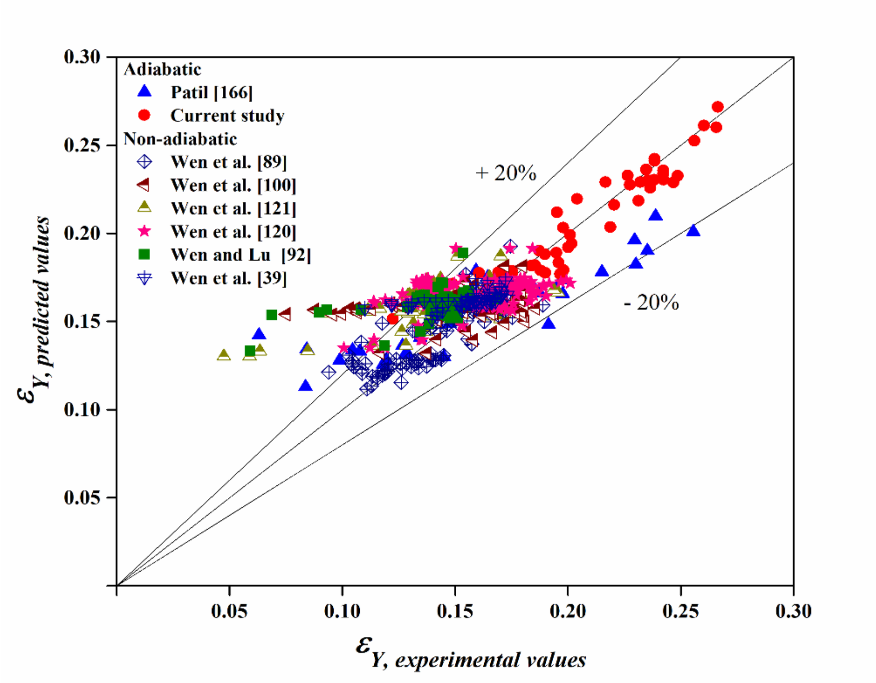

Fig. 4.17 Comparison between predicted dehumidification effectiveness of present correlation with different experimental datasets

4.6.2 Development of regeneration effectiveness correlation

The regeneration process is driven by the simultaneous heat and mass transfer between air and desiccant. The magnitude of both heat and mass transfer driving potential plays a significant role in the regeneration process. Hence, two driving parameters in non-dimensional form; sensible heat transfer potential $\left(\frac{T_{s,in} - T_{a,in}}{T_{a,in}}\right)$ and mass transfer potential

$\left(\frac{\omega_{eqls,in}-\omega_{a,in}}{\omega_{eqls,in}}\right)$ between solution and air were considered in the model equation. The significant of the rest parameters is explained in previous section 4.6.1. The newly proposed regeneration effectiveness correlation for the falling film towers is shown in Eq. (4.11).

$$\varepsilon_{Y,reg} = 0.379\left(\frac{F_s}{F_g}\right)^{0.302}\left(\frac{\gamma_c}{\gamma_s}\right)^{0.406}\left(\frac{A_{ext}}{A}\right)^{0.273}\left(\dot{m}_{a,in}\right)^{-0.012}\left(\dot{m}_{s,in}\right)^{0.086}$$

$$\left(\frac{T_{s,in}-T_{a,in}}{T_{a,in}}\right)^{-0.051}\left(\frac{\omega_{eqls,in}-\omega_{a,in}}{\omega_{eqls,in}}\right)^{0.566}\left(1+\frac{T_{w,in}}{T_{s,in}}\right)^{-0.031} \tag{4.11}$$

4.6.2.1 Performance of regeneration effectiveness correlation

The performance of the current correlation was evaluated against nine experimental studies and its performance was further compared with existing correlations. Table 4.4 presents the performance comparison between the current and the existing falling film correlations. The current model showed good prediction accuracy for all the validated datasets. The MAPE of the current model for nine datasets was 16.5%, which was 7.0% lower than the next best model of Wen et al. [101] out of available correlation in the open literature. Around 66.7% and 78.7% of the data points were within the error band of ±20% and ±30% respectively, for the current model, while both were 57.0% and 67.5% for the model reported by Wen et al. [101].

Table 4.4 Summary of comparative performance analysis of the present and previous regeneration effectiveness correlations

Experimental study	Yin et al. [82]	Patil [167]	Present study	Yin et al. [82]	Yin et al. [132]	#Mun et al. [107]	Wen et al. [170]	Wen et al. [101]	Wen et al. [136]		Overall MAPE
Data points (U/A)	18/18	39/39	43/43	26/26	10/10	16/32	121/121	90/90	42/42	46/46	
Desiccant	LiCl	LiCl	LiCl	LiCl	LiCl	LiCl	LiCl	LiCl	LiCl	KCOOH	
Tower	Adiabatic			Non-adiabatic							
Prediction of correlations against the experimental dataset (MAPE)											
Patil [167]	18.9	15.3	46.9	9.3	12.8	13.2	53.7	27.4	64.6	307.0	65.0
Wen et al. [101]	36.1	37.9	52.6	50.1	22.7	52.2	15.5	11.3	14.5	6.2	23.5
Current model	14.0	14.1	16.0	28.8	17.2	12.6	18.7	15.4	14.9	11.5	16.5

Data points with $\left(\frac{\dot{m}_{s,}}{\dot{m}_a} < 0.1\right)$not considered, U/A- utilized /available data points.

Fig. 4.18 shows the comparison between the predicted and experimental regeneration effectiveness for the current correlation against nine datasets. The current model is tested for the following range of the operating parameters: $m_{a,in} = 0.020 - 0.090\ kg/s,\ m_{s,in} = 0.003 - 0.210\ kg/s,\ T_{a,in} = 21 - 46.5$°C, $T_{s,in} = 48 - 77.1$°C, $\omega_{a,in} = 6.3 - 24.9\ g/kg$, $X_{s,in} = 25 - 42.4\ \%\ (LiCl)$, and 68% $(KCOOH)$.

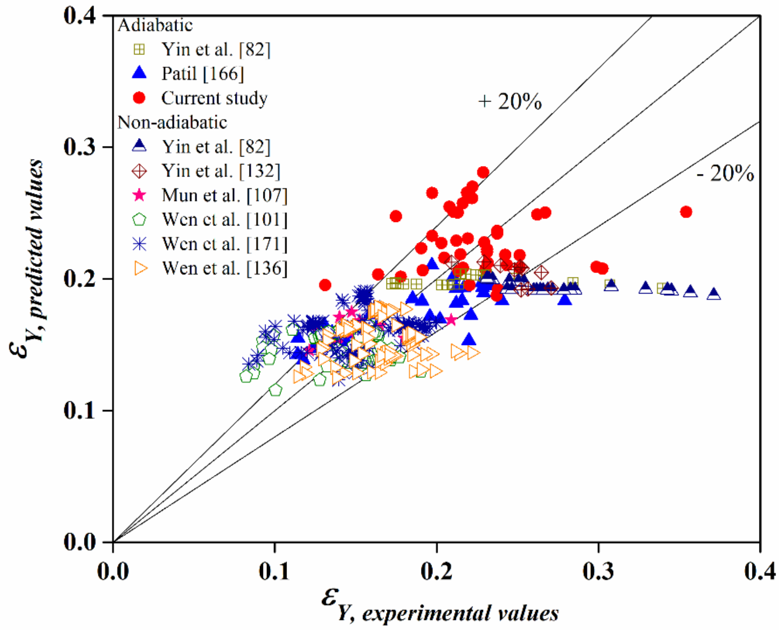

Fig. 4.18 Comparison between the predicted regeneration effectiveness of current correlation with different experimental datasets.

4.7 Conclusion

Experimental investigation on the dehumidification and regeneration performance of vertical PP CCS was carried out in this study, and a comparison between CCS and PS was also presented under the influence of pertinent parameters of air and desiccant solution. The dehumidification/regeneration rate and dehumidification/regeneration effectiveness were used as the performance indicators. The followings are the main conclusions drawn from the current Chapter.

1. The Plain PP CCS surface provided 21.0 – 200.0% and 13.9 – 196.7% improvement in the dehumidification rate and dehumidification

effectiveness in comparison to the Plain PP PS. Similarly, it offered 18.6 – 91.7% and 14.9 – 83.9% improvement in the regeneration rate and regeneration effectiveness over the Plain PP PS.

2. Modified PP CCS offered dehumidification rate and dehumidification effectiveness improvement of 18.2 – 61% and 18.9 – 64.8% over Plain PP CCS whereas the Modified PP PS offered 38.1 – 128.7% and 49.3 – 152.4% improvement over poorly wetted Plain PP PS. However, the same modified surface could offer improvement of 1.1 – 34.5% and 1.3 – 33.4% only in the regeneration rate and regeneration effectiveness compared to the Plain PP CCS. The operating mass flow rate above 100% surface wetting condition was identified as the expected reason behind it. Hence, another set of regeneration experiments are carried out at ~60% wetting condition for both the CCS surfaces, 22.9 – 84.5% and 28.0 – 80.3% improvement in the regeneration rate and regeneration effectiveness was observed for the Modified PP CCS surface. Hence, it is established that the performance enhancement through surface modification techniques is more extrusive for surfaces with poor wetness and operating at partial wetted conditions.

3. Two parameters, including mass flow rates of solution and air, showed a strong influence on the performance indices of PP solid CCS.

4. Spilling of the desiccant solution at high solution flow rates and non-uniform biased airflow distribution across solid surfaces are identified as the two main limitations of the CCS. Hence, proper size selection based on the liquid flow rate across the dehumidifier/regenerator is very crucial in case CCS are used as desiccant- air contact facilitator.

5. A generalized dehumidification effectiveness is proposed to predict the predict the performance of adiabatic and non-adiabatic falling film tower using enthalpy potential, mass transfer potential, non-dimensional parameters influencing wetness of the solid surface, mass flow rate of the solution and mass flow rate of the air. The proposed correlation predicted 83.3% data points of eight experimental dehumidification studies (two adiabatic and six non-adiabatic) within an error band of ±20% for 660 number of experimental readings.

6. Similarly, a new empirical correlation has been developed for the regeneration effectiveness of falling film towers. The developed regeneration effectiveness correlation showed a good prediction response, 66.7% data out of 451 number of experimental readings (taken from nine different experimental studies) are within ±20% error band. In comparison to the dehumidification correlation, the regeneration correlation showed poor predictability. The above is possibly due to a significant variation in solution operating parameters for regenerators, unlike dehumidifiers.

CHAPTER 5

HEAT AND MASS TRANSFER CHARACTERISTICS

5.1 Introduction

Extensive studies on heat and mass transfer coefficient analysis have been reported on packing bed LDS while for falling film tower it is comparatively less and that too on regeneration process is almost nil. Moreover, the existing heat and mass transfer correlation are not suitable for simulation/modelling of low flow plastic falling film dehumidifier/regenerator. From experimental dehumidification and regeneration investigations in Chapter 4, it is found that that the circular cylinder surface is more superior than plate surface for the development of low flow falling film dehumidifiers and regenerators. However, in addition to performance analysis of dehumidifier and regenerators, evaluation of heat and mass transfer coefficient of plastic CCS is essential for progress and development of low flow plastic falling film LDS. This chapter aims to comprehensively investigate the heat and mass transfer behaviour of CCS for dehumidification and regeneration process using numerical finite difference method. Apart from the above, new heat and mass transfer coefficient correlation are proposed for dehumidifiers and regenerators. The developed correlation will be useful for design and optimization of low flow falling film liquid desiccant systems.

5.2 Heat and mass transfer coefficient evaluation method

From literature survey, it is found that there are different methods to determine the heat and mass transfer coefficients. These methods have been summarized in Chapter 2 (section 2.14.3).

In the beginning, Chung et al. [61] used numerical integration techniques to determine the mass transfer coefficient of a packed bed tower by using Eqs. (5.1) and (5.2).

$$h'_m = \left(\frac{\dot{m}_a}{aZ}\right) \int_{y_{A,in}}^{y_{A,out}} \frac{(1-y_A)*M}{(1-y_A)(y_A - y_A^*)} dy_A \quad (5.1)$$

$$h_t = \frac{\dot{m}_a (C_{p,air} + Y_A C_{p,w})}{aZ} ln \frac{T_{a,in} - T_i}{T_{a,in} - T_i} \quad (5.2)$$

where, h'_m is the mass transfer coefficeint in unit (Kmol/m^{2}s). However, due to the lengthy numerical procedures, most subsequent researchers used Eq. (5.3) and Eq. (5.4) to calculate the overall heat and mass transfer coefficient associated with the dehumidification and regeneration process.

$$h_t = \frac{Q}{\int_0^L \Delta T(z) W dz} = \frac{Q}{A\, \Delta T_m} \quad (5.3)$$

$$h_m = \frac{\dot{m}_{abs}/\dot{m}_{reg}}{\int_0^L \Delta\omega(z) W dz} = \frac{\dot{m}_{abs}/\dot{m}_{reg}}{A\, \Delta\omega_m} \quad (5.4)$$

where, h_m is the mass transfer coefficient in units g/m^2 s

The most important point in the above Eqs. (5.3) and (5.4) is to determine the average temperature (ΔT_m) and humidity potential ($\Delta\omega_m$) for liquid desiccant-air interaction. Saman and Alizadeh [102], Yin et al. [82], Bansal et al. [59], and Wen et al. [149] calculated mass transfer coefficient following Eq. (5.3), the potential of mass transfer operation ($\Delta\omega_m$) was taken corresponding to the inlet conditions of air and solution $(\omega_{a,in} - \omega_{eqls,in})$ as shown in Eq. (5.5)

$$h_m = \frac{\dot{m}_{abs}}{A\,(\omega_{a,in} - \omega_{eqls,in})} \quad (5.5)$$

Liu et al. [171], Dong et al. [109], and Peng et al. [137] calculated ΔT_m and $\Delta\omega_m$ based on the logarithmic mean temperature and humidity difference as given by Eqs. (5.6) and (5.7).

$$h_t = \frac{Q}{A\, \Delta T_{LMTD}} \quad (5.6)$$

$$h_m = \frac{\dot{m}_{abs}}{A\, \Delta\omega_{LMWD}} \quad (5.7)$$

Where, ΔT_{LMTD} and $\Delta\omega_{LMWD}$ are logarithmic mean temperature and humidity difference calculated as follows

$$\Delta T_{LMTD} = \frac{(T_{s,in}-T_{a,out})-(T_{s,out}-T_{a,in})}{ln\frac{(T_{s,in}-T_{a,out})}{(T_{s,out}-T_{a,in})}} \text{ and}$$

$$\Delta\omega_{LMWD} = \frac{(\omega_{eqls,in}-\omega_{a,out})-(\omega_{eqls,out}-\omega_{a,in})}{ln\frac{(\omega_{eqls,in}-\omega_{a,out})}{(\omega_{eqls,out}-\omega_{a,in})}}$$

Unlike conventional heat exchangers and packed bed columns, the overall heat and mass transfer coefficient based on the inlet or logarithmic potential difference approach is recommended for the falling film tower. As transfer potential (especially mass transfer), observe a drastic change in the slope on account of inadequate cooling/heating before the inlet of dehumidifier/regenerator as well as a significant change in solution temperature due to the heat of condensation/evaporation of water. An evaluation method capable of tracking the changes in temperature (ΔT_m) and humidity potential ($\Delta\omega_m$) along the tower length would give the accurate estimate of heat and mass transfer coefficients.

5.3 Experimental variation of the mass transfer coefficient of the dehumidifier

Fig. 5.1 shows the value of the mass transfer coefficients obtained by applying the above-discussed approaches on experimental observations of [112].

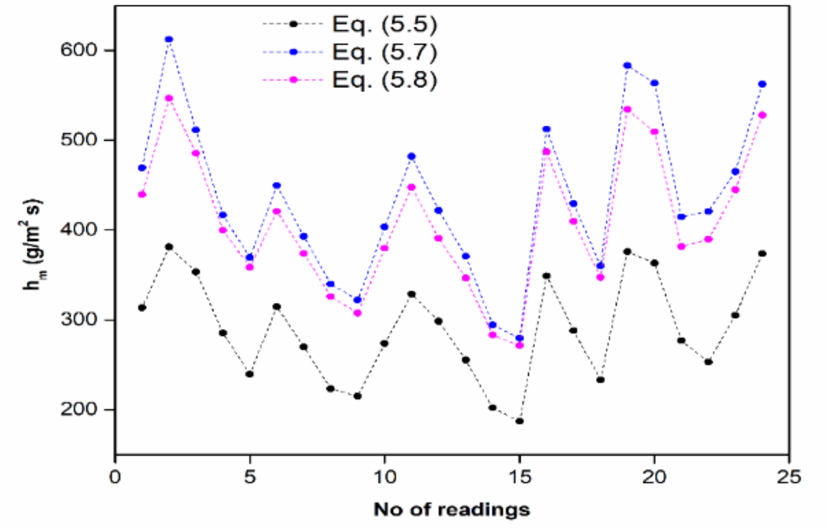

Fig. 5.1 Mass transfer coefficient obtained using (Eqs. (5.5), (5.7) and (5.8)) for experimental readings of Prieto et al. [112].

$$h_m = \left(\frac{\dot{m}_a}{A}\right) \int_{\omega_{a,in}}^{\omega_{a,out}} \frac{(1-\omega_a)*}{(1-\omega_a)(\omega_a - \omega_{eqls})} d\omega_a \tag{5.8}$$

To have consistent units of the mass transfer coefficient for comparison purposes, a modified form of Eq. (5.1) i.e., Eq. (5.8) is utilized. Eq. (5.5) under predicts the mass transfer coefficient. It considers hypothetical mass transfer potential, which is not available in the counter flow and the crossflow designs across any location. It varies continuously along the length of the tower. In analogy to heat exchanger studies, the log mean humidity difference method (Eq. (5.7)) tries to trace the actual humidity profile of air and solution and represent a close approximation to the actual mass transfer coefficient. It is also evident from Fig. 5.1 that although the value obtained from the log mean humidity difference closely follows the numerical integration prediction yet the error between the two goes up to 10.7%. Hence, the mass transfer coefficient in the current study is calculated by the numerical integration approach. A separate code is developed in MATLAB (R2020b) for the mass transfer coefficient calculation using Eq. (5.8), and Simpson's 3/8 method is used for numerical integration purposes. Later on, the same code is used to calculate the mass transfer coefficient of different experimental datasets [28,89,91,100,121,122,137,167]. Adaption of the same approach for mass transfer coefficient estimation facilitated the generalized correlation development.

5.3.1 Experimental variation of mass transfer coefficients

The experimental variation of mass transfer coefficients of the CCS (Plain and Modified) is investigated under the influence of the pertinent parameters of air and desiccant solution. Further, to reveal the benefits of the CCS, the performance of the circular cylinder geometry is compared with the plate surface study of Patil [167]. The range of independent parameters is given in Table 4.1.

5.3.1.1 Impact of mass flow rate of solution

Fig. 5.2 shows the impact of the mass flow rate of the solution on the mass transfer coefficient and the change in specific humidity of the solid circular cylindrical surface, and it also presents the behaviour of the plate surfaces. With an increase in the mass flow rate of solution, both mass transfer coefficient and change in specific humidity increase for solid circular cylinder and plate surfaces. The increase in the mass transfer coefficient occurs due to two distinct reasons: activation of new surface area on the solid surfaces for the simultaneous heat and mass transfer operation (Fig. 3.1), and the maintenance of high mass flow rate potential ($\omega_a - \omega_{eqls}$) throughout the length of the tower as solution observes less increase in ω_{eqls} across the column at high flow rates. The average h_m of Plain PP CCS is found 17.6 g/m^{2}s, which is almost 38.2% superior to the Plain PP PS average mass transfer coefficient of 12.7 g/m^{2}s for the studied range of the mass flow rate of the solution. The difference in the mass transfer coefficient between the Plain PP CCS and Plain PP PS rises until 0.077 kg/s, and then the mass transfer coefficient on the Plain PP CCS becomes almost constant. It is clear from the wetness curve (Fig. 3.1) that the cylindrical surface attains saturated condition (~100%) corresponding to the above mass flow rate conditions. Liquid spilling out of the CCS at higher flow rates seems to be the expected reason.

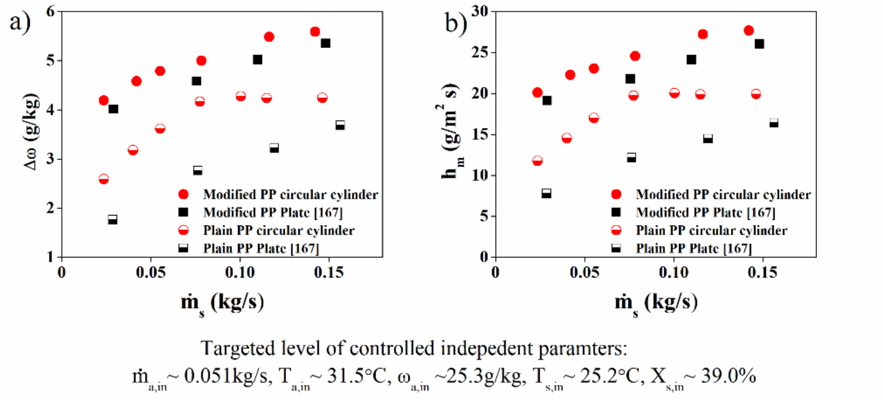

Fig. 5.2 Impact of the mass flow rate of the solution on a) mass transfer coefficient and b) change in specific humidity of air

Modified surfaces enjoy a superior mass transfer coefficient in comparison to their counterparts. The radially inclined grooves (opposite to the direction of falling liquid film) help in retarding the fluid flowing over it by applying an opposing drag force (shear). Also, the accumulation of the fluid inside these grooves forms a stagnant liquid layer over the solid surface that reduces the impact of the hydrophobic nature of the plastic surface on falling film. Thus, it contracts much slowly on the Modified surfaces in comparison to the plain surfaces. Improved wetness of the solid surface boosts up the mass transfer coefficient of air for Modified PP surfaces. Average mass transfer coefficient increases to 24.2 g/m^2 s (37.6% increment) for the CCS and 22.8 g/m^2 s (79.1% increment) for the PS through the application of Modified surface. As Plain PP CCS enjoys much superior wetting than Plain PP PS, the influence of mechanical surface modification is not that strong compared to the PS. Therefore, surface modification is more critical for surfaces associated with poor wetting, i.e., Plain PP PS. The mass transfer coefficient of the Modified circular cylinder is 9.4% higher than the Modified PP PS. Hence, for the development of low flow plastic falling film tower based-liquid desiccant systems, the CCS is more advantageous than the PS. Careful selection of cylindrical surface diameter based on operating flow conditions is an essential concern to avoid operating the cylindrical surface with saturated (complete wetting) overflow conditions.

5.3.1.2 Impact of mass flow rate of air

Fig. 5.3 demonstrates the impact of the air mass flow rate on the mass transfer coefficient and change in specific humidity of the CCS and PS. The mass transfer coefficient for both surfaces increase, whereas the change in specific humidity decreases with an increase in the air mass flow rate. More air flow rate indicates higher air velocity, which results in the reduction of the boundary layer thickness on the airside. It, in turn, reduces the mass transfer resistances, and consequently, the mass transfer coefficient increases. On the other hand, an increase in the air velocity shortens the duration of contact between air and desiccant solution. Therefore, the change in specific humidity of air across the dehumidifier decreases. The air side mass transfer coefficient improves from 15.2 - 19.8 g/m^2 s for the Plain PP CCS, whereas it increases only 9.6 - 13.6 g/m^2 s for the Plain PP PS as the mass flow rate of air increases from 0.032 to 0.062 kg/s. The mass transfer coefficient of the Plain PP CCS becomes flat at higher flow rates ($\dot{m}_a$ > 0.052 kg/s); the non-uniform distribution of air across the CCS appears to be the expected reason behind the observed trend. The mass transfer coefficient of the Modified PP PS increases from 15.4 to 23.1 g/m^2 s, whereas it increases from 20.3 to 25.9 g/m^2 s for the Modified PP CCS. The above observation also seems to be influenced by the increasing impact of non-uniform air distribution across circular cylindrical surfaces at higher mass flow rates. However, the Modified PP CCS maintains a linear trend even at higher flow rates due to superior wetting characteristics. The air flow non-uniformity across the parallel surface of the falling film tower can be normalized by providing suitable design baffles.

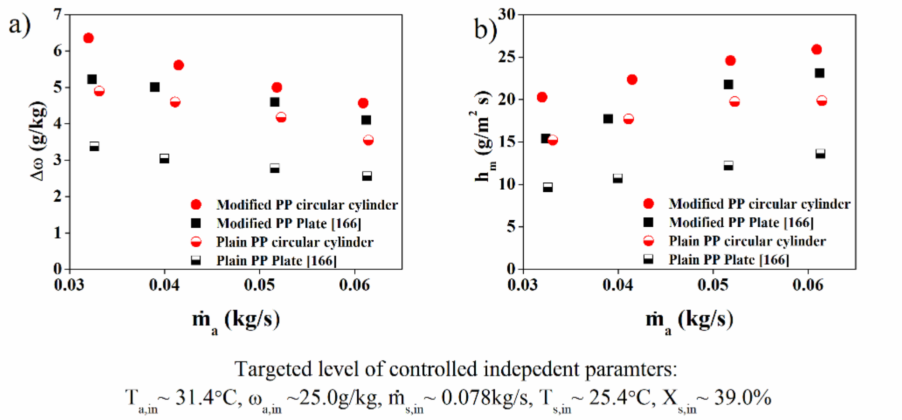

Fig. 5.3 Impact of the mass flow rate of air on a) mass transfer coefficient and b) change in specific humidity of air

5.3.1.3 Impact of inlet solution temperature

The influence of desiccant solution inlet temperature on the performance of plate and circular cylinder surfaces is shown in Fig. 5.4. The mass transfer coefficient and change in specific humidity both decrease with an increase in the solution temperature. The change in specific humidity of air reduces due to the decreased driving mass potential between the desiccant and air, as the surface vapor pressure of the desiccant solution increases with an increase in solution temperature. The Plain PP CCS offers 55.3 – 82.0% improvement in the mass transfer coefficient than the Plain PP PS for the studied range of solution temperature. The Modified PP CCS offers 24.6 – 37.1% improvement in the mass transfer coefficient than the Plain PP CCS. Two contradictory influences governing the mass transfer coefficient decrease: diminishing mass transfer potential due to the increase in the solution temperature and a positive influence of the solution temperature rise on the wetted area (due to the decrease in the viscosity of the solution) and the diffusion coefficient of the solution. The negative influence of the decrease in the mass transfer potential dominates over the positive influence of an increase in the wetted area and diffusion rate. The mass transfer coefficient of CCS is less impacted by the increase in the desiccant solution inlet temperature, unlike the PS. The solution temperature gradually rises as it flows over the solid surface due to the exothermic dehumidification process. The solution temperature rise over one solid surface does not influence the performance of other cylindrical bodies. In contrast, it seems to have a significant influence on the performance of the PS. The above-mentioned reason also appears to be responsible for the inferior performance of Modified PP PS than Plain PP CCS at the high-temperature region ($T_s > 29°C$). Therefore, in a high solution temperature region, the mass transfer coefficient of the Plain PP CCS even supersedes over the Modified PP PS.

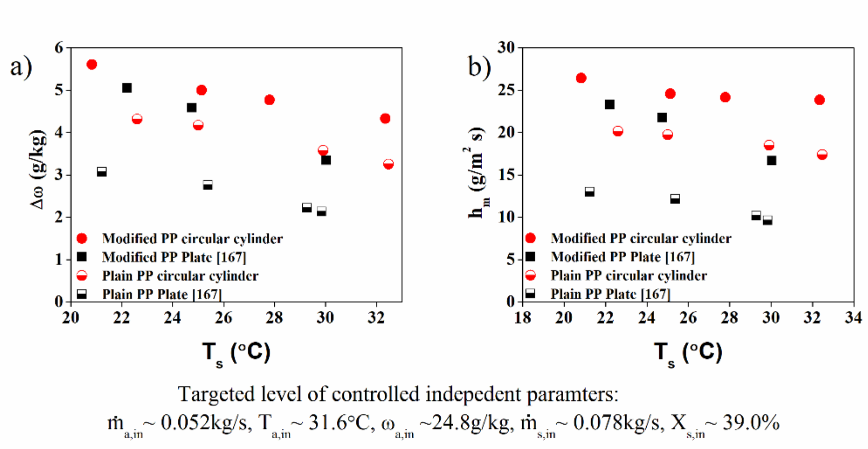

Fig. 5.4 Impact of inlet solution temperature on a) mass transfer coefficient and b) change in specific humidity of air

5.3.1.4 Impact of air inlet temperature

Fig. 5.5 shows the variation in the mass transfer coefficient and the change in specific humidity of air for different kinds of PP surfaces against the inlet air dry bulb temperature. The inlet air temperature has shown a weak impact on the change in specific humidity and the mass transfer coefficient of circular cylindrical surfaces. The air temperature is expected to negatively influence the performance of falling film towers as they can be operated at much lower $\dot{m}_s/\dot{m}_a$ than the packed bed towers. Therefore, sensible heating of the solution at higher air temperatures will become authoritative in limiting the mass transfer between liquid desiccant and air. However, for the studied range of T_a $(26 - 36\ °C)$, the influence is found to be negligible as air temperature does not control the limiting parameters (wetting area and mass transfer driving potential) directly. Except for the Plain PP CCS, the mass transfer coefficient remains almost constant for the rest of the surfaces against T_a. The observed trend is found fluctuating for the Plain PP CCS, and the cumulative effect of the undesired fluctuations in the dependent parameters seems responsible for the above fluctuations. The average mass transfer coefficient of the Plain PP and the Modifier PP CCS are found ~18.3 g/m^2 s and ~25.5 g/m^2 s, respectively.

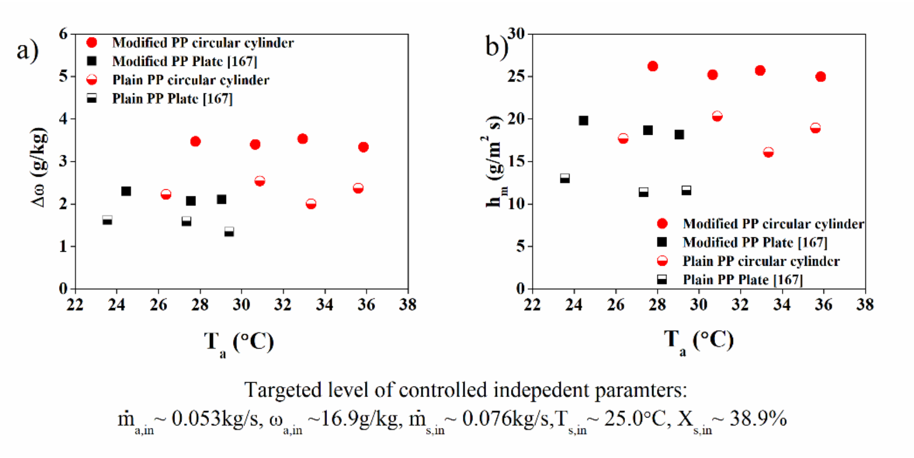

Fig. 5.5 Impact of inlet air temperature on a) mass transfer coefficient and b) change in specific humidity of air

5.3.1.5 Impact of inlet solution concentration

Fig. 5.6 presents the effect of change in the solution concentration on the mass transfer coefficient and change in specific humidity of the CCS and PS. The change in specific humidity increases with an increase in the inlet solution concentration. The solution equilibrium vapor pressure decreases with the increase in the concentration of the desiccant solution at a given temperature, which leads to a higher input mass transfer potential. Consequently, the change in specific humidity of the air increases. As the dehumidification rate and driving mass transfer potential both increase with an increase in the solution concentration, the mass transfer coefficient has an almost flat trend for the Plain PP and the Modified PP CCS. The average mass transfer coefficient of the Plain PP CCS is found 144.6% higher than the Plain PP PS. The Modified PP CCS average mass transfer coefficient is 28.5% higher than the Plain PP

CCS. It is worth noting that the Plain PP CCS performance is superior to the Modified PP PS for the entire tested range of the solution concentration. At high temperatures ($T_s > 29°C$), the Plain PP CCS outperforms the Modified PP plate (Ref. Section. 5.3.1.3). The performance difference between the two diminishes at higher concentration levels as the mechanical surface modification (groves opposite to the direction of flow) facilitates in overcoming the negative influence of the increase in viscosity of the solution on the wetted area of the solid surface.

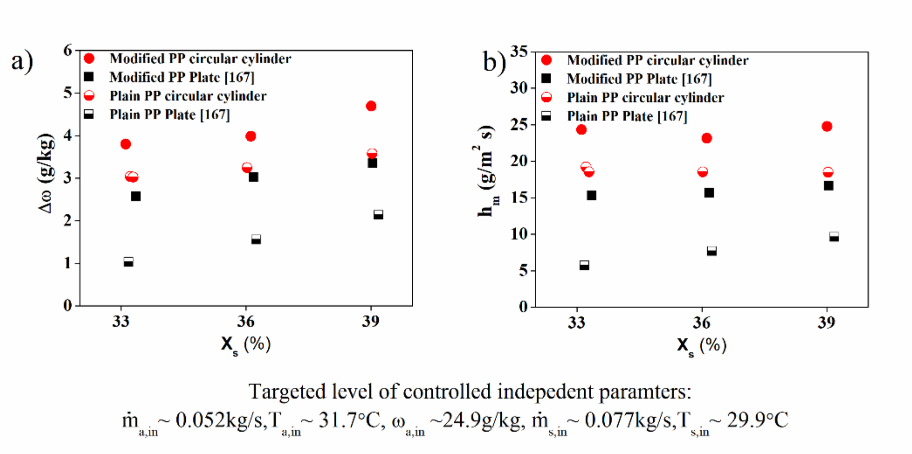

Fig. 5.6 Impact of inlet solution concentration on a) mass transfer coefficient and b) change in specific humidity of air

5.3.1.6 Impact of inlet specific humidity of air

Fig. 5.7 depicts the influence of the inlet air humidity ratio on the performance indices of the circular cylinder and plate surfaces. The higher humidity level of air corresponds to a higher mass transfer potential between desiccant and process air, while other independent parameters are kept constant. Hence, as a result, the change in specific humidity rises linearly with the increase in inlet specific humidity of the air. In contrast to the change in specific humidity curve, the mass transfer coefficient curve does not show much sensitivity to the change in $\omega_{a,in}$ for any of the studied surfaces. As both parts of Eq. 5.4, numerator - dehumidification rate and denominator -the mass transfer potential improve with an increase in inlet specific humidity of process air, which is responsible for the flatness of the mass transfer curve. As shown in Fig. 5.7, the mass transfer coefficient of the Plain and Modified PP CCS varied around a constant value of 20.2 g/m^2 s and 25.3 g/m^2 s respectively, when the inlet humidity ratio changed from 15.3 to 25.4 g/kg. The mass transfer coefficient of the Plain PP CCS is found 59.6 - 109.8% superior to the Plain PP PS. Similarly, the performance of the Modified PP CCS is found 22.7 - 28.8% superior to the Plain PP CCS.

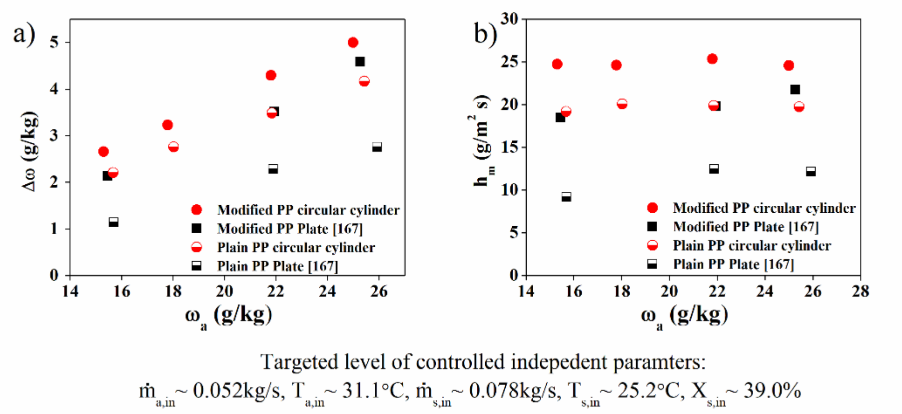

Fig. 5.7 Impact inlet specific humidity of air on a) mass transfer coefficient and b) change in specific humidity of air

5.3.2 Development of new generalized Sh number correlation

From literature survey it is found that unlike the packed bed towers, very few correlations of the Sh number are available for the falling film tower. The existing correlations in falling film towers were developed considering experimental/numerical observations on the stainless-steel metallic plates and tube surfaces, which are expected to over predict the performance of the plastic falling film towers used in the current study as the wetness behaviour of the metallic and plastic surfaces vary drastically. So far, there is no common consensus on the generalized correlations for mass transfer coefficient prediction in liquid desiccant falling film towers. Almost every correlation severely failed when it is cross-checked against other's experimental datasets. Hence, a generalized mass transfer correlation is needed for the falling film towers, which can capably predict the accurate mass transfer coefficient of the metallic/plastic surfaces for adiabatic and non-adiabatic cases. An accurate mass transfer coefficient will be very useful in the modelling and simulation of falling film towers.

In the current study, Sh number correlation for falling film dehumidifiers is expressed in the non-dimensional form, as shown in Eq. (5.9). The enthalpy difference $\left(\frac{h_a - h_{eqls}}{h_{eqls}}\right)$ and moisture difference $\left(\frac{\omega_{a,-}\omega_{eqls}}{\omega_{eqls}}\right)$ between air and liquid desiccant are included as the governing parameters to represent the concurrent thermal energy and moisture exchange between air and solution. Apart from the above, falling film behaviours and its wetting characteristics on the solid surface, and the solution thermophysical properties considerably affect the mass transfer performance.

$$Sh_a = a\left(\frac{F_s}{F_g}\right)^b \left(\frac{Y_c}{Y_s}\right)^c \left(\frac{A_{ext}}{A}\right)^d \left(\frac{\dot{m}_a}{\dot{m}_s}\right)^e \left(\frac{h_a - h_{eqls}}{h_{eqls}}\right)^f \left(\frac{\omega_{a,-}\omega_{eqls}}{\omega_{eqls}}\right)^g \left(1 + \frac{T_s}{T_w}\right)^h (Re_a)^i (Sc_a)^j (Re_s)^k \tag{5.9}$$

The definitions of different non-dimensional numbers used are as follows.

$$Sh_a = \frac{h_m\, t}{\rho_a D_a} \tag{5.10}$$

$$Re_a = \frac{\rho_a V_a\, t}{\mu_a} \tag{5.11}$$

$$Sc_a = \frac{\mu_a}{\rho_a D_a} \tag{5.12}$$

$$Re_s = \frac{4\dot{m}_s}{\mu_s W} \tag{5.13}$$

Nine experimental datasets are selected for the purpose of model development and validation. The details of the dehumidifier and operating conditions of different studies are given in Table 5.1. Three experimental studies of different natures: Plastic adiabatic (current study), metallic adiabatic study on vertical tube [91] and metallic non-adiabatic study on the plate [89] are used in statistical regression analysis to determine the coefficients a, b, c, d, e, f, g, h, i, j and k of Eq.

(5.9). Equation (5.14) shows the final form of the newly proposed correlation of the current study.

$$Sh_a = 0.051\left(\frac{F_s}{F_g}\right)^{0.276}\left(\frac{Y_c}{Y_s}\right)^{0.329}\left(\frac{A_{ext}}{A}\right)^{0.474}\left(\frac{\dot{m_a}}{\dot{m_s}}\right)^{-0.067}\left(\frac{h_a - h_{eqls}}{h_{eqls}}\right)^{-0.193}\left(\frac{\omega_a - \omega_{eqls}}{\omega_{eqls}}\right)^{0.349}\left(1 + \frac{T_s}{T_w}\right)^{-0.217}(Re_a)^{0.654}(Sc_a)^{0.333}(Re_s)^{0.216} \quad (5.14)$$

The accuracy of the new Sh number correlation is checked by validating it with the current and other experimental datasets. Table 5.2 shows the analytical performance comparison between current and existing falling film Sh number correlations. The MAPE is calculated using (Eq. 5.15).

$$MAPE\ (\%) = \frac{\sum_1^N \left|\frac{Sh_{exp} - Sh_{pred}}{Sh_{pred}}\right|}{N} \text{ x } 100 \quad (5.15)$$

Table 5.1 Dehumidifier details and operating conditions of experimental studies

Study	Solid surface-liquid desiccant	Type of dehumidifier	Dehumidifier size	Air channel gap	Operating conditions					
					Air (inlet)			Desiccant (inlet)		
					$\dot{m}_a$ (kg/s)	T_a (°C)	ω_a (g/kg)	$\dot{m}_s$ (kg/s)	T_s (°C)	X_s (%)
Wen et al. [28]	S.S-LiCl, S.S-KCOOH	Non-adiabatic: Vertical Plate	500 x 500 mm	40 mm	0.020-0.060	29.0-36.0	16.0-25.0	0.080-0.150	27.0-35.0	35, 70.3
Wen et al. [89]	Al-LiCl	Non-adiabatic: Vertical Plate	500 x 500 mm	30 mm	0.021-0.058	27.0-36.0	17.2-24.3	0.050-0.120	25.0-34.0	35.0-38.0
Cheng et al.	S.S-LiCl	Adiabatic: Vertical tube	1030 x 58 mm	58 mm	0.070-0.370	30.0	18.6-19.2	0.090	26.0-36.0	29.9-31.6
Wen et al. [100]	S.S-LiCl	Non-adiabatic: Vertical Plate	500 x 500 mm	40 mm	0.023-0.060	29.8-35.5	16.2-23.4	0.082-0.148	27.8-35.0	25.0-35.0
Wen et al. [121]	S.S-LiCl	Non-adiabatic: Vertical Plate	500 x 500 mm	30 mm	0.023-0.07	28.0-36.4	16.5-24.6	0.085-0.162	28.0-35.0	32.0-40.0

Wen et al [122]	S.S-LiCl	Non-adiabatic: Vertical Plate	500 x 500 mm	40 mm	0.023-0.060	29.9-36.7	17.0-24.2	0.085-0.150	28.2-34.2	35.0
Peng et al. [137]	S.S-LiCl, S.S-$CaCl_2$	Non-adiabatic: Vertical tube	1030 x 58 mm	58 mm	0.070-0.380	32.0-36.0	21.0-30.0	0.060-0.110	26.0-34.0	27.0-37.0
Patil [167]	PP-LiCl	Adiabatic: Vertical plate	400 x 700 mm	70 mm	0.032 - 0.062	23.0-30.0	15.0-27.0	0.026-0.156	21.2-30.8	36.0-42.4

The current correlation presented good agreement with all the datasets. However, for the experimental observation of Cheng et al. [91] and Wen et al. [100], the MAPE of the present correlation is found more than 20%. As shown in Fig. 5.8, the MAPE of the current model is 16.6%, 70.0% and 88.6% of the data points fall within the error band of ± 20% and ± 30% respectively, while the MAPE of the second best correlation [137] is 23.1%, 49.9% and 69.9% of the data points fall within error band of ± 20% and ± 30%, respectively.

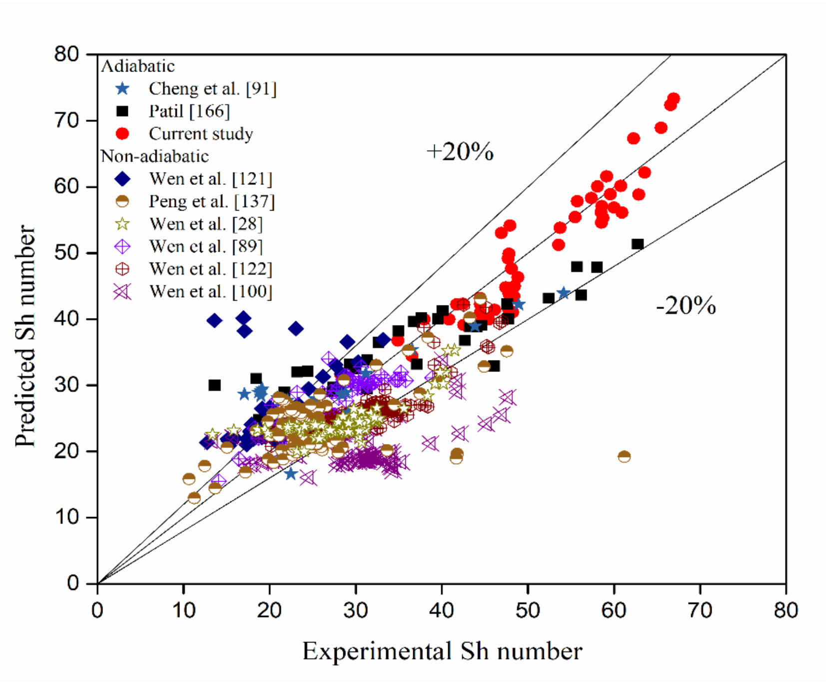

Fig. 5.8 Comparison between experimental and predicted Sh number for different datasets.

Table 5.2 Performance comparison of current and existing falling film Sh number correlations

Experimental studies	Cheng et al. [91]	Patil [167]	Current study	Wen et al. [28]		Wen et al. [89]	Wen et al. [100]	Wen et al. [121]	Wen et al.[122]	Peng et al.[137]		MAPE (overall)
Type of desiccant	LiCl	LiCl	LiCl	LiCl	KCOOH	LiCl	LiCl	LiCl	LiCl	LiCl	$CaCl_2$	
Number of data points	22	33	47	49	58	85	100	129	154	60	60	
Type of tower	Adiabatic			Non-adiabatic								
MAPE of correlation for each dataset												
Wen et al. [28]	211.9	90.3	32.8	8.5	7.8	24.8	20.4	105.9	30.4	342.7	269.3	88.5
Yin et al. [132]	45.7	54.4	67.2	81.7	83.0	66.3	82.9	75.0	82.8	43.1	45.2	70.8
Peng et al. [137]	24.4	32.2	47.9	22.6	47.9	18.7	24.1	18.9	22.7	7.0	5.8	23.1
Current study	23.7	19.4	6.0	18.4	17.8	8.3	29.0	17.7	14.3	12.7	17.3	16.6

5.4 Heat and mass transfer characteristics of regenerator

The regenerator plays a critical role in the overall efficiency and energy-economic viability of the LDS. However, in comparison to experimental heat and mass transfer studies on falling film dehumidification process, the heat and mass transfer study on regeneration process is almost negligible. Apart from mass transfer potential, the heat transfer potential in the regeneration process is significantly higher as compared to dehumidifier. Hence, evaluation of heat transfer coefficients along with mass transfer coefficient becomes vital for development of falling film liquid desiccant regenerators. As discussed in section 5.3, the numerical integration technique following Chung's [17] (Eq. 5.1) was applied to study the mass transfer characteristic of the dehumidifier. However, the preceding method may not be suitable for the regeneration process as the variation in ω_{eqls} is significantly higher due to high heat transfer between air and solution. In addition, the conventional approach of 100% wetting of the working surface was assumed for the dehumidification mass transfer study. In the regeneration study, the Eqs. (5.3) and (5.4) are solved by finite difference method to determine the heat and mass transfer coefficient.

5.4.1 Numerical Modelling

In the regenerator, the liquid desiccant distributed from the top interacts with the counter-flowing process air. Fig. 5.9 shows the liquid desiccant falling film pattern on the solid surface during partial wetted conditions (a) in actual and (b) assumed in the current numerical modelling. In the current study, two distinct approaches are followed for numerical modelling. In the first method: the conventional approach is followed, solid surface assumed to be fully wetted irrespective of desiccant flow rate conditions. In the second approach (which is presented in detail afterwards): the actual wetting of the solid surface has been used to estimate heat and mass transfer coefficient initially. Based on the above two approaches heat and mass transfer coefficient correlations are developed. Later on, these correlations are compared for their ability to predict the performance of the falling film tower operating as regenerator in the wide range of operating conditions (including partial and full wetted zones). On the wetted portion of the solid surface, coupled heat and mass transfer occurs between the air and the liquid desiccant solution. Convective heat transfer happening between dry part of the solid surface and flowing air across it has also been considered in the current study. As convective heat transfer happening between dry portions of solid surface and flowing air across becomes influential at partial wetting conditions. Fig. 5.10 shows the control volume diagram of the regenerator. The 'W_w' represents the partial wetted width of desiccant solution (partial wetting conditions) on solid PP surface, and 'W_d' represents the width of the dry part of the solid surface. The 'W_w' is calculated following Eq. (5.16).

$$W = A_W/H \tag{5.16}$$

Where, A_w is the average wetted area. Fig. 5.9 shows the falling film pattern on solid surface. Fig. 5.10 shows the control volume diagram of the regenerator.

The following assumptions are made for developing the numerical model:

1. The heat and mass transfer process occurs between air and solution only.
2. The humidity, temperature, and concentration gradient exit along the flow direction.
3. The liquid on the solid surfaces flows with constant width at different flow rates.

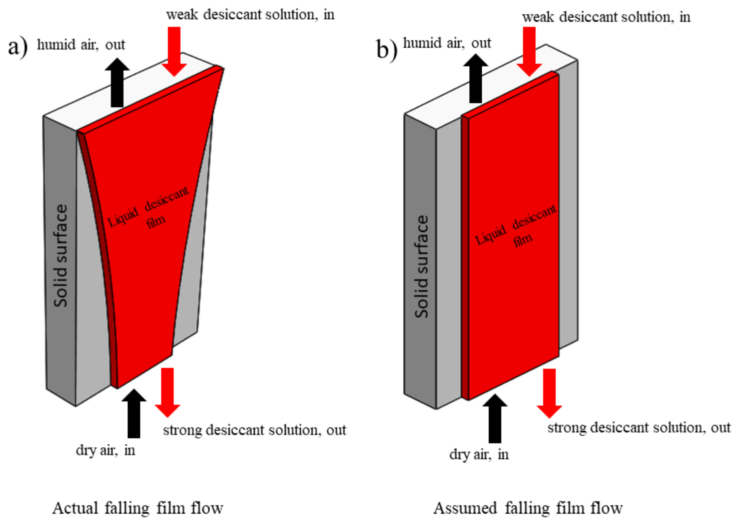

Fig. 5.9 Falling film flow pattern on solid surface a) actual b) assumed

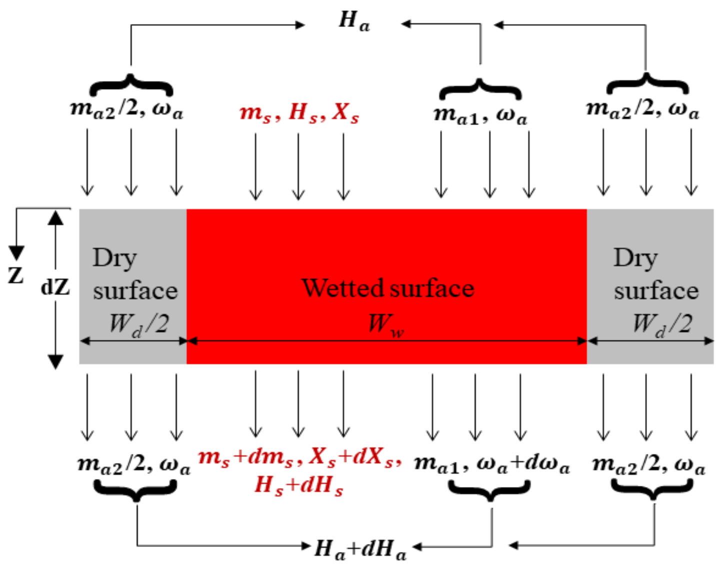

Fig. 5.10 Control volume diagram

5.4.2 Mass balance of the control volume:

Mass of water exiting the wetted surface of control volume= mass of water entering the wetted surface of control volume+ mass transfer from desiccant solution to air.

$$m_a(\omega_a + d\omega_a) = m_a\omega_a + h_m(\omega_{eqls} - \omega_a)W_w dz \tag{5.17}$$

$$m_{a1}\frac{d\omega_a}{dz} = h_m W_w(\omega_{eqls} - \omega_a) \tag{5.18}$$

Where, m_{a1} is the fraction of the mass flow rate of air interacting with the wetted part of the solid surface. It is estimated as $m_{a1} = WF * m_a$

5.4.3 Energy balance of the control volume:

Enthalpy of air exiting the control volume= enthalpy of air entering the control volume + enthalpy change of air due to heat and mass transfer with liquid desiccant on the wetted surface of control volume+ enthalpy change of air due to heat transfer between air and the dry surface of the control volume.

$$\boldsymbol{m_a(H_a + dH_a) = m_a H_a + h_t W_w(T_s - T_a)dz + h_m W_w\left(\omega_{eqls} - \omega_a\right)h_{fg}dz + h_d W_d(T_d - T_a)dZ} \quad (5.19)$$

$$\boldsymbol{m_a dH_a = h_t W_w(T_s - T_a)dz + h_m W_w\left(\omega_{eqls} - \omega_a\right)h_{fg}dz + h_d W_d(T_d - T_a)dZ} \quad (5.20)$$

Where h_d is the heat transfer coefficient between air and the dry surface control volume. It is estimated as

$$Nu_d = \frac{h_{dW_d}}{k_a} = 0.664 R_e^{0.5} P_r^{0.3}$$

The enthalpy change of air can be expressed as

$$\boldsymbol{dh_a = C_{pm} dT_a + h_{fg} d\omega_a} \quad (5.21)$$

Hence, using Eq. (5.18) and Eq. (5.20), the Eq. (5.21) can be written as

$$\boldsymbol{m_a C_{pm} \frac{dT_a}{dz} = h_t W_w(T_s - T_a) + h_d W_d(T_d - T_a)} \quad (5.22)$$

Finally, by applying mass and energy balance, the mass flow rate, concentration, and temperature change of desiccant solution for the control volume can be obtained using Eqs. (5.23), (5.24) and (5.25).

$$\boldsymbol{\frac{d\left(m_s(1 - X_s)\right)}{dz} = h_m W\left(\omega_{eqls} - \omega_a\right)} \quad (5.23)$$

$$\boldsymbol{\frac{d(m_s h_s)}{dz} = h_t W(T_s - T_a) + h_m W\left(\omega_{eqls} - \omega_a\right)h_{fg}} \quad (5.24)$$

$$\boldsymbol{d(m_s X_s) = 0} \quad (5.25)$$

5.4.4 Heat and mass transfer coefficients evaluation method

The overall heat and mass transfer coefficient associated with coupled heat and mass transfer interaction during dehumidification/regeneration process are calculated following Eqs. (5.26) and (5.27).

$$h_t = \frac{Q}{\int_0^L \Delta T(z)(W_w)dz} = \frac{Q}{A\,\Delta T_m} \tag{5.26}$$

$$\boldsymbol{h_m} = \frac{\dot{m}_{reg}}{\int_0^L \Delta\omega(z) W_w dz} = \frac{\dot{m}_{reg}}{A\,\Delta\omega_m} \tag{5.27}$$

The most important point is to determine the average potential of (ΔT_m) and $(\Delta\omega_m)$ for liquid desiccant-air interaction. Previous studies [136,137] calculated ΔT_m and $\Delta\omega_m$ based on the inlet temperature $(T_{s,in} - T_{a,in})$ and humidity $(\omega_{eqls,in} - \omega_{a,in})$ potential difference, and logarithmic mean temperature and humidity difference as given by Eqs. (5.28) and (5.29).

$$\Delta T_{LMTD} = \frac{(T_{s,in} - T_{a,out}) - (T_{s,out} - T_{a,in})}{ln\frac{(T_{s,in} - T_{a,out})}{(T_{s,out} - T_{a,in})}} \tag{5.28}$$

$$\Delta\omega_{LMWD} = \frac{(\omega_{eqls,in} - \omega_{a,out}) - (\omega_{eqls,out} - \omega_{a,in})}{ln\frac{(\omega_{eqls,in} - \omega_{a,out})}{(\omega_{eqls,out} - \omega_{a,in})}} \tag{5.29}$$

Unlike conventional heat exchangers and packed bed columns, the overall heat and mass transfer coefficient based on the inlet or logarithmic potential difference approach is recommended for the falling film tower. As transfer potential (especially mass transfer), observe a drastic change in the slope on account of inadequate cooling/heating before the inlet of dehumidifier/regenerator as well as a significant change in solution temperature due to the heat of condensation/evaporation of water. An evaluation method capable of tracking the changes in transfer potential along the tower length would give the accurate estimate of heat and mass transfer coefficients. The current study adopts the numerical finite difference method to solve the non-linear coupled differential equation (Eqs. (5.17-5.25)) at partial wetting (actual) wetting conditions of solid surface. MATLAB (R2022b) is utilized to carry out the numerical work. Fig. 5.11 shows the flow chart for heat and mass transfer calculation. The procedure adopted for numerical computation is explained in detail as follows:

1. The inlet and outlet experimental values of air and desiccant solution and average wetted width of the desiccant film (calculated by Eq. (5.16)) and with of the dry part of solid surface are considered as known parameters.

2. Assume two initial sets of heat and mass transfer coefficients (h_{t1}, h_{m1}), and (h_{t2}, h_{m2}). For the speedy convergence of assumed values to exact heat and mass transfer coefficient, assumptions are made based on experimental data. The (h_{t1}, h_{m1}) is set following logarithmic mean temperature and humidity potential, and (h_{t2}, h_{m2}) is set based on (the maximum temperature and humidity potential (it may not be true for internally cooled or heated absorber/regenerator)/terminal temperature and humidity potential across the regenerator.

3. Governing differential equations (Eqs. 5.17-5.25) for each control volume (from top to bottom of tower) are solved by the Fourth order Runge-Kutta method. Simultaneously, Newton's forward difference method is used to calculate the outlet conditions of desiccant solution for each control volume through mass and energy balance equations (Eqs. 5.23-5.25). Procedure 3 in the first step is repeated for two sets of (h_{t1}, h_{m1}), and (h_{t2}, h_{m2}) values.

4. The calculated values at the bottom of tower $T_{a,in,cal}$, $\omega_{a,in,cal}$ are compared with experimental conditions $T_{a,in,exp}$, $\omega_{a,in,exp}$ and check for convergence. If the desired accuracy is not obtained, then Newton-secant method is applied to determine the new values of h_t and h_m.

5. Steps 3 to 4 are repeated until the desired accuracy is achieved between the calculated value of inlet air conditions and their experimental values. The arrived values h_t and h_m are exact estimation of heat and mass transfer coefficient.

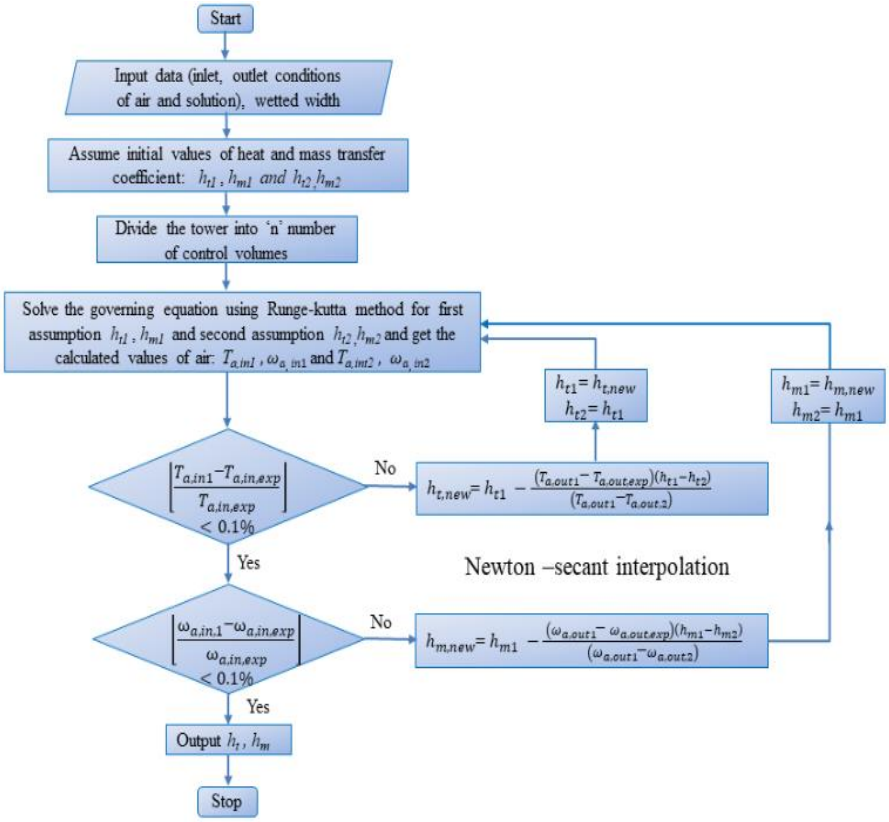

Fig. 5.11 Flow chart for calculation of h_t and h_m

5.5 Experimental variation of heat and mass transfer coefficients

The effect of essential parameters, including air and solution mass flow rate, air temperature and humidity ratio, and desiccant solution temperature, on heat and mass transfer coefficient is studied. Initially, experiments were conducted to get the outlet parameters of air and solution and then, based on numerical modelling and experimental readings, the heat and mass transfer coefficient was calculated. The operating rang of parameters is given in Chapter 4 (Table 4.1).

5.5.1 Effect of mass flow rate of solution

Fig. 5.12 shows the heat and mass transfer behaviour of different PP surfaces with an increase in the mass flow rate of solution. The observed variation of transfer coefficients can be explained by considering two different operating zones of mass flow rate range of C.C.S: first, the partial surface wetting zone and second, the complete surface wetting zone. In partial surface wetting zone of Plain C.C.S. ($\dot{m}_s$ < 0.120 kg/s) and Modified C.C.S. ($\dot{m}_s$ < 0.100 kg/s), mass transfer coefficients of both PP surfaces increased with an increase in the mass flow rate of solution. The increasing trend can be explained as follows: At very low rate the liquid flow starts from the top of the surface in the form of isolated liquid rivulets, angular orientation of the solid surface promotes frequent mixing between isolated liquid rivulets, which obstruct the growth of the concentration boundary layer. As the flow rate increases, these liquid rivulets spread radially on the surface of the circular cylinder, consequently the liquid film thickness decreased. In addition, the fluctuation of falling film liquid wave increases which reduces the mass transfer resistance at the interface between liquid desiccant and air. Hence, the mass transfer coefficient increases with increase in mass flow rate of desiccant solution in the partial wetted zone conditions. On the contrary, the heat transfer coefficient decreased with increase in mass flow rate of solution in the partial wetting zone. The contrary nature of the coupled heat and mass transfer process (efficient mass transfer leads to rapid reduction in solution temperature due to endothermic regeneration process) might be expected reason for the decreasing heat transfer coefficient in the partial wetted zone.

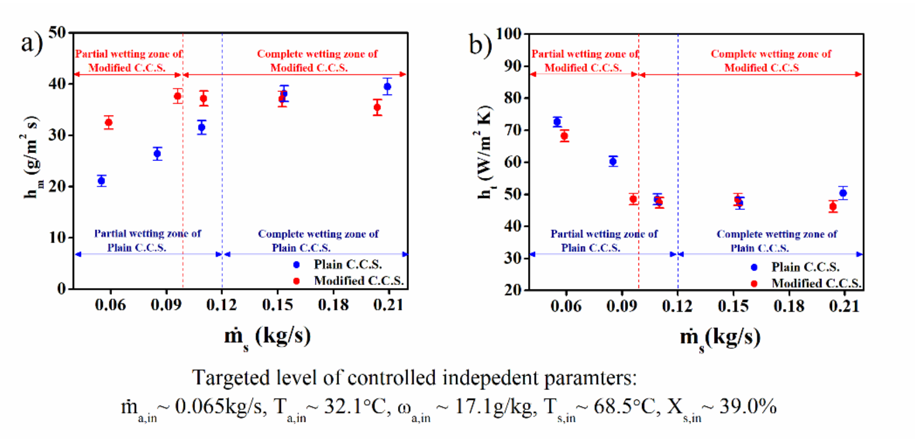

Fig. 5.12 Effect of mass flow rate of solution on a) mass transfer coefficient and b) heat transfer coefficient.

The inclined groove on the Modified surface promotes radial spreading of the liquid film towards the dry patches, facilitating in the formation of thin liquid film that enjoys frequent renewal. Further, inclined groves enhanced the formation of liquid waves, which also improves the mass transfer process. All these features of Modified C.C.S. surface help in improving the mass transfer coefficient. In the partial wetting operating zone, the mass transfer coefficient of Modified C.C.S. is found 35.8% higher than Plain C.C.S. However, the heat transfer coefficient of the Modified C.C.S. is found to be 10.1% lower than Plain C.C.S. The endothermic nature of the regeneration process seems to be responsible reason for the observed behaviour. In the complete surface wetting zone of Plain C.C.S. ($\dot{m}_s > 0.120$ kg/s) and Modified C.C.S. ($\dot{m}_s > 0.100$ kg/s), Heat and mass transfer coefficients of the Plain C.C.S. continuously increases at high mass flow rates, whereas, for Modified C.C.S. the mass transfer coefficient decreases, and heat transfer coefficient fluctuates at high flow rates. The above observations seem to be governed under the following contradictory influences. With increase in mass flow rate after complete surface wetting; initially the thickness of falling film increases, thus the boundary layers of the liquid phase decrease and it reduces the resistance of heat and mass transfer operations. With further increase in the mass flow rate; spilling of the liquid starts from the solid surface, hence, increase in heat and mass transfer coefficient stop with mass flow rate of the desiccant solution. Modified C.C.S. surface reaches complete surface wetting conditions much earlier than Plain C.C.S.

It is evident from the above discussion that the performance difference between Plain and the Modified surface mainly depends on the desiccant flow rate (liquid loading conditions: partial or fully wetted condition). To ascertain the behaviour of above observation, two other strong independent parameters: air mass flow rate and desiccant inlet temperature are also studied at partial wetted conditions ($\dot{m}_s \sim 0.060\ \mathrm{kg/s}$), whereas the effect of process air temperature and humidity are analysed at full wetted condition. The above variation is also intended to get generalized nature of the heat and mass transfer coefficient equations so that developed equations can capably facilitate the numerical simulation needs of partial and fully wetted operating conditions of the falling film tower.

5.5.2 Effect of mass flow rate of air

The effect of the mass flow rate of air on the heat and mass transfer regeneration characteristic is depicted in Fig. 5.13 at partial wetting conditions of studied surfaces ($\dot{m}_s \sim$ 0.060 kg/s). For the studied range of air mass flow rate from 0.030 kg/s to 0.065 kg/s, the transfer coefficients of Plain C.C.S. increased from 14.4 g/m^{2}s to 21.1 g/m^{2}s and from 43.4 W/m^2 K to 72.6 W/m^2 K, respectively. Similarly, the Modified C.C.S. transfer coefficients increased from 24.3 g/m^{2}s to 32.5 g/m^{2}s and from 35.3 W/m^2 K to 68.3 W/m^2 K, respectively. The increase in air mass flow rate disturbs the growth of boundary layer thickness on the airside, which in turn decreases the heat and mass transfer resistance. Therefore, the overall transfer coefficients increased with the mass flow rate of air. The average mass transfer coefficient of Modified C.C.S. is higher than Plain C.C.S. by 65.3% for the tested conditions, while the heat transfer coefficient of Modified C.C.S. is 7.9% lower than Plain C.C.S. Endothermic nature of the regeneration process seems to be the expected reason behind it. The same reason seems to be also responsible for the slight convergence of heat transfer coefficient characteristics of the Plain and Modified C.C.S. as mass flow rate of air is increased. The higher air mass flow rate indicates higher air velocity. Air at very high flow rate start influencing the liquid film (wave formation) flowing over the solid surface. The influence of above effect seems less significant for the Modified C.C.S. surface as it already enjoys the stronger liquid wave formation due to the presence of inclined grooves. Hence, Plain C.C.S. surface enjoy almost linear increase in mass transfer coefficient at highest mass flow rate of air unlike the Modified C.C.S. Consequently, the heat transfer coefficient of the Modified C.C.S. slightly improves at highest mass flow rate of air.

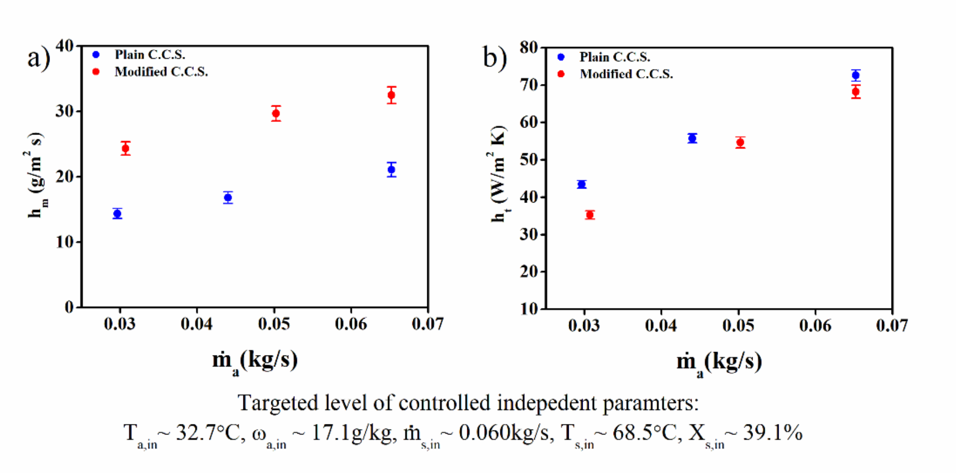

Fig. 5.13 Effect of mass flow rate of air on a) mass transfer coefficient and b) heat transfer coefficient

5.5.3 Effect of liquid desiccant inlet temperature

Fig. 5.14 shows the effect of liquid desiccant inlet temperature on heat and mass transfer characteristics of CCS surfaces at partial wetting conditions. The transfer coefficients of Plain C.C.S. and Modified PP C.C.S. increased with increase in solution temperature from 60.4 ºC to 68.6 ºC. The mass transfer coefficients of Plain C.C.S. and Modified C.C.S. increased from 13.2 g/m^{2}s to 21.1 g/m^{2}s and from 28.2 g/m^{2}s to 32.5 g/m^{2}s, respectively. Similarly, the heat transfer coefficients of Plain C.C.S. and Modified PP C.C.S. increased from 65.0 W/m^{2}K to 72.6W/m^{2}K and from 56.6 W/m^{2}K to 68.3 W/m^{2}K, respectively. With increase in solution temperature the falling film thickness of the isolated liquid rivulets on C.C.S. reduces due to a decrease in the viscosity and surface tension of the desiccant solution. The reduction in liquid film thickness enhances the diffusion heat and mass transfer between solution and air due to decrease in the overall heat and mass transfer resistance. The average mass transfer coefficient of the Modified C.C.S. is found to be 74.8% superior to Plain C.C.S., and the heat transfer coefficient of the Plain C.C.S. is found to be 12.4% superior to Modified C.C.S. The difference in the transfer coefficient values between Plain and Modified C.C.S. decreased with an increase in solution temperature. As the Plain C.C.S. suffers from low wettability compared to Modified

C.C.S., the reduction in the liquid film thickness with the increase in solution temperature is higher for the Plain C.C.S. in comparison to Modified C.C.S. Hence, the mass transfer coefficient increases rapidly for the Plain C.C.S. in comparison to Modified C.C.S. The Plain C.C.S. surface enjoys higher heat transfer coefficient than Modified C.C.S. surface, convective heat transfer happening between dry part of the solid surface and air seems to be expected reason behind it. The heat transfer coefficient behaviour between Plain and Modified C.C.S. is due to coupled heat and mass transfer characteristics.

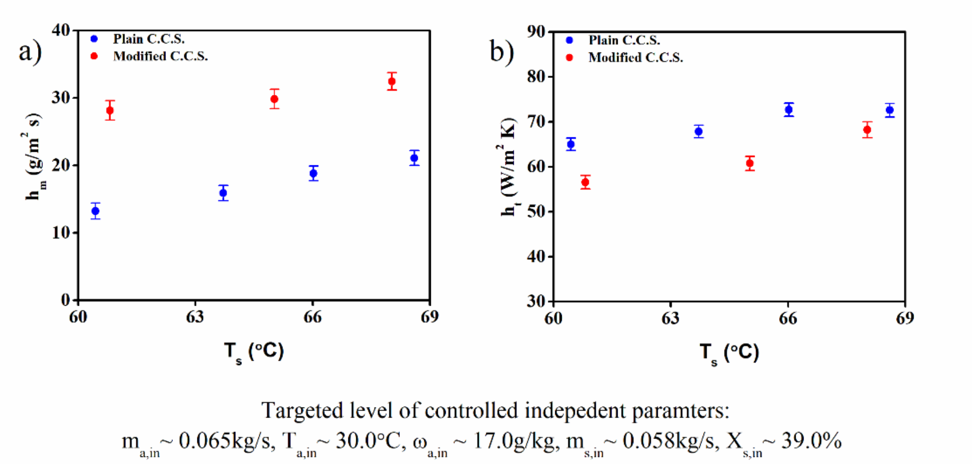

Fig. 5.14 Effect of liquid desiccant inlet temperature on a) mass transfer coefficient and b) heat transfer coefficient

5.5.4 Effect of air inlet dry bulb temperature

Fig. 5.15 shows the regeneration characteristic for the variation of inlet air temperature from 30.5ºC to 44.2ºC at complete wetting conditions ($\dot{m}_s$~ 0.153 kg/s) of Plain and Modified PP CCS. The increasing air temperature neither affects the wetting characteristic nor the thermophysical properties of solution. Hence, the mass transfer coefficient almost maintains a flat trend for the studied range of air temperature. As the Modified C.C.S. attains full wetting condition much earlier than Plain C.C.S. then liquid splashing starts on it. A slightly better mass transfer coefficient has been observed for the Plain C.C.S. in comparison to Modified C.C.S. On the contrary, the heat transfer coefficient value decreases with increase in temperature. The increase in the air viscosity with increase in inlet air temperature seems to be the expected reason for the observed trend. However, at higher temperatures the effect of increase in air viscosity on the Modified C.C.S. in comparison to Plain C.C.S. is found to be less. Superior wetting characteristics of the Modified C.C.S. might be the expected reason. The average value of transfer coefficients for Plain C.C.S. are 37.9 g/m^2s and 41.0 W/m^2K, and the average value of transfer coefficient for Modified C.C.S. are 36.2 g/m^2s and 43.2 W/m^2K, respectively.

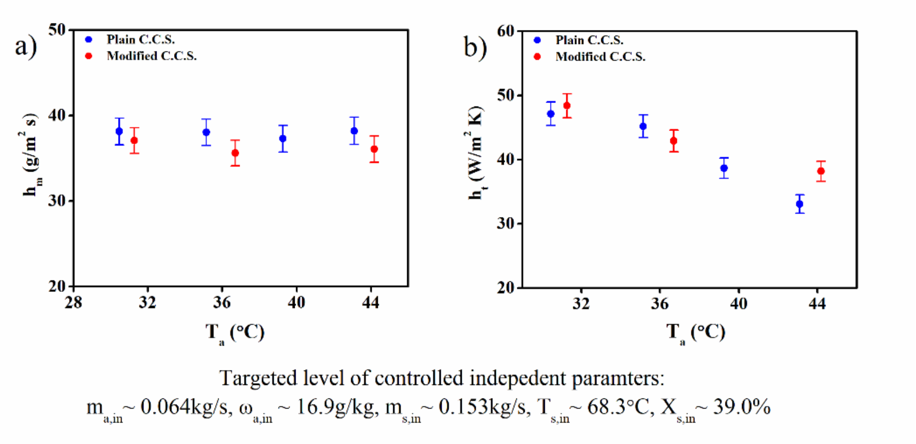

Fig. 5.15 Effect of air inlet temperature on a) mass transfer coefficient and b) heat transfer coefficient

5.5.5 Effect of air inlet specific humidity

Fig. 5.16 illustrates the regeneration behavior of Plain PP CCS and Modified PP CCS at various air inlet humidity values. Increasing the humidity of dry air decreases the moisture diffusivity rate between desiccant and air. Consequently, the mass transfer coefficients of Plain and Modified PP C.C.S. decreased with increase in air humidity ratio. However, at higher humidity levels, as the moist air approaches the saturation level (100% relative humidity), the mass transfer coefficient trend of Plain and Modified C.C.S. tend to become stable. On the contrary, the increase in air humidity value does not present any significant effect on the heat transfer coefficient of Plain and Modified C.C.S. The fluctuations in the values of heat transfer coefficients might be due to undesired variation in the inlet values of other independent parameters of air and solution, which could not be maintained strictly at the constant values. As the operating mass of the solution is well above the saturation limit (100% wetting conditions) of the studied surfaces, the Plain and Modified C.C.S. almost show equivalent values of transfer coefficients. The average value of transfer coefficients for both Plain and Modified PP C.C.S. are ~36.1 g/m^2s and ~46.1 W/m^2K, respectively.

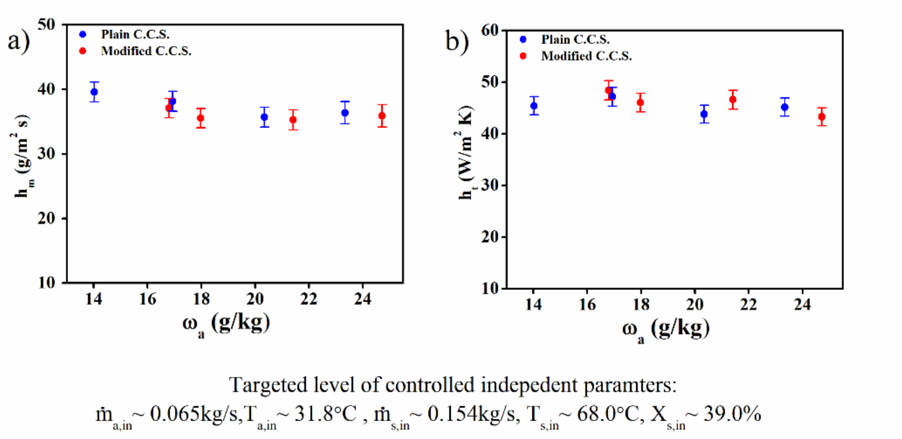

Fig. 5.16 Effect of air specific humidity ratio on a) mass transfer coefficient and b) heat transfer coefficient

5.5.6 Variation of Lewis number (Le)

The Le number is a dimensionless number that relates the heat and mass transfer coefficients in the coupled heat and mass transfer process. It is defined as,

$$Le = \frac{h_t}{h_m * C_{pm}} \tag{5.26}$$

Previous studies [126,134] obtained the heat transfer coefficients under the assumptions of unity Lewis number (Le). However, this approximation may be true for the air-water system, but in LDAC where complex coupled heat and mass transfer occurs due to chemical dehumidification/humidification, the unity Le number may be inaccurate. In the current study, the Le number is derived from coupled heat and mass transfer process via numerical differentiation.

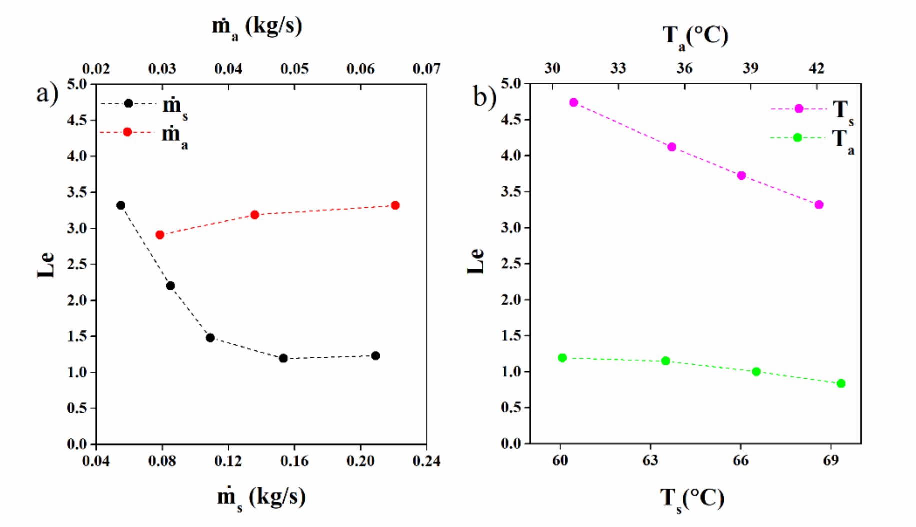

Fig. 5.17 Variation of Lewis number of CCS for varying a) air and solution mass flow rate b) air and solution temperature

Fig. 5.17 shows the variation of Le number for different operating parameters. It is found that Le number decreased from 3.3 to 1.2 with the increase in the mass flow rate of solution and increased from 2.9 to 3.3 for increasing air mass flow rate. Further, Le number varied from 4.7 to 3.3 and from 0.8 to 1.2 for increasing desiccant solution and air temperature. The overall range of the Lewis number was found to be from 0.8 to 4.7 in the current study.

5.6 Development of Sh and Nu number correlation

The heat and mass transfer coefficient derived from the experimental data by numerical technique were utilized for correlation model development. Heat and mass transfer correlations on packed bed towers are widely reported [61,64,79,126–131]. In contrast, correlations on falling film towers are comparatively less, and that too on regeneration heat and mass transfer coefficient is very few [135,136]. The existing regeneration correlation are developed for vertical plastic/metallic PS considering complete surface wetting assumption. It is clear from the section 5.5.1 that heat and mass transfer coefficient characteristics are entirely distinct in the partial wetted zones compared to fully wetted zones. Hence, the past correlations that are developed from experimental observations of fully wetted conditions or fully wetted assumption under partial liquid loading conditions will not suffice the requirement of modelling of partial wetted zones experimental observations. Therefore, a new generalized correlation is needed for the development of low flow plastic surface-based regenerators that can capably help in the modelling of plastic regenerator operating in the partial or fully wetted zones.

Developing a correlation that can consider the influence of all parameters requires extensive experimentation to generate a substantial number of datasets. Practically, such massive data generation is not technically possible for many parameters. On the other hand, it is not feasible to conduct experiments for all parameters due to the associated cost incurred in undesired experiments. Hence, the authors have restricted investigation with selected air and solution operating parameters (Table A2). In order to compare the efficacy of current approach (considering actual wetting characteristics) with previously followed practice (assuming 100 percent wetting assumption), two different Nu and Sh correlations have been developed and compared to predict experimental observations of regeneration process at partial wetted conditions. Apart from common air and solution operating parameters, the correlation equation includes heat and mass transfer driving potential to represent the coupled heat and mass transfer interaction and solution side Reynolds number to incorporate the influences of thermo-physical properties of the desiccant solution. Eqs. (5.27) and (5.28) show the newly proposed Sh and Nu correlation for falling film regenerators in dimensionless form.

$$Sh = \frac{h_m\, t}{\rho_a D_a} = a\left(\frac{A_w}{A}\right)^b \left(\frac{m_{s,in}}{m_{a,in}}\right)^c \left(\frac{T_{s,in} - T_{a,in}}{T_{a,in}}\right)^d \left(\frac{\omega_{eqls,in} - \omega_{a,in}}{\omega_{eqls,in}}\right)^e (Re_a)^f (Sc_a)^g (Re_s)^h \tag{5.27}$$

$$Nu = \frac{h_t\, t}{k_a} = a'\left(\frac{A_w}{A}\right)^{b'} \left(\frac{m_{s,in}}{m_{a,in}}\right)^{c'} \left(\frac{T_{s,in} - T_{a,in}}{T_{a,in}}\right)^{d'} \left(\frac{\omega_{eqls,in} - \omega_{a,in}}{\omega_{eqls,in}}\right)^{e'} (Re_a)^{f'} (Pr_a)^{g'} (Re_s)^{h'} \tag{5.28}$$

The data points of the current study and Kumar et al. [150] are used in regression analysis for finding the coefficients of Eqs. (5.27-5.28). Eqs (5.29-5.30) shows the final form of the newly proposed Nu and Sh correlation.

$$Sh_{pw} = 4.92\left(\frac{A_w}{A}\right)^{0.676}\left(\frac{m_{s,in}}{m_{a,in}}\right)^{0.209}\left(\frac{T_{s,in}-T_{a,in}}{T_{s,in}}\right)^{0.008}\left(\frac{\omega_{eqls,in}-\omega_{a,in}}{\omega_{eqls,in}}\right)^{0.431}$$

$$(Re_a)^{0.533}(Sc_a)^{0.33}(Re_s)^{-0.282} \tag{5.29}$$

$$Nu_{pw} = 1.93\left(\frac{A_w}{A}\right)^{-0.504}\left(\frac{m_{s,in}}{m_{a,in}}\right)^{-0.197}\left(\frac{T_{s,in}-T_{a,in}}{T_{s,in}}\right)^{0.40}\left(\frac{\omega_{eqls,in}-\omega_{a,in}}{\omega_{eqls,in}}\right)^{-0.176}$$

$$(Re_a)^{0.396}(Pr_a)^{0.33}(Re_s)^{0.210} \tag{5.30}$$

Equations (5.31-5.32) show the final form of Nu and Sh correlations developed assuming 100% wetting conditions for low flow rate readings also.

$$Sh_{cw} = 0.92\left(\frac{m_{s,in}}{m_{a,in}}\right)^{-0.0086}\left(\frac{T_{s,in}-T_{a,in}}{T_{s,in}}\right)^{-0.474}\left(\frac{\omega_{eqls,in}-\omega_{a,in}}{\omega_{eqls,in}}\right)^{0.320}$$

$$(Re_a)^{0.492}(Sc_a)^{0.35}(Re_s)^{0.015} \tag{5.31}$$

$$Nu_{cw} = 0.456\left(\frac{m_{s,in}}{m_{a,in}}\right)^{-0.069}\left(\frac{T_{s,in}-T_{a,in}}{T_{s,in}}\right)^{0.443}\left(\frac{\omega_{eqls,in}-\omega_{a,in}}{\omega_{eqls,in}}\right)^{-0.131}$$

$$(Re_a)^{0.616}(Pr_a)^{0.420}(Re_s)^{0.080} \tag{5.32}$$

Developed Sh and Nu number correlations (Eqs. (5.29-5.30)) and (Eqs. (5.31-5.32)) are separately used to estimate the outlet condition of air following Eq. (5.18) and Eq. (5.22) with actual wetting and complete wetting assumptions. Fig. 5.18 shows the comparison between the experimental and predicted $\Delta\omega_a$ and ΔT_a values of Plain and Modified C.C.S. at different mass flow rate of solution using correlations developed through partial wetting, complete wetting and Kim et al. [135] correlations. The existing Nu and Sh numbers correlations of falling film regenerator by Kim et al. [135] severely under predicted $\Delta\omega_a$ and ΔT_a values observed during experimentation of Plain and Modified C.C.S. Differences in the wetting characteristic of C.C.S. and

P.S., liquid air flow arrangement and low liquid desiccant loading rates (forcing liquid flow in the form of thick individual liquid rivulets, not as a thin continuous falling film) seem to be expected reasons behind it. The developed Sherwood number correlation through partial wetting approach (Sh_{PW}) predicted $\Delta\omega_a$ values of the Plain and Modified PP C.C.S. with MAPE of 5.0% and 4.7%, respectively whereas the developed Sherwood number correlation with complete wetting assumption (Sh_{CW}) predicted these experimental observations with MAPE of 14.8% and 19.1%, respectively. Similarly, Nusselt number correlation developed by partial wetting approach (Nu_{PW}) predicted ΔT_a values of Plain C.C.S. and Modified C.C.S. with MAPE of 4.0% and 6.3%, while Nusselt number correlation developed with complete wetting assumption (Nu_{CW}) predicted ΔT_a values of the Plain C.C.S. and Modified C.C.S. with MAPE of 10.9% and 17.2% respectively. It is clear that the partial wetting correlations (Sh_{PW} and Nu_{PW}) predicted experimental $\Delta\omega_a$ and ΔT_a values of the Plain and Modified C.C.S. for partial as well as complete wetting operating zones with good accuracy compared to complete wetting correlations (Sh_{CW} and Nu_{CW}); developed assuming full wetting of the solid surface. As complete wetting approach assumes that entire solid surface area is available for simultaneous heat and mass transfer operation between liquid desiccant and air, it would have underpredicted heat and mass transfer coefficient values in the partial wetting zone. As regression process tries to normalize the errors of partial and complete wetting zones together, the developed Sh_{CW} and Nu_{CW} number correlations showed poorer response in both partial and fully wetted zones. Hence, complete wetting correlations are not suitable for modelling and load calculation needs of the partial wetting zones. Sh_{PW} and Nu_{PW} number correlations had shown good response for the partial as well as full wetted operating conditions. These equations should be utilized for the diversified need of modelling under partial and fully wetted operating conditions.

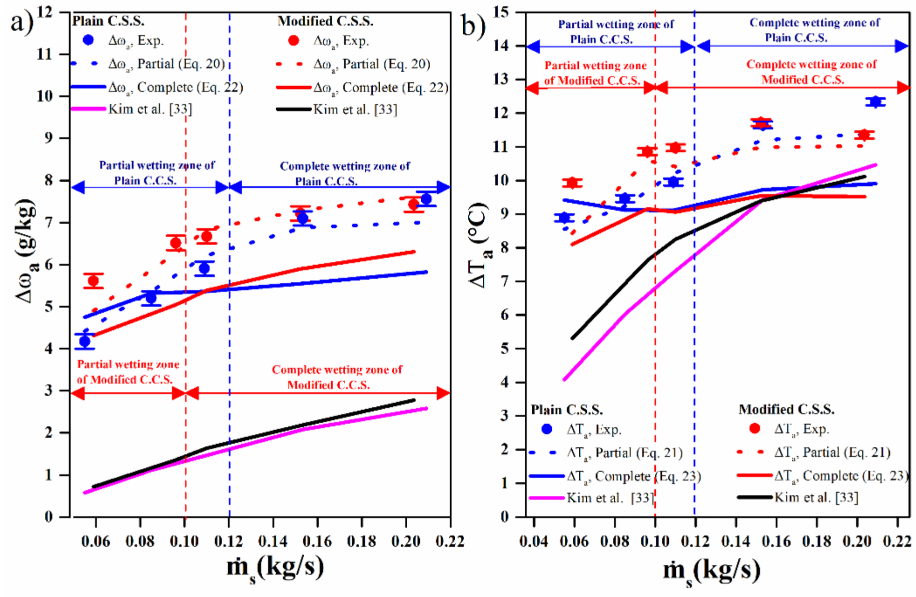

Fig. 5.18 Comparison between experimental and predicted values of CCS for change in a) air humidity ratio and b) air temperature at varying mass flow rate of desiccant solution

In order to confirm the ascendency of the partial wetting approach compared to complete wetting approach, the performance of the developed correlations is also checked against the experimental readings of P.S. [150]. Fig. 5.19 illustrates the prediction of $\Delta\omega_a$and ΔT_a for the experimental observations of P.S. [150] through developed correlations of partial wetted (Sh_{PW} and Nu_{PW}) and complete wetted (Sh_{CW} and Nu_{CW}) assumptions. Kim et al. [135] correlations underpredicted experimental $\Delta\omega_a$ and ΔT_a values of Plain and Modified P.Ss. The Sh_{PW} and Sh_{CW} correlations predicted experimental $\Delta\omega_a$ values of Plain P.S. with MAPE of 7.6% and 45.2%, respectively. Which proves that for poorly wetted surfaces and at low flow rate operating conditions (with partial wetting of the surface), the empirical equation developed through the consideration of heat transfer from the dry parts over the solid surface provides more accurate prediction in comparison to the conventional complete wetting approach. The Sh_{PW} and Sh_{CW} predicted experimental observations of the Modified P.S. with MAPE of 4.4% and 9.5%, respectively. Sh_{PW} correlation closely traces the experimental observation unlike Sh_{CW} correlation for both cylindrical and plate surfaces. Only for the Modified P.S., the Nu_{CW} provided better prediction of ΔT_a than Nu_{PW}. It may be possibly due to the liquid splashing out of the solid surface at high flow rates.

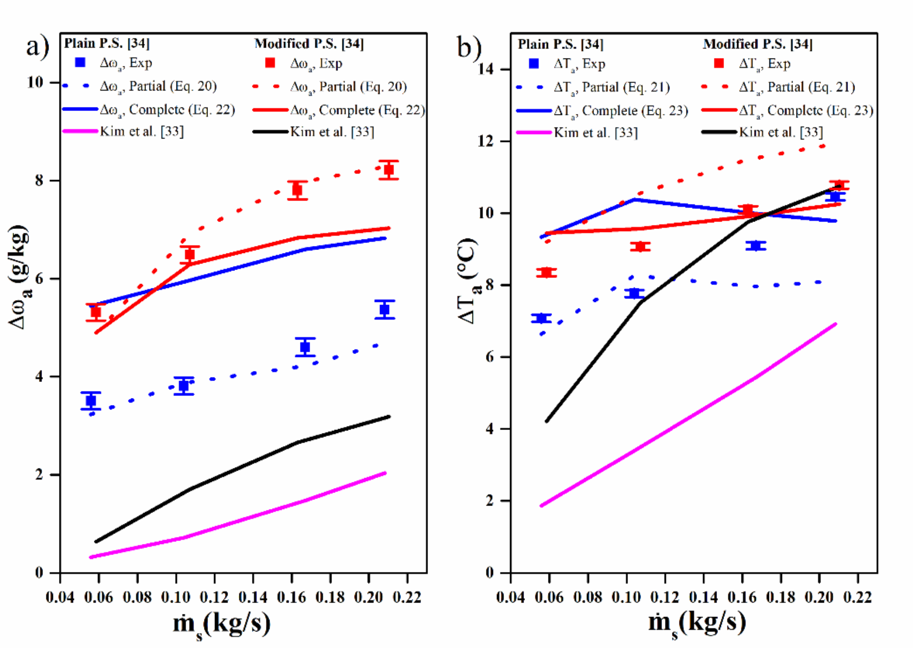

Fig. 5.19 Comparison between experimental and predicted values of PS for change in a) air humidity ratio and b) air temperature at varying mass flow rate of desiccant solution

Fig. 5.20 shows the parity plot for Sh and Nu correlation at partial and complete wetting conditions. 86.4% and 77.3% of datapoints lies within ±15% error band for Sh_{PW} and Nu_{PW} correlation, respectively, whilst for the Sh_{CW} and Nu_{CW} correlation it is 30.3% and 63.6%, respectively.

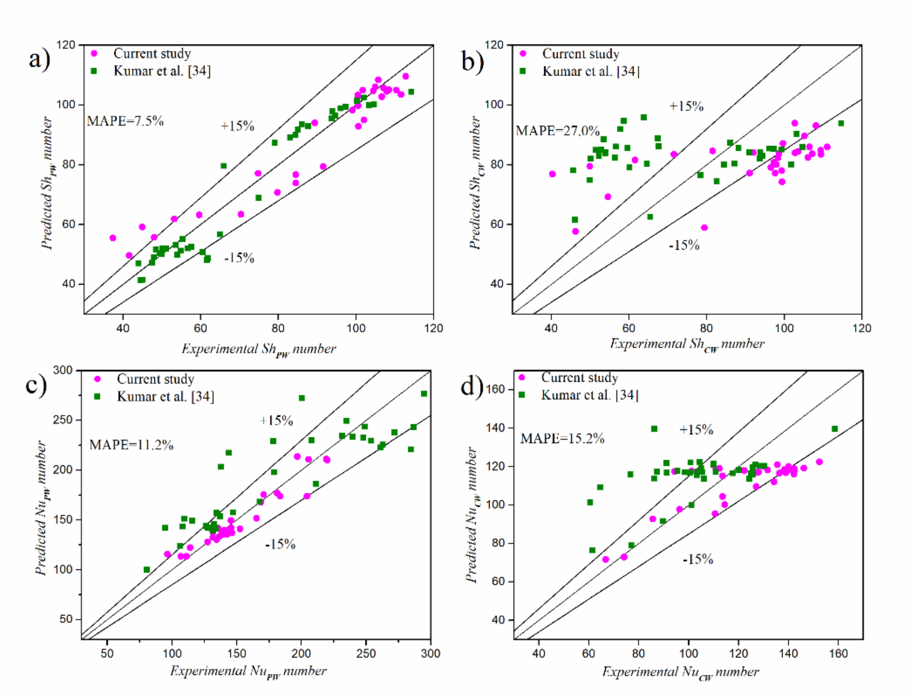

Fig. 5.20 Comparison between experimental and predicted Sh and Nu number at partial wetting condition (a and c) and complete wetting conditions (b and d) for different datasets.

5.7 Conclusion

Experimental test was conducted to investigate the heat and mass transfer characteristic of the plastic CCS dehumidifier and regenerator. The numerical finite difference technique was applied to evaluate the heat and mass coefficients of CCS dehumidifier and regenerator. Experimental variation of heat and mass transfer coefficients was studied under wide range of operating parameters of air and solution. Following are the main conclusions drawn from the current Chapter.

1. For the dehumidification process, the CCS has shown superior mass transfer characteristics than the PS for each analysed air and solution parameter. The enhancement in the mass transfer coefficient offered by CCS over PS was found in the range of 21.2 - 237.0% for the current study with an average improvement of 65.3%. The Modified surface intensified the mass transfer coefficient of circular cylinders from 20.0 to 65.0% for the studied parameters. Hence, vertical circular cylinder surfaces are more suitable for the development of low flow falling film LDS.

2. A new generalized empirical correlation to predict the Sh number of dehumidifiers was developed by incorporating new pertinent parameters, such as wetting characteristics difference, flow dynamics, enthalpy potential and sensible cooling information. The proposed correlation presented a good prediction response against nine experimental studies (three adiabatic and six non-adiabatic) and the error was bounded within ± 20% and ± 30% for the predicted 70.0% and 88.6% data. The developed correlation would be helpful for engineers and scientists who are interested in simulation and modelling of falling film dehumidifiers.

3. For regeneration process, in partial wetting operating zone ($\dot{m}_s$ ~ 0.060 kg/s), the average mass transfer coefficient of the Modified C.C.S. is found superior to Plain C.C.S. by 73.0%, whereas average heat transfer coefficient of Plain C.C.S. is found 12.4% higher than Modified C.C.S. The basic nature of coupled heat and mass transfer processes might be the expected reasons.

4. In complete wetting operating zone ($\dot{m}_s$ ~ 0.153 kg/s), no significant difference was found between the transfer coefficients of Plain and Modified PP CCS. To ascertain the above behaviour, the performance of the Plain PP CCS surface and Modified PP CCS surfaces are experimentally compared against the partial loading condition for $\dot{m}_s$ and T_S, and complete wetting condition for T_a and ω_a. Experimental findings proved that the benefits of surface modification techniques can be realized mainly at low liquid flow rates (partial wetting conditions).

5. Existing falling film regenerator correlation and correlations developed from complete wetting assumption failed to predict the experimental observations of partial wetting conditions. Hence, new generalized correlations have been developed considering the actual wetting factor at partial wetting conditions. The newly developed correlations predict the experimental outlet air humidity and air temperature values of CCS with better accuracy compared to correlations developed by complete surface wetting assumption.

6. The correlations developed at actual wetting conditions predict the air outlet conditions of C.C.S. and P.S. [150] with good accuracy in partial and complete wetted zone compared to correlations developed at complete wetting assumption. Hence, the partial wetting correlation must be used for prediction of experimental observations. The overall MAPE of Sh_{PW} and Nu_{PW} correlation against current study and P.S. [150] is 7.5% and 11.2%, respectively while the overall MAPE of Sh_{CW} and Nu_{CW} is 27.0% and 15.2%, respectively. The developed partial wetting correlations will be helpful for designing and developing falling film towers operated in wide range of liquid flow rate conditions.

7. For fully wetted conditions, the variation of Le number is found to be from 0.8 to 1.2 whereas, variation of Le number for partial wetting conditions is from 1.4 to 4.7. Hence, assumption of unity Lewis number for poor wetting characterise surface and surface operating at partial wetting conditions would result in underprediction of outlet air condition.

.

CHAPTER 6

ANN MODELLING OF FALLING FILM DEHUMIDIFIERS

6.1 Introduction

Analytical models are challenging to solve due to complex nature of heat and mass transfer process in liquid desiccant. They have limited prediction ability and mostly rely on verification from experiment data. Finite difference models require few assumptions but involve extensive calculations and consume a lot of computational time. Empirical models developed based on experimental/numerical data have limited generalizability and are valid for fitted range of datasets. In recent years, to accurately reproduce the experimental observation intelligent computing technique such as ANN models have emerged as the popular choice among the researchers. In the current Chapter 6, neural network technique is used to developed data-driven models of falling film dehumidifier.

6.2 Artificial neural network (ANN) working principle.

ANN are non-linear information processing structure inspired from the way human brain works, basically it is tries to imitate the learning and memorizing mechanism of brain [153,157]. Analogous to biological neurons structure, ANN is composed of multiple information processing units called neurons which are associated to each other by connecting links (weights). The ANN learns itself by creating a input-output mapping without knowing the explicit information of mathematical relationships between input and output data [153]. The neurons perform mathematical operations on data, which is then passed to neuron in next layer for further processing. Fig. 6.1 displays the simple structure of ANN. Every ANN structure consists of three essential elements: 1) connecting links (weights) 2) summing node with an activation function and 3) externally applied bias.

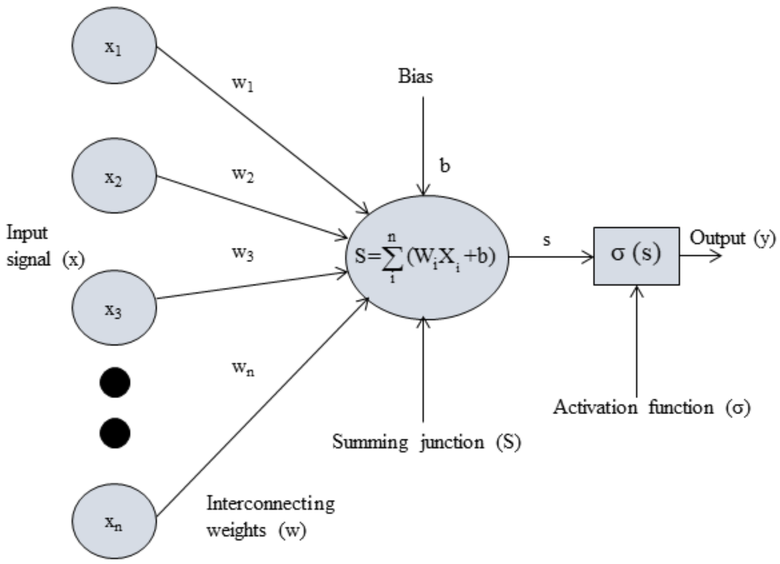

Fig. 6.1 General structure of ANN [172]

The x_1, x_2 …x_n are the input signal; w_1, w_2…w_n are called weights of neuron; b is the bias; σ is the activation function and y is the output signal of the neuron. The value of neuron (S) is the weighted sum of values of all neurons and connecting weights plus the bias. Mathematically, the value of a neuron can be expressed as,

$$y = \sigma[\sum_i^n (w_i x_i + b)] \tag{6.1}$$

The weight and bias are selected randomly, or they can be predefined. The weight indicates the strength of the connection, and bias indicates whether the neuron is active or not. Activation functions are non-linear transformation that is performed over each input signal. There are various activation functions available such as linear, sigmoid, hyperbolic tangent, etc. out of which sigmoid is the most used transfer function

$$f(x) = \frac{1}{1+e^{(-x)}} \tag{6.2}$$

The feed-forward back propagation (FFBP) is the most popular and widely used ANN [173,174]. The structure of FFBP is shown in Fig. 6.2. FFBP consists of an input layer, an output layer, and a single/multi-hidden layer between the input-output layer. The information is passed from the input layer to the output layer in feed-forward fashion. During training, the FFBP learns by acquiring new weights and bias based on input-output data mapping; the output generated in the output layer is matched with the desired output. The error between the ANN output and actual output is fed back to adjust the weight till the desired minimum error is obtained.

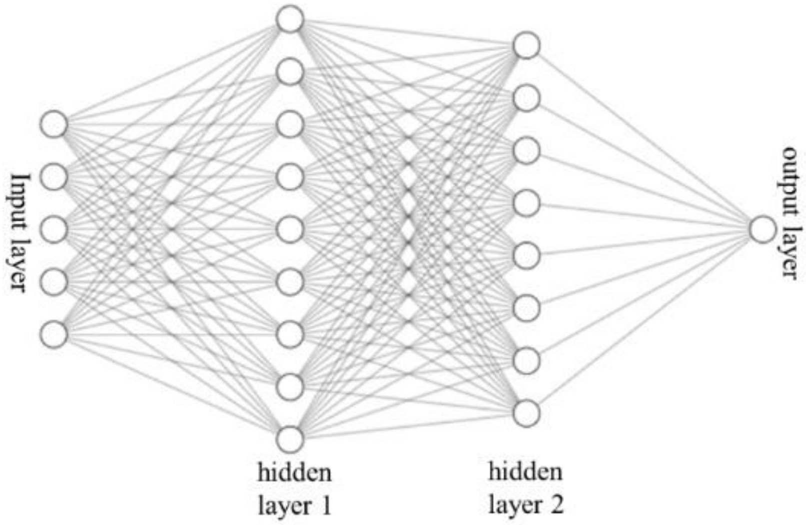

Fig. 6.2 Multilayer FFBP neural network

6.3 Selection of input parameters and its significance.

From the experimental data analysis, it was found that the parameters of air (temperature, humidity, and mass flow rate) and desiccant solution (temperature, concentration, and mass flow rate) have significant impact on dehumidification rate and dehumidification effectiveness. Hence, all the influencing parameters from the air side ($m_{a,in}, T_{a,in,}\omega_{a,in}$) and solution side ($m_{s,in,}T_{s,in}, \omega_{eqls}$) are considered as input to the ANN. Total six variables are selected as input to ANN. The dehumidification rate and dehumidification effectiveness are expressed as functions of the following variables.

$$\dot{m}_{abs}/\varepsilon_{Y,abs} = f\left(\frac{H}{W}, \frac{\gamma_c}{\gamma_s}, m_a, m_s, \ (h_{a,in} - h_{eqls,in}), (\omega_{a,in} - \omega_{eqls})\right) \qquad (6.3)$$

The enthalpy difference ($h^* = h_{a,in} - h_{eqls,in}$) and moisture difference ($\omega^* = \omega_{a,in} - \omega_{eqls}$) represent the simultaneous heat and mass transfer between air and solution. The ratio of the surface energy of solid surface and liquid desiccant $\left(\gamma^* = \frac{\gamma_c}{\gamma_s}\right)$ is utilized to signify the wetting characteristic of plastic/metallic surfaces and liquid desiccant. The shape factor $\left(S^* = \frac{H}{W}\right)$ is included to differentiate the size of the dehumidifier corresponding to different datasets. The mass flow rate of air and desiccant solution ($\dot{m}_a$ and $\dot{m}_s$) are included as independent parameters due to different thermophysical properties.

6.4 Input-output dehumidifier datasets and Pre-processing

In addition to the experimental observation from our studies, the datasets from other available studies on falling film dehumidifiers are considered for developing the ANN model. Table 6.1 shows the details of different dehumidification studies used for training and testing the ANN model. The datasets covered wide range of operating parameters of different liquid desiccant-solid surface combinations of both adiabatic and non-adiabatic studies. The total number of data points utilized for the ANN model is 1650. Around 60% of the data is used for training and the remaining data is used as validation data (15%) and test data (25%). Before training and simulation, the input and output data points are normalized according to Eq. (6.4).

$$Z_{\text{norm}} = 0.1 + 0.8\,\frac{(Z_i - Z_{\min})}{(Z_{\max} - Z_{\min})} \qquad (6.4)$$

Z_{min} and Z_{max} are the maximum and minimum values of a particular parameter, and X_i is any value of that parameter. The normalization scales down the datasets from wide range to same range for input and output data, which ensures better training and generalizability [175].

Table 6.1 Details of the dehumidification studies utilized for ANN modelling

Study	Adiabatic/Non-Adiabatic	Solid surface-desiccant	Data points	Operating parameters					
				$\dot{m}_a$ (kg/s)	T_a (°C)	ω_a (g/ kg)	$\dot{m}_s$ (kg/s)	T_s (°C)	X_s (%)
Training dataset									
Yin et al. [82]	Adiabatic	S.S-LiCl	27	0.055-0.083	30.5-30.9	10.6-13.4	0.103	20.6-28.9	37.7-38.8
	Non-adiabatic	S.S-LiCl	35	0.048-0.086	30.5-30.9	10.6-13.4	0.103	23.5-31.5	37.7-38.8
Luo et al. [86]	Non-adiabatic	S.S-LiCl	127	0.020-0.060	24.0-35.0	17.8-24.0	0.030-.047	17.3-30.0	34.7-40.7
Liu et al. [171]	Non-adiabatic	PP-LiBr	12	0.121-0.180	33.5-36.3	15.2-18.9	0.044-0.134	28.6-31.5	38.9-42.1
Turgut and Coban [97]	Non-adiabatic	S.S-LiCl	16	0.210-0.800	25.4-35.0	16.1-23.1	0.120-0.460	21.1-29.4	40.0
Prieto et al. [112]	Non-adiabatic	PP-LiCl	50	0.178-0.378	27.0-33.6	9.0-13.4	0.042-0.117	17.0-25.0	35.3-35.9

Dong et al. [88]	Non-adiabatic	TiO_2-LiCl	114	0.028-0.070	26.4-39.0	11.6-25.8	0.010-0.045	25.9-26.4	38.8
Wen et al. [89]	Non-Adiabatic	Al-LiCl	85	0.021-0.058	27.0-36.0	17.2-24.3	0.050 0.120	25.0-34.0	35.0 38.0
Wen et al. [122]	Non-Adiabatic	S.S-LiCl	154	0.023-0.060	29.8-36.4	17.0-24.7	0.081-0.158	28.0-34.8	35.0
Wen et al. [39]	Non-Adiabatic	S.S-LiCl	53	0.032	29.0-36.0	16.7-24.9	0.010-0.178	27.9-35.3	70.3
Wen et al. [92]	Non-Adiabatic	S.S-LiCl	243	0.023	28.0-36.4	15.0-24.0	0.080-0.160	26.0-35.0	32.0-38.0
Peng et al [137]	Non-Adiabatic	S.S-LiCl	120	0.070-0.038	28.0-32.5	20.9-30.3	0.060-0.112	26.0-34.0	27.0-46.0
Cheng et al. [91]	Adiabatic	S.S-LiCl	22	0.07-0.37	30.0	18.6-19.2	0.090-0.910	26.0-36.0	29.9-31.6
Zhi et al. [113]	Adiabatic	PTFE-LiCl	20	0.030-0.070	25.0	13.9	0.043-0.054	27.5	40.0
Wen et al. [28]	Non-Adiabatic	S.S-LiCl, HCOOK	107	0.029-0.050	29.8-35.5	16.2-25.1	0.080-0.150	27.3-34.5	35.0, 70.3
Current study	Adiabatic	PP-LiCl	47	0.032-0.07	26.0-36.0	15.3-25.4	0.023-0.146	20.8-32.5	33.0-39.0
Test data set									

Wen et al[121]	Non-adiabatic	S.S-LiCl	129	0.023-0.070	28.0-36.4	16.3-24.7	0.082-0.162	28.0-35.0	35.0
Dong et al. [109]	Non-adiabatic	Titanium S.S, PTFE-LiCl	111	0.030-0.080	28.3-40.2	14.0-24.6	0.016-0.047	18.8-30.1	38.0
Wen et al. [100]	Non-Adiabatic	S.S-LiCl	100	0.023-0.060	28.5-36.3	16.1-24.7	0.070-0.149	27.8-35.2	25.0, 35.0
Gao et al. [133]	Adiabatic	S.S-LiCl	30	0.100-0.510	27.0-38.0	8.5-21.3	0.052-0.448	16.0-32.0	30.0-42.0
Khan et al.. [151]	Adiabatic	PP-LiCl	48	0.032-0.07	26.0-36.0	15.3-25.4	0.023-0.146	20.8-32.5	36.0-42.0

6.5 ANN model training and simulation.

The ANN has excellent prediction capability, but this has been reported mainly for training datasets [154,158,174]. The ANN model, which is good at predicting the training data, may perform poorly for test data sets (data not considered for training the ANN model). In generality, the ANN matches the training datasets so closely that it loses generalizability over the unseen data. Hence, an optimal/best ANN model is the one that can give good performance to both training and test datasets. Hitherto, there is no exact criterion for determining the best/optimum ANN model because there are many parameters that affect the network performance, such as the training algorithm, training function, transfer function, number of inputs, learning rate, and training ratio, which need to fix/tested before proposing the best/optimal ANN model. The other challenge associated with ANN is the selection of number of hidden layers and neurons. The neural network's performance is significantly influenced by the number of hidden layer and neurons. The selection of both of them is arbitrary, and there is no concrete evidence regarding the definite number of hidden layer and neurons in network structure [176].

Fig. 6.3 shows the flow chart of current ANN model. The model is tested with different hidden neuron varying from one to twenty. Because of the randomness in the initialization of weight and bias, each ANN model with different hidden neurons is iterated one hundred times. The TrainBr (Bayesian regularization) is used as training function with 80: 20 as training ratio. In 80:20 training ratio, around 20% of data (testing data) is utilized to test the network's performance during training and stop the training algorithm once the generalization starts improving. Table 6.2 shows the different parameters used for training the ANN model. A MATLAB (R2022b) code is programmed to carry out the training and testing of ANN. The algorithm stops when the lowest mean-square error (MSE) value is obtained. One epoch indicates one training and learning cycle (Fig. 6.3).

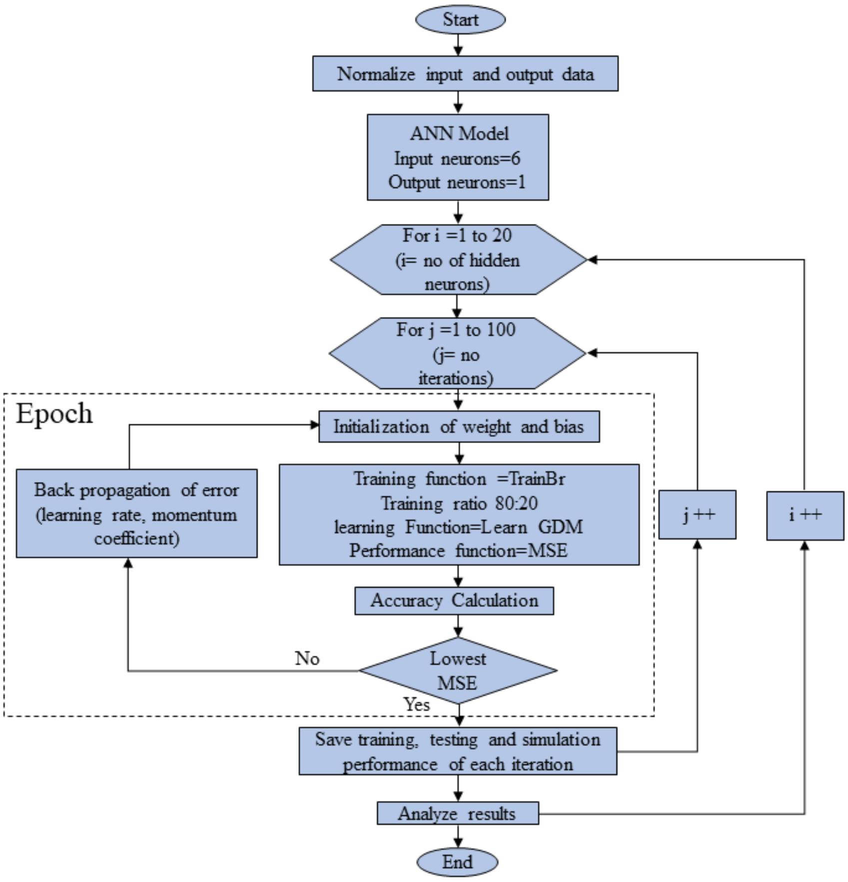

Fig. 6.3 Flow chart of ANN modelling

.

Table 6.2 Training parameters of ANN

Training Parameters	Type/Value
Training function	TRAINBR
Training ratio	80:20
Learning function	LEARNGDM
Performance function	MSE
Transfer function	TANSIG, PURELIN
Epochs	10000
Error goal	1x 10^{-7}
Learning rate	0.005
Momentum factor	0.1

6.6 Optimal ANN model

Fig. 6.4 shows the variations of MSE for training and test data of dehumidification rate and dehumidification effectiveness model. The trained and test MSE decreased gradually with an increase in the number of hidden neurons and attained the same level at six neurons. The testing performance fluctuates with a further increase in the number of neurons, and no significant change is observed in the training performance. Hence, the ANN model with six hidden neurons is considered the optimum. The ANN training is improved at higher hidden neurons, but the testing deteriorates. Fig. 6.5 shows the optimal ANN model for falling film dehumidifier.

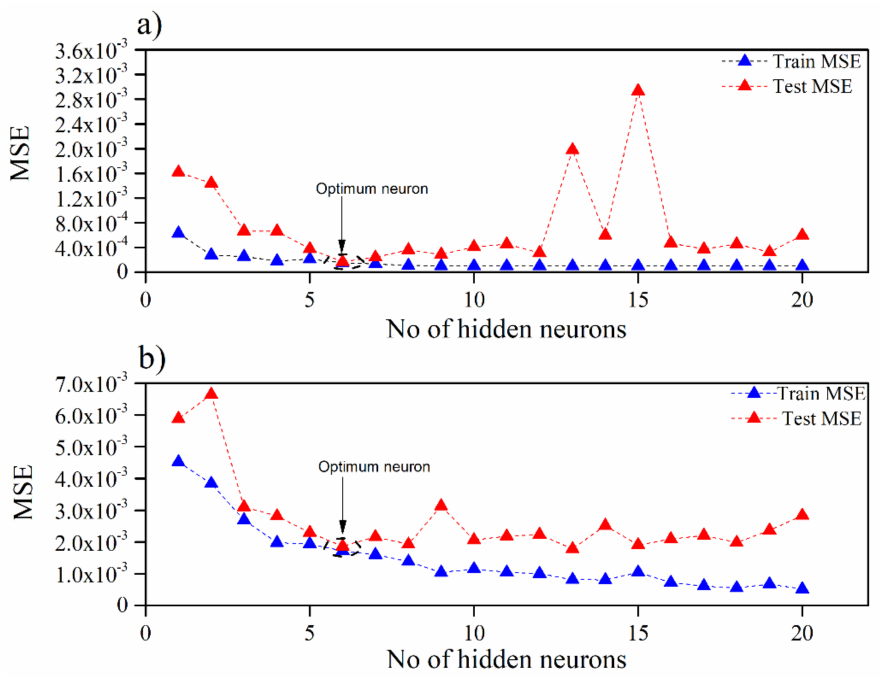

Fig. 6.4 MSE variation with different hidden neurons a) dehumidification rate b) dehumidification effectiveness

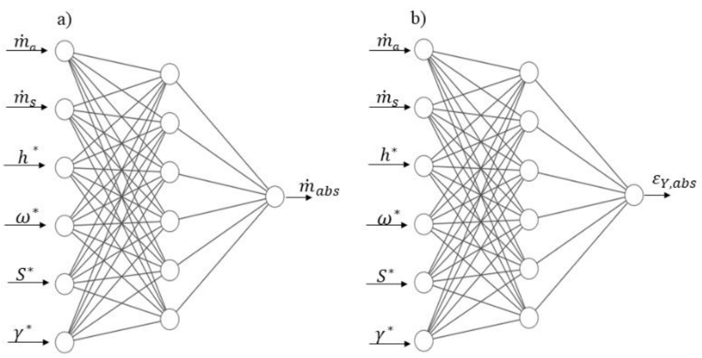

Fig. 6.5 Optimal ANN model for a) dehumidification rate and b) dehumidification effectiveness

6.7 Performance of optimal ANN model.

Table 6.3 shows the performance comparison of the current ANN model with the previous ANN model of Mohammed et al. [154] on a MAPE basis for the. To avoid biasness, the result of the previous model is obtained following the procedure shown in Fig. 6.3 considering TrainLM as the training function. The current dehumidification rate model showed good performance for training, validation, and test data. The MAPE of training, validation, and tes is found to be 2.7%, 2.1%, and 3.0% lower than the model of Mohammad et al. [154]. The effectiveness ANN model showed comparable performance for training and testing but higher accuracy for predicting the test datasets, with MAPE 7.3% lower than the previous model [154]. That proves the usefulness of the current ANN for predicting the dehumidification rate and effectiveness for experimental observations.

Table 6.3 Performance comparison of current with previous ANN model [154]

Dehumidification rate			
Study and ANN model	Training (MAPE)	Validation (MAPE)	Testing (MAPE)
Mohammed et al. [154] (6-3-3-1)	6.9	6.5	9.1
Current model (6-6-1)	4.2	4.4	6.1
Dehumidification effectiveness			
Mohammed et al. [154] (6-6-6-1)	9.9	9.7	17.5
Current model (6-6-1)	10.4	10.4	10.2

6.8 Influence of different input variables

Apart from the influence of different variable used in the current study, the variable used in empirical correlation by different authors [73,100,147] for the prediction performance of liquid desiccant is tested as input for both dehumidification rate and dehumidification effectiveness ANN models. Table 6.4 shows the impact of a number of inlet parameters on the performance of ANN. The ANN with 3,5 and 9 input variables are tested. As shown in Table 6.4, the number of hidden neurons is kept the same in each ANN model for comparison purposes. The current optimal ANN model outperformed the other models for both the dehumidification rate and effectiveness model. However, the 9-6-1 model performed well for training data but poorly for simulating datasets. However, the 5-6-1 model presented better performance only for dehumidification rate model. Hence, the ANN with six input variables might be the optimal model for predicting the training and test datasets.

Table 6.4 Impact of number of input parameters on ANN

		Dehumidification rate		
Studies	ANN structure	Training (MAPE)	Validation (MAPE)	Testing (MAPE)
Qi et al.[147]	9-6-1	5.7	6.8	45.2
Wang et al. [73]	5-6-1	6.4	6.1	13.3
Wen et al. [100]	3-6-1	7.6	8.5	9.7
Current study	6-6-1	4.2	4.4	6.1
		Dehumidification effectiveness		
Qi et al.[147]	9-6-1	11.3	11.6	27.0
Wang et al. [73]	5-6-1	13.2	11.7	17.5
Wen et al. [100]	3-6-1	16.3	19.0	29.8
Current study	6-6-1	10.4	10.4	10.2

6.9 Conclusion

The ANN modelling work was carried out to develop a generalized predictive model for falling film adiabatic and non-adiabatic dehumidifiers. The following conclusion are drawn from the above study.

1. The optimal neural network is obtained at six hidden neurons and the best ANN model is 6-6-1 and 6-6-1 for dehumidification rate and effectiveness, respectively.
2. The current single-layer ANN model has shown superior performance compared to the previous multilayer ANN model. The MAPE between experimental and ANN for training and test data in the case of dehumidification rate is 4.2% and 6.1%, respectively, while for the effectiveness model, it is 10.4% and 10.2%, respectively.
3. It was found that increasing the number of neurons/hidden layer improved the accuracy the of training datasets but yielded poor testing performance. Adding of the additional neurons/layers will also increase the computation time.
4. The current six input variables have shown the superior performance on the dehumidification rate and effectiveness of ANN models compared to inlet parameters from other studies.

CHAPTER 7

OVERALL CONCLUSIONS AND FUTURE SCOPE

7.1 Overall conclusion

8. The CCS promotes the formation of stable falling film by allowing effective radial spreading and intense mixing of rivulets on the CCS. Liquid film shrinkage in the downward direction on CCS is found smaller than it was reported for the PS [165]. In fact, liquid film extends in the downward direction at a low flow rate even due to the mixing of isolated liquid rivulets. The improved wetting behavior of the CCS facilitated in intensifying the dehumidification and regeneration performance achievable through PS. The improvement in the dehumidification rate and dehumidification effectiveness offered by the Plain PP CCS over Plain PP PS for the tested conditions are 55.9% and 52.3%, respectively. Similarly, the improvement in the regeneration rate and regeneration effectiveness offered by the Plain PP CCS over Plain PP are 50.5% and 52.2%, respectively. This proves the usefulness of the CCS surface over the PS for the development of the low flow liquid desiccant falling film systems.

9. The Modified surface further elevated the performance of Plain CCS by retaining the liquid film in the stretched condition within the grooves Further, inclined groves promoted the formation of liquid waves, which also improved the performance. The Modified CCS intensified the dehumidification rate and dehumidification effectiveness by 31.3% and 30.2%, respectively. However, the same surface Modification intensified the dehumidification rate and dehumidification effectiveness of PS by 64.4% and 67.0%, respectively. For regeneration process, the Modified CCS enhanced the regeneration rate and regeneration effectiveness of CCS by 3.0% and 4.0% only. The operating flow of above complete surface wetting conditions might be the expected reasons. However, at partial wetting conditions, the surface modification offered 38.7% and 39.7% improvement in regeneration rate and regeneration effectiveness. Thus, the importance of the surface modification technique is more prominent for the poorly wetted surface and surface operating at partial wetting conditions.

10. Two parameters, including mass flow rates of solution and air, showed a strong influence on the dehumidification performance indices of CCS. The dehumidification rate of the Plain PP CCS was saturated at the high mass flow rates of the air and solution. However, Modified PP CCS maintained an increasing trend up to a high range of the mass flow rates of the air and the solution. Spilling of the desiccant solution at a high solution flow rate and non-uniform biased airflow distribution appeared to be two main limitations of the CCS.

11. For dehumidification process, at high solution temperatures ($T_s > 29$), the dehumidification rate the Plain PP CCS was found even higher than Modified PP PS and also for the studied range of the desiccant solution concentration. However, at high concentration levels, the performance of both surfaces started approaching the same value. The desiccant viscosity seems to be the main reason behind the above observations.

12. The regeneration performance of the Plain PP CCS even exceeded the performance of the Modified PP PS at lower solution temperature and higher air humidity levels. Hence, operating conditions should be appropriately considered to avoid the cost incurred due to surface modification.

13. The proposed dehumidification and regeneration effectiveness correlation presented good accuracy on validation with experimental studies. The dehumidification correlation predicted eight datasets with overall MAPE of 11.7% and the regeneration correlation predicted nine datasets with an overall MAPE of 16.5%.

14. The mass transfer coefficient of the Modified PP CCS for the dehumidification process was found to be 20.0 to 65.0% higher than the Plain PP CCS. Thus, mechanical surface modification technique can play a crucial role in intensifying the performance of poorly wetted plastic surfaces equivalent to metallic surfaces.

15. The proposed generalized Sh number correlation showed good accuracy against plastic/metallic surface of adiabatic and non-adiabatic falling film dehumidifiers. The overall MAPE of the correlation was 16.6% for nine experimental dehumidification studies (three adiabatic and six non-adiabatic).

16. In partial wetting zone of CCS ($\dot{m}_s$ < 0.110 kg/s), the mass transfer coefficient of the Modified PP CCS is found to be superior to Plain PP CCS by 24.0%, whereas heat transfer coefficient of Plain PP CCS was found to be 9.4% higher than Modified PP CCS. In complete wetting zone ($\dot{m}_s$ > 0.110 kg/s), no significant difference was found between the transfer coefficients of Plain and Modified PP CCS.

17. The correlations developed at partial wetting conditions (i.e., actual wetting conditions) predict the experimental outlet air humidity and air temperature values of CCS with good accuracy compared to correlations developed at complete surface wetting assumption. The overall MAPE of Sh_{pw} and Nu_{pw} correlation against current study and PS [167] is 9.1% and 14.0% respectively while the overall MAPE of Sh_{cw} and Nu_{cw} is 23.8% and 24.5%, respectively. The developed correlation correlations will be helpful for designing, optimizing, and developing falling film LDS.

18. The current single layer ANN model has shown superior performance compared to previous multilayer ANN model. The MAPE between experimental and ANN for training and simulation data in case of dehumidification rate are 4.2% and 6.1% respectively, while for the effectiveness model it is 10.4% and 10.2%, respectively.

7.2 Future scope

Following are the suggestions for future work:

1. The circular cylinder surface has proven to be a superior geometry over plate surface for liquid desiccant dehumidification as well as regeneration. Hence, the findings of the current study can be extended for the development of small-compact size low flow hybrid liquid desiccant system targeted for end-user residential/commercial applications.
2. The finding of the current study could also be useful to carry out a comparative simulation study between packed bed LDS, low-flow falling film hybrid LDS and other conventional air-conditionings systems using commercially available building energy simulation packages like Trnsys, Energy plus, Open Studio for different thermal comfort conditions of building occupants.

APPENDIX A

Uncertainty analysis

The range and accuracy of the different measuring instruments used in the current study are listed in Table 1. The uncertainty associated with performance indicators is estimated following the root sum square (RSS) technique described by Moffat [177]. According to this technique, the uncertainty involved in any dependent variable *Y*, which is a function of many independent variables *x1*, *x2*, *x3*, *x4*, …., can be evaluated as per Eq. (A.1).

$$\Delta_Y = \sqrt{\left(\frac{\partial Y}{\partial X_1}\Delta_{X_1}\right)^2 + \left(\frac{\partial Y}{\partial X_2}\Delta_{X_2}\right)^2 + \left(\frac{\partial Y}{\partial X_3}\Delta_{X_3}\right)^2 + \left(\frac{\partial Y}{\partial X_4}\Delta_{X_4}\right)^2 \ldots.} \quad \text{(A.1)}$$

Where, Δ_Y is the overall uncertainty associated with dependent variable *Y*, and $\Delta_{X1 \ldots X4 \ldots}$ is the overall uncertainty associated with independent variables $X_1 \ldots X_4 \ldots$.

Uncertainty calculation for absorption readings following Moffat [177] RSS method

Temperature

Overall uncertainty in the measurement of the temperature is measured by the temperature of the particular point and internal reference temperature of the data logger.

$\Delta T = T_1 - T_2$

$T_2 = 0\ ^0C$ (internal reference temperature of the data logger)

$$\frac{\partial \Delta T}{\partial T_1} = 1$$

$\delta_T = \delta_{T_1} = \delta_{T_2} = 0.1\ ^0C$

$$\frac{\partial \Delta T}{\partial T_2} = 0$$

$$\delta_{\Delta T} = \sqrt{\left(\frac{\partial \Delta T}{\partial T_1}\delta_{T_1}\right)^2 + \left(\frac{\partial \Delta T}{\partial T_2}\delta_{T_2}\right)^2}$$

$$\delta_{\Delta T} = \sqrt{(1 * 0.1)^2 + (0 * 0.1)^2}$$

$\delta_{\Delta T} = 0.1\ ^0C$

Humidity of moist air

Humidity is the function of DBT and WBT of moist air:

$$\delta_{\omega_a} = \sqrt{\left(\frac{\partial \omega_a}{\partial DBT}\delta_{DBT}\right)^2 + \left(\frac{\partial \omega_a}{\partial WBT}\delta_{WBT}\right)^2}$$

$$\omega_a = \frac{0.622\ P_v}{P_{atm} - P_v}$$

Where, P_v is calculated using Modified Apjohn equation

$$P_v = P_v' - \frac{1.8 * P_{atm} * (DBT - WBT)}{2700}$$

where P_v' is function of WBT

$$\ln(P_v') = \left[\frac{C_1}{WBT} + C_2 + C_3 * WBT + C_4 * WBT^2 + C_5 * WBT^3 + C_6 * \ln(WBT)\right]$$

$$P_v' = e^{\left[\frac{C_1}{WBT} + C_2 + C_3 * WBT + C_4 * WBT^2 + C_5 * WBT^3 + C_6 * \ln(WBT)\right]}$$

where C_1 = -5800.22, C_2 = -5.51626, C_3 = -0.04864, C_4 = 4.17648E-05, C_5 = -1.44521E-08, C_6 = 6.545967 and WBT in K

$$\frac{\partial P_v'}{\partial WBT} = e^{\left[\frac{-C_1}{WBT} + C_2 + C_3 * WBT + C_4 * WBT^2 + C_5 * WBT^3 + C_6 * \ln(WBT)\right]} * \left[C_1 * \frac{1}{WBT^2} + 0 + C_3 + 2 * C_4 * WBT + 3 * C_5 * WBT^2 + C_6 * \frac{1}{WBT}\right]$$

$$\frac{\partial P_v{}'}{\partial WBT} = e^{\left[\frac{-C_1}{WBT}+C_2+C_3*WBT+C_4*WBT^2+C_5*WBT^3+C_6*\ln(WBT)\right]} * \left[\frac{C_1}{WBT^2} + C_3 + 2*C_4*WBT + 3*C_5*WBT^2 + \frac{C_6}{WBT}\right]$$

For a typical condition of the air at the inlet of the dehumidifier (DBT = 31.8 ^{0}C and WBT =29.5 ^{0}C)

$$\frac{\partial P_v{}'}{\partial WBT} = e^{\left[\frac{-5800.22}{302.6}-5.51626-0.04864*302.6+4.17648E-05*302.6^2-1.44521E-08*302.6^3+6.545967*\ln(302.6)\right]} * \left[\frac{5800.22}{302.6^2} - 0.04864 + 2*4.17648E-05 * 4.17648E-05 - 3*-1.44521E-08*302.6^2 + \frac{6.545967}{302.6}\right]$$

$$\frac{\partial P_v{}'}{\partial WBT} = 0.2371\ kPa/K$$

P_{atm} = 101.325 kPa (Atm pressure)

$P_v{}'$ = 4.1256kPa (saturated vapor pressure at WBT)

P_v = 3.9703 kPa (saturated vapor pressure at Dew PT)…..calculated from Modified Apjohn Equation.

$$P_v = P_v{}' - \frac{1.8*P_{atm}*(DBT-WBT)}{2700}$$

$$\omega_a = \frac{0.622*\left[P_v{}' - \frac{1.8*\ P_{atm}*(DBT-WBT)}{2700}\right]}{P_{atm} - \left[P_v{}' - \frac{1.8*\ P_{atm}*(DBT-WBT)}{2700}\right]}$$

$$\omega_a = \frac{0.622*P_v{}' - \frac{0.622*1.8*\ P_{atm}*(DBT-WBT)}{2700}}{P_{atm} - P_v{}' + \frac{1.8*\ P_{atm}*(DBT-WBT)}{2700}}$$

$$\omega_a = \frac{2700*\ 0.622*P_v{}' - 0.622*1.8*\ P_{atm}*(DBT-WBT)}{2700*P_{atm} - 2700*P_v{}' + 1.8*\ P_{atm}*(DBT-WBT)}$$

$$\frac{\partial \omega_a}{\partial DBT} = \frac{\left\{\begin{array}{c}\left[(2700 * P_{atm}) - (2700 * P_v{}') + \left(1.8 * P_{atm} * (DBT - WBT)\right)\right] * [0 - (0.622 * 1.8 * P_{atm})] - \\ {[2700 * 0.622 * P_v{}' - 0.622 * 1.8 * P_{atm} * (DBT - WBT)] * [1.8 * P_{atm}]}\end{array}\right\}}{\left\{\left[(2700 * P_{atm}) - (2700 * P_v{}') + \left(1.8 * P_{atm} * (DBT - WBT)\right)\right]^2\right\}}$$

$$\frac{\partial \omega_a}{\partial DBT} = \frac{\left\{\begin{array}{c}\left[\left(-0.622 * 1.8 * 2700 * P_{atm}{}^2\right) + (2700 * 0.622 * 1.8 * P_{atm} * P_v{}') - \left(0.622 * 1.8^2 * P_{atm}{}^2 * (DBT - WBT)\right)\right] - \\ \left[(1.8 * P_{atm} * 2700 * 0.622 * P_v{}') - \left(0.622 * 1.8^2 * P_{atm}{}^2 * (DBT - WBT)\right)\right]\end{array}\right\}}{\left\{\left[(2700 * P_{atm}) - (2700 * P_v{}') + \left(1.8 * P_{atm} * (DBT - WBT)\right)\right]^2\right\}}$$

$$\frac{\partial \omega_a}{\partial DBT} = \frac{\left\{\begin{array}{c}\left[(-0.622 * 1.8 * 2700 * 101.325^2) + (2700 * 0.622 * 1.8 * 101.325 * 4.1256) - \left(0.622 * 1.8^2 * 101.325^2 * (31.8 - 29.5)\right)\right] - \\ \left[(1.8 * 101.325 * 2700 * 0.622 * 4.1256) - \left(0.622 * 1.8^2 * 101.325^2 * (31.8 - 29.5)\right)\right]\end{array}\right\}}{\left\{\left[(2700 * 101.325) - (2700 * 4.1256) + \left(1.8 * 101.325 * (31.8 - 29.5)\right)\right]^2\right\}}$$

$$\frac{\partial \omega_a}{\partial DBT} = -0.0004490 \text{ kg/kg of dry air/ K}$$

$$\frac{\partial \omega_a}{\partial WBT} = \frac{\left\{\begin{array}{c}\left\{\left[(2700 * P_{atm}) - (2700 * P_v{}') + \left(1.8 * P_{atm} * (DBT - WBT)\right)\right] * \left[\left(2700 * 0.622 * \frac{\partial P_v{}'}{\partial WBT}\right) - \left((0.622 * 1.8 * P_{atm}) * (-1)\right)\right]\right\} - \\ \left\{\left[(2700 * 0.622 * P_v{}') - \left(0.622 * 1.8 * P_{atm} * (DBT - WBT)\right)\right] * \left[0 - \left(2700 * \frac{\partial P_v{}'}{\partial WBT}\right) + (1.8 * P_{atm})(-1)\right]\right\}\end{array}\right\}}{\left\{\left[(2700 * P_{atm}) - (2700 * P_v{}') + \left(1.8 * P_{atm} * (DBT - WBT)\right)\right]^2\right\}}$$

$$\frac{\partial \omega_a}{\partial WBT} = \frac{\left\{\begin{array}{c}\left\{\left[(2700 * P_{atm}) - (2700 * P_v{}') + \left(1.8 * P_{atm} * (DBT - WBT)\right)\right] * \left[\left(2700 * 0.622 * \frac{\partial P_v{}'}{\partial WBT}\right) + (0.622 * 1.8 * P_{atm})\right]\right\} - \\ \left\{\left[(2700 * 0.622 * P_v{}') - \left(0.622 * 1.8 * P_{atm} * (DBT - WBT)\right)\right] * \left[-2700 * \frac{\partial P_v{}'}{\partial WBT} - 1.8 * P_{atm}\right]\right\}\end{array}\right\}}{\left\{\left[(2700 * P_{atm}) - (2700 * P_v{}') + \left(1.8 * P_{atm} * (DBT - WBT)\right)\right]^2\right\}}$$

$$\frac{\partial \omega_a}{\partial WBT} = \frac{\left\{\begin{array}{c}\left\{\left[(2700 * 101.325) - (2700 * 4.1256) + \left(1.8 * 101.325 * (32.3 - 29.3)\right)\right] * [(2700 * 0.622 * 0.2371) + (0.622 * 1.8 * 101.325)]\right\} - \\ \left\{\left[(2700 * 0.622 * 4.1256) - \left(0.622 * 1.8 * 101.325 * (32.3 - 29.3)\right)\right] * [-2700 * 0.2371 - 1.8 * 101.325]\right\}\end{array}\right\}}{\left\{\left[(2700 * 101.325) - (2700 * 4.1256) + \left(1.8 * 101.325 * (32.3 - 29.3)\right)\right]^2\right\}}$$

$$\frac{\partial \omega_a}{\partial WBT} = 0.002025 \text{ kg/kg of dry air/ K}$$

$$\delta_{\omega_a} = \sqrt{\left(\frac{\partial \omega_a}{\partial DBT}\,\delta_{DBT}\right)^2 + \left(\frac{\partial \omega_a}{\partial WBT}\,\delta_{WBT}\right)^2}$$

$$\delta_{\omega_a} = \sqrt{(-0.0004490 * 0.1)^2 + (0.002025 * 0.1)^2}$$

$$\delta_{\omega_a} = 0.000208\ kg/kg\ of\ dry\ air$$

Change in humidity ratio ($\Delta\omega$)

For typical dehumidification condition ($\omega_{a,in}$ = 25.4 g/kg of dry air and $\omega_{a,out}$ = 21.3 g/kg of dry air)

$$\Delta\omega = \left(\omega_{a,out} - \omega_{a,in}\right)$$

$$\frac{\partial \Delta\omega a}{\partial \omega_{a,in}} = -1$$

$$\frac{\partial \Delta\omega a}{\partial \omega_{a,out}} = 1$$

$$\delta_{\Delta\omega_a} = \sqrt{\left(\frac{\partial \Delta\omega a}{\partial \omega_{a,in}}\delta_{\omega_{a,in}}\right)^2 + \left(\frac{\partial \Delta\omega a}{\partial \omega_{a,out}}\delta_{\omega_{a,out}}\right)^2}$$

$$\delta_{\Delta\omega_a} = \sqrt{\left(0.000208 * (-1)\right)^2 + (0.000208 * 1)^2}$$

$\delta_{\Delta\omega_a}$ = 0.000207 * $\sqrt{2}$ = 0.00029274 kg/kg of dry air

$\delta_{\Delta\omega_a} \approx$ 0.3 g/kg of dry air

Density of the moist air

Density is the function of DBT and specific humidity of the moist air:

$$\delta_{\rho a} = \sqrt{\left(\frac{\partial \rho_a}{\partial DBT}\delta_{DBT}\right)^2 + \left(\frac{\partial \rho_a}{\partial \omega_a}\delta_{\omega_a}\right)^2}$$

Density of air is calculated from the following equation, ASHRAE, Handbook of Fundamentals (1997):

$$\rho_a = \frac{p}{0.2871\, T(1+1.6078\omega)}$$

For a typical condition of the air at the inlet of the dehumidifier (DBT = 31.8 ^{0}C and WBT = 29.5^{0}C)

$$\frac{\partial \rho_a}{\partial DBT} = -3.65E-03\,\frac{kg}{m^3}\;K^{-1}$$

$$\frac{\partial \rho_a}{\partial \omega_a} = -1.7183\,\frac{kg}{m^3}\,.\left(\frac{kg}{kg\;dry\;air}\right)^{-1}$$

$$\delta_{\rho a} = \sqrt{(-3.65E-03 * 0.1)^2 + (-1.7183 * 0.000208)^2}$$

$\delta\rho_a$ = 5.11E-04 kg/m^3

Uncertainty in moisture transfer rate

$$\dot{m}_{abs} = m_{da}(\omega_{a,out} - \omega_{a,in})$$

$$\dot{m}_{abs} = \rho_a * V_a * A * (\Delta\omega)$$

For a typical dehumidification condition (DBT = 31.8 ^{0}C and WBT = 29.5 ^{0}C)

Va = 2.45 m/s

ρ_a = 1.14 kg/m^3

$\omega_{a,in}$ = 25.4 g/kg of dry air

$\omega_{a,out}$ = 21.3 g/kg of dry air

A = 0.25 * 0.075 m^2 = 0.01875 m^2

$$\delta_{\dot{m}_{abs}} = \sqrt{\left(\frac{\partial\dot{m}_{abs}}{\partial\rho_a}\delta_{\rho_a}\right)^2 + \left(\frac{\partial\dot{m}_{abs}}{\partial V_a}\delta_{V_a}\right)^2 + \left(\frac{\partial\dot{m}_{abs}}{\partial\Delta\omega_a}\delta_{\Delta\omega_a}\right)^2 + \left(\frac{\partial\dot{m}_{abs}}{\partial A}\delta_A\right)^2}$$

$$\frac{\partial\dot{m}_{abs}}{\partial\rho_a} = V_a * A * (\omega_{a,out} - \omega_{a,in})$$

$$\frac{\partial\dot{m}_{abs}}{\partial\rho_a} = 2.45 * 0.01875 * (0.0254 - 0.0213)$$

$$\frac{\partial\dot{m}_{abs}}{\partial\rho_a} = 1.91\text{E-}04 \ \frac{kg}{s} \cdot \left(\frac{kg}{m^3}\right)^{-1}$$

$$\delta_{V_a} = 0.2 + 0.01 * 2.45$$

$$\delta_{V_a} = 0.224 \approx 0.22 \text{ m/s}$$

$$\frac{\partial\dot{m}_{abs}}{\partial V_a} = \rho_a * A * (\Delta\omega)$$

$$\frac{\partial\dot{m}_{abs}}{\partial V_a} = 1.14 * 0.01875 * (0.0254 - 0.0213)$$

$$\frac{\partial \dot{m}_{abs}}{\partial V_a} = 8.91\,E - 05\,\frac{kg}{s}\,.\left(\frac{m}{s}\right)^{-1}$$

$$\frac{\partial \dot{m}_{abs}}{\partial \Delta\omega_a} = \rho_a * V_a * A$$

$$\frac{\partial \dot{m}_{abs}}{\partial \Delta\omega_a} = 1.14 * 2.45 * 0.01875$$

$$\frac{\partial \dot{m}_{abs}}{\partial \Delta\omega_a} = 5.23\,E - 02\ \ \frac{kg}{s}\,.\left(\frac{kg}{kg}\right)^{-1}$$

$$A = L_1 * L_2$$

$$\delta_A = \sqrt{\left(\frac{\partial A}{\partial L_1}\delta_{L_1}\right)^2 + \left(\frac{\partial A}{\partial L_2}\delta_{L_2}\right)^2}$$

$$\frac{\partial A}{\partial L_1} = L_2 = 0.075\,m$$

$$\frac{\partial A}{\partial L_2} = L_1 = 0.25\,m$$

$$\delta_A = \sqrt{(0.075 * 0.001)^2 + (0.25 * 0.001)^2}$$

$$\delta_A = 0.000261\ \mathrm{m}^2$$

$$\frac{\partial \dot{m}_{abs}}{\partial A} = \rho_a * V_a * (\Delta\omega)$$

$$\frac{\partial \dot{m}_{abs}}{\partial A} = 1.14 * 2.45 * (0.0254 - 0.0213)$$

$$\frac{\partial \dot{m}_{abs}}{\partial A} = 1.16\,E - 02\ \ \frac{kg}{s}\,.(m^2)^{-1}$$

$$\delta_{\dot{m}_{abs}} = \sqrt{\left(\frac{\partial \dot{m}_{abs}}{\partial \rho_a}\delta_{\rho_a}\right)^2 + \left(\frac{\partial \dot{m}_{abs}}{\partial V_a}\delta_{V_a}\right)^2 + \left(\frac{\partial \dot{m}_{abs}}{\partial \Delta\omega_a}\delta_{\Delta\omega_a}\right)^2 + \left(\frac{\partial \dot{m}_{abs}}{\partial A}\delta_A\right)^2}$$

$$\delta_{\dot{m}_{abs}} = \sqrt{(1.91E - 04 \ * 5.11E - 04)^2 + (8.91\,E - 05 * 0.023)^2 + (5.23\,E - 02 \ * 0.0003)^2 + (1.16\,E - 02 \ * 0.000261)^2}$$

$$\delta_{\dot{m}_{abs}} \approx 0.010\ \mathrm{g/s}$$

Uncertainty in humidity effectiveness

$$\varepsilon_Y = \frac{(\omega_{a,out} - \omega_{a,in}) * 100}{(\omega_{a,eqls} - \omega_{a,in})}$$

$$\delta_{\varepsilon_Y} = \sqrt{\left(\frac{\partial \varepsilon_Y}{\partial \omega_{a,in}} \delta_{\omega_{a,in}}\right)^2 + \left(\frac{\partial \varepsilon_Y}{\partial \omega_{a,out}} \delta_{\omega_{a,out}}\right)^2 + \left(\frac{\partial \varepsilon_Y}{\partial \omega_{a,eqls}} \delta_{\omega_{a,eqls}}\right)^2}$$

For typical absorber condition (DBT = 31.8 ^{0}C, WBT = 29.5 ^{0}C, $T_{s,in}$ = 25.01 ^{0}C, $X_{s,in}$ = 38.9%, $\omega_{a,in}$ = 0.0254 kg/kg of dry air, $\omega_{a,out}$ = 0.0213 kg/kg of dry air and $\omega_{a,eqls}$ = 0.0404 kg/kg of dry air)

$$\omega_{a,eqls} = \frac{0.622\, P_v}{P_{atm} - P_v}$$

where $P_v = f(T_{s,in}, X_{s,in})$ as per Chaudhari and Patil [R1]

$$P_v = \exp\left(A + \frac{B}{T_{s,in}} + \frac{C}{T_{s,in}^2}\right)$$

where

Pv in mm of Hg, Patm = 760 mm of Hg for this calculation

$$A = 8.202988 - 0.1353801 * m + 0.0179222 * m^2 - 0.0005292 * m^3$$

$$B = -1727.8 + 58.3845 * \mathrm{m} - 10.208 * \mathrm{m}^2 + 0.3125\, \mathrm{m}^3$$

$$C = -95014.0 - 4701.526 * \mathrm{m} + 929.081 * \mathrm{m}^2 - 31.766\, \mathrm{m}^3$$

where m is molality of desiccant, mol/kg and $T_{s,in}$ in K

$$\omega_{a,eqls} = \frac{0.622\, exp\left(A + \frac{B}{T_{s,in}} + \frac{C}{T_{s,in}^2}\right)}{P_{atm} - exp\left(A + \frac{B}{T_{s,in}} + \frac{C}{T_{s,in}^2}\right)}$$

$$\frac{\partial \omega_{a,eqls}}{\partial T_{s,in}} = \frac{\left\{\left(P_{atm} - \exp\left(A + \frac{B}{T_{s,in}} + \frac{C}{T_{s,in}^2}\right)\right) * 0.622\, exp\left(A + \frac{B}{T_{s,in}} + \frac{C}{T_{s,in}^2}\right)\left[\left(B * \frac{-1}{(T_{s,in})^2}\right) + \left(C * \frac{-2}{(T_{s,in})^3}\right)\right]\right\} - \left\{0.622\, exp\left(A + \frac{B}{T_{s,in}} + \frac{C}{T_{s,in}^2}\right) * \left[-\exp\left(A + \frac{B}{T_{s,in}} + \frac{C}{T_{s,in}^2}\right) * \left(B * \frac{-1}{(T_{s,in})^2}\right) - \left(C * \frac{-2}{(T_{s,in})^3}\right)\right]\right\}}{\left(P_{atm} - \exp\left(A + \frac{B}{T_{s,in}} + \frac{C}{T_{s,in}^2}\right)\right)^2}$$

The calculated values are A = 8.42, B = -2094.57and C -63684.27

$$\frac{\partial \omega_{a,eqls}}{\partial T_{s,in}} = 4.5967E-05 \text{ kg/kg of dry air/ K}$$

$$\frac{\partial \omega_{a,eqls}}{\partial X_{s,in}} = \frac{\left\{\left(P_{atm} - \exp\left(A + \frac{B}{T_{s,in}} + \frac{C}{T_{s,in}^{2}}\right)\right) * \left[0.622\, exp\left(A + \frac{B}{T_{s,in}} + \frac{C}{T_{s,in}^{2}}\right)\left(\left(\frac{\partial A}{\partial X_{s,in}}\right) + \left(\frac{1}{T_{s,in}} * \frac{\partial B}{\partial X_{s,in}}\right) + \left(\frac{1}{T_{s,in}^{2}} * \frac{\partial C}{\partial X_{s,in}}\right)\right)\right]\right\} - \left\{0.622\, exp\left(A + \frac{B}{T_{s,in}} + \frac{C}{T_{s,in}^{2}}\right) * \left[-\exp\left(A + \frac{B}{T_{s,in}} + \frac{C}{T_{s,in}^{2}}\right)\left(\left(\frac{\partial A}{\partial X_{s,in}}\right) + \left(\frac{1}{T_{s,in}} * \frac{\partial B}{\partial X_{s,in}}\right) + \left(\frac{1}{T_{s,in}^{2}} * \frac{\partial C}{\partial X_{s,in}}\right)\right)\right]\right\}}{\left(P_{atm} - \exp\left(A + \frac{B}{T_{s,in}} + \frac{C}{T_{s,in}^{2}}\right)\right)^{2}}$$

$$\frac{\partial A}{\partial X_{s,in}} = 0.04491, \frac{\partial B}{\partial X_{s,in}} = -36.829, \frac{\partial C}{\partial X_{s,in}} = 1717.430$$

$$\frac{\partial \omega_{a,eqls}}{\partial X_{s,in}} = -9.60E-05\left(\frac{kg}{kg\ of\ dry\ air}\right) / \left(\frac{kg\ of\ salt}{kg\ of\ solution}\right)$$

$$\delta_{\omega_{a,eqls}} = \sqrt{\left(\frac{\partial \omega_{a,eqls}}{\partial T_{s,in}} \delta_{T_{s,in}}\right)^{2} + \left(\frac{\partial \omega_{a,eqls}}{\partial X_{s,in}} \delta_{X_{s,in}}\right)^{2}}$$

$$\delta_{\omega_{a,eqls}} = \sqrt{(4.5967E-05 * 0.1)^{2} + (-9.60E-05 * 0.003)^{2}}$$

$$\delta_{\omega_{a,eqls}} = 4.61E-06 \text{ kg/kg of dry air}$$

$$\varepsilon_{Y} = \frac{(\omega_{a,in} - \omega_{a,out})}{(\omega_{a,in} - \omega_{eqls})}$$

$$\frac{\partial \varepsilon_{Y}}{\partial \omega_{a,in}} = \frac{\left((\omega_{a,in} - \omega_{eqls}) * (1)\right) - \left((\omega_{a,in} - \omega_{a,out}) * (1)\right)}{(\omega_{a,in} - \omega_{eqls})^{2}}$$

$$\frac{\partial \varepsilon_{Y}}{\partial \omega_{a,in}} = \frac{(\omega_{a,in} - \omega_{eqls}) + (\omega_{a,in} - \omega_{a,out})}{(\omega_{a,in} - \omega_{eqls})^{2}}$$

$$\frac{\partial \varepsilon_{Y}}{\partial \omega_{a,in}} = \frac{(0.0254 - 0.00402) + 0.0042}{(0.0254 - 0.00402)^{2}}$$

$$\frac{\partial \varepsilon_{Y}}{\partial \omega_{a,in}} = 37.6357 \text{ kg of dry air /kg}$$

$$\frac{\partial \varepsilon_{Y}}{\partial \omega_{a,out}} = \frac{(-1)}{(\omega_{a,in} - \omega_{eqls})}$$

$$\frac{\partial \varepsilon_Y}{\partial \omega_{a,out}} = \frac{-1}{(0.0254 - 0.00402)}$$

$$\frac{\partial \varepsilon_Y}{\partial \omega_{a,out}} = -46.746 \text{ kg of dry air /kg}$$

$$\frac{\partial \varepsilon_Y}{\partial \omega_{a,eqls}} = \frac{\left(\omega_{a,in} - \omega_{a,out}\right) * (-1) * (-1)}{\left(\omega_{a,in} - \omega_{eqls}\right)^2}$$

$$\frac{\partial \varepsilon_Y}{\partial \omega_{a,eqls}} = \frac{\left(\omega_{a,in} - \omega_{a,out}\right)}{\left(\omega_{a,in} - \omega_{eqls}\right)^2}$$

$$\frac{\partial \varepsilon_Y}{\partial \omega_{a,eqls}} = \frac{(0.0254 - 0.0213)}{(0.0254 - 0.00402)^2}$$

$$\frac{\partial \varepsilon_Y}{\partial \omega_{a,eqls}} = 9.10994 \text{ kg of dry air /kg}$$

$$\delta_{\varepsilon_Y} = \sqrt{(37.635782 \ * 0.000208)^2 + (-46.746 * 0.000208)^2 + (9.10994 * 4.61E - 06)^2}$$

$$\delta_{\varepsilon_Y} = 0.0124770 \approx 1.24\%$$

Table A1 Dehumidification experimental observations on Plain and Modified PP CCS.

Sr. No.	$\dot{m}_{a,in}$ (kg/s)	$\dot{m}_{s,in}$ (kg/s)	$T_{a,in}$ (^{0}C)	$\omega_{a,in}$ (g/kg)	$\omega_{a,out}$ (g/kg)	$T_{s,in}$ (^{0}C)	$X_{s,in}$ (%)	ϵ_{Y} (%)
				Plain PP CCS				
1	0.052	**0.024**	32.0	25.3	22.7	25.5	39.0	12.2
2	0.051	**0.040**	31.5	25.3	22.1	25.2	39.0	15.0
3	0.051	**0.055**	31.7	25.1	21.5	25.6	38.9	17.3
4	0.052	**0.077**	31.8	25.4	21.3	25.0	38.9	19.5
5	0.051	**0.101**	31.9	25.3	21.0	25.1	39.0	20.1
6	0.052	**0.115**	31.7	25.4	21.2	25.2	39.1	19.8
7	0.053	**0.146**	31.7	25.7	21.5	25.1	39.2	19.5
8	**0.033**	0.078	30.9	25.1	20.2	25.1	39.2	23.1
9	**0.041**	0.079	31.0	25.0	20.4	25.3	39.2	21.9
10	**0.061**	0.078	31.4	25.0	21.5	25.4	39.0	16.9
11	**0.070**	0.078	32.0	25.1	22.0	25.1	39.1	14.9
12	0.052	0.076	31.3	25.0	20.7	**22.6**	39.1	20.0
13	0.052	0.078	31.6	24.8	21.2	**29.9**	39.0	18.5
14	0.052	0.077	32.0	25.0	21.7	**32.5**	39.0	17.5
15	0.052	0.078	**26.4**	16.7	14.5	25.2	39.1	17.5

16	0.053	0.076	**30.9**	16.9	14.4	25.0	38.9	19.7
17	0.052	0.077	**33.4**	16.5	14.5	25.2	39.0	16.1
18	0.052	0.078	**35.6**	16.7	14.3	25.3	39.0	18.8
19	0.052	0.077	31.7	24.9	21.9	29.9	**33.2**	19.0
20	0.051	0.078	31.9	24.9	21.9	29.8	**33.3**	18.7
21	0.052	0.078	31.9	24.8	21.6	30.0	**36.0**	18.4
22	0.052	0.079	31.9	**15.7**	13.5	25.4	39.1	19.0
23	0.052	0.077	30.5	**18.0**	15.3	25.4	39.0	19.8
24	0.052	0.078	29.6	**21.8**	18.4	25.3	39.0	19.6
Modified PP CCS								
1	0.051	**0.024**	31.2	24.9	20.7	25.3	39.0	20.2
2	0.051	**0.042**	31.0	24.8	20.2	25.2	39.1	22.0
3	0.051	**0.055**	31.1	25.1	20.3	25.3	39.1	22.7
4	0.052	**0.078**	31.0	25.0	20	25.1	39.0	23.8
5	0.052	**0.116**	31.2	25.1	19.6	25.0	39.1	26.0
6	0.051	**0.142**	31.3	25.0	19.4	25.1	39.0	26.6
7	**0.032**	0.078	30.7	24.9	18.5	25.3	39.0	30.5
8	**0.042**	0.077	31.1	25.1	19.5	25.0	39.1	26.6
9	**0.061**	0.077	31.3	25.1	20.5	25.1	39.1	21.7
10	**0.070**	0.078	31.4	25.1	20.8	25.2	39.0	20.4

11	0.051	0.076	31.2	24.9	19.3	**20.8**	39.0	25.6
12	0.052	0.076	31.1	25.1	20.4	**27.8**	39.0	23.5
13	0.052	0.077	31.1	25.0	20.7	**32.4**	39.0	23.2
14	0.053	0.078	**27.8**	18.2	14.7	25.3	39.0	24.7
15	0.052	0.077	**30.7**	18.1	14.7	25.3	39.0	24.2
16	0.051	0.078	**32.9**	18.3	14.8	25.3	39.0	24.9
17	0.052	0.077	**35.9**	18.1	14.8	25.4	39.0	23.8
18	0.051	0.077	31.3	25.1	21.3	30.3	**33.1**	23.8
19	0.052	0.076	31.2	25.1	21.0	30.1	**36.1**	22.6
20	0.051	0.077	31.3	24.9	20.2	30.0	**39.0**	24.2
21	0.052	0.078	31.3	**15.3**	12.6	25.2	39.0	23.6
22	0.052	0.078	31.1	**17.8**	14.6	25.2	39.0	23.5
23	0.052	0.078	30.2	**21.8**	17.5	25.2	39.0	24.2

Table A2 Regeneration experimental observations on Plain and Modified PP CCS.

Sr. No.	**$\dot{m}_{a,in}$ (kg/s)**	**$\dot{m}_{s,in}$ (kg/s)**	**$T_{a,in}$ (^0C)**	**$\omega_{a,in}$ (g/kg)**	**$\omega_{a,out}$ (g/kg)**	**$T_{s,in}$ (^0C)**	**$X_{s,in}$ (%)**	**$\in_Y$(%)**
				Plain PP CCS				
1	0.065	**0.055**	30.8	17.1	21.3	68.6	39.1	13.1
2	0.066	**0.085**	32.1	17.1	22.3	68.5	39.0	16.4
3	0.065	**0.109**	32.3	17.2	23.1	68.3	39.1	19.1
4	0.064	**0.153**	30.5	16.9	24.0	67.9	39.0	23.2
5	0.066	**0.209**	30.2	17.0	24.5	68.2	39.0	24.2
6	**0.033**	0.158	31.1	18.3	27.1	68.0	39.1	30.3
7	**0.052**	0.158	30.7	18.1	25.8	68.4	39.0	25.1
8	**0.075**	0.158	32.1	18.3	23.9	68.2	39.1	19.0
9	**0.085**	0.159	30.8	18.5	23.9	68.3	39.0	17.8
10	0.064	0.163	31.7	18.2	23.7	**64.6**	39.0	25.1
11	0.064	0.158	31.0	18.3	25.1	**68.1**	39.0	23.0
12	0.064	0.157	30.5	18.6	27.1	**71.5**	39.0	21.9
13	0.064	0.160	31.0	18.0	28.9	**75.8**	39.0	20.5
14	0.065	0.154	**35.1**	17.0	24.3	68.4	39.1	23.1
15	0.065	0.153	**39.3**	16.5	23.8	68.3	39.1	23.1

16	0.065	0.154	**43.1**	16.9	24.5	68.4	39.0	23.7
17	0.065	0.153	30.7	16.9	27.6	68.1	**34.2**	20.3
18	0.064	0.155	30.2	17.0	26.1	68.4	**36.4**	21.3
19	0.065	0.157	30.7	16.7	23.0	68.4	**40.5**	23.7
20	0.065	0.156	30.4	16.8	21.6	68.3	**42.3**	23.7
21	0.065	0.149	31.4	**14.0**	22.0	68.0	39.1	23.7
22	0.064	0.154	31.8	**20.3**	26.7	68.7	39.1	22.0
23	0.065	0.152	32.4	**23.3**	28.7	68.0	39.0	21.6
Modified PP CCS								
1	0.065	**0.059**	32.7	17.1	22.7	68.5	39.0	17.5
2	0.065	**0.096**	31.5	17.3	23.8	68.6	39.1	20.5
3	0.065	**0.110**	32.0	16.8	23.5	68.6	39.1	20.8
4	0.065	**0.152**	31.3	16.8	24.0	68.7	39.1	22.2
5	0.064	**0.204**	32.1	16.9	24.4	68.6	39.0	22.9
6	**0.033**	0.160	31.1	18.2	29.1	68.5	39.0	35.4
7	**0.052**	0.158	31.1	17.9	26.0	68.5	39.0	26.2
8	**0.073**	0.158	31.8	18.2	24.8	68.5	39.0	21.3
9	**0.086**	0.159	31.2	17.9	24.2	68.7	39.0	19.7
10	0.065	0.160	31.8	18.5	24.1	**64.3**	39.0	26.7
11	0.064	0.158	31.3	18.0	24.8	**68.6**	39.0	22.0

12	0.064	0.159	33.4	18.5	27.3	**71.9**	39.1	22.2
13	0.064	0.161	31.3	18.1	28.5	**74.6**	39.0	21.0
14	0.065	0.153	**36.7**	17.1	24.2	68.6	39.0	22.0
15	0.064	0.151	**40.2**	16.7	23.9	68.7	38.9	21.9
16	0.064	0.154	**44.2**	16.9	24.4	68.6	38.9	22.9
17	0.065	0.154	32.0	16.9	27.4	68.5	**34.4**	19.7
18	0.065	0.153	32.3	17.2	25.5	68.3	**37.1**	21.2
19	0.065	0.156	32.0	16.8	21.8	68.4	**42.3**	24.4
20	0.064	0.152	31.6	**21.4**	27.3	68.6	39.1	21.5
21	0.065	0.155	33.1	**24.7**	30.0	68.4	38.9	21.6

Table A3 Regeneration experimental observations on Plain and Modified PP CCS at low flow rate

Sr. No.	$\dot{m}_{a,in}$ (kg/s)	$\dot{m}_{s,in}$ (kg/s)	$T_{a,in}$ (^{0}C)	$\omega_{a,in}$ (g/kg)	$\omega_{a,out}$ (g/kg)	$T_{s,in}$ (^{0}C)	$X_{s,in}$ (%)	$\in_{Y}$(%)
1	**0.030**	0.057	29.8	16.9	23.3	68.1	39.2	21.2
2	**0.044**	0.060	30.2	17.1	22.1	68.5	39.2	16.1
3	0.065	0.060	29.8	16.6	18.0	**60.4**	39.1	9.2
4	0.064	0.058	29.8	16.7	19.0	**63.7**	39.1	10.8
5	0.065	0.057	30.0	16.8	20.0	**66.0**	39.1	12.2
				Modified PP CCS				
1	**0.030**	0.058	30.3	16.9	26.3	68.5	39.1	29.6
2	**0.050**	0.056	30.6	16.7	23.5	68.4	39.0	21.1
3	0.064	0.056	30.8	17.0	19.6	**60.8**	39.0	16.6
4	0.064	0.058	30.8	17.0	21.1	**65.0**	38.9	17.1

References

[1] Xiong J., Lian Z., Zhou X., You J., Lin Y. (2015), Effects of temperature steps on human health and thermal comfort, Build Environ, 94, 144–154.

[2] Ortiz M.A., Kurvers S.R., Bluyssen P.M. (2017), A review of comfort, health, and energy use: Understanding daily energy use and wellbeing for the development of a new approach to study comfort, Energy Build, 152, 323–335.

[3] Chinazzo G., Wienold J., Andersen M. (2019), Daylight affects human thermal perception, Sci Rep, 9, 1–15.

[4] Bichowsky F.R., Kelley G.A. (1935), Concentrated Solutions in Air-Conditioning, Ind Eng Chem, 27, 879–882.

[5] Lof G. (1955), Cooling with solar energy, Congress on Solar Energy, Tucson, Arizona, 171–189.

[6] A.Kakabaev, A.Khandurdyev (1969), Absorption solar refrigeration unit with open regeneration of solution, App Sol Energy, 5, 28–32.

[7] Nakoryakov V.E., Branch S. (1977), Combined heat and mass transfer during absorption in drops and films, 32, 243–247.

[8] Factor H.M., Grossman G. (1980), A packed bed dehumidifier regenerator for solar air conditioning with liquid desiccants, Sol Energy, 24, 541–550.

[9] Collier R.K., Arnold F., Barlow R. (1981), An Overview of Open-Cycle Desiccant Cooling Systems and Materials, J Sol Energy Eng, 1065, 1–27.

[10] Peng C.P., Howell J.R. (1982), Analysis of open inclined surface solar regenerators for absorption cooling applications--comparison between numerical and analytical models, Sol

Energy, 28, 265–268.

[11] Michel J.W., Perez-Blanco H. (1985), Influence of Surfactant additive on Absorption Heat Pump Performance, ASHRAE Trans, 91, 1847.

[12] Ullah M.R., Kettleborough C.F., Gandhidasan P. (1988), Effectiveness of Moisture Removal for an Adiabatic Counterflow Packed Tower Absorber Operating with CaCl2-Air Contact System, J Sol Energy Eng, 110, 98.

[13] Ziegler F.; Grossman G. (1996), Heat-transfer enhancements by additives, Int J Refrig, 19, 301–309.

[14] Oberg V., Goswami D.Y. (1998), A review of Liquid Desiccant Cooling, Adv Sol Energy - An Annu Rev Res Dev, 12, 430–470.

[15] Killion J.D., Garimella S. (2001), A critical review of models of coupled heat and mass transfer in falling-film absorption, Int J Refrig, 24, 755–797.

[16] Johannsen A., Grossman G., Africa S., Grossman G. (1983), Performance simulation of regenerating type solar collectors, Sol Energy, 30, 87–92.

[17] Chung T.W., Hines A.L., Novosel D. (1995), Dehumidification of moist air with simultaneous removal of selected indoor pollutants by triethylene glycol solutions in a packed-bed absorber, Sep Sci Technol, 30, 1807–1832.

[18] Lai M.-H., Chang Y.-N., Wang C.-M., Wu H., Chung T.-W. (2003), Analysis of the Absorption-Dehumidification Process Variables Using the Experimental Design Methodology, Sep Sci Technol, 38, 2447–2464.

[19] Wu H., Feng T.C., Chung T.W. (2006), Discussions of mass transfer performance and empirical correlations for VOCs absorbed by triethylene glycol solution, Ind Eng Chem Res, 45,

8689–8696.

[20] Giampieri A., Ma Z., Smallbone A., Roskilly A.P. (2018), Thermodynamics and economics of liquid desiccants for heating, ventilation and air-conditioning – An overview, Appl Energy, 220, 455–479.

[21] Ertas A., Anderson E.E., Kiris I. (1992), Properties of a New Liquid Desiccant Solution- Lithium Chloride and Calcium Chloride Mixture, Sol Energy, 49, 205–212.

[22] Ertas A., Gandhidasan P., Kiris I., Anderson E.E. (1994), Experimental study on the performance of a regeneration tower for various climatic conditions, Sol Energy, 53, 125–130.

[23] Lazzarin R.M., Gasparella A., Longo G.A. (1999), Chemical dehumidification by liquid desiccants: theory and experiment, Int J Refrig, 22, 334–347.

[24] Liu X.H., Yi X.Q., Jiang Y. (2011), Mass transfer performance comparison of two commonly used liquid desiccants: LiBr and LiCl aqueous solutions, Energy Convers Manag, 52, 180–190.

[25] Longo G.A., Gasparella A. (2015), Three years experimental comparative analysis of a desiccant based air conditioning system for a flower greenhouse: Assessment of different desiccants, Appl Therm Eng, 78, 584–590.

[26] Bouzenada S., Kaabi A.N., Frainkin L., Salmon T., Léonard A. (2016), Experimental Comparative Study on Lithium Chloride and Calcium Chloride Desiccants, Procedia Comput Sci, 83, 718–725.

[27] Koronaki I.P., Christodoulaki R.I., Papaefthimiou V.D., Rogdakis E.D. (2013), Thermodynamic analysis of a counter flow adiabatic dehumidifier with different liquid desiccant materials, Appl Therm Eng, 50, 361–373.

[28] Wen T., Luo Y., Wang M., She X. (2021), Comparative study on the liquid desiccant dehumidification performance of lithium chloride and potassium formate, Renew Energy, 167, 841–852.

[29] Bhowmik M., Muthukumar P., Anandalakshmi R. (2021), Experimental investigation on structured packed bed liquid desiccant dehumidifier: An optimal mixture design of experiments strategy, Int J Refrig, 122, 232–244.

[30] Jiang X., He H., Li X., Mao H. (2020), Performance analysis and mixing ratio selection of mixed liquid desiccant for a dehumidification system, Indoor Built Environ, 29, 711–720.

[31] Luo Y., Shao S., Xu H., Tian C. (2011), Dehumidification performance of [EMIM]BF4, Appl Therm Eng, 31, 2772–2777.

[32] Luo Y., Shao S., Qin F., Tian C., Yang H. (2012), Investigation on feasibility of ionic liquids used in solar liquid desiccant air conditioning system, Sol Energy, 86, 2718–2724.

[33] Qu M., Abdelaziz O., Sun X.G., Yin H. (2017), Aqueous solution of [EMIM][OAc]: Property formulations for use in air conditioning equipment design, Appl Therm Eng, 124, 271–278.

[34] Watanabe H., Komura T., Matsumoto R., Ito K., Nakayama H., Nokami T., Itoh T. (2019), Design of ionic liquids as liquid desiccant for an air conditioning system, Green Energy Environ, 4, 139–145.

[35] Maekawa S., Matsumoto R., Ito K., Nokami T., Li J.-X., Nakayama H., Itoh T. (2020), Design of quaternary ammonium type-ionic liquids as desiccants for an air-conditioning system, Green Chem Eng, 1, 109–116.

[36] Conde M.R. (2004), Properties of aqueous solutions of lithium and calcium chlorides: Formulations for use in air conditioning equipment design, Int J Therm Sci, 43, 367–382.

[37] Kaita Y. (2001), Thermodynamic properties of lithium bromide ± water solutions at high temperatures Â te Â s thermodynamiques des solutions bromure de Proprie Â ratures e Â leve Â es lithium / eau aux tempe, Int J Refrig, 24.

[38] Patterson M., Perez-Blanco H. (1988), Numerical fits of the properties of lithium-bromide water solutions, ASHRAE Trans, 94, 2379–88.

[39] Wen T., Wang M., Chen Y., He W., Luo Y. (2019), Thermal properties study and performance investigation of potassium formate solution in a falling film dehumidifier/regenerator, Int J Heat Mass Transf, 134, 131–142.

[40] Nasr-El-Din H.A., Al-Otaibi M.B., Al-Aamri A.M., Ginest N. (2005), Surface tension of completion brines, Proc - SPE Int Symp Oilf Chem, 643–654.

[41] Oliveira A.C., Afonso C.F., Riffat S.B., Doherty P.S. (2000), Thermal performance of a novel air conditioning system using a liquid desiccant, System, 20, 1213–1223.

[42] Kessling W., Laevemann E., Kapfhammer C. (1998), Energy storage for desiccant cooling systems component development, Sol Energy, 64, 209–221.

[43] Jain S., Dhar P.L.L., Kaushik S.C.C. (1994), Evaluation of liquid desiccant based evaporative cooling cycles for typical hot and humid climates, Heat Mass Transf, 14, 621–632.

[44] Peña X., Alonso L., Diaz de Mendibil A., Prieto J., Gommed K. (2019), Hybrid liquid desiccant system design and operation under high latent load conditions in Taiwan, Int J Refrig, 105, 41–49.

[45] Yadav Y.K. (1995), Vapour-compression and liquid-desiccant hybrid solar space-conditioning system for energy conservation, Renew Energy, 6, 719–723.

[46] Chen Y., Yin Y., Zhang X. (2014), Performance analysis of a hybrid air-conditioning system dehumidified by liquid desiccant with low temperature and low concentration, Energy Build, 77, 91–102.

[47] Van W.M., Lin T.F. (1990), Combined heat and mass transfer in natural convection between vertical parallel plates with film evaporation, Int J Heat Mass Transf, 33, 529–541.

[48] Matsuda A., Choi K.H., Hada K., Kawamura T. (1994), Effect of pressure and concentration on performance of a vertical falling-film type of absorber and generator using lithium bromide aqueous solutions, Int J Refrig, 17, 538–542.

[49] Hoffmann L., Greiter I., Wagner A., Weiss V., Alefeld G. (1996), Experimental investigation of heat transfer in a horizontal tube falling film absorber with aqueous solutions of LiBr with and without surfactants, Int J Refrig, 19, 331–341.

[50] Deng S.M., Ma W.B. (1999), Experimental studies on the characteristics of an absorber using LiBr/H2O solution as working fluid, Int J Refrig, 22, 293–301.

[51] Takamatsu H., Yamashiro H., Takata N., Honda H. (2003), Vapor absorption by LiBr aqueous solution in vertical smooth tubes, Int J Refrig, 26, 659–666.

[52] Kim D.S., Infante Ferreira C.A. (2009), Flow patterns and heat and mass transfer coefficients of low Reynolds number falling film flows on vertical plates: Effects of a wire screen and an additive, Int J Refrig, 32, 138–149.

[53] Shi C., Chen Q., Jen T.C., Yang W. (2010), Heat transfer performance of lithium bromide solution in falling film generator, Int J Heat Mass Transf, 53, 3372–3376.

[54] Papaefthimiou V.D., Koronaki I.P., Karampinos D.C., Rogdakis E.D. (2012), A novel approach for modelling LiBreH2O falling

film absorption on cooled horizontal bundle of tubes, Int J Refrig, 35, 1115–1122.

[55] Michel B., Le Pierrès N., Stutz B. (2017), Performances of grooved plates falling film absorber, Energy, 138, 103–117.

[56] Kumar L., Lee S., Garimella S. (2019), Heat and mass transfer models for horizontal-tube falling-film ammonia-water absorption Lalit, Int J Refrig, 107, 84–97.

[57] Chung T.W., Wu H. (2000), Comparison between spray towers with and without fin coils for air dehumidification using triethylene glycol solutions and development of the mass-transfer correlations, Ind Eng Chem Res, 39, 2076–2084.

[58] Yin Y., Zhang X. (2010), Comparative study on internally heated and adiabatic regenerators in liquid desiccant air conditioning system, Build Environ, 45, 1799–1807.

[59] Bansal P., Jain S., Moon C. (2011), Performance comparison of an adiabatic and an internally cooled structured packed-bed dehumidifier, Appl Therm Eng, 31, 14–19.

[60] Patnaik S., Lenz T.G., Löf G.O.G. (1990), Performance studies for an experimental solar open-cycle liquid desiccant air dehumidification system, Sol Energy, 44, 123–135.

[61] Chung T.W., Glosh T.K., Hines A.L. (1996), Comparioson between Random and Structured Packings for Dehumidification of Air by Lithium Chloride Solutions in a Packed Column and Their Hear and Mass Transfer Correlations, Ind Eng Chem Res, 35, 192–198.

[62] Fumo N., Goswami D.Y. (2002), Study of an aqueous lithium chloride desiccant system: Air dehumidification and desiccant regeneration, Sol Energy, 72, 351–361.

[63] Gandhidasan P., Al-Farayedhi A.A., Antar M.A. (2002),

Investigation of heat and mass transfer in a gauze-type structured packing liquid desiccant dehumidifier, Int J Energy Res, 26, 1035–1044.

[64] Elsarrag E., Magzoub E.E.M., Jain S. (2004), Mass-transfer correlations for dehumidification of air by triethylene glycol in a structured packed column, Ind Eng Chem Res, 43, 7676–7681.

[65] Abu-Arabi M.K., Abdul-Wahab S.A., Goosen M.F.A. (2006), Study of desiccant regeneration in a structured packed tower, Sep Sci Technol, 41, 1679–1695.

[66] Liu X.H., Zhang Y., Qu K.Y., Jiang Y. (2006), Experimental study on mass transfer performances of cross flow dehumidifier using liquid desiccant, Energy Convers Manag, 47, 2682–2692.

[67] Yin Y., Zhang X., Chen Z. (2007), Experimental study on dehumidifier and regenerator of liquid desiccant cooling air conditioning system, Build Environ, 42, 2505–2511.

[68] Longo G.A., Gasparella A. (2009), Experimental analysis on desiccant regeneration in a packed column with structured and random packing, Sol Energy, 83, 511–521.

[69] Babakhani D., Soleymani M. (2009), An analytical solution for air dehumidification by liquid desiccant in a packed column, Int Commun Heat Mass Transf, 36, 969–977.

[70] Bassuoni M.M. (2011), An experimental study of structured packing dehumidifier/regenerator operating with liquid desiccant, Energy, 36, 2628–2638.

[71] Gao W.Z., Liu J.H., Cheng Y.P., Zhang X.L. (2012), Experimental investigation on the heat and mass transfer between air and liquid desiccant in a cross-flow dehumidifier, Renew Energy, 37, 117–123.

[72] Park J.Y., Yoon D.S., Lee S.J., Jeong J.W. (2016), Empirical

model for predicting the dehumidification effectiveness of a liquid desiccant system, Energy Build, 126, 447–454.

[73] Wang L., Xiao F., Zhang X., Kumar R. (2016), An experimental study on the dehumidification performance of a counter flow liquid desiccant dehumidifier, Int J Refrig, 70, 289–301.

[74] Mohamed A.S.A., Ahmed M.S., Hassan A.A.M., Hassan M.S. (2016), Performance evaluation of gauze packing for liquid desiccant dehumidification system, Case Stud Therm Eng, 8, 260–276.

[75] Longo G.A., Gasparella A. (2005), Experimental and theoretical analysis of heat and mass transfer in a packed column dehumidifier/regenerator with liquid desiccant, Int J Heat Mass Transf, 48, 5240–5254.

[76] Dong C., Qi R., Lu L., Wang Y., Wang L. (2017), Comparative performance study on liquid desiccant dehumidification with different packing types for built environment, Sci Technol Built Environ, 23, 116–126.

[77] Dong H.W., Cho H.J., Park J.Y., Jeong J.W. (2019), Optimum regeneration temperature of a desiccant solution in a packaged liquid desiccant-assisted air conditioning unit, Int J Refrig, 101, 155–166.

[78] Gu Y., Zhang X. (2020), Performance investigation on the liquid desiccant regeneration using rotating packed bed, Int J Refrig, 109, 45–54.

[79] Zhang L., Hihara E., Matsuoka F., Dang C. (2010), Experimental analysis of mass transfer in adiabatic structured packing dehumidifier/regenerator with liquid desiccant, Int J Heat Mass Transf, 53, 2856–2863.

[80] Jain S., Dhar P.L., Kaushik S.C. (2000), Experimental studies on the dehumidifier and regenerator of a liquid desiccant cooling

system, Appl Therm Eng, 20, 253–267.

[81] Ren C.Q., Tu M., Wang H.H. (2007), An analytical model for heat and mass transfer processes in internally cooled or heated liquid desiccant-air contact units, Int J Heat Mass Transf, 50, 3545–3555.

[82] Yin Y., Zhang X., Wang G., Luo L. (2008), Experimental study on a new internally cooled/heated dehumidifier/regenerator of liquid desiccant systems, Int J Refrig, 31, 857–866.

[83] Liu X.H., Chang X.M., Xia J.J., Jiang Y. (2009), Performance analysis on the internally cooled dehumidifier using liquid desiccant, Build Environ, 44, 299–308.

[84] Zhang T., Liu X., Jiang J., Chang X., Jiang Y. (2013), Experimental analysis of an internally-cooled liquid desiccant dehumidifier, Build Environ, 63, 1–10.

[85] Qi R., Lu L., Yang H., Qin F. (2013), Influence of plate surface temperature on the wetted area and system performance for falling film liquid desiccant regeneration system, Int J Heat Mass Transf, 64, 1003–1013.

[86] Luo Y., Wang M., Yang H., Lu L., Peng J. (2015), Experimental study of internally cooled liquid desiccant dehumidification: Application in Hong Kong and intensive analysis of influencing factors, Build Environ, 93, 210–220.

[87] Dong C., Lu L., Qi R. (2017), Model development of heat/mass transfer for internally cooled dehumidifier concerning liquid film shrinkage shape and contact angles, Build Environ, 114, 11–22.

[88] Dong C., Lu L., Wen T. (2017), Experimental study on dehumidification performance enhancement by TiO 2 superhydrophilic coating for liquid desiccant plate dehumidifiers, Build Environ, 124, 219–231.

[89] Wen T., Lu L., Dong C., Luo Y. (2018), Development and experimental study of a novel plate dehumidifier made of anodized aluminum, Energy, 144, 169–177.

[90] Qi R., Dong C., Zhang L.Z. (2019), Development of liquid-air mass transfer correlations for liquid desiccant dehumidification considering the liquid/air contact and film instability, Int J Heat Mass Transf, 141, 491–502.

[91] Cheng X., Peng D., Yin Y., Xu S., Luo D. (2019), Experimental study and performance analysis on a new dehumidifier with outside evaporative cooling, Build Environ, 148, 200–211.

[92] Wen T., Lu L. (2019), Numerical and experimental study on internally cooled liquid desiccant dehumidification concerning film shrinkage shape and vapor condensation, Int J Therm Sci, 136, 316–327.

[93] Wen T., Luo Y., Lu L., He W. (2020), Enhancing the falling film dehumidification performance from the prospective of CFD simulation, Int J Heat Mass Transf, 151, 119459.

[94] Lu H., Lu L., Gao X. (2021), Mass transfer enhancement of falling film liquid desiccant dehumidification by micro-baffle plates, Int J Heat Mass Transf, 169, 120945.

[95] Lowenstein A. (2008), Review of liquid desiccant technology for HVAC applications, HVAC R Res, 14, 819–839.

[96] Luo Y., Shao S., Xu H., Tian C., Yang H. (2014), Experimental and theoretical research of a fin-tube type internally-cooled liquid desiccant dehumidifier, Appl Energy, 133, 127–134.

[97] Turgut O.E., Çoban M.T. (2016), Experimental and numerical investigation on the performance of an internally cooled dehumidifier, Heat Mass Transf, 52, 2707–2722.

[98] Wen T., Lu L., Yang H., Luo Y. (2018), Investigation on the

Regeneration and Corrosion Characteristics of an Anodized Aluminum Plate Regenerator, Energies, 11, 1209.

[99] Jaradat M. (2019), Thermochemical energy storage in low flow liquid desiccant regenerator, Int Energy J, 19, 159–176.

[100] Wen T., Lu L., Nie Y., Zhong H. (2019), Development and investigation on the dehumidification and corrosion resistance performance of a new mixed liquid desiccant, Int J Heat Mass Transf, 130, 72–82.

[101] Wen T., Lu L., Li M., Zhong H. (2018), Comparative study of the regeneration characteristics of LiCl and a new mixed liquid desiccant solution, Energy, 163, 992–1005.

[102] Saman W.Y., Alizadeh S. (2002), An experimental study of a cross-flow type plate heat exchanger for dehumidification/cooling, Sol Energy, 73, 59–71.

[103] Alizadeh S., Saman W.Y. (2002), Modeling and performance of a forced flow solar collector/regenerator using liquid desiccant, Sol Energy, 72, 143–154.

[104] Mesquita L.C.S., Harrison S.J., Thomey D. (2006), Modeling of heat and mass transfer in parallel plate liquid-desiccant dehumidifiers, Sol Energy, 80, 1475–1482.

[105] Chen L., Li Z., Guo Z.Y. (2009), Experimental investigation of plastic finned-tube heat exchangers, with emphasis on material thermal conductivity, Exp Therm Fluid Sci, 33, 922–928.

[106] Gommed K., Grossman G., Prieto J., Ortiga J., Coronas A. (2015), Experimental comparison between internally and externally cooled air-solution contactors, Sci Technol Built Environ, 21, 267–274.

[107] Mun J.H., Jeon D.S., Kim Y.L., Kim S.C. (2016), A study on the regeneration performance characteristics of an internally heated

regenerator in a liquid desiccant system, J Mech Sci Technol, 30, 1343–1349.

[108] Park J.Y., Kim B.J., Yoon S.Y., Byon Y.S., Jeong J.W. (2019), Experimental analysis of dehumidification performance of an evaporative cooling-assisted internally cooled liquid desiccant dehumidifier, Appl Energy, 235, 177–185.

[109] Dong C., Lu L., Wen T. (2018), Investigating dehumidification performance of solar-assisted liquid desiccant dehumidifiers considering different surface properties, Energy, 164, 978–994.

[110] Mortazavi M., Nasr Isfahani R., Bigham S., Moghaddam S. (2015), Absorption Characteristics of Falling Film Lithium Bromide (LiBr) Solution over a Finned Structure, Energy, 87, 270–278.

[111] Lee J.H., Jung C.W., Chang Y.S., Chung J.T., Kang Y.T. (2016), Nu and Sh correlations for LiCl solution and moist air in plate type dehumidifier, Int J Heat Mass Transf, 100, 433–444.

[112] Prieto J., Ortiga J., Coronas A. (2017), Experimental performance of polymeric air-solution contactors for liquid desiccant systems, Appl Therm Eng, 121, 576–584.

[113] Zhi J., Dong C., Guo M., Qi R., Zhang L. zhi (2019), Wettability and performance enhancement with durable super-hydrophilic surfaces for plastic liquid desiccant dehumidification systems, Energy Build, 187, 77–85.

[114] Jaradat M., Fleig D., Vajen K., Jordan U. (2019), Investigations of a dehumidifier in a solar-assisted liquid desiccant demonstration plant, J Sol Energy Eng Trans ASME, 141, 1–10.

[115] Yi Y., Hu T., Xie X., Jiang Y. (2020), The influence of a vertical chevron corrugated plate on wetting and thermal performance of a detachable plate-type falling film absorber, Appl Therm Eng, 179, 115704.

[116] Ahmadi M., Ahmadi B., Bigham S. (2022), Wickability-optimized textured liquid-desiccant air dehumidifiers for independent moisture management in energy-efficient buildings, Energy Convers Manag, 260, 115637.

[117] Zheng G.S., Worek W.M. (1995), Effect of additives on the regeneration of a dilute absorbent, J Thermophys Heat Transf, 9, 743–748.

[118] Ali A., Vafai K. (2004), An investigation of heat and mass transfer between air and desiccant film in an inclined parallel and counter flow channels, Int J Heat Mass Transf, 47, 1745–1760.

[119] Abu-Hamdeh N.H., Almitani K.H. (2016), Solar liquid desiccant regeneration and nanofluids in evaporative cooling for greenhouse food production in Saudi Arabia, Sol Energy, 134, 202–210.

[120] Cihan E., Kavasoğulları B., Demir H. (2017), Enhancement of performance of open liquid desiccant system with surface additive, Renew Energy, 114, 1101–1112.

[121] Wen T., Lu L., Dong C. (2018), Enhancing the dehumidification performance of LiCl solution with surfactant PVP-K30, Energy Build, 171, 183–195.

[122] Wen T., Lu L., Zhong H. (2018), Investigation on the dehumidification performance of LiCl/H2O-MWNTs nanofluid in a falling film dehumidifier, Build Environ, 139, 8–16.

[123] Lun W., Li K., Liu B., Zhang H., Yang Y., Yang C. (2018), Experimental analysis of a novel internally-cooled dehumidifier with self-cooled liquid desiccant, Build Environ, 141, 117–126.

[124] Khan A.Y., Ball H.D. (1992), Development of a generalized model for performance evaluation of packed-type liquid sorbent dehumidifiers and regenerators, ASHRAE Trans, 98, 525–533.

[125] Stevens D.I., Braun J.E., Klein S.A. (1989), An effectiveness model of liquid-desiccant system heat/mass exchangers, Sol Energy, 42, 449–455.

[126] Liu X.H., Jiang Y., Qu K.Y. (2007), Heat and mass transfer model of cross flow liquid desiccant air dehumidifier/regenerator, Energy Convers Manag, 48, 546–554.

[127] Langroudi L.O., Pahlavanzadeh H., Mousavi S.M. (2014), Statistical evaluation of a liquid desiccant dehumidification system using RSM and theoretical study based on the effectiveness NTU model, J Ind Eng Chem, 20, 2975–2983.

[128] Chen Y., Zhang X., Yin Y. (2016), Experimental and theoretical analysis of liquid desiccant dehumidification process based on an advanced hybrid air-conditioning system, Appl Therm Eng, 98, 387–399.

[129] Varela R.J., Yamaguchi S., Giannetti N., Saito K., Harada M. (2018), General correlations for the heat and mass transfer coefficients in an air- solution contactor of a liquid desiccant system and an experimental case application, Int J Heat Mass Transf, 120, 851–860.

[130] Su W., Li W., Sun B., Zhang X. (2019), Experimental study and correlations for heat and mass transfer coefficients in the dehumidifier of a frost-free heat pump system, Int J Heat Mass Transf, 131, 450–462.

[131] Lim H., Lee S.-J., Su Y., Jeong J.-W. (2021), Experimental study and prediction model of a liquid desiccant unit for humidification during the heating season, J Build Eng, 45, 103549.

[132] Yin Y., Zhang X., Peng D., Li X. (2009), Model validation and case study on internally cooled/heated dehumidifier/regenerator of liquid desiccant systems, Int J Therm Sci, 48, 1664–1671.

[133] Gao W.Z., Shi Y.R., Cheng Y.P., Sun W.Z. (2013), Experimental

study on partially internally cooled dehumidification in liquid desiccant air conditioning system, Energy Build, 61, 202–209.

[134] Lee J.H., Ro G.H., Kang Y.T., Chang Y.S., Kim S.C., Kim Y.L. (2016), Combined heat and mass transfer analysis for LiCl dehumidification process in a plate type heat exchanger, Appl Therm Eng, 96, 250–257.

[135] Kim T.H., Chang Y.S., Kang B.H. (2016), Regeneration performance of liquid desiccant on the surface of a plate-type heat exchanger, J Therm Sci Technol, 11, 1–10.

[136] Wen T., Luo Y., Sheng L. (2020), Experimental study on the corrosion behavior and regeneration performance of KCOOH aqueous solution, Sol Energy, 201, 638–648.

[137] Peng D., Xu S., Yang H. (2020), Heat and mass transfer characteristics and dehumidification performance improvement of an evaporatively-cooled liquid dehumidifier, Appl Therm Eng, 178, 115579.

[138] Chung T.W. (1994), Predictions of moisture removal efficiencies for packed-bed dehumidification systems, Gas Sep Purif, 8, 265–268.

[139] Khan A.Y. (1994), Sensitivity analysis and component modelling of a packed-type liquid desiccant system at partial load operating conditions, 18, 643–655.

[140] Chung T.W., Luo C.M. (1999), Vapor pressures of the aqueous desiccants, J Chem Eng Data, 44, 1024–1027.

[141] Martin V., Goswami D.Y. (2000), Effectiveness of Heat and Mass Transfer Processes in a Packed Bed Liquid Desiccant Dehumidifier/Regenerator, HVAC&R Res, 6, 21–39.

[142] Abdul-Wahab S.A., Zurigat Y.H., Abu-Arabi M.K. (2004), Predictions of moisture removal rate and dehumidification

effectiveness for structured liquid desiccant air dehumidifier, Energy, 29, 19–34.

[143] Liu X.H., Qu K.Y., Jiang Y. (2006), Empirical correlations to predict the performance of the dehumidifier using liquid desiccant in heat and mass transfer, Renew Energy, 31, 1627–1639.

[144] Chung T., Lai C., Wu H. (1999), Analysis of Mass Transfer Performance in an Air Stripping Tower, Sep Sci Technol, 34, 2837–2851.

[145] Liu X.H., Jiang Y., Chang X.M., Yi X.Q. (2007), Experimental investigation of the heat and mass transfer between air and liquid desiccant in a cross-flow regenerator, Renew Energy, 32, 1623–1636.

[146] Moon C.G., Bansal P.K., Jain S. (2009), New mass transfer performance data of a cross-flow liquid desiccant dehumidification system, Int J Refrig, 32, 524–533.

[147] Qi R., Lu L., Yang H. (2013), Development of simplified prediction model for internally cooled / heated liquid desiccant dehumidification system, Energy Build, 59, 133–142.

[148] Qi R., Lu L., Yang H. (2014), Quick performance prediction for internally cooled/heated liquid desiccant dehumidification system, Build Serv Eng Res Technol, 35, 99–112.

[149] Wen T., Lu L., Dong C., Luo Y. (2018), Investigation on the regeneration performance of liquid desiccant by adding surfactant PVP-K30, Int J Heat Mass Transf, 123, 445–454.

[150] Kumar R., Patil D., Xiao F., Lu T. (2019), Performance intensification of regeneration process for non-corrosive plastic plate vertical falling film tower, Appl Therm Eng, 162, 114301.

[151] Khan R., Patil D.A., Kumar R. (2022), Development of high

performance vertical falling film plastic dehumidifier exploiting surface modification technique, J Sol Energy Eng, 144, 1–40.

[152] Gandhidasan P., Mohandes M.A. (2008), Predictions of vapor pressures of aqueous desiccants for cooling applications by using artificial neural networks, Appl Therm Eng, 28, 126–135.

[153] Gandhidasan P., Mohandes M.A. (2011), Artificial neural network analysis of liquid desiccant dehumidification system, Energy, 36, 1180–1186.

[154] Mohammad A.T., Mat S. Bin, Sulaiman M.Y., Sopian K., Al-abidi A.A. (2013), Implementation and validation of an artificial neural network for predicting the performance of a liquid desiccant dehumidifier, Energy Convers Manag, 67, 240–250.

[155] Mohammad A.T., Mat S. Bin, Sulaiman M.Y., Sopian K., Al-Abidi A.A. (2013), Artificial neural network analysis of liquid desiccant dehumidifier performance in a solar hybrid air-conditioning system, Appl Therm Eng, 59, 389–397.

[156] Mohammad A.T., Mat S. Bin, Sulaiman M.Y.Y., Sopian K., Al-abidi A.A. (2013), Artificial neural network analysis of liquid desiccant regenerator performance in a solar hybrid air-conditioning system, Sustain Energy Technol Assessments, 4, 11–19.

[157] Zendehboudi A., Tatar A., Li X. (2017), A comparative study and prediction of the liquid desiccant dehumidifiers using intelligent models, Renew Energy, 114, 1023–1035.

[158] Longo G.A., Ortombina L., Zigliotto M. (2018), Application of Artificial Neural Network (ANN) for modelling H2O/KCOOH (potassium formate) dynamic viscosity, Int J Refrig, 86, 435–440.

[159] Aly A.A., Saleh B., Bassuoni M.M., Alsehli M., Elfasakhany A., Ahmed K.I.E. (2019), Artificial neural network model for performance evaluation of an integrated desiccant air

conditioning system activated by solar energy, AIMS Energy, 7, 395–412.

[160] Lowenstein A. (1994), Low-Flow Internally-Cooled Liquid-Desiccant Absorber.

[161] Lowenstein A., Slayzak S., Kozubal E. (2006), A zero carryover liquid-desiccant air conditioner for solar applications, *ASME International Solar Energy Conference, Denver, Colorado, July 8–13*, 1–11.

[162] Abdel-Salam A.H., McNevin C., Crofoot L., Harrison S.J., Simonson C.J. (2016), A field study of a low-flow internally cooled/heated liquid desiccant air conditioning system: Quasi-steady and transient performance, J Sol Energy Eng Trans ASME, 138, 25–28.

[163] Jaradat M., Addy J., Ajen K., Fleig D., Jordan U. (2015), Experimental Evaluation of a Novel Tube Bundle Solar Driven Liquid Desiccant Regenerator, *International Solar Energy Society, Aix-Les-Bains(France), 16-19 September*, 1–10.

[164] Qi R., Dong C., Zhang L.Z. (2020), A review of liquid desiccant air dehumidification: From system to material manipulations, Energy Build, 215, 109897.

[165] Patil D., Kumar R., Xiao F. (2016), Wetting enhancement of polypropylene plate for falling film tower application, Chem Eng Process Process Intensif, 108, 1–9.

[166] Kumar R., Patil D., Xiao F., Aras P. (2017), Experimental investigation of maldistribution in vertical plate falling film tower, Chem Eng Commun, 204, 1237–1245.

[167] Patil D. (2021), Development of high performance falling film tower for liquid desiccant application, PhD Thesis, IIT Indore,India.

[168] Wang B., Tian R. (2019), Investigation on flow and breakdown characteristics of water film on vertical corrugated plate wall, Ann Nucl Energy, 127, 120–129.

[169] Guichet V., Jouhara H. (2020), Condensation, evaporation and boiling of falling films in wickless heat pipes (two-phase closed thermosyphons): A critical review of correlations, Int J Thermofluids, 1–2, 100001.

[170] Wen T., Lu L., Zhong H., Dong C. (2018), Experimental and numerical study on the regeneration performance of LiCl solution with surfactant and nanoparticles, Int J Heat Mass Transf, 127, 154–164.

[171] Liu J., Zhang T., Liu X., Jiang J. (2015), Experimental analysis of an internally-cooled / heated liquid desiccant dehumidifier / regenerator made of thermally conductive plastic, Energy Build, 99, 75–86.

[172] Haykin S. (2005), *Neural Networs A Comprehensive Foundation*, Pearson Prentice Hall, Singapore.

[173] Kizilkan Ö. (2011), Thermodynamic analysis of variable speed refrigeration system using artificial neural networks, Expert Syst Appl, 38, 11686–11692.

[174] Zhi L.-H., Hu P., Chen L.-X., Zhao G. (2018), Viscosity prediction for six pure refrigerants using different artificial neural networks, Int J Refrig, 88, 432–440.

[175] Mawson V.J., Hughes B.R. (2020), Deep learning techniques for energy forecasting and condition monitoring in the manufacturing sector, Energy Build, 217, 109966.

[176] Mohanraj M., Jayaraj S., Muraleedharan C. (2012), Applications of artificial neural networks for refrigeration, air-conditioning and heat pump systems - A review, Renew Sustain Energy Rev, 16, 1340–1358.

[177] Moffat R.J. (1988), Describing the uncertainties in experimental results, Exp Therm Fluid Sci, 1, 3–17.